AD-A051 850 SCIENTIFIC SYSTEMS INC CAMBRIDGE MA F/G 1/3
GLOBAL STABILITY AND CONTROL ANALYSIS OF AIRCRAFT AT HIGH ANGLE--ETC(U)
JUN 77 R K MEHRA, W C KESSEL, J V CARROLL N00014-76-C-0780
UNCLASSIFIED SSI-TR-77-1 ONR-CR215-248-1 NL

1 OF 3
AD
A051850

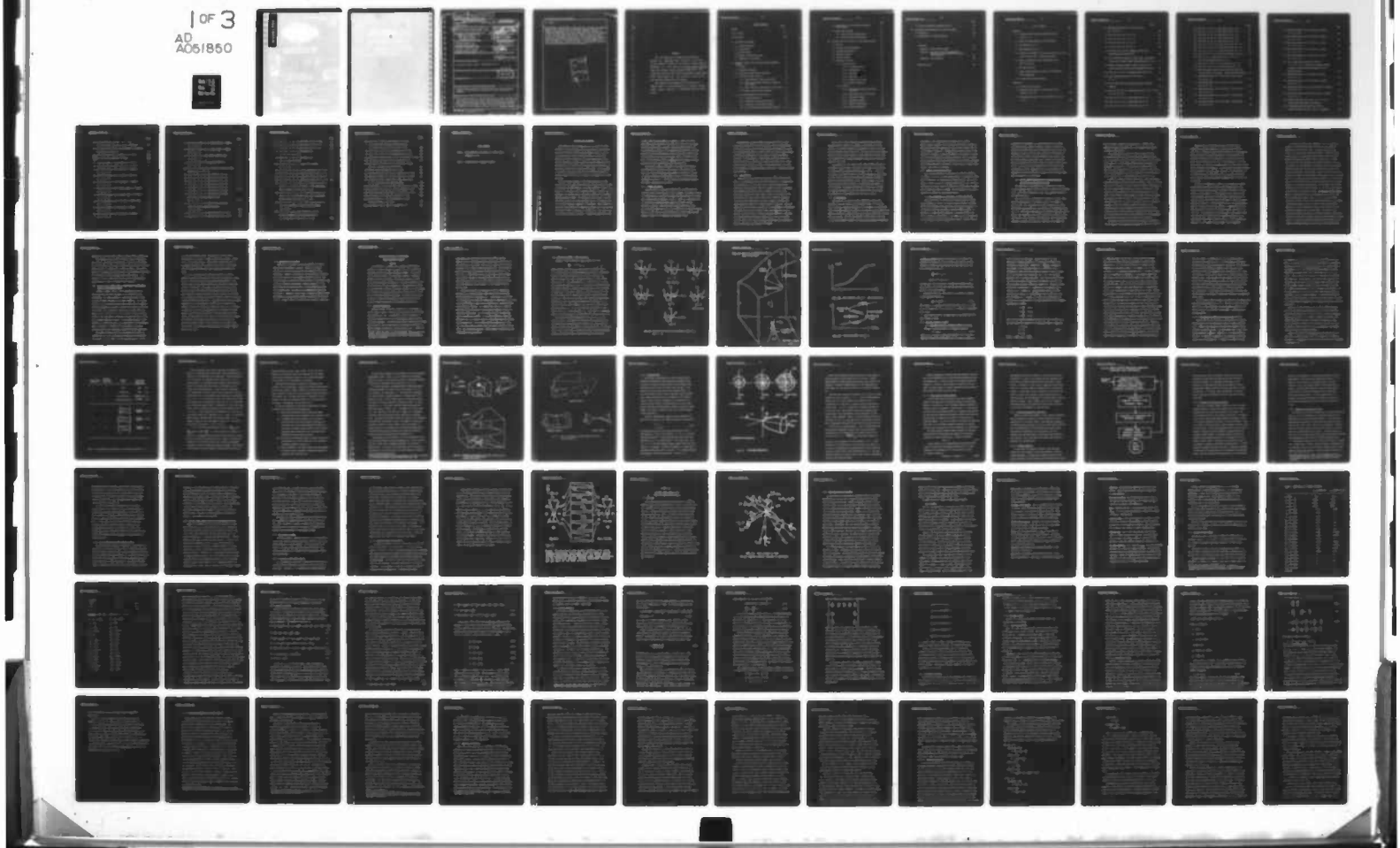

(18) ONR (19) CR215-248-1

SECURITY CLASSIFICATION OF THIS PAGE (When Data Entered)

REPORT DOCUMENTATION PAGE

READ INSTRUCTIONS BEFORE COMPLETING FORM

1. REPORT NUMBER: ONRCR-215-248-1	2. GOVT ACCESSION NO.
3. RECIPIENT'S CATALOG NUMBER: (10) 1	
4. TITLE (and Subtitle): (6) Global Stability and Control Analysis of Aircraft at High Angles-of-Attack.	5. TYPE OF REPORT & PERIOD COVERED: (9) Annual Technical Report - 1 Jun 76 - 31 May 77
	6. PERFORMING ORG. REPORT NUMBER: (14) SSI-TR-77-1
7. AUTHOR(s): (10) Raman K. Mehra, William C. Kessel, James V. Carroll	8. CONTRACT OR GRANT NUMBER(s): (15) N00014-76-C-0781 new
9. PERFORMING ORGANIZATION NAME AND ADDRESS: Scientific Systems, Inc. 1640 Massachusetts Avenue Cambridge, Massachusetts 02138	10. PROGRAM ELEMENT, PROJECT, TASK AREA & WORK UNIT NUMBERS: (12) 255p.
11. CONTROLLING OFFICE NAME AND ADDRESS: The Office of Naval Research Technology Projects Division, Code 211 Arlington, Virginia 22217	12. REPORT DATE: (11) 30 Jun 77
	13. NUMBER OF PAGES: 241
14. MONITORING AGENCY NAME & ADDRESS (if different from Controlling Office)	15. SECURITY CLASS. (of this report): Unclassified
	15a. DECLASSIFICATION/DOWNGRADING SCHEDULE

16. DISTRIBUTION STATEMENT (of this Report)

Approved for public release: Distribution unlimited

DDC RECEIVED MAR 28 1978 F

17. DISTRIBUTION STATEMENT (of the abstract entered in Block 20, if different from Report)

18. SUPPLEMENTARY NOTES

19. KEY WORDS (Continue on reverse side if necessary and identify by block number)

Aircraft Stability and Control, Bifurcation Analysis, Catastrophe Theory, Atmospheric Flight Mechanics, Nonlinear Systems, High Angle-of-Attack Phenomena.

20. ABSTRACT (Continue on reverse side if necessary and identify by block number)

Aircraft dynamic behavior at high angles-of-attack is highly non-linear and, in the past, there has been a lack of suitable techniques for analyzing the global behavior of nonlinear systems. This report describes a new approach based on Bifurcation Analysis and Catastrophe Theory Methodology (BACTM). The approach has been applied to specific jump, hysteresis and limit cycle phenomena such as roll-coupling, pitch-up, wing rock, buffeting, departure

DD FORM 1 JAN 73 1473 EDITION OF 1 NOV 65 IS OBSOLETE S/N 0102-014-6601 |

20. cont'd

and divergence. Three different aircraft have been considered for comparison purposes, and it has been shown how different types of instabilities and families of limit cycles arise as the control variables are varied. A complete representation of the aircraft equilibrium and bifurcation surfaces is given in an eight dimensional space consisting of roll rate, pitch rate, yaw rate, angle-of-attack, sideslip angle, elevator, aileron and rudder deflections. Two dimensional projections of the equilibrium and bifurcation surfaces provide pictorial representations of the aircraft global stability and control behavior at high angles-of-attack. The use of BACTM for spin entry, spin prevention, stability augmentation at high angles-of-attack and nonlinear system identification are also considered.

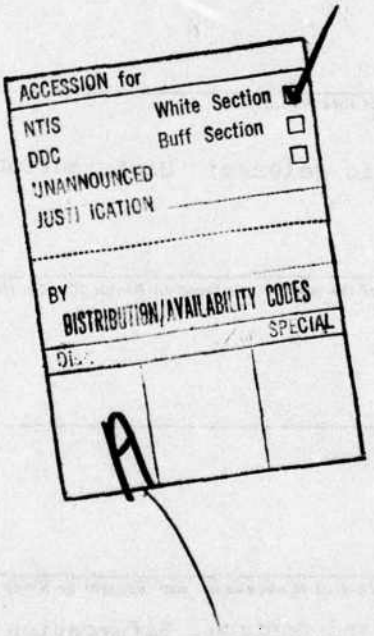

PREFACE

This investigation was conducted by Scientific Systems, Inc., Cambridge, Mass. from June 1, 1976 under Contract N00014-76-C-0780 for the Office of Naval Research, Washington, D.C. This report is the first annual technical report and includes results through 31 May, 1977. The sponsoring office was the Vehicle Technology Program headed by Mr. David Siegel, CDR. P.R. "Bob" Hite served as the Navy Technical Monitor for the Program.

The principal investigator for the study was Dr. Raman K. Mehra. He was assisted by Mr. William C. Kessel and Dr. James V. Carroll. A.C. Mulholland typed the final report.

Table of Contents

List of Figures

Page:

Page:

Page:

Page:

Page:

List of Tables

I. Introduction and Summary

High angle-of-attack phenomena have been of interest to aerodynamicists, aircraft designers, pilots and control system analysts ever since the advent of modern high performance aircraft. Due to the concentration of inertia along the fuselage, the modern jet fighters are highly susceptible to post-stall departures and spin. Extensive wind-tunnel testing and radio-controlled flight testing has been done over the last twenty years to gain better understanding of the dynamic instabilities at high angles-of-attack. A basic problem has existed in interpreting this data and in making predictions of aircraft dynamic behavior so as to achieve close agreement with flight test data.

Aircraft dynamic behavior at high angles-of-attack is highly nonlinear and, in the past, there has been a lack of suitable techniques for analyzing the global behavior of nonlinear systems. Under an on-going project with the Office of Naval Research, Scientific Systems, Inc. has developed a new approach based on Bifurcation Analysis and Catastrophe Theory Methodology (BACTM). The approach has been applied to specific jump, hysteresis and limit cycle phenomena such as roll-coupling, pitch-up, wing rock, buffeting, departure and divergence. Three different aircraft have been considered for comparison purposes, and it has been shown how different types of instabilities and families of limit cycles arise as the control variables are varied. A complete representation of the

aircraft equilibrium and bifurcation surfaces is given in an eight dimensional space consisting of roll rate, pitch rate, yaw rate, angle-of-attack, sideslip angle, elevator, aileron and rudder deflections. Two dimensional projections of the equilibrium and bifurcation surfaces provide pictorial representations of the aircraft global stability and control behavior at high angles-of-attack. The use of BACTM for spin entry, spin prevention, stability augmentation at high angles-of-attack and nonlinear system identification are also considered.

This chapter presents a discussion of the high angle-of-attack stability problem followed by a brief survey of the previous work in this area. The new methodology called BACTM is introduced in section 1.3 and the significant results obtained during the current study are summarized in section 1.4. The last section in this chapter discusses the overall organization of the report.

(1.1) Problem Description.

Aircraft motion at high angles-of-attack (α) is characterized by large deviations in both state and control variables. Linearized analysis of aircraft stability and control provides only limited localized information regarding aircraft behavior at high α. There is a conspicuous lack of techniques for analyzing global stability and large maneuver response of aircraft. Only specialized nonlinear phenomena such as roll-coupling and spin have been partially analyzed in an isolated fashion. There is a clear need for a unified approach to analyze global aircraft behavior at high α in an integrated and systematic manner.

A methodology for global stability analysis and control is also a first step towards safer piloting procedures, stability augmentation, control system design, aircraft model structure determination and design. A suitable methodology must contribute towards solutions to these problems in addition to simply giving a yes/no type of information regarding stability. In other words, the global stability analysis should also provide guidelines for stabilizing an unstable nonlinear system. Since aircraft behavior at high α is known to exhibit discontinuous and limit cycle phenomena, the methodology should also be able to predict and explain such phenomena.

(1.2) Previous Work

Early work on high α stability and control during the forties and fifties, concentrated mainly on qualitative description and understanding of the phenomena [1,2,3,4,5]. The study of specific phenomena was motivated by observed flight behavior. Attempts were made to understand these pheomena and to correct them via changes in aircraft design. Conventional analysis techniques based on steady state assumptions and linearization were used to obtain quantitative information. However, a lack of suitable experimental facilities, analysis techniques and meager computing capabilities hindered progress in this area. The major emphasis during the sixties was placed on the establishment of experimental facilities such as radio-controlled flights and wind-tunnels for spin testing. At the same time, simulation techniques were used to reproduce with six degree-of-freedom models behavior typical of high α flights [6,7,8]. Again, due to lack of analytical techniques, only limited progress has been made using simulation techniques.

Recent work in high α areas covers a wide spectrum of subjects ranging from basic research in aerodynamics, wind tunnel and flight testing [9] to advanced mathematical techniques for stability analysis [10] and parameter identification [11]. The highly nonlinear and complex nature of aircraft dynamic behavior at high α coupled with poorly understood aerodynamics has presented formidable difficulties to significant progress in this area.

The motivation for the research effort reported here came from an involvement of the principal investigator with a study of the stability of chemical reactions using Catastrophe Theory [12,13]. It was conjectured that the discontinuous and limit cycle phenomena at high angles-of-attack could be analyzed using results from Topology, Bifurcation Analysis and Catastrophe Theory [14,15]. Recent analysis of the roll-coupling problem by Schy and Hannah [16] provided further support to this conjecture. The results presented here have not only confirmed our original conjecture, but have also provided additional insights and revealed new dynamic phenomena that can occur at high α.

(1.3) New Methodology

The application of recent abstract mathematical results from Topology, Bifurcation Analysis and Catastrophe Theory to the aircraft high α stability problem has resulted in the development of a new methodology called BACTM (Bifurcation Analysis and Catastrophe Theory Methodology). BACTM is applicable to other nonlinear systems such as submarines, missiles, and power systems. The four main theorems on which BACTM is based are (i) the Center Manifold Theorem; (ii) Classification Theorem of Elementary

Catastrophes; (iii) Hopf Bifurcation Theorem; and (iv) Global Implicit Function Theorem. These theorems are discussed in Chapter II and Appendix A and their application to the aircraft stability problem is discussed in Chapter III. The application of BACTM provides global information regarding aircraft dynamic behavior with respect to changes in initial state parameters, and control variables. The use of BACTM requires advanced computational techniques which are extremely important for obtaining quantiative information needed for stability augmentation, control, identification and design.

(1.4) Summary of Significant Results

Since detailed quantitative results of the study are presented in Chapters II and III, we briefly summarize here, in qualitative terms, what are believed to be some of the significant results. The current study is the first phase of a continuing research effort and, therefore, represents only a first step in the direction of methodology development and potential applicability of BACTM. The contributions of the present study may be divided into three general areas:

(i) A New Methodology for the Analysis of Nonlinear Systems

Bifurcation Analysis and Catastrophe Theory Methodology (BACTM), shown schematically in Fig. 2.8, which is based on several important results from Topology, Catastrophe Theory and Bifurcation Analysis, is a powerful new tool for the study of nonlinear dynamic systems. It allows one to study the global behavior of nonlinear systems in an $(n + m)$ dimensional space where n is the number of state variables and m is the number of control variables in the system. A direct outcome

of applying this methodology is a characterization of the stable and unstable regimes, stability boundaries, domains of attraction, bifurcation and jump surfaces and the existence of limit cycles. The methodology can also be used for model reduction or simplification (using the center manifold theorem), feedback control system design for producing almost linear behavior for a nonlinear system, model structure determination and input design for nonlinear system identification. It also gives a clear representation of those cases where linearization is valid. More importantly, it gives guidelines for extending the linearized model so as to make it valid for those cases where nonlinearities are significant.

(ii) Unified Improved Understanding of Aircraft Stability and Control at High Angles-of-Attack.

The application of Catastrophe Theory and Bifurcation Analysis to three different aircraft models has provided an improved understanding of the various jump, hysteresis and limit cycle phenomena observed at high angles-of-attack.

The three aircraft are designated as aircraft A, B and H. Their physical characteristics are presented in Table 2 of Chapter III. (See also Sec. 3.3). Aircraft A is an F100A; aircraft B is a small maneuverable single-engined jet, and aircraft H is a swept-wing fighter, the F-80A. Even though these models do not represent modern day fighter planes, their importance lies in their extensive use in previous work (see Chapter III for discussion and references). Use of these models, therefore, provides a solid basis for comparison of the BACTM with

other techniques, especially analytic results. BACTM has been demonstrated using these models, and it is currently being applied to modern fighter planes.

It has been shown for aircraft B that the bifurcation and catastrophe surfaces are of the "butterfly"-type. The projection of the bifurcation surface in the control-state space onto the control plane results in a pattern which somewhat resembles the shape of a butterfly. See Figs. 2.9, 3.10, and 3.11 for examples. See also Fig. 3.13 and the discussion in Sec. 3.6.1.3 relating to the bifurcation to an autorotational state for aircraft B as δe increases from 0° to 12°, with $\delta a = \delta r = 0°$ (the bifurcation occurs at $\delta e = 9.3°$).

A bifurcation surface divides regions in the control space where different numbers of equilibrium states are possible. Thus, as controls vary in such a way as to cross the bifurcation surface, catastrophes in the form of sudden "jumps" between equilibrium solutions occur. The solution is said to bifurcate to a new equilibrium branch in state space. The bifurcation surface marks the boundary between the stable and unstable equilibrium solutions. See the discussion of Sec. 2.2, and particularly Figs. 2.1 and 2.2 for a better picture of bifurcation phenomena. Note that hysteresis effects are prevalent where bifurcations occur; which introduces the possibility that control recovery actions, which are effective in stable and/or linear regions of the equilibrium state space, may be ineffective or actually enhance the destabilizing motions, once a bifurcation has occurred.

The physical mechanism causing jumps in the case of aircraft B can be related to roll-coupling first observed by Phillips in 1948 [6].

Careful study of time-history motions of aircraft B and H indicates that yaw rate behavior is an indicator of an oncoming jump. This is because of coupling effects between roll and yaw motions which are enhanced by the peculiar geometry of high performance jet aircraft, particularly their small moment of inertia about the roll axis. See the discussion in Sec. 3.6.1.5 and especially 3.6.1.6 for more details. Our analysis, furthermore, predicts several other effects such as hysteresis and divergence. It also indicates coordinated aileron-elevator maneuvers that avoid jumps. See Sec. 3.7 for a discussion of this BACTM application. Even the critical roll rates are predicted more accurately since the simplifying assumptions used by Phillips [1] are avoided.

We have also examined the physical causes of jumps more closely and developed indicators of incipient jump phenomena which can be useful to the pilot during flight. One promising indicator of catastrophic, or jump, behavior is total vehicle kinetic energy and its time derivative. When monitored during dynamic response studies of aircraft B and H, the kinetic energy was observed to experience sudden changes - in advance of a similar change of any of the state variables - when the controls had moved from a stable to a jump-producing value. This was clearly the case for the aircraft B model (See Figures 3.29 and 3.30); the presence of oscillatory terms in the aircraft H case (Figures 3.92 and 3.93)indicates that low-pass filtering or a more sophisticated "jump alarm" criterion than the one which sufficed for aircraft B - i.e., change of sign in dE/dt - may be developed.

For aircraft H, time history analysis has revealed families of limit cycles in a five-dimensional space which have not been obtained analytically in any previous study. A time history plot, shown in Fig. 3.50, clearly shows limit cycle behavior. This plot is seen to be the result of behavior predicted by inspection of the related equilibrium surface plots, shown in Figs. 3.48 and 3.49. In these plots, both limit cycle amplitude and hysteresis effects are indicated, in addition to the specification of the values of control (δa, aileron deflection) which will cause limit cycle behavior for aircraft H in this flight condition. See also Figs. 3.87 and 3.88, which show limit cycles for aircraft H in the state space (four plots of p vs. (q,r,α,β)); and Fig. 3.90, which shows how a change in δe from 2° to -2° causes the motion to leave the limit cycle and settle (after some severe transient behavior) at a stable equilibrium point. The existence of limit cycle phenomena has been postulated previously, but the analysis has generally been confined to two-dimensional cases. The existence of Hopf Bifurcations in aircraft dynamics has been demonstrated for the first time. The bifurcation plots shown in Figs. 3.51 and 3.52 are generated explicitly by BACTM. They are also related geometrically to the family of equilibrium surfaces (Figs. 3.48 and 3.49 being representative members), in that the bifurcation surfaces are the projection of the equilibrium surfaces onto the control space. The "folds" in the equilibrium surfaces cause regions of differing numbers of equilibrium solutions to exist; the bifurcation surfaces are the boundaries to these regions. The physical mechanisms causing these limit cycles are not completely understood except in special cases such as wing-rock and

buffeting (even in these cases, there are several physical explanations).

Other phenomena that are easily analyzed using this methodology are "pitch-up", autorotation and divergence. Most of these phenomena are not described precisely in the literature and the general conditions under which they are observed are not known accurately. Our approach gives an exact quantitative representation of these phenomena and reveals this dependence on aircraft parameters and control systems. It is possible therefore to study techniques for avoiding these phenomena through changes in design or through control strategies.

(iii) Implications for Model Structure Determination and Controller Design at High Angles-of-Attack.

A number of areas in which the above improved understanding of the high angle-of-attack phenomena can be utilized have been investigated. Two common problems in aircraft model identification are model structure determination and model validation. It is easily inferred from the Catastrophe Theory generic models that the observed bifurcation behavior can be used to identify and validate the structure of the model. This has important implications for input design and flight testing. The basic idea is that the model structure should be chosen in such a way that it is capable of matching the jump and limit cycle phenomena observed in flight. At high angles-of-attack, these phenomena are dominant and their proper representation by a mathematical model is essential. Such models are also necessary for studying entry into spin and for investigating recoveries from spin conditions.

By studying different aircraft and by analyzing the effect of feedback, we have shown how bifurcation surfaces can be modified and even avoided in certain cases. This has important implications for

aircraft and controller design. The bifurcation surfaces may be used directly in the design of stability augmentation systems. (Refer to Sec. 3.7 for more details). Results there indicate that plots of the bifurcation surfaces are a useful tool for defining relationships among the control variables which avoid regions where bifurcations occur.

In Sec. 3.7, bifurcation and equilibrium surfaces are used to develop an aileron-rudder-interconnect (ARI) control augmentation system for use in high angle-of-attack lateral-directional maneuvers. This study was done with the aircraft H model, and time history comparisons of ARI vs. non-ARI ($\delta r = 0°$) systems show clearly that ARI not only enhances stability but improves performance characteristics. The ARI gains developed by BACTM are effective because of their direct reliance on the bifurcation surfaces, which contain important stability information. A linear ARI model was used in Sec. 3.7 for illustrative purposes; however BACTM allows for a more general, global ARI-type relationship which explicitly accounts for elevon (δe) deflections as well. It is possible to expand the criteria for the bifurcation loci themselves to develop further criteria for the ARI surface in the three dimensional control space. Results presented in this report show that the ARI gains plotted as a function of equilibrium angle-of-attack, as derived from the bifurcation surfaces, behave in much the same way, with roughly equivalent values, as the ARI gains derived by other, less-global, methods [11,15 of Ch. III].

(1.5) Organization of the Report

The report is organized into two main chapters (II and III) supported by two appendices (A and B). Chapter II contains a discussion of the Bifurcation Analysis and Catastrophe Theory Methodology. Chapter III contains all the aircraft global stability and control results for three example aircrafts (A,B and H). The study of aircraft H involving nonlinear kinematic and aerodynamic terms is most comprehensive representing a complete description of the equilibrium and bifurcation surfaces in an eight-dimensional space $(p,q,r,\alpha,\beta,\delta a,\delta e,\delta r)$. Conclusions and recommendations are stated in Chapter IV. Appendix A contains exact statements of BACTM theorems and Appendix B contains detailed algebraic calculations for aircraft B and H. A list of symbols and nomenclature is included in Appendix C.

II. Bifurcation Analysis and Catastrophe Theory Methodology (BACTM)*

OVERVIEW

In this chapter, we describe from a general system theoretic viewpoint, the basic principles and applications of the Bifurcation Analysis and Catastrophe Theory Methodology (BACTM). After giving a brief historical survey, the terminology of BACTM is introduced through an illustrative example. The four main theorems of BACTM are discussed thereafter in Section 2.3. The exact statements of the main theorems are contained in Appendix A. The application of BACTM to nonlinear dynamic systems is discussed in Section 2.4. Other methods for the analysis of nonlinear systems are outlined in Section 2.5 and their relationship to BACTM is duscussed. The specific applications of BACTM for Global Stability Analysis, Control System Design and Nonlinear System Identification, are described in Section 2.6.

(2.1) Historical Background

Nonlinear dynamic systems are extremely rich in their behavior and are known to exhibit a wide variety of bifurcation and catastrophe jump phenomena [37, 38]. In recent years, several developments in differential topology have led to a fairly general classification of bifurcation phenomena. Following the publication of the thought-provoking book by Thom [1], various applications of Catastrophe and Bifurcation Theory by Zeeman have appeared in the literature [2,3,4]. A number of

*Certain readers may prefer to go through Chapter 3 before reading this chapter. This process would help in associating various abstract quantities and concepts defined here with specific aircraft physical variables and phenomena.

these applications have been to social and biological systems, where the lack of a mathematical model causes serious difficulties in the application of the theory. This has led to some recent criticism of Zeeman's work on Applied Catastrophe Theory [34]. The engineering applications of Catastrophe Theory and Bifurcation Analysis, on the other hand, are well founded since they are based on physical models [5,6,7,28,29]. Perhaps the most common engineering applications of Bifurcation Analysis are in the fields of Elastic Stability of Structures [39], Nonlinear Circuit Analysis [37] and Chemical Kinetics [28,30,35,40].

A study of the bifurcation phenomena in ordinary differential equations was started by Poincare around 1892 [8] and was extended further by Andronov and Pontryagin [10]. A new impetus was provided in recent years by the theory of singularities of smooth maps [11,12,13,14]. A full understanding of these results requires use of advanced concepts from differential topology. Our approach here will be to illustrate important concepts and results through specific examples, relevant to engineering applications. We shall discuss four main theorems that are the cornerstones of BACTM: (i) the Center Manifold or Reduction Theorem [7,15]; (ii) the main theorem of Catastrophe Theory due to Thom [1] and Mather [14] ; (iii) the Hopf Bifurcation Theorem [15] ; and (iv) the Global Implicit Function Theorem of Palais [17] and its extensions. For illustrative purposes, a simple example of bifurcations and catastrophes is presented first.

(2.2) Illustrative Example: Cusp Catastrophe

Consider a scalar differnetial equation model of the form

$$\frac{dx}{dt} = - x^3 + c_1 x + c_2 \qquad (2.1)$$

where x denotes state and (c_1, c_2) denote control variables. Since it is a scalar system, the stable equilibrium points may be represented as the minima of the potential function $\phi = x^4/4 + c_1 (x^2/2) + c_2 x$. These are shown in Fig. [2.1] for different values of c_2 and a fixed value of $c_1 = -3$. It is clear from Fig. [2.1] that for $|c_2| > 2$, only one minimum exists whereas for $|c_2| < 2$, two minima and one maximum exist. The maximum represents an unstable equilibrium point so that the system can never stay in that state. Suppose c_2 is varied slowly from -3 to 3 in such a manner that the system state x reaches an equilibrium value for each c_2. Then the state will stay in the right hand minimum corresponding to x_1 till this minimum coalesces with the maximum at $c_2 = 2$. At this point with a small change in c_2, the state will jump catastrophically from x_1 to x_2. If c_2 is now reversed, the system will stay in state x_2 until $c_2 = -2$ and then jump to x_1. Thus there is a hysteresis effect in that the location of the jump depends on the past history of c_2.

We now draw a three-dimensional picture in the (x, c_1, c_2) space (see Fig. [2.2]). The surface of equilibrium points is called M and its projection on the control space is denoted by C. Notice that the region in control space over which M is triple-sheeted (i.e., the function $f(x,c) = 0$ has three roots) is enclosed by a cusp. The boundary between regions with different number of equilibrium points is called the

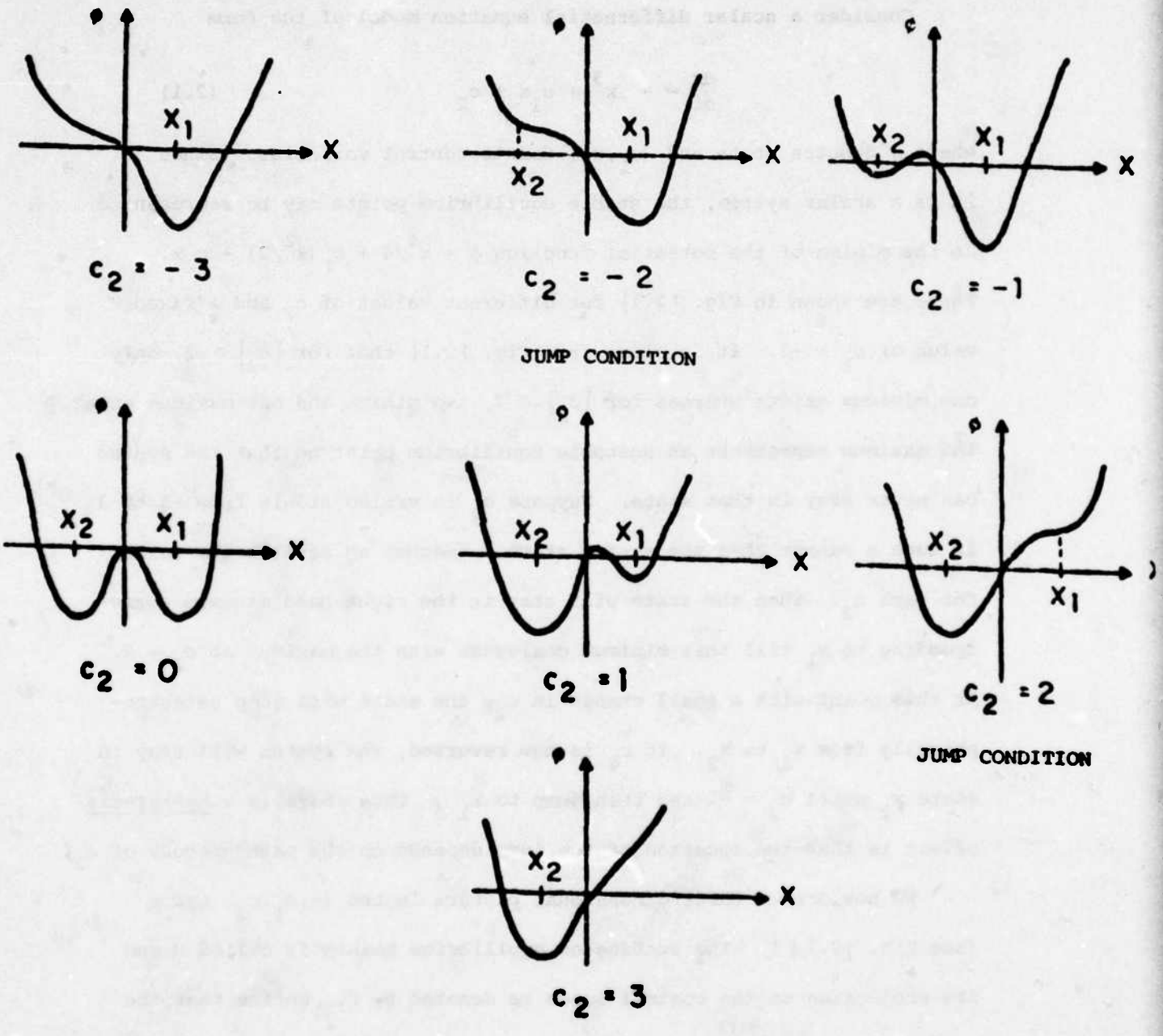

Fig. 2.1: Potential function $\phi(x,c)$ for different values of c_2 and $c_1 = -3$.

Fig. 2.2: Qualitative Representation of Cusp Catastrophe

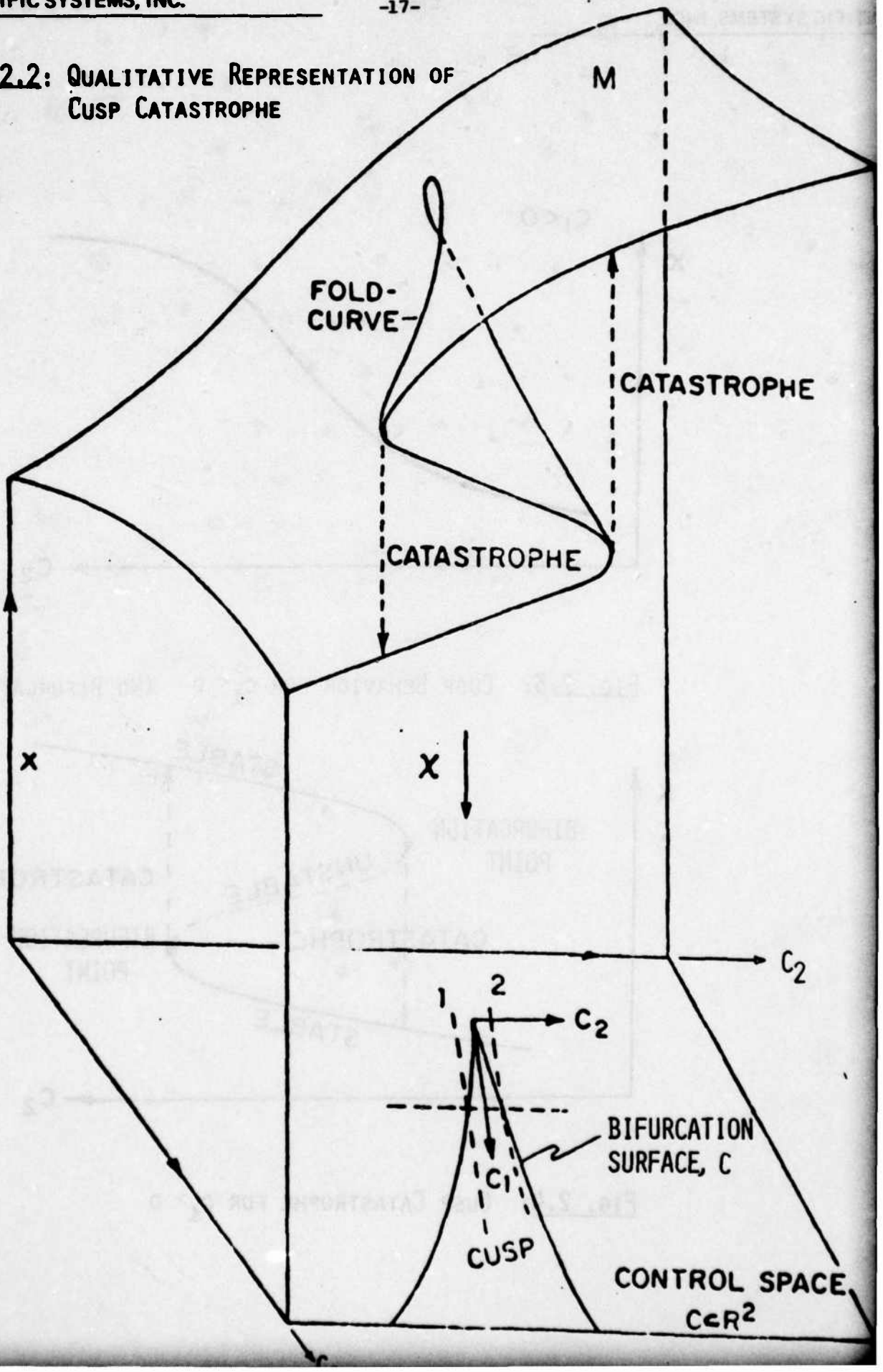

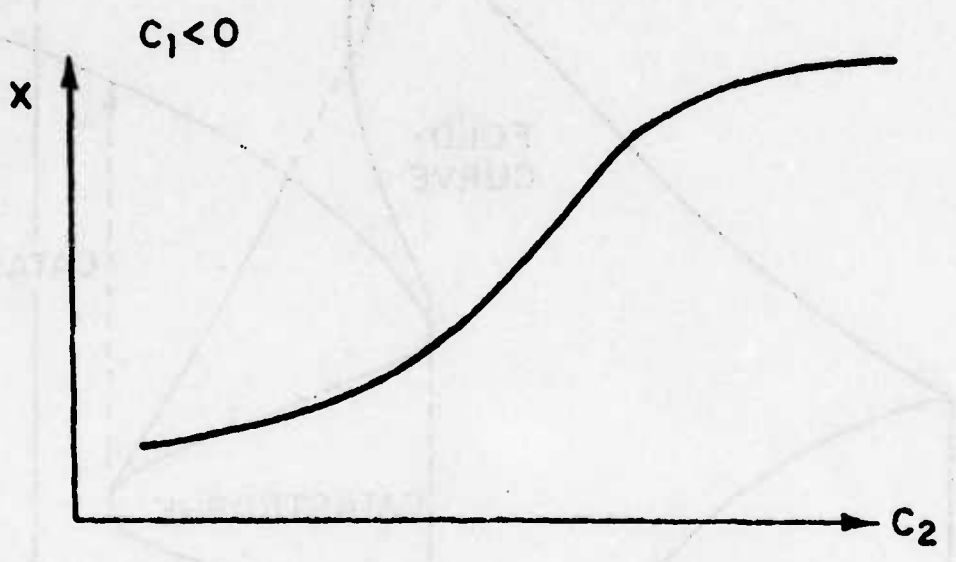

FIG. 2.3: CUSP BEHAVIOR FOR $C_1 < 0$ (NO BIFURCATION)

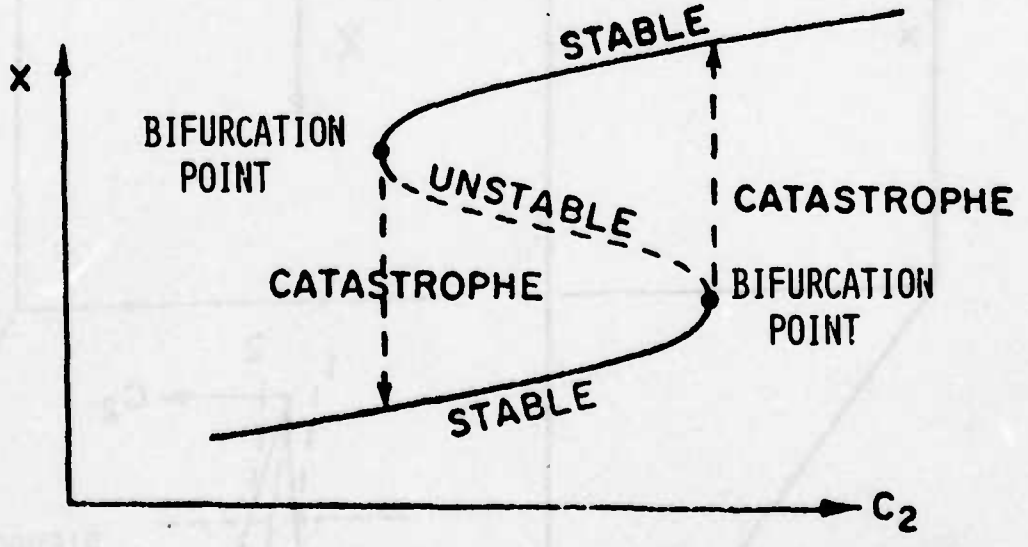

FIG. 2.4: CUSP CATASTROPHE FOR $C_1 > 0$

Bifurcation Surface since the equilibrium solutions separate (or bifurcate) from each other at this surface. The equations for the Bifurcation Surface are easily derived by setting both $f(x,c)$ and $\partial f(x,c)/\partial x$ equal to zero, i.e.

$$\frac{\partial f}{\partial x} = 3x^2 + c_1 = 0 \tag{2.2}$$

$$f(x,c) = x^3 + c_1 x + c_2 = 0 \tag{2.3}$$

In other words, the coalescing of a minimum and a maximum creates and inflection point at which the first and the second derivatives of $\phi(x,c)$ vanish simultaneously.

Elminating x from Eqs. (2.2) and (2.3), we obtain the equation of the bifurcation surface as

$$\frac{1}{27} c_1^3 + \frac{1}{4} c_2^2 = 0 \tag{2.4}$$

The variable c_1 is called a splitting factor since for $c_1 < 0$, there is no catastrophe (Fig. [2.3]) and for $c_1 > 0$, there is a catastrophe (Fig. [2.4]).

Having defined some of the terminology, we now discuss the four main theorems of BACTM.

(2.3) Four Main Theorems of BACTM*

(2.3.1) The Center Manifold or Reduction Theorem [18,19,20]:

Consider a system described by a differential equation

$$\dot{x} = f(x,c) \tag{2.5}$$

where x is n × 1 vector of state variables and c is m × 1 vector of

*The exact statements of these theorems are contained in Appendix A.

control variables and parameters. Suppose that for c = 0, the system has an equilibrium point at x = 0 (this can be achieved by a translation in state space). Assume that $F = \frac{\partial f}{\partial x}\Big|_{\substack{x=0 \\ c=0}}$, representing the dynamics of the linearized system, has k eigenvalues on the imaginary axis (zeros and purely imaginary eigenvalues being included). Out of the remaining (n-k) eigenvalues, let j be in the left half plane and ℓ be in the right half plane. Also, divide the eigenvectors of F into three groups corresponding to the imaginary axis, left half plane and right half plane eigenvalues respectively. Arrange the eigenvectors of F corresponding to k eigenvalues on the imaginary axis as columns of an $n \times k$ matrix E_o. Similarly define matrices of eigenvectors $E_-(n\times j)$ and $E_+(n \times \ell)$ corresponding to the left-half and right-half eigenvalues of F. Consider, now, coordinate transformations or projections of the state vector x onto the space spanned by the different eigenvectors as follows:

$$u = E_o^T x \qquad (k \times 1)$$

$$v = E_-^T x \qquad (j \times 1)$$

$$w = E_+^T x \qquad (\ell \times 1)$$

Then the Center Manifold Theorem states that Eq. (2.5) is locally (i.e., for small deviations) equivalent to the following system of equations:

$$\begin{aligned} \dot{u} &= g(u,c) \\ \dot{v} &= A_- v \\ \dot{w} &= A_+ w \end{aligned} \qquad (2.6)$$

where $A_- = E_-^T F E_-$ and $A_+ = E_+^T F E_+$.

The important thing to notice in Eq. (2.6) is that the equations for v and w are linear and that the dimension k is generally much smaller than n. In fact, the maximum value of k depends on the dimension m of the control vector c. For example, if m = 1, only the cases k = 1 (a single zero eigenvalue) and k = 2 (a pair or purely imaginary eigenvalues) are obtained in a "structurally stable" way. Other values of k are not structurally stable since a small change in the dynamics of the system can move the extra eigenvalues away from the imaginary axis. Notice further that a minimum of three control variables are required to place two eigenvalues of F simultaneously at the origin (alternatively to reduce the rank of F by two). General relationships of this type between m and k have been given by Arnold [7].

A direct consequence of Eq. (2.6) is that the bifurcational study of the original nonlinear system is reduced to a much smaller system of dimension k. The theorem also implies that any results that are obtained on the u-system may be generalized to higher dimensional systems by the process of building on or "suspension" [7] with linear systems having eigenvalues with non-zero real parts. For applications, the most significant consequence of the theorem is perhaps the central importance of the eigenvalues on the imaginary axis. The nonlinear character of the system is essentially unfolded through these eigenvalues. Therefore, the determination of surfaces in the control and parameter space where one or more eigenvalues cross the imaginary axis is of paramount importance in studying the behavior of nonlinear systems. These surfaces may be obtained analytically from models or inferred experimentally

for real systems. In BACTM (see Fig. 2.8), the given equations of motion for a system (viz. Eq. (2.5)) are linearized around each equilibrium point, either analytically or numerically. The eigenvalues of each linearized system are computed to determine the control conditions at which the eigenvalues cross the imaginary axis. There are cases (e.g. aircraft B) for which only one eigenvalue crosses the imaginary axis. Using the Center Manifold Theorem, we can, therefore, study their bifurcation behavior in terms of a single state variable. The Center Manifold Theorem essentially generalizes and extends the linearization procedure used so commonly in control applications. More importantly, it reveals when linearization would break down and how the model may be extended to capture the "essential" nonlinearities of the system.

We now discuss theorems by Thom [1] and Hopf [16] that characterize the bifurcational behavior for k = 1,2. The classification for higher values of k is still incomplete, but the phenomena exhibited by the above two cases is so rich that a large number of applications are already possible.

(2.3.2) Main Theorem of Elementary Catastrophe Theory [1,14].

This theorem provides a complete classification of the bifurcational behavior of finite dimensional systems of gradient-type for $m \leq 5$. Gradient-type systems are such that their dynamics locally minimize a potential function. For such systems f(x,c) in Eq. (2.5) can be expressed as $\frac{-\partial}{\partial x}\phi(x,c)$ where $\phi(x,c)$ is a scalar potential function. An important consequence of this assumption is that the linear part of the dynamic viz. $F = \partial^2\phi/\partial x^2$ is a symmetric matrix

and therefore has only real eigenvalues. It can be shown [1,7] that for $m \leq 5$, only the cases $k = 1$ and 2 can be obtained in a structurally stable way (or occur in "general position" [7] i.e., a slight change in the function $\phi(x,c)$ or the parameters would not eliminate the above singularities) whereas higher order singularities of F, i.e., $k \geq 3$ do not appear in control space dimension of less than 6 in a structurally stable way. This can also be seen from the fact that F may be decomposed into the product of a non-singular lower triangular matrix W with an upper triangular matrix G via Gaussian elimination. Then, for a stable rank deficiency of 3 in F, a minimum of six elements in the the last three rows of G must be zero [35], which requires having six independently varying control parameters. In some practical applications, the special structure of F may lead to stronger results, allowing one to narrow down the classification of singularities and the resulting bifurcations.

Based on the above discussion and the Center Manifold Theorem, the local classification of bifurcations for all finite dimensional gradient type systems for $m \leq 5$ can be reduced to systems of dimension one ($k = 1$) and two ($k = 2$). However, a complete classification of singularities depends further on the nature of higher order terms in the Taylor series expansion of the function $g(u,c)$ (cf. Eq. (2.6)). The general theorem by Thom [1] is given in Appendix A. We consider here the case of four control variables.

Table 1 lists the seven catastrophes given by Thom [1] for the case of $m = 4$. The first four are called cuspoids and correspond to the case $k = 1$, whereas the last three are called umbilics and correspond to the case $k = 2$.

Control Space Dimension, m	Reduced State Space Dimension, k	Generic g(x,c)	Description Name of the Catastrophe	
1	1	$-(x^2-c)$	FOLD	(2.7)
2	1	$-(x^3+c_1x-c_2)$	CUSP	(2.8)
3	1	$-(x^4+c_1x^2+c_2x-c_3)$	SWALLOW TAIL	(2.9)
4	1	$-(x^5+c_1x^3+c_2x^2+c_3x-c_4)$	BUTTERFLY	(2.10)
3	2	$-\begin{pmatrix} x_1^2+c_1x_2-c_2 \\ x_2^2+c_1x_1-c_3 \end{pmatrix}$	HYPERBOLIC UMBILIC	(2.11)
3	2	$-\begin{pmatrix} x_1^2-x_2^2+c_1x_1-c_2 \\ -2x_1x_2+c_1x_2-c_3 \end{pmatrix}$	ELLIPTIC UMBILIC	(2.12)
4	2	$-\begin{pmatrix} 2x_1x_2+2c_1x-c_2 \\ x_2^3+c_2x_2-c_4 \end{pmatrix}$	PARABOLIC UMBILIC	(2.13)

Table 1: Seven Elementary Catastrophes for Control Space Dimension, m = 4.

The classification within each of the above two categories is based on the codimension of the singularity, which qualitatively is an indication of the degeneracy of the singularity. The exact definition of the codimension of a singularity may be found in ref. [1], but roughly speaking, the codimension may be inferred from the number of Taylor series coefficients that vanish in the expansion of $g(x,c)$ around a given equilibrium point. In this sense, all equilibrium points [equivalently critical points of $\phi(x,c)$] around which the linearized system has no zero eigenvalues are singularities of codimension zero. For $k = 1$, it is clear that at least one (linear) Taylor coefficient must vanish in the expansion of $g(u,c)$ [cf. Eq. (2.6)] but higher order coefficients may also vanish. The dimension of the control space m again limits the number of cases that are to be considered since for $m = 4$ and $k = 1$, only singularities of codimension $d \leq 4$ can occur in a structurally stable way. Similarly, for $k = 2$, and $m = 4$, only three umbilic types of singularities occur as shown in Table 1. As an example, consider the cusp catastrophe of section 2.2. The function $g(u,c)$ takes the form $g(u,c) = -(u^3 + c_1 u + c_2)$.

At $u = 0$, the first two derivatives of $g(u,c)$ viz $\left.\frac{\partial g}{\partial u}\right|_{u=0}$ and $\left.\frac{\partial^2 g}{\partial u^2}\right|_{u=0}$ vanish, whereas $\frac{\partial^3 g}{\partial u^3} = -6$. Thom [1] shows that the above $g(\cdot)$ function is representative of the class of smooth functions for which the first two partial derivatives are zero. However, to achieve this condition in a "structurally stable" way, at least two independent parameters or control variables ($m=2$) must be available. The specific control values can then be obtained by simply setting the first two

partial derivatives of g(u,c) equal to zero. If only one control variable is available and the first two partials of g(u,c) happen to be zero for a particular value of c, then a slight perturbation in the function g(u,c) would destroy this property.

We now discuss the genericity property of the models listed in Table 1 for each catastrophe. These are the simplest representations of equivalence classes of dynamic systems in the sense that all other dynamic systems in a given class can be obtained by smooth deformations of the generic ones. The exact definition of equivalence is rather technical, but should be considered carefully in every application of the theorem. (See Appendix A for this definition).

The practical importance of the generic representation of Table 1 in applications derives from the following facts:

(i) Their global bifurcation behaviors have been studied extensively and are well documented in the literature [1,21].

(ii) In system identification problems, one or more model structures have to be postulated based on physical considerations and on the observed qualitative properties of the system. The generic models provide a library with well-understood dynamic properties and are, therefore, ideal candidates for choosing model structures.

(iii) The validity of the generic models for physical systems can be extended by use of the building on or the "suspension" procedure discussed in Section 2.3.1.

(iv) The low dimension of the generic models makes them amenable for further study in problems of experimental design and optimal control (see Section 2.6).

For illustrative purposes, we show diagrams of the seven elementary catastrophes in Figs. 2.5 and 2.6. Only selected three dimensional sections are shown.* We now discuss the nature of equilibrium surfaces and phase plane trajectories for the cuspoids (cf Fig. 2.5).

For a Cusp Catastrophe, the maximum number of equilibrium points (stable and unstable) for a given value of the controls c is 3 and for a Butterfly, the same number is 5. Each equilibrium corresponds to a minimum (stable), maximum (unstable) or inflexion point of the potential function. At the inflexion point, the second derivative of the potential function vanishes and a bifurcation occurs. In higher dimensions ($n > 1$), the nature of nonzero eigenvalues modifies the state space portrait (see Eq. (2.6)). For example, one can get nodes (i.e., all eigenvalues of the same sign), saddles (i.e., eigenvalues of opposite signs) and bifurcation points (one or more eigenvalues zero). The nodes may be further divided into sources or sinks depending on whether they are unstable or stable. The domains of attraction of the sinks are defined in terms of separatrices of the saddles. At bifurcation points, the determinant of the linearized dynamic matrix F vanishes and this provides one method for locating the bifurcation surfaces without solving explicitly for eigenvalues of F.

The discussion in this subsection (2.3.2) has concentrated on the case of real eigenvalues crossing the imaginary axis. We now consider the case in which a pair of complex eigenvalues of F crosses the imaginary axis. It is shown in the next section that this results in bifurcation to a limit cycle known as the Hopf Bifurcation, provided certain conditions are satisfied.

*For detailed representation of these catastrophes, the reader is referred to the extensive computer study of Woodstock and Poston [21].

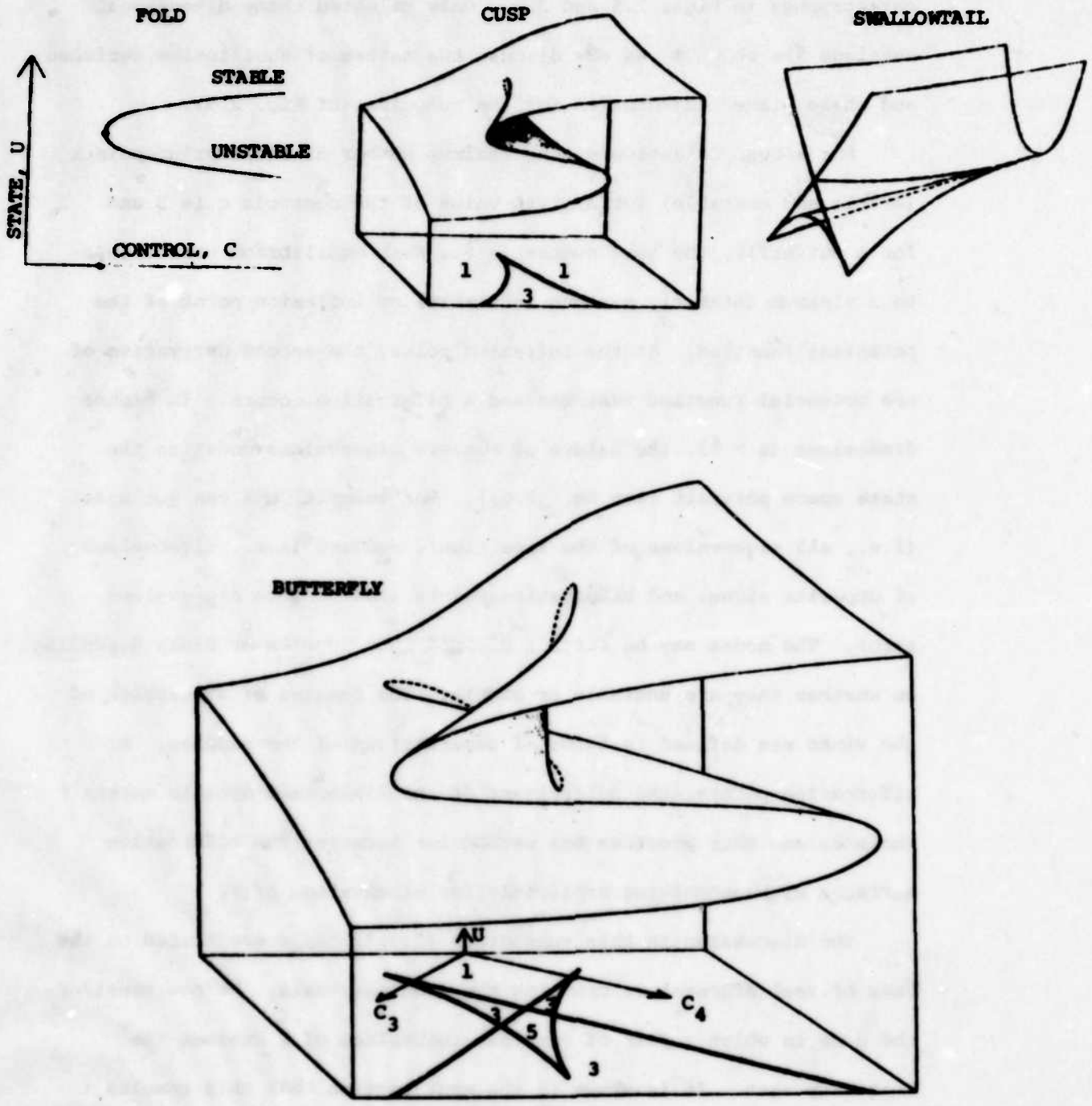

Fig. 2.5: Elementary Catastrophes in One State Variable and One or Two Control Variable Space. (Cuspoids from Table 1).

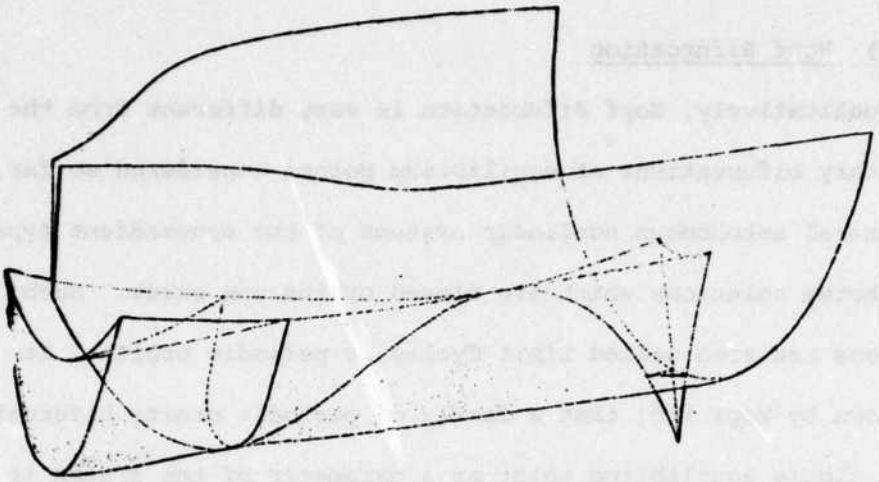

PARABOLIC UMBILIC

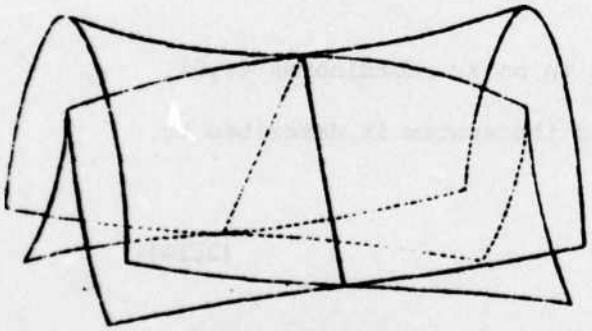

HYPERBOLIC UMBILIC

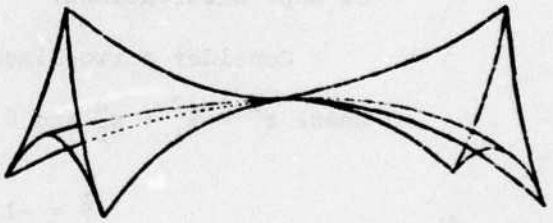

ELLIPTIC UMBILIC

Fig. 2.6: Umbilic Catastrophes in Three-Dimensional Control Space (See Table 1).

(2.3.3) Hopf Bifurcation

Qualitatively, Hopf Bifurcation is very different from the elementary bifurcations of equilibrium points considered so far. For general autonomous nonlinear systems of the nongradient type, equilibrium solutions which are closed orbits can exist. Such solutions are also called Limit Cycles or periodic orbits. It was shown by Hopf [16] that a family of periodic orbits bifurcates from a simple equilibrium point as a parameter of the system is varied in such a way that a complex pair of eigenvalues of the linearized system crosses the imaginary axis with nonzero speed. Before discussing the Hopf Bifurcation Theorem, we present a simple example. The reader is referred to Ref. [5] for further examples of Hopf Bifurcations.

Consider a two-dimensional system in polar coordinates (r,θ), where $r^2 = x_1^2 + x_2^2$ and $\theta = \tan^{-1}\frac{x_2}{x_1}$ and the system is described by

$$\begin{aligned} \dot{\theta} &= -1 \\ \dot{r} &= r(c-r^2) \end{aligned} \tag{2.14}$$

The equilibrium solutions must satisfy the equation $r(c-r^2) = 0$ which implies $r = 0$ and $r = \sqrt{c}$ provided $c > 0$. For $c < 0$, only the equilibrium solution $r = 0$ exists and the sign of the linear term coefficient i.e. $c < 0$ indicates that $r = 0$ is a spiral sink. But for $c > 0$, $r = 0$ solution becomes unstable (spiral source) and a new solution $r = \sqrt{c}$ emerges. The latter corresponds to a stable limit cycle whose radius grows as $\sqrt{c}$. The point $c = 0$ is weakly attracting and represents a Hopf Bifurcation point. (See Fig. 2.7).

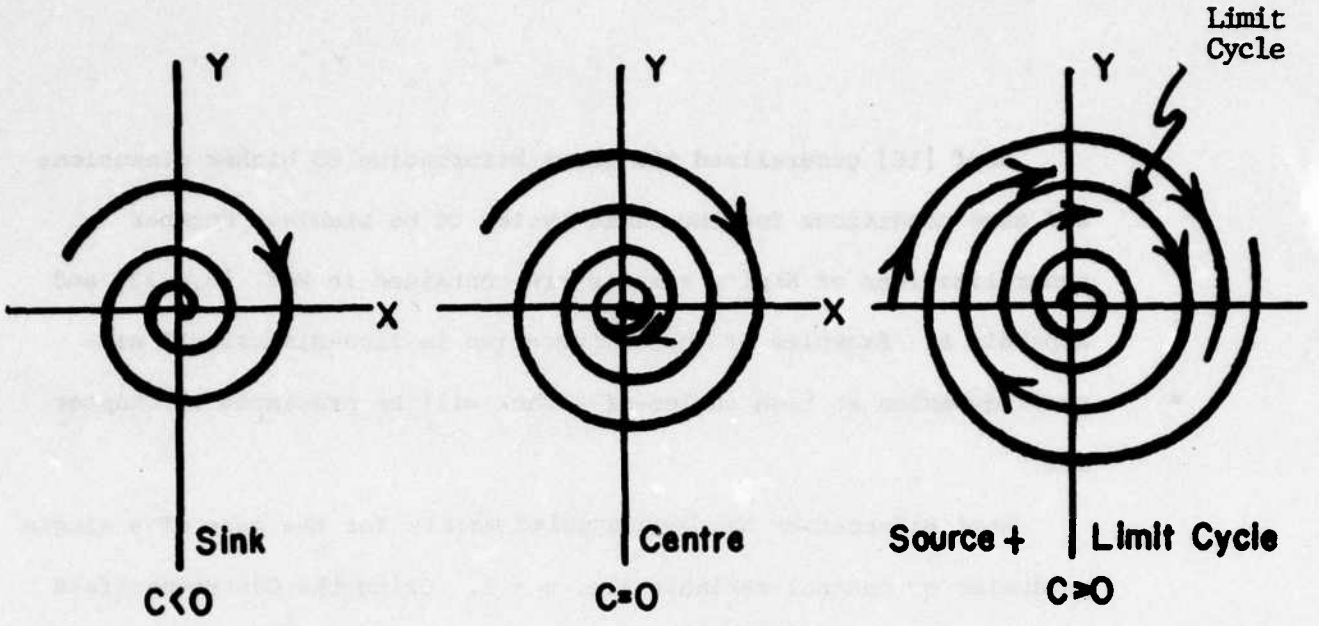

(A) Vectorfields.

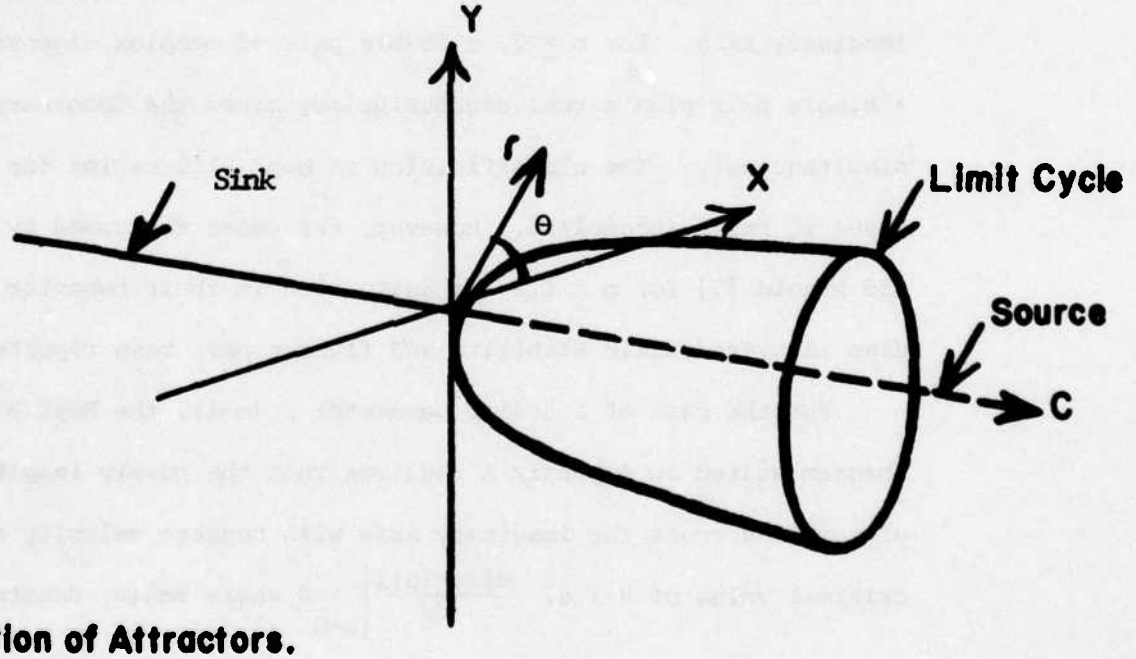

(B) Evolution of Attractors.

FIG. 2.7: The Hopf Bifurcation

Hopf [16] generalized the above bifurcation to higher dimensions and gave conditions for the limit cycles to be stable. Further generalizations of Hopf's results are contained in Ref. [5,6,23] and Appendix A. Examples of Hopf Bifurcation in five-dimensional aircraft dynamics at high angles-of-attack will be presented in Chapter III.

Hopf Bifurcation has been studied mainly for the case of a single parameter or control variable i.e. $m = 1$. Using the Centre-manifold theorem, this case can be studied in two dimensions since $k = 2$ corresponding to a single pair of complex eigenvalues crossing the imaginary axis. For $m \geq 2$, a double pair of complex eigenvalues or a single pair plus a real eigenvalue may cross the imaginary axis simultaneously. The classification of Hopf Bifurcation for these cases is still incomplete. However, the cases discussed by Taken [23] and Arnold [7] for $m = 1,2$ are quite rich in their behavior and their uses in Hydrodynamic Stability and flutter have been reported [7,24].

For the case of a scalar parameter μ ($m=1$), the Hopf Bifurcation theorem stated in Appendix A requires that the purely imaginary eigenvalues cross the imaginary axis with nonzero velocity at the critical value of μ i.e. $\left.\frac{d[Re\lambda(\mu)]}{d\mu}\right|_{\mu=0} > 0$ where $Re\lambda(\mu)$ denotes the real part of the eigenvalue of F which vanishes at $\mu = 0$. If this condition is not satisfied and an even derivative with respect to μ of $Re\lambda(\mu)$ is nonvanishing, then depending upon its sign, either two families of limit cycles or none may bifurcate at $\mu = 0$. If an odd derivative of $Re\lambda(\mu)$ is nonzero, then at least locally a one parameter family of limit cycles will exist.

Another requirement of the Hopf Bifurcation theorem is that the rest of the eigenvalues be in the left half plane bounded away from the imaginary axis. It turns out that for the aircraft application (Chapter III, aircraft H) this condition is satisfied for all the cases of interest since one is mainly interested in those situations where stability is lost for the first time.

(2.3.4) Global Implicit Function Theorem

It may be seen from the discussion so far that an important problem in the application of Bifuraction Analysis and Catastrophe Theory is the solution of a set of nonlinear algebraic equations for different values of a parameter or control vector c. In particular, the bifurcation and catastrophe behavior is intimately connected with the fact that these equations have multiple solutions which bifurcate from each other or coalesce as the vector c is varied over its admissible domain. It is also of interest to determine the conditions under which a set of nonlinear algebraic equations has a unique solution since this implies the lack of catastrophic or jump behavior.

The global implicit function theorem of Palais [17] has been used extensively in establishing the uniqueness of equilibrium solutions in nonlinear networks [25]. Consider the equation

$$f(x,c) = 0 \tag{2.17}$$

Palais' theorem (or its generalization by Kuh and Hajj [26]) states two conditions for uniqueness of solutions viz. (i) non-vanishing of the determinant of $F = \partial f/\partial x$ for all (x,c), and (ii) "growth conditions".

$$||f(x,c)|| \to \infty \text{ as } ||x|| \to \infty \tag{2.18}$$

The importance of the first condition is clear from the discussion in Sections 2.3.1 and 2.3.2 for systems with real eigenvalues of F since the first condition implies precisely the absence of bifurcations. In Chapter 3, we will use this theorem and certain special cases of it to study the effect of feedback control on bifurcation surfaces. In particular, if one is interested in control laws that change the structure of a nonlinear system from bifurcational to nonbifurcational, then the importance of the global implicit function theorems is obvious. Notice, however, that the case of complex eigenvalues leading to Hopf Bifurcations needs further study since in this case the determinant of F does not vanish.

(2.4) A Unified Methodology for Applications

Based on the above four theorems, a fairly complete methodology has been developed for studying the global stability and control characteristics of nonlinear systems. This methodology complements and extends previous approaches to nonlinear system stability analysis such as Liapunov methods and two-dimensional phase plane methods. We describe this methodology here in some detail since it is different from other applications of Catastrophe Theory reported in the literature. Fig. (2.8) shows the four basic steps involved in BACTM which are discussed below.

(2.4.1) Problem Formulation

In this step, the variables of interest in the system are divided into state variables x and control variables c (this may include parameters). The qualitative difference between the two types of variables is that the former are fast-varying and the latter

FIG. 2.8: Steps in BACTM (Bifurcation Analysis and Catastrophe Theory Methodology)

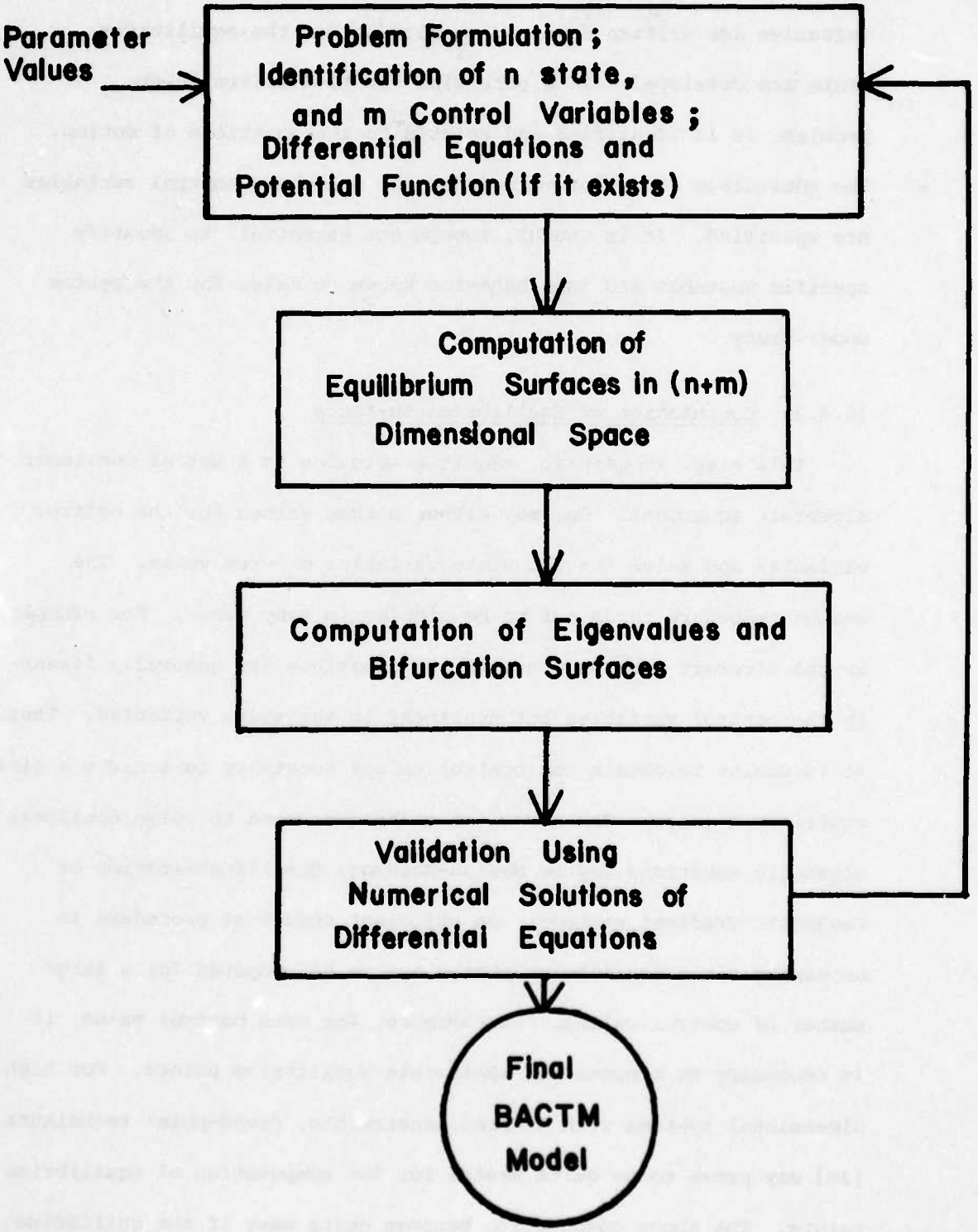

are slow-varying. Next, the equations of motion for the state variables are written down and conditions for the equilibrium state are developed. If a potential function exists in the problem, it is identified and related to the equations of motion. The admissible ranges of values for the state and control variables are specified. It is useful, though not essential, to identify specific unstable and jump behavior known to exist for the system under study.

(2.4.2) Computation of Equilibrium Surfaces

This step, in general, requires solution to a set of nonlinear algebraic equations. One may either assume values for the control variables and solve for the state variables or vice versa. The second procedure turns out to be simpler in many cases. For example, in the aircraft case, the equilibrium equations are generally linear in the control variables but nonlinear in the state variables. Thus, it is easier to obtain the control values necessary to achieve a given equilibrium state. The numerical techniques used to solve nonlinear algebraic equations may be Newton-Raphson, Quasilinearization or Conjugate Gradient methods. An efficient numerical procedure is necessary since equilibrium states are to be computed for a large number of control values. Furthermore, for each control value, it is necessary to compute all admissible equilibrium points. For high dimensional systems with several constraints, fixed-point techniques [36] may prove to be quite useful for the computation of equilibrium points. The above computation becomes quite easy if the quilibrium

equations can be reduced to a single nonlinear equation as will be demonstrated in the aircraft B case considered in Section 3*. In addition, if this equation is a polynomial equation, then the reduction to one of the canonical models of Catastrophe Theory is possible. Since the global behavior of these canonical models is well-understood, the equilibrium surfaces and the bifurcation surfaces are obtained easily. In the more general case, it is possible to employ Quasilinearization techniques to generate all the branches of equilibrium solutions by varying one parameter at a time.

(2.4.3) Computation of Bifurcation Surface

The surface in the control parameter space of singular equilibrium points at which the eigenvalues of the linearized system cross the imaginary axis are called Bifurcation Surfaces. At these surfaces, equilibrium solutions branch out and either new equilibrium points or periodic orbits (limit cycles) are born or are destroyed. Therefore, Bifurcation Surfaces represent jump surfaces at which the system may jump from one equilibrium state to another. In systems obeying the Delay rule [1], the jumps occur only when the current stable equilibrium state disappears by collision with an unstable equilibrium state.

The analytical calculation of the bifurcation surfaces is possible only in simple cases. Therefore, efficient numerical techniques have to be devised to solve the set of nonlinear algebraic equations representing the Bifurcation surfaces. Thom's classification theorem of

*The justification for this reduction is provided by the Centre Manifold Theorem (Section 2.3.1) since for aircraft B only a single real eigenvalue crosses the origin under all admissible control variations.

Catastrophe Theory [1] and Taken's classification theorem on Hopf Bifurcations [41] can be used to describe the qualitative behavior of the bifurcation surfaces near the singular equilibrium points. On the other hand, if the bifurcation surfaces are obtained numerically or experimentally, then the classification theorems can be used for validation of the results.

The location of singular equilibrium points can be done simultaneously with the computation of the equilibrium surface if a Newton-type algorithm or Quasilinearization is used. The extra work involved is a calculation of the eigenvalues of the jacobian matrix or a check for the location of eigenvalues on the imaginary axis. In fact, starting from one branch of equilibrium points, one may generate other branches by proper calculation at the singular equilibrium points. The bifuraction to limit cycles, however, would require special calculations such as converting the equilibrium equations to polar coordinates or the construction of Poincare maps [5].

(2.4.4) Use of Bifurcation and Equilibrium Surfaces

An amazing amount of dynamical information is compressed in the bifurcation and equilibrium surfaces. The jump phenomena, hysteresis effects, divergence properties, limit cycles and domains of attraction can all be inferred from these diagrams. It is also possible to devise control laws that will move the system from one equilibrium state to another minimizing a certain cost function. The design of control inputs to identify the model structure can also be based on the above

information. The chief characteristic of these surfaces is that they contain global information regarding the system. It may seem that for high dimensional systems, an excessive amount of computation is required to obtain these surfaces. On the other hand, the computations involved are much less than the numerical solution of the equations of motion for a large number of control histories. The latter approach is routinely used on most practical systems, but can miss many significant phenomena since the number of cases to be considered is extremely large. The case of aircraft dynamics at high angles-of-attack is a good example of this situation.

(2.5) Relationship to Other Methods for Nonlinear System Analysis

BACTM may be thought of as an extension of the classical phase plane method from two to higher dimensions with special emphasis on topological properties of equilibrium and bifurcation surfaces. Two of the other common methods for nonlinear system analysis are (i) Liapunov methods and (ii) Describing function methods [44]. Liapunov methods (first, second and extensions by Lure, Popov and others [42]), are useful for determining whether a given equilibrium point or trajectory is stable in the sense of Liapunov Stability. The main difficulty in the use of these methods lies in the construction of Liapunov Functions. Takahashi et al. [43] state that the difficulty of finding Liapunov functions is of the same order as that of finding analytical solutions to differential equations. Even if a suitable Liapunov function can be found, its use in computing the domain of attraction and in control system synthesis may be very limited. BACTM,

on the other hand, does not suffer from any of these deficiencies since its use can be reduced to straightforward computational steps. In a sense BACTM is more general, since Liapunov theorems and extensions can be used as part of BACTM to analyze the stability of equilibrium points. In fact, the First Method of Liapunov is used during step 2.4.4 and in those cases where only a single real eigenvalue crosses the imaginary axis (e.g. aircraft B, Chapter III), the use of BACTM leads to a potential function which can be used to construct a suitable Liapunov function.

The describing function techniques [44] are inherently limited due to assumptions of harmonic inputs and specific nonlinearities. They cannot be expected to provide the global type of topological information which is necessary for a complete understanding of the aircraft nonlinear phenomena at high angles-of-attack.

(2.6) Applications of BACTM

As described earlier, BACTM leads directly to an understanding of the global stability behavior of nonlinear systems as control and system parameters are varied globally. Two other applications of BACTM are (i) input design and model structure determination for nonlinear systems and (ii) nonlinear control system design. These are discussed below.

(2.6.1) Nonlinear System Identification

The identification of nonlinear systems of unknown structure is of great practical importance, but woefully little has been done in this field. In Section 2.3, we discussed four different theorems,

all of which have implications for nonlinear system identification. The center manifold theorem allows us to reduce the dimensionality of the system and provides guidelines for deciding whether a nonlinear model is required and of what dimension. For example, suppose the unknown system is perturbed around an equilibrium point and its linearized dynamics is identified using standard identification techniques [33]. If the identified eigenvalues and their standard deviations indicate that all the eigenvalues are far removed from the imaginary axis, then the identified linearized model can be regarded as satisfactory. On the other hand, if the 95% confidence limits around the identified eigenvalues enclose the imaginary axis, then a need for the addition of nonlinearities is indicated. (If the confidence limits are too wide, one may repeat the experiment and collect further data to narrow the confidence limits). The eigenspace corresponding to the eigenvalues that are most likely to cross the imaginary axis would exhibit the "essential" nonlinearity.

(2.6.2) Nonlinear Control System Design

A standard requirement in control system design is to place the poles of the system in the left half plane. It is clear from the theorems of Section 2.3 that, if a control law achieves this requirement for a nonlinear system at all points in the state and control space, and the "growth condition" is satisfied, then the close-loop would be bifurcation-free. This powerful result which follows almost trivially from the above theorems is not widely appreciated in the control literature. It may, however, account for the success of linearized techniques that are commonly used in control system design.

A more difficult problem to solve is to design controllers that do not allow the eigenvalues of the linearized system to cross the imaginary axis. The problem is solved easily for the generic models (2.7)-(2.13) since the behavior of these models is well-understood. For example, in the cusp model Eq. (2.8), negative feedback on c_2 viz. $c_2 = (-k_1 x + k_o)$ has the effect of changing c_1 to $(c_1 + k_1)$. If c_1 is negative, then by choosing $k_1 > c_1$ the bifurcations are eliminated. The same effect can be achieved for the "Butterfly" case, Eq. (2.10), by choosing $c_4 = -(k_1 x + k_2 x^2 + k_3 x^4 + k_o)$ and choosing the gains (k_1, k_2, k_3) in such a way that the case shown at the top of Fig. 2.9 (unique equilibrium point) is achieved. For more general models, the control parameters $(c_1 \ldots c_4)$ are nonlinear functions of the physical control variables. In such cases, a feedback law on a physical control has the effect of changing more than one control parameter in the generic models. The design of bifurcation-free control laws is more complicated in these cases. However, we do have a clear cut methodology to proceed and to study the effect of different control laws on the bifurcation behavior of the system.

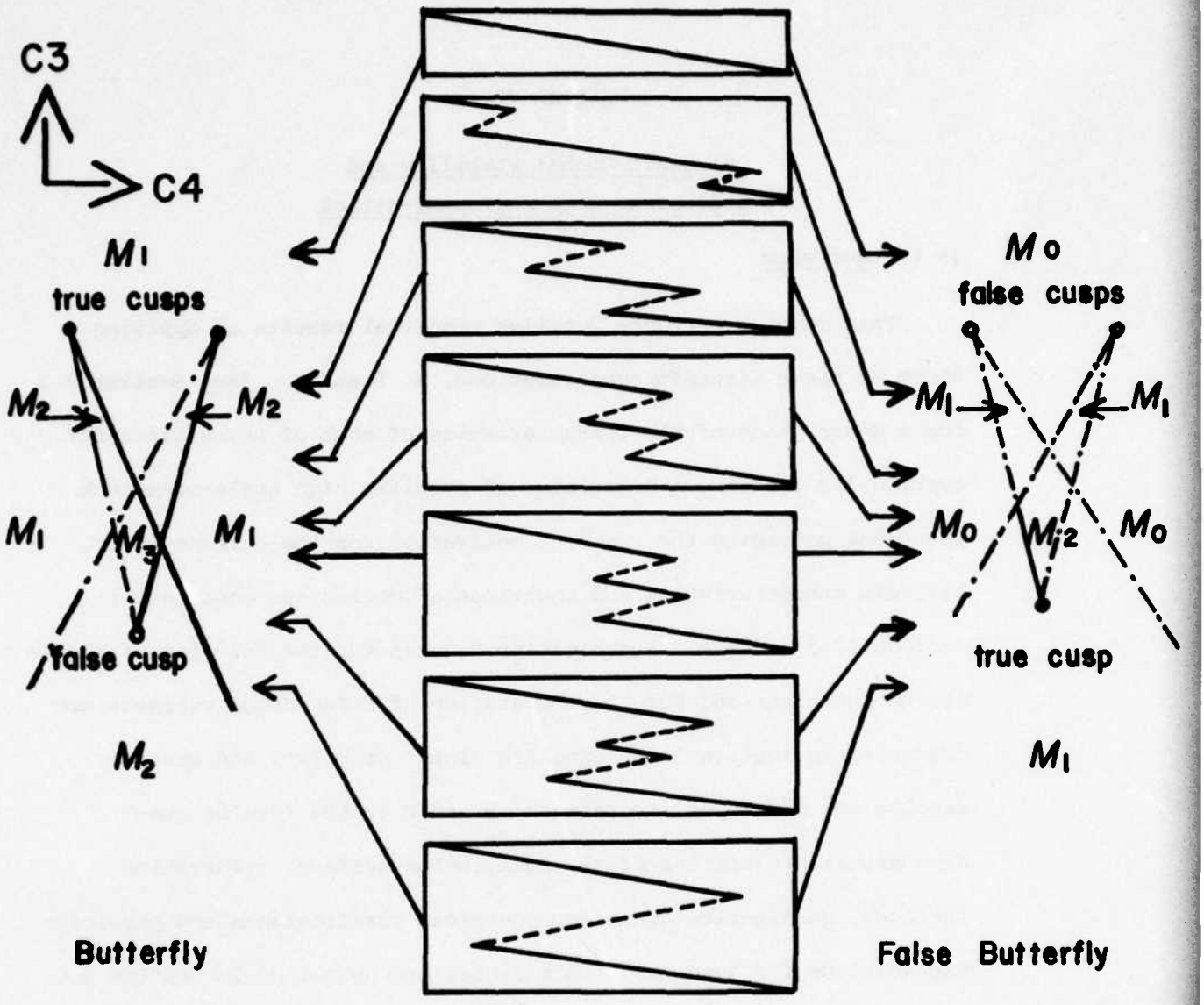

FIG 2.9: The butterfly and false butterfly: partitions of the control manifold in the "butterfly" cross sections ($c_1 < 0$). The vignettes show the schematic cross sections of the behavior set Σ at various stations (for the butterfly, the solid lines represent stable, observable behavior, and the dotted lines represent unstable, unobservable behaviour, and vice versa for the false butterfly).

CHAPTER III

Aircraft Global Stability and Control at High-Angles-of-Attack

(3.1) Overview

This chapter presents detailed numerical results of applying BACTM to three aircraft configurations, A, B and H. (See Section 3.3 for a description of the characteristics of each of these aircraft). Section 3.2 contains a discussion of specific high angle-of-attack phenomena providing the main motivation for the current study. Aircraft characteristics and equations of motion are contained in Sections 3.3 and 3.4. Numerical procedures for the solution of equilibrium equations and for the computation of bifurcation surfaces are discussed in Section 3.5. Specific global stability and control results for models of aircrafts A, B and H in the form of two-dimensional projections of the equilibrium surface, bifurcation surfaces, qualitative dynamics, numerical verifications and physical explanations for jumps and limit cycles are contained in Section 3.6. (This section contains the major numerical results of the current study). Certain control and stability augmentation aspects of the model for aircraft B are discussed in Section 3.7. Figure 3.1 defines and shows the various forces, moments, angular velocities and angular position for an aircraft.

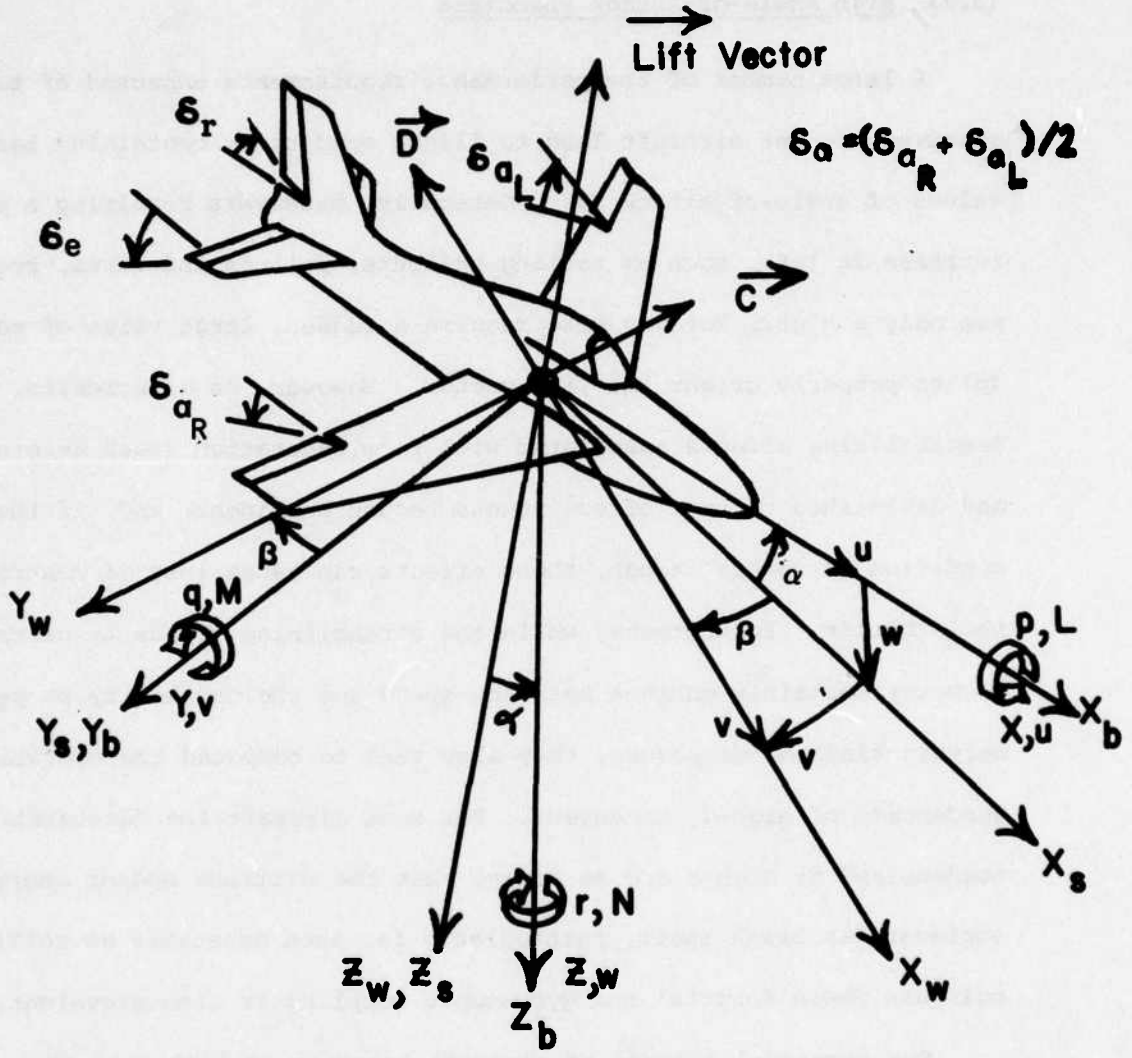

FIG. 3.1: Body system of axes.
Arrows indicate positive direction of quantities.

(3.2) High Angle-of-Attack Phenomena

A large number of the performance requirements expected of today's maneuverable jet aircraft lead to flight conditions containing large values of angle-of-attack (α). Generally, maneuvers requiring a rapid increase in lift, such as rolling pullouts, pullups and turns, require not only a high α, but may also require a sudden, large value of roll rate (p) to properly orient the lift vector. However, as α increases, many destabilizing effects associated with flow separation (such as stalling) and diminished control effectiveness become prominent; and, if the flight condition is severe enough, these effects can cause loss of control of the aircraft. Furthermore, while the streamlining trends in aircraft geometry certainly enhance both the speed and the capability to perform certain kinds of maneuvers, they also tend to compound the destabilizing tendencies of high-α maneuvers. For some aircraft the "destabilizing tendencies" at high α are so severe that the airframe and/or control surfaces can break apart, particularly for such maneuvers as rolling pullouts where inertial and gyroscopic coupling is also prevalent.

The essential feature of aircraft behavior at high α is that it is nonlinear in nature. Predominant nonlinear characteristics are jump and limit cycle phenomena. The large-disturbance nature of such motions implies, furthermore, the presence of significant coupling between the longitudinal and lateral modes. Hence, separation of modes based on small-disturbance linearized theory is no longer valid. Given a significant roll rate p and high angle-of-attack α, the coupling phenomenon produces high sideslip

angles (β) which may generate hinge moments surpassing the structural limits of the vertical tail. Whether or not structural integrity remains, quite often this condition induces jump and limit cycle behavior which leads to departure and subsequent loss of control.

Prominent features of flight in high α regimes include:

- Roll Coupling:

The roll coupling problem is an old one dating back to the introduction of jet aircraft. Phillips [4] produced his results in 1948, and the bulk of the main results, including the high angle-of-attack phenomena, were obtained in the middle fifties (see Pinsker [13] and Rhoades and Schuler [1], for example). Certain vertical tail failures were caused by maneuvers combining a simultaneous roll and pull-up (rolling pull-out). Large sideslip angles, generated by the combination of roll rate and high angle-of-attack, were responsible.

Previous work in this area, while quite often very productive, has been hampered by the lack of adequate mathematical tools for dealing with the nonlinear models which are required to simulate the high-α maneuvers. Therefore, the studies tend to be locally concentrated, so that at least quasi-linear methods are applicable. The risk is, of course, that it is thereby possible to overlook regions in the control space in which "catastrophic" phenomena occur.

For aircraft with a short wing span and having most of their weight in the fuselage, and performing rolling maneuvers, their "catastrophic" phenomena assume the form of sudden changes in the values of the dynamic, or state, variables. Such "jumps" tend to occur almost entirely without warning, with very little, if any, change in control settings. The roll coupling problem, then, does

exhibit many of the properties of those dynamic systems which may be dealt with using BACTM. Later sections of this chapter will show that BACTM is a useful tool for analyzing in a global manner the nonlinear behavior of aircraft performing high-α, rolling maneuvers.

- Low Rudder Effectiveness: This is a consequence of the vertical tail (hence, rudder) descending further into the wing's wake as α increases; it can lead to nose slice (see below). Large negative values of α also inhibit rudder control effectiveness. Result is weakening of "weathercock stability" moment (C_{n_β}).
- Reduced Dihedral Effect: Related to the reasons for reduced rudder effectiveness, in that the tail is in the wing's wake, so that its lift due to sideslip β is reduced.
- Stall: The stall angle-of-attack, α_{STALL}, is the angle of maximum usable lift at a given flight condition. Beyond this α, while there may be greater lift potential, severe longitudinal and/or lateral-directional instability will most likely arise, with ensuing loss of control.
- Wing Rock: Uncommanded lateral-directional motions, in the form of roll oscillations.
- Nose Slice: Uncommanded lateral-directional motion, in the form of yaw excursions. Also known as "directional divergence" [2].

- Departure: Aircraft motions immediately following loss of control. Many of these motions will shortly be identified as "jump phenomena".

- Post Stall Gyration: Uncontrollable motions about more than one body axis following departure, e.g., a rapid roll after initial yaw divergence ("roll departure").

- Spin: Sustained yaw rate r at angles-of-attack greater than α_{STALL}. If α is positive the condition is called "erect spin"; if negative, "inverted spin".

- Incipient Spin: In the initial stages of spin, there is often insufficient balance of the aerodynamic and inertial moments, giving rise to an incipient spin condition. When these moments are in balance, the condition is called "developed spin".

- Recovery Roll: This is roll rate occuring in the initial phase of recovery from spin or departure. As α gets smaller during recovery, the residual values of roll and yaw rates generate a "pitch up" tendency, delaying the reduction in α.

- Pre-Stall Buffeting: For α less than α_{STALL}, buffeting intensifies somewhat, and a "nose-rise" tendency develops. This buffeting typically does not provide adequate warning of an oncoming stall condition. However the BACTM presented here is able to indicate beforehand the flight condition(s) under which buffeting type of conditions will give rise to "jump" catastrophes.

Finally, typical of the phenomena less directly due to high angle-of-attack, but nonetheless amplified by it, is that of adverse aileron yaw, in which the rolling motion of the wings generates an α differential along the wing. This $\Delta\alpha$ produces an (abetting) lift differential and a drag differential which induces yawing motion in the adverse sense of the rolling motion.

Not all of the above characteristics of high α flight are hazardous. Some are merely bothersome, reducing control effectiveness, while others, such as the reduced dihedral effect, may actually aid the pilot in reestablishing solid control of his vehicle, if he has an understanding of how to utilize it.*

It will be seen later that many of these phenomena can be categorized, predicted, and, ultimately, controlled by utilizing the BACTM methodology, presented in this report.

(3.3) Aircraft Characteristics

The aircraft used in this study are identified, respectively, as aircraft A, B and H. In future work, it is hoped to apply the results of this study to an aircraft of particular interest to the Navy, such as the F-14.

In general, aircraft A and B are distinguished from aircraft H in that the latter is modelled by nonlinear aerodynamic coefficients, while aircraft A and B are modelled only with linear coefficients (see Table 2).

The data available on aircraft A allowed study of the roll-coupling problem for zero values of δe (elevator angle) and δr (rudder angle) only.

*For "pitch-down" maneuvers (see Etkin, p.153), $\delta e > 0$, negative α converts to negative β via the rolling motion. This makes the dihedral destabilizing, so that reduction of the dihedral effect is desirable.

TABLE 2: CHARACTERISTICS OF EXAMPLE AIRPLANES

	A/C A (Haddad [3])	A/C B (Etkin [5], p.447)
m, slugs	745	186.3
I_x, slug - ft^2	10976	1700
I_y, slug - ft^2	57100	12400
I_z, slug - ft^2	64975	13600
C_{y_β}, per radian	-0.28	-0.081
C_{y_r}, per radian	0.34	0.
C_{y_p}, per radian	0.15	0.
C_{L_α}, per radian	3.85	4.35
C_{m_α}, per radian	-0.36	-0.435
C_{m_q}, per radian	-3.5	-9.73
$C_{m_{\dot\alpha}}$, per radian	-1.25	-2.1
C_{n_β}, per radian	0.057	0.0218
C_{n_r}, per radian	-0.095	-0.0424
C_{n_p}, per radian	-0.034	0.
C_{ℓ_p}, per radian	-0.255	-0.442
C_{ℓ_r}, per radian	0.09	0.0309
C_{ℓ_β}, per radian	0.06	-0.081
$C_{\ell_{\delta a}}$, per radian	-0.044	-0.24
$C_{\ell_{\delta e}}$, per radian	0.	0.
$C_{\ell_{\delta r}}$, per radian	0.	0.
$C_{m_{\delta e}}$, per radian	0.	-1.07
$C_{n_{\delta e}}$, per radian	0.	0.
$C_{n_{\delta r}}$, per radian	0.	0.
$\bar{q}$, lb/ft^2	197	297.3

V, ft/sec	691	500
s, ft^2	377	216
$\bar{c}$, ft	11.3	6.
b, ft	36.6	36.0

AIRCRAFT H (Ref. [1]). Mach = 0.9; h = 20,000 ft.

$i_1 = (I_z - I_y)/I_x$ $\quad i_2 = (I_z - I_x)/I_y$ $\quad i_3 = (I_y - I_x)/I_z$

$i_1 = .727$ $\quad i_2 = .949$ $\quad i_3 = .716$

$y_\beta = -.196$	$n_p = .002$
$y_{\delta a} = -.0071$	$n_{p\alpha} = -1.578$
$y_{\delta r} = 0.$	$n_{\delta a} = -.921$
$z_\alpha = -1.$	$n_{\delta r} = -6.51$
$z_{\delta e} = -.168$	$\ell_\beta = -9.99$
$\overline{m_\alpha} = -22.95$	$\ell_{\alpha\delta a} = 63.5$
$\overline{m_q} = -.987$	$\ell_q = .107$
$m_{\delta e} = -28.37$	$\ell_r = .126$
$m_{\dot{\alpha}} = -.173$	$\ell_p = -3.933$
$m_\alpha = -23.18$	$\ell_{\beta\alpha} = -684.4$
$m_q = -.814$	$\ell_{r\alpha} = 8.39$
$n_\beta = 5.67$	$\ell_{\delta a} = -45.83$
$n_{\alpha\delta a} = 1.132$	$\ell_{\delta r} = -7.64$
$n_r = -.235$	$z_q = -.006$

Control derivatives with respect to both δa (aileron angle) and δe were available for aircraft B and this allowed a study of the roll coupling, autorotation and divergence problems. Aircraft H, taken from Rhoades and Schuler [1] and Hacker and Oprisiu [6] contains significant nonlinearities in the aerodynamic model, and also gyroscopic effects due to engine rotation (ℓ_q, m_p, m_r and m_q). Note that "normalized" aero coefficients, such as ℓ_β, which are used by Hacker and Oprisiu, relate to the more conventional, "dimensionless" coefficients, say C_{ℓ_β}, via the factors $F_1 = \bar{q}\, S / I_x$ for coefficients C_{ℓ_β}, $C_{\ell_{\delta a}}$; or $F_2 = F_1(b/(2V))$, for coefficients such as C_{ℓ_p} and C_{ℓ_r}. Phenomena such as bifurcations to limit cycles were predicted and verified for aircraft H. Aircraft A, taken from Haddad [3] , is an F100A. Aircraft B is a small jet airplane taken from Etkin [5]. It has been used extensively in the literature (see Schy and Hannah [7]) and has been exhaustively studied here, along with aircraft H. The bifurcational properties of aircraft H are studied here for the first time. The aircraft A and B are chosen for analysis here because of the amount of study they have already been subject to, with regard to roll-coupling and similar phenomena. Therefore, it is meaningful to compare the results presented in this report with earlier work. With regard to aircraft H, the above is true, as well as the fact that it is a more comprehensive model - i.e., more non-linear coupling terms are present, with values for the coefficients of these terms specified at the appropriate flight conditions. These extra terms for aircraft H also introduce limit cycle phenomena which are known to exist in modern fighter aircrafts. For aircraft A and B nonlinear aerodynamic data was not available to permit similar analysis.

The algorithms used have been kept general so that the effect of additional nonlinearities is easily studied. In this report, only the effect of varying the physical controls ($\delta e, \delta a, \delta r$) is studied, but the same approach

can be used for studying the effects of aerodynamic and other aircraft parameter variations on the stability properties of the aircraft.

(3.4) Equations of Motion

The most general set of equations of motion used in this study is for aircraft H. The equations for aircraft A and B can be derived by setting some of the parameters in the aircraft H model to zero. Notation and terminology used here is taken from Hacker and Oprisiu [6] and is given in Appendix C. The complete system, then, is

$$\dot{p} = \ell_\beta \beta + \ell_{\alpha\delta a} \Delta\alpha\delta a + \ell_q q + \ell_r r + \ell_{\beta\alpha} \beta\Delta\alpha + \ell_{r\alpha} r\Delta\alpha + \ell_p p - i_1 qr + \ell_{\delta a} \delta a + \ell_{\delta r} \delta r \tag{3.1}$$

$$\dot{q} = \bar{m}_\alpha \Delta\alpha + \bar{m}_q q + i_2 pr + m_{\delta e} \delta e - m_{\dot{\alpha}} p\beta \tag{3.2}$$

$$\dot{r} = n_\beta \beta + n_{\alpha\delta a} \Delta\alpha\delta a + n_r r + n_p p + n_{p\alpha} p\Delta\alpha - i_3 pq + n_{\delta\alpha} \delta a + n_{\delta r} \delta r \tag{3.3}$$

$$\dot{\alpha} \simeq q - p\beta + z_\alpha \Delta\alpha + z_{\delta e} \delta e + (g/V)(\cos\theta \cos\phi - \cos\theta_o) \tag{3.4}$$

$$\dot{\beta} = y_\beta \beta + p(\sin\alpha_o + \Delta\alpha) - r\cos\alpha_o + y_{\delta a} \delta a + y_{\delta r} \delta r + (g/V)\cos\theta \sin\phi \tag{3.5}$$

$$\dot{\phi} = p + q \tan\theta \sin\phi + r \tan\theta \cos\phi \tag{3.6}$$

$$\dot{\theta} = q \cos\phi - r \sin\phi \tag{3.7}$$

In eqs. (3.1) to (3.7) the air density, speed and aerodynamic coefficients are assumed to be constant. These equations also include the usual assumptions that $\Delta\alpha$ and δe are measured from trim settings for steady, straight flight, and that $u \approx V$, $\alpha = \alpha_o + \Delta\alpha \approx w/V$, and $\beta \approx v/V$. Note, however, that the complete rotational coupling and gravity terms such as $n_{p\alpha}, \ell_{\beta\alpha}$, etc., introduce coupling terms into the equations. While

such terms are nonlinear in the variables, the coefficients are assumed to be constant over the flight regimes of interest. It is also noted that the aircraft principal axes have been used here for convenience (one benefit being that inertia products vanish), as opposed to the stability axes. The latter are defined as the set of wind axes at a certain steady-flight reference condition, most commonly with sideslip angle $\beta = 0$. Stability axes are generally the reference axes in which the aerodynamic coefficients (stability derivatives) are derived, using wind tunnel data; however, transformations to body principal axes of these coefficients are straightforward.

The complete set of equations includes the x-axis force equation and the kinematic equation for yaw angle, ψ. However, under the assumption of constant speed, and noting that ψ is not an element in any of the other equations save its own kinematic equation, the full system reduces to the system of seven equations presented here, which hereafter shall be called "complete". In order to successfully explore the high angle-of-attack phenomena described in Section 3.2, it is not possible to introduce the usual set of assumptions about the aircraft dynamics which lead to a decoupling of the above equations into a longitudinal and lateral set, each of which may be separately analyzed. However, it is often profitable to neglect the gravity terms, as is done in the derivation of the equilibrium surfaces and in the examination of "jump" phenomena, which are not seen to depend appreciably on gravity effects. When this is done, the kinematic equations for roll (ϕ) and pitch (θ) decouple from the five force/moment equations for the states (p,w,r,α,β), leaving five differential equations,

$$\dot{p} = \ell_\beta \beta + \ell_{\alpha\delta a} \Delta\alpha\delta a + \ell_q q + \ell_r r + \ell_{\beta\alpha} \beta\Delta\alpha + \ell_p p - i_1 qr + \ell_{\delta a} \delta a + \ell_{\delta r} \delta r \tag{3.8}$$

$$\dot{q} = \bar{m}_\alpha \Delta\alpha + \bar{m}_q q + i_2 pr + m_{\delta e} \delta e - m_{\dot{\alpha}} p\beta \tag{3.9}$$

$$\dot{r} = n_\beta \beta + n_{\alpha\delta a} \Delta\alpha \delta a + n_r r + n_p p + n_{p\alpha} p \Delta\alpha - i_3 pq + n_{\delta a} \delta a + n_{\delta r} \delta r \tag{3.10}$$

$$\dot{\alpha} = q - p\beta + z_\alpha \Delta\alpha + z_{\delta e} \delta e \tag{3.11}$$

$$\dot{\beta} = y_\beta \beta + p(\sin \alpha_o + \Delta\alpha) - r \cos \alpha_o + y_{\delta a} \delta a + y_{\delta r} \delta r \tag{3.12}$$

The neglected weight effects have an important influence on peak responses, so that if high accuracy is desired, the complete set should be used in generating time histories (Schy and Hannah [7]). The qualitative properties of the solution may, however, be studied from Eqs. (3.8) to (3.12). For either set, the following notation is used:

$$\bar{m}_\alpha = m_\alpha + m_{\dot{\alpha}} z_\alpha \tag{3.13}$$

$$\bar{m}_q = m_q + m_{\dot{\alpha}} \tag{3.14}$$

$$i_1 = (I_z - I_y)/I_x \tag{3.15}$$

$$i_2 = (I_z - I_x) I_y \tag{3.16}$$

$$i_3 = (I_y - I_x)/I_z \tag{3.17}$$

Also $y = Y(g/WV)$, $z = Z(g/WV)$, $\ell = L/I_x$, $m = M/I_y$, $n = N/I_z$. Dotted symbols denote time derivatives. The aerodynamic forces are y and z, and the aerodynamic moments are ℓ, m, and n. The notation ℓ_β, say, is standard for the expression $\frac{\partial \ell}{\partial \beta}$, and implies a linearization of the contribution of sideslip to roll rate. Such linearization, unfortunately, is necessary due to limited data. Finally, the state vector is

$(p,q,r,\alpha,\beta,\theta,\phi)$ or (p,q,r,α,β), depending on the set used, and the control vector is $(\delta e,\delta a,\delta r)$, representing angular deflection commands for elevator, aileron, and rudder, respectively.

(3.5) Solution Procedures

In the actual implementation of the BACTM method (see Fig. 2.8) computer programs were developed which perform four basic tasks: 1) evaluationg the equilibrium solutions for the equations of motion (Section 3.4); 2) determining the stability of an aircraft at these equilibrium solutions; 3) computing the bifurcation surface (control values at which a stable equilibrium solution bifurcates from an unstable one); and 4) numerical integration of the equations of motion with respect to time, for specified control inputs. The last program produces a calculated time history of the behavior of an aircraft, and is used as a verification of the correctness of the results obtained from the first three steps. The BACTM method, programmed as described above, has been applied to the three aircraft (A, B and H) described in Section 3.3. See Table 2 for their physical characteristics. The programs use the most general set of equations of motion [Section 3.4 Eqs. (3.1-3.7)] for all the aircraft, typically by setting some of the parameters to zero. In this manner, while doing the time history solutions, the influence of force or moment terms of interest may be studied, e.g., the effect of gravity on the motions.

In finding the equilibrium or steady-state solutions for the aircraft under study, gravity was ignored (see Section 3.6.1.6 and 3.6.2.6 for a discussion of the consequences of such an assumption), and $\dot{p}$, $\dot{q}$, $\dot{r}$, $\dot{\alpha}$, and $\dot{\beta}$ were set to zero in Eq. (3.1)-(3.5). The last four of the resulting five equations were solved for $\bar{\alpha}$, $\bar{\alpha}$, $\bar{q}$, and $\bar{r}$ respectively* and the expressions obtained were substituted into

*A bar over a variable denotes its equilibrium value.

Eq. (3.1), giving rise to an 11th degree polynomial in equilibrium roll rate, $\bar{p}$, with an additional $\bar{p}^{-1}$ term. The resulting equation has the following form:

$$f_1(\bar{p},\delta e,\delta r)\delta a^4 + f_2(\bar{p},\delta e,\delta r)\delta a^3 + f_3(\bar{p},\delta e,\delta r)\delta a^2 + f_4(\bar{p},\delta e,\delta r)\delta a + f_5(\bar{p},\delta e,\delta r) = 0. \tag{3.18}$$

Eq. (3.18) is a 4th degree polynomial in δa. Solutions to this equation may be studied by fixing δe and δr, and solving δa for a wide range of values of $\bar{p}$. See Appendix B for definitions of the f_i.

Since the coefficient of the δa^4 term is very small for the aircraft considered, a simple cubic equation was solved using Newton's method.* In solving Eq. (3.3) for $\bar{\alpha}$, it was found that the resulting expression has a denominator which is a function of δa and $\bar{p}$. Thus

$$\bar{\alpha} = \frac{N(\delta a,\delta e,\delta r,\bar{p})}{D(\bar{p},\delta a,\delta e,\delta r)} . \tag{3.19}$$

No solution will exist at any point where D is equal to zero. Such points do occur for some values of parameters for aircraft H and correspond to more than one eigenvalue crossing the imaginary axis simultaneously. The study of these singular points would involve umbilics or the Hopf bifurcation.

When the model for aircraft B is considered (see Etkin [5] and also Schy and Hannah [9]), the equations are simplified a great deal since all the nonlinear aerodynamic terms are neglected. Eq. (3.18) becomes linear in $(\delta a,\delta e,\delta r)$ and the bifurcation surfaces are obtained by solving two

*Neglecting the $-i_1\overline{qr}$ term in Eq. (3.8) results in a cubic equation. On the other hand, neglecting $n_{\alpha\delta a}$ yields a quadratic equation in δa.

linear equations, viz (see Schy [9] for details):

$$f_4(\bar{p},\delta e,\delta r)\ \delta a + f_5(\bar{p},\delta e,\delta r) = 0 \tag{3.20}$$

$$\frac{\partial f_4}{\partial \bar{p}}\ \delta a + \frac{\partial f_5}{\partial \bar{p}} = 0 \tag{3.21}$$

It is further observed that Eq. (3.20) is a fifth-degree polynomial in p so that the most general catastrophe that can be observed is of "butterfly" type. See Section 2.3.2 and in particualr, Eq. (2.10). This fact is verified by solving Eq. (3.2) and (3.21) parametrically in p (see Section 3.6.1.3). An eigenvalue analysis around each equilibrium point shows that no stable autonomous limit cycles exist in this case.

The above method for determining the equilibrium surfaces often encountered difficulties in that for some values of the controls and flight condition the derivation was invalid, and care had to be taken to recognize these conditions. Further, for each specific application of the program to a different set of equations, the program had to be rewritten, after a long and tedious algebraic effort. As a result it was decided to solve the set of nonlinear equations numerically for one set of control values and continue the solution for the other set of control values in terms of a differential equation that uses the length of the arc along a solution path as the independent variable. The details of this technique will be provided in a forthcoming report.

The linearized stability analysis was used to determine the stability of a given equilibrium solution. If the equations of motion are written as,

$$\begin{aligned}
\dot{p} &= f_p(p,q,r,\alpha,\beta,\ \delta a,\delta e,\delta r)\\
\dot{q} &= f_q(p,q,r,\alpha,\beta,\ \delta a,\delta e,\delta r)\\
&\vdots\\
\dot{\beta} &= f_\beta(p,q,r,\alpha,\beta,\ \delta a,\delta e,\delta r)
\end{aligned} \tag{3.22}$$

then the linearized system matrix F is defined as,

$$F = \begin{bmatrix} \frac{\partial f_p}{\partial p} & \frac{\partial f_p}{\partial q} & \frac{\partial f_p}{\partial r} & \frac{\partial f_p}{\partial \alpha} & \frac{\partial f_p}{\partial \beta} \\ \frac{\partial f_q}{\partial p} & \cdots & & & \frac{\partial f_q}{\partial \beta} \\ \vdots & & & & \\ \frac{\partial f_\beta}{\partial p} & \cdots & & & \frac{\partial f_\beta}{\partial \rho} \end{bmatrix} \qquad (3.23)$$

where the partials are evaluated at a given equilibrium, or trim, setting $\bar{x} = (\bar{p}, \bar{q}, \bar{r}, \bar{\alpha}, \bar{\beta})$. If the real parts of all eigenvalues of F are negative, the equilibrium is stable and is indicated by an "S" on the equilibrium plots. A real eigenvalue which is positive indicates an unstable equilibrium solution and is denoted on plots as "U". Finally, complex eigenvalues with a positive real component indicate an unstable focus with a possibility of a surrounding limit cycle, indicated by "L". It should be noted that since each equilibrium solution has five corresponding eigenvalues it is possible to have a combination of the above conditions, leading to points denoted by "UL", "UUU", etc.

Of particular importance is the condition arising when a change of control input causes an eigenvalue to change from a negative real part (stable) to a positive real part (unstable). The set of control values at which such a change occurs (i.e. at least one eigenvalue equals zero) constitute the bifurcation surface. This surface is determined by solving the following set of six equations obtained from Eqs. (3.1)-(3.5) and Eq. (3.23):

$$f_p(p,q,r,\alpha,\beta,\delta a,\delta e,\delta r) = 0$$

$$f_q(p,q,r,\alpha,\beta,\delta a,\delta e,\delta r) = 0$$

$$f_r(p,q,r,\alpha,\beta,\delta a,\delta e,\delta r) = 0$$

$$f_\alpha(p,q,r,\alpha,\beta,\delta a,\delta e,\delta r) = 0 \qquad (3.24)$$

$$f_\beta(p,q,r,\alpha,\beta,\delta a,\delta e,\delta r) = 0$$

$$\det\left|F(p,q,r,\alpha,\beta,\delta a,\delta e,\delta r)\right| = 0$$

In the (δa,δe) plane, (δr fixed), this means solving a set of six equations in seven unknowns, producing a one dimensional surface.

Finally, the most straightforward task is to numerically integrate the equations of motion to produce time histories. This is accomplished using a fourth order Runge-Kutta integration routine. The program is written to integrate either the set of five equations of motion (gravity neglected) or the complete set of seven equations with gravity included. The presence of gravity couples Eq. (3.6) and (3.7) into the Eq. (3.1) to (3.5).

(3.6) Discussion of Results

This section is divided into two main subsections viz. section 3.6.1 on aircrafts A and B and section 3.6.2 on aircraft H. Each subsection is further divided into discussions of equilibrium surfaces (3.6.1.1, 3.6.2.1),

nonlinear root locus (3.6.1.2, 3.6.2.1), bifurcation surfaces (3.6.1.3, 3.6.2.2, 3.6.2.3), qualitative dynamics (3.6.1.4, 3.6.2.4), numerical verifications (3.6.1.5, 3.6.2.5) and physical explanations (3.6.1.6, 3.6.2.6). Figures 3.2 to 3.102, which pertain to Sections (3,6.1) through (3.7), appear at the end of Section (3,7),

(3.6.1) Aircrafts A and B

Figures (3.2) through (3.25) pertain to aircraft A and B. We describe them in detail below.

(3.6.1.1) Equilibrium Surface

Fig. (3.2) shows the equilibrium roll rate $\bar{p}$ plotted against the aileron angle δa for aircraft A (F100A). The other control variables ($\delta e, \delta r$) are zero. A maximum of five steady states (3 stable and 2 unstable) are possible. It is clear from the figure that once δa increases beyond $\pm 8°$ (approximately) a jump in roll rate will occur since the middle stable equilibrium branch disappears. A physical explanation for this phenomenon which is related to roll coupling will be given in section 3.6.

Aircraft B: Figs. (3.3) and (3.4) show the behavior of equilibrium roll rate with respect to δa for a pitch up elevator ($\delta e = -2°$) and a pitch down elevator ($\delta e = 2°$). A marked difference in equilibrium behavior is noticed for the two cases. For the pitch up elevator, only one stable (S) equilibrium state exists for $-20° \leq \delta a \leq 20°$ so that for all practical purposes, the aircraft is stable in pitch up except for very high values of $|\delta a| (>20°)$. For a pitch down elevator (Fig. 3.4), five equilibrium states (3 stable, 2 unstable) exist in the approximate* range $4° < \delta a < 4°$ and one stable equilibrium point exists for $|\delta a| > 9°$. As δa is increased

*The exact critical values for δa will be given in section 3.6.1.5.

from zero, the roll rate increases almost linearly until $\delta a \approx 4^\circ$ at which point a jump occurs to a value on the upper equilibrium branch. Figs. (3.5)-(3.8) show the behavior of equilibrium yaw rate $\bar{r}$, sideslip angle $\bar{\beta}$, angle-of-attack $\bar{\alpha}$, and pitch rate $\bar{q}$ versus aileron deflection, δa. At $\delta a \approx \pm 4$, similar jumps occur in other states and the direction and size of the jumps can be easily observed from the above figures. If the direction of δa is reversed, a second jump would be observed at $|\delta a| \approx 9^\circ$, resulting mainly in a reversal of the direction of roll rate. Notice that, without changing δe, it is not possible to bring the roll rate back to zero in a smooth fashion. The other possibility is to produce via some control action a large change in the initial state of the aircraft so that it lies in the domain of attraction of the inner roll rate equilibrium branch. The important point is that after a jump has occurred, the hysteresis effect due to separated domains of attraction prevents the aircraft from returning to prejump conditions unless a coordinated control action is taken or an abrupt reverse change in the aircraft state is made by some other means. These aspects of qualitative dynamics will be discussed further in sections 3.6.1.4 and 3.6.1.5.

(3.6.1.2) Nonlinear Root Locus

Figure 3.9 shows a nonlinear root locus plot obtained by varying the equilibrium roll rate from -500 deg/sec to 500 deg/sec and computing the eigenvalues of the linearized system around different equilibrium points for $\delta e = 2^\circ$. It is noticed that a real eigenvalue crosses the origin precisely at those points where bifurcations occur. Referring to the Center Manifold Theorem, it can be seen that the bifurcation behavior for this case can be studied in terms of one state variable. We have chosen the roll rate as the single variable, but it is possible to choose any other state variable in the

present case. The reduction of the bifurcation behavior to one dimension is achieved easily for aircraft A and B since their model does not contain nonlinear aerodynamic terms. As discussed in Appendix B, if the equilibrium equations are solved for $\bar{q}$, $\bar{r}$, $\bar{\alpha}$ and $\bar{\beta}$ in terms of $\bar{p}$, then the following fifth order polynomial equation in $\bar{p}$ is obtained.

$$f_1\bar{p}^5 + f_2\bar{p}^4 + f_3\bar{p}^3 + f_4\bar{p}^2 + f_5\bar{p} + f_6 = 0 \qquad (3.25)$$

where, for aircraft B,

$f_1 = -21.6$

$f_2 = -326.4\ \delta a$

$f_3 = 50.3\ \delta e + 358.9$

$f_4 = 5412.6\ \delta a$

$f_5 = 11752.8\ \delta e - 1525.9$

$f_6 = -23015\ \delta a$

Notice that f_1 is constant, (f_2, f_4, f_6) depend linearly on δa and (f_3, f_5) depend linearly on δe. We can reduce the above equation to the canonical Butterfly model of Catastrophe Theory [1] by the following change of variables:

$$b = \bar{p} - f_2/5f_1 \qquad (3.26)$$

Eq(3.26) is derived by using the fact that the only difference between Eq(3.25) and Eq(2.10) is that the coefficient of the quartic term is zero in the latter case. When the expression $\bar{p} = b + f_2/5f_1$ is substituted in Eq(3.25) and binomial series expansions are used, it is found that

the coefficients c_1, c_2, c_3 and c_4 in Eq(2.10) correspond to

$$c_1 = \frac{-3f_2^2}{5f_1^2} + \frac{3f_3^3}{2f_1} \tag{3.27}$$

$$c_2 = \frac{8f_2^3}{25f_1^3} - \frac{6f_3f_2}{5f_1^2} + \frac{2f_4}{f_1} \tag{3.28}$$

$$c_3 = \frac{-9}{125}\frac{f_2^4}{f_1^4} + \frac{9}{25}\frac{f_3f_2^3}{f_1^3} - \frac{6}{5}\frac{f_4f_2}{f_1^2} + \frac{3f_5}{f_1} \tag{3.29}$$

$$c_4 = \frac{24}{3125}\frac{f_2^5}{f_1^5} - \frac{6}{125}\frac{f_3f_2^3}{f_1^4} - \frac{6}{5}\frac{f_5f_2}{f_1^2} + \frac{6f_6}{f_1} \tag{3.30}$$

The canonical model has the form:

$$\dot{b} = 6b^5 + 4c_1b^3 + 3c_2b^2 + 2c_3b + c_4 \tag{3.31}$$

(3.6.1.3) Bifurcation Surface

The bifurcation plot for Eq. (3.31) is well-known "Butterfly" which was shown in Fig. 2.9 using c_3 and c_4 as the control variables. The bifurcation plot and the three-dimensional Catastrophe diagram for aircraft B using (δa,δe) as the control variables is shown in Figs. 3.10 and 3.11. Notice the interesting fact that if $\delta a = 0$ and δe is increased from 0 to 12°, one crosses point C corresponding to $\delta e = 9.3°$ at which the equilibrium state ($\delta a = 0$, $\delta r = 0$, $\bar{p} = 0$, $\bar{r} = 0$, $\bar{\beta} = 0$) becomes unstable. This is also shown in Fig. 3.12 which should be compared with Figs. 3.3 and 3.4 for $\delta e = \pm 2°$. It is clear from Figs. 3.11 and 3.12 that autorotation and departure would occur at this value of δe. Fig. 3.12 shows that, at $\delta e = 12°$, the central branch has become an unstable one, while it is seen to be stable in Figs. 3.3 and 3.4, where $\delta e = \pm 2°$. An analytical criterion has been developed for the determination of critical

δe at which autorotation would occur and is given in Appendix B (section B.2).

Figure 3.13 shows the behavior of equilibrium roll rate with respect to δe for $\delta a = 0°$. The presence of a bifurcation point at $\delta e = 9.3°$ is demonstrated beautifully, with two solutions branching off in opposite directions. Notice that locally in the neighborhood of $(\dot{\overline{p}} = 0, \delta e = 9.3°)$, there are either 3 or 1 equilibrium solutions, but globally there are either 5 or 3 equilibrium solutions. A local bifurcation analysis would simply indicate a loss of stability at $\delta e = 9.3°$, but the global analysis also indicates the resulting autorotation equilibrium state after the jump. In the case of Fig. 3.13, the choice between positive and negative roll rates would be almost random depending on the sign of a perturbation in roll rate at $\delta e = 9.3°$.

(3.6.1.4) Qualitative Dynamics for Aircraft A and B

Having generated the equilibrium and bifurcation surfaces, it is now possible to derive from them (Figs. 3.2-3.13 , for example) extremely useful information about the aircraft behavior. Fig. (3.2) shows a plot of the equilibrium (or steady state) roll rate $\bar{p}$ for aircraft A as a function of aileron angle, with $\delta e = 0^{o}$. Note that there are values of δa for which five solutions of $\bar{p}$ exist.* The stability and instability properties of the equilibrium points are also indicated in Fig. 3.2. Starting with a state in the linear region of the figure (i.e. around $\bar{p} = 0$, $\delta a = 0$), small aileron inputs show a (linear) variation of $\bar{p}$ with δa. Similar plots of $\bar{\alpha}$ vs. δa and $\bar{\beta}$ vs. δa show that $\bar{\alpha}$ *remains near its trim setting and* $\bar{\beta}$ *remains small,* for small δa. However, it is clear from the figure that at values of about $\pm$ 8° for δa, the basic solution "disappears", and a "jump" occurs from one equilibrium point to another. The well documented and much utilized criterion of Phillips [8] gives a much higher value of critical δa of about 15°. Time histories of p vs. δa show that the tendency is for the state to jump to an "attractor" state - in this case, a jump to the upper "S" line, (solution branch (2)) which is a stable equilibrium manifold, rather than the "U" unstable solution. However, the new stable solution represents a large change in the value of $\bar{p}$. Furthermore, the other states will experience jumps, for example $\bar{\alpha}$ from a small positive to large negative value.

*The presence of the qr term in the set of equilibrium equations would generate a ninth order polynomial in $\bar{p}$, gravity neglected. See Section 3.6.2.

Other interesting features of plots like Fig. 3.2 will be discussed below in conjunction with Etkin's aircraft B [5], which has received much more extensive analysis here.

For aircraft B, the elevator is first set at either $\pm 2°$, to correspond closely with the studies done earlier, e.g. Etkin [5] and Schy and Hannah [9]. When $\delta e = -2°$ (pitch up) a unique equilibrium state exists for a large range of δa values ($\pm$ 20°), as seen in Fig. (3.3). A large change in the shape of this curve is noted in Figure (3.4), which corresponds to $\delta e = + 2°$ (pitch-down). Here, five possible equilibrium values of $\bar{p}$ exist around $\delta a = 0°$, three of which are stable. This lack of symmetry about δe is a result of the nonlinearity of the equations. Again, there are no gravity terms, and the $(-i_1\ qr)$ term in the roll moment equation, Eq. (3.8) is neglected in generating the curves of Fig. (3.3) through Fig. (3.4).* The equilibrium solutions of yaw rate, sideslip, angle-of-attack, and pitch rate are shown, respectively, in Figs. (3.5,3.6, 3.7,3.8). In all these figures, note that there are two sets of equilibrium states at which jumps may occur, $\delta a = \pm 4°$ and $\pm$ 9°. For example, the motion could begin for $\delta a = 0°$ (δe is held at +2°); as $|\delta a|$ moves beyond 4°, the equilibrium values of the state will change suddenly to new, larger values. The yaw-rate $\bar{r}$ undergoing a large change in particular (nose slice) while $\bar{\alpha}$ changing sign from negative to positive, are two of the most drastic effects, although all five states experience jumps, phenomena closely related to departure and post stall gyration phenomena described in Rutan, et al. [10]. From this initial jump, the equilibrium states

*The effect of the qr term is found to be negligible, as will be demonstrated for the model of aircraft H.

will vary smoothly with increasing $|\delta a|$, even though the "equlibrium" state, with its high values, is hardly a physically desirable situation, being characterized by severe coupling on all axes. If $|\delta a|$ is then reduced to 0°, it will be noted that there is no smooth mechanism to return the equilibrium solutions to their original linear, small-value condition by using δa alone.* That is, one expects a hysteresis condition, resulting in an autorotational state (sustained rolling motion for $\delta a = 0°$). Results presented in Sec. 3.6.1.5 will indeed confrm this and other observations.

An asymptotically stable autorotational steady state is actually dangerous if the stationary value of at least one other variable than $\bar{p}$ is high. This would then induce either large angles of attack or sideslip or high rates of pitch or yaw. To continue changing $|\delta a|$ in the same direction, increasing it to 9°, will initiate the second jump condition. The change in values for this jump are even more severe than for the inner jump ($|\delta a| = 4°$).

Figure (3.9) shows a locus of the eigenvalues of the linearized system, plotted as a function of $\bar{p}$. Critical roll rates (i.e, where jumps occur) correspond to values at which an eigenvalue crosses the imaginary axis. Note especially that only a real eigenvalue moves over to the right half plane in Fig. (3.9). Therefore, only elementary catastrophes, i.e., jumps from one equilibrium point to another, are observed. More generally (see discussion of aircraft H in Sec. 3.6.2), bifurcations to limit cycles may occur when a complex pair of eigenvalues crosses the imaginary axis.

*It is possible to force the aircraft out of this equilibrium state, but this would require a large transient or external force to cross the domain of attraction.

The bifurcation plot, shown in Fig. (3.10)* for aircraft B in the (δa,δe) control plane indicates that instability is possible for $\delta a = 0$ and δe increased beyond 9°. The phenomenon here is autorotation and departure, and Figs. 3.11 and 3.12 amplify this prediction. Based on an analytical criterion, the δe at which departure occurs in this case is 9.3°, which corresponds to an α of -16.3°. The analytical criterion is very easy to apply and involves the solution of at most a quadratic equation in δe. (See Appendix B)

(3.6.1.5) Numerical Verification.

Time history plots obtained by the integration of differential equations (3.8) to (3.12) for aircraft B are shown in Fig. (3.14). Also given are the (δa,δe) control histories (this model does not contain rudder derivatives so that $\delta r \equiv 0$ is implied). The state variables have initial values of zero. Over the first 20 seconds, δe was fixed at 2° (pitch down) and δa varied in steps from 0° to 10°, and back to 0°. These inputs were chosen to verify the jump and hysteresis phenomena predicted from Figs. (3.4) to (3.8). Note that the steady state variables jump shortly after δa changes to 10° and reach values which closely correspond to those predicted by the equilibrium surface plots of Figs. (3.4) to (3.8). Furthermore, the return of δa to 0° at t = 10 seconds does not return $\bar{p}$ to zero, but results in a rather severe autorotational condition, a clear example of hysteresis. Changing δe properly can induce recovery from this autorotation involving the roll axis. The strategy for δe may

*The numbers on the figure indicate the number of possible equilibrium solutions in that region.

be derived from Fig. (3.10); i.e., to move the control point out of the Butterfly pocket, where the states are multi-valued, to the single-valued region of small motions, set $\delta e = 0°$. This was done, at t = 20 seconds, in Fig. (3.14), and the variables do indeed jump toward the initial state at t = 0. It should be obvious that the (global) surface of Fig. (3.11) can be used as a starting point to derive control strategies which will transfer the aircraft from one equilibrium state to another without jumps.

In order to investigate more closely the physical nature of the jump phenomenon (see next section), several time histories were run in the "inner jump" region ($|\delta a| \gtrsim 4°$) of the well-treated pitch down case ($\delta e = 2°$), and some of these are shown in Figs. (3.15) to (3.24). For all of these cases, the initial value of the state variables is zero.

Figure (3.15) shows how the state variables respond to step variations in δa, for a fixed δe ($\approx 2°$). Each setting of δa is held for 3 seconds, to allow the system to reach its equilibrium state. As can be seen, there is a definite jump, occurring betwen t = 6 and t = 9 sec. The jump is especially sharp for the variables r and α, and in all cases these time histories reflect exceptionally well the behavior predicted by their respective equilibrium curves (Figs. [3.4] to [3. 8]). Note how β, q and r decrease in magnitude after the jump, and note how α changes sign from negative to positive, as Fig. (3.7) predicts. (This particular feature must be especially disconcerting to the unsuspecting pilot, who initially commanded a pitch down mode). There is no evidence either in the equilibrium plots or in the time histories of self-induced buffeting phenomena or wing rock (a more complicated model, A/C H, does exhibit these

and other limit cycle motions - see Sec. 3.6.2); however, Fig. (3.15) does evidence many of the phenomena typical of the high angle-of-attack regime described in Sec, (3.2) and extensively elsewhere, including reduced rudder effectiveness, nose slice and departure. Noteworthy is the observation that it is possible to exploit the excellent correspondence between the equilibrium curves and the time histories by using the equilibrium plots, which have the advantage both of being relatively inexpensive to generate and of being global in nature. It is also possible to identify the flight conditions and control settings which lead to harmful high-α motions.

The yaw rate curve of Fig. (3.15) seems particularly sensitive to incipient jump conditions (the reasons for this will be given in the next section), and it provides a clue that, while the jump has clearly been initiated by the time $\delta a = 6°$, nevertheless an inspection of smaller values of δa might prove fruitful.

Figures (3.16) to (3.18) each show time history plots for one setting of δa per solution, again with zero initial conditions. For $\delta a = 3°$ (Fig. [3.16]), there is no jump, although it takes upwards of 8 to 9 sec. to bring the system to steady state. Then, as is quite accurately predicted by the corresponding equilibrium curves (Figs. [3.4] to [3.8]), a jump occurs for $\delta a = 4°$ at about 6 sec. into the solution (Fig.[3.17]). Yaw rate is the cleanest, and also the earliest, indicator of the jump situation. Pitch rate experiences a marked increase in amplitude as early as 1.5 sec; however, the same thing happens

in the (stable) $\delta a = 3°$ case, except that q manages to return to a value in the steady state somewhat close to its "first plateau" value prior to t = 1.5 sec. The mechanism, then, influencing this pre-jump behavior in q is not related to conditions causing the jump, but is a result of the (nonlinear) lateral-longitudinal coupling in the equations. In the jump case, yaw rate changes sign (neglecting the cross-over at about 1.5 sec. due to Dutch roll transients), upsetting the moment balance in the pitch moment equation, which forces q to keep growing. Since r manages to stay positive at $\delta a = 3°$, the coupling influence on q is a stabilizing one. Similarly, none of the jump changes in the other variables precedes the change in r.

Finally, the case $\delta a = 5°$ is presented in Fig. (3.18) to show that a more extreme jump setting will cause the jump to begin sooner. The jump does not come to completion noticeably quicker, however.

The above observations indicate strongly that the region in control space for which a jump will occur is separated from the stable region by a distinct boundary (in fact, the bifurcation line of Fig. [3.10]). There is no intermediate region in which a jump may or may not occur. One can expect, then, the highly nonlinear situation of one value of δa producing well-behaved, stable, motions, yet a value $(\delta a + \varepsilon)$ causing a jump. Bifurcation Theory implies this, the above observations support the contention, and the plots of Figs. (3.19) - (3.22) tend to verify it. For example, $\delta a = 3.7°$ (Fig. [3.20]) is clearly stable while $\delta a = 3.9°$ is not (Fig. [3.22]). As before, the initial value of all state variables is zero. From the data which generated the

bifurcation surface of Fig. (3.10), the critical value of δa is given as 3.828°. This is in close agreement with the results presented below, considering the effect of nonlinearities in Liapunov's First Method would slightly reduce the stability limits.

While the examination of time history plots adds much insight to the understanding of jump phenomena, there are pitfalls; it is possible to overlook conditions which indicate an incipient jump. This is illustrated by the $\delta a = 3.8°$ case, Fig. (3.21). Through t = 12 sec., everything seems to be well-behaved, although a sharp-eyed observer might detect that, unlike the $\delta a = 3.6, 3.7°$ cases, a steady state has not been reached. Compare in particular the A and R (α and r) plots in each of Figs. 3.20 ($\delta a = 3.7°$) and 3.21 ($\delta a = 3.8°$). Note that they have achieved a steady state condition in the 3.7° case while there is (barely!) noticeable oscillation still occurring for $\delta a = 3.8°$. Note also in the 3.8° case that the Q and B (q and β) plots continue to move away from the origin, which is not the case when $\delta a = 3.7°$. Further, r has gone negative at around 10.5 sec., and the previous discussion indicates, therefore, that the problem may have reached an incipient jump condition.

Therefore, the $\delta a = 3.8°$ solution was run for 24 seconds and Fig. (3.23) shows clearly that a jump has occurred. Besides showing that as little as a 0.1° change in δa can produce significantly greater changes in the aircraft's behavior, due to bifurcation phenomena, there is also manifested a definite "caveat" against relying too heavily on time histories to define the stability behavior. The expense of generating these runs (compounded, of course, as the model becomes more complex) and the fact that only a point-by-point examination over the control space is possible, preclude exclusive use of the time histories for a definitive evaluation of high-α performance, even though useful insight may be derived

from solutions taken at selected points of interest. The problem with using time histories to define the global bifurcation surface is compounded further by two facts: (1) the search procedure is iterative in nature, since one is wise to initiate it with a "coarser" grid of control settings (Figs. [3.16] to [3.18]), and then proceed to a "finer" grid (Figs. [3.19] to [3.22]); (2) as is evident by the $\delta a = 3.8°$ example, the closer one is to the bifurcation surface, the longer it takes for the jump to initiate; which, if nothing else, adds to the computational requirements.

The next section attempts to explain what is happening physically during a jump, and will report on initial investigations into a formulation whose implementation has the potential of providing the pilot (or autopilot) with on-board real-time warning of incipient jump.

(3.6.1.6) Physical Explanation.

In the previous section, predictions derived from an inspection of the global equilibrium and bifurcation surfaces, regarding the behavior of a jet aircraft (B) in high angle-of-attack regimes, were seen to be readily verified by integrating the system equations (3.8) to (3.12). The detail of these verifications resulted in some further insight as to the mechanism causing a jump condition, and in Sec. 3.6.1.5 some of the observed kinematics were described - specifically: (1) the sensitivity of yaw rate r to jump conditions ("jump conditions" being the change in the control settings for a particular equilibrium solution in a direction which would cause the equilibrium solution to "jump" to a different branch. See, for example, Fig. 3.4, where a jump condition exists if δa increases from some value less than about 4° to a value greater than 4°). (2) the importance of coupling as a mechanism for either stabilizing or destabilizing

the motion; (3) the manner in which the coupling mechanism and the change of sign in r interact to bring about incipient jump (and nose slice).

The computer runs which generated the time history plots presented in the previous section were modified to provide time history plots of roll and yaw moment terms which comprise the right-hand side of equations (3.8) to (3.12). Note the absence of gravity terms in these equations. The terms are clustered into groups for plotting, as follows (Notation is for aircraft H, which is a more complete formulation):

Roll (Eq. 3.8)

Aerodynamic terms

$$A = \ell_\beta \beta + \ell_p p + \ell_r r$$

Control terms

$$C = \ell_{\delta a} \delta a + \ell_{\delta r} \delta r$$

Inertia term

$$I = -i_1 qr$$

Nonlinear terms

$$N = \ell_{\alpha\delta a} \alpha\delta a + \ell_q q + \ell_{\beta\alpha} \beta\alpha + \ell_{r\alpha} r\alpha$$

Yaw (Eq. 3.10)

Aerodynamic terms

$$A = n_\beta \beta + n_r r + n_p p$$

Control terms

$$C = n_{\delta a} \delta a + n_{\delta r} \delta r$$

Inertia terms

$$I = -i_3 pq$$

Nonlinear terms

$$N = n_{\alpha\delta a}\alpha\delta a + N_{p\alpha}p\alpha$$

Each of these four terms, together with its respective moment ($\dot{p}$ or $\dot{r}$), is plotted against time. ([$\dot{p}$ or $\dot{r}$] = A+C+I+N) It should be noted that N≡0 in both roll and yaw for aircraft B. These terms, however, do appear in the results for aircraft H. A typical plot, the roll equation, is shown in Fig. 3.24. This plot represents the case: aircraft B, $\delta a = 3.7°$, $\delta e = 2°$, $\delta r = 0°$; the companion state variable time history is given in Fig. 3.20. In Fig. 3.24, all terms are converted to units of deg/sec^2. Also, the roll axis I-term is scaled by a factor of 100 in order to detect its behavior. This term has little effect on the presence and magnitude of jumps, obviously, but is presented for completeness. A run made with $i_1=0$ produced essentially the same results, as discussed below. The yaw axis I-term, however, is most emphatically not insignificant.

An inspection of a set of these plots for aircraft B in the flight conditions depicted by Figs. 3.20 and 3.23 (the $\delta a=3.7°$ and $3.8°$ cases respectively) leads to the following conclusion (Figs. 3.24 to 3.27):

The mechanism of the jump is related directly to the inertia properties of the aircraft, the particular flight condition and the degree of control surface deflection. As Rhoades and Schuler [1] aptly state it, the "real villains" are the ($i_2 pr$) and ($-i_3 pq$) inertia coupling

terms which appear, respectively, in the pitch and yaw moment equations. To a certain degree, the relationship between inertia coupling and jump phenomena has also received widespread recognition among other investigators (e.g., Phillips [4], Etkin[5], Pinsker[13], and Schy and Hannah [9]). The flight condition and degree of control surface deflection are also important factors, however. Along with the vehicle geometry, these factors determine whether the state of the vehicle is in a region of incipient jump, or whether it evolves to a stable steady state.

Further, for the specific case of aircraft B initiating a roll maneuver in a pitch-down elevator setting, the lateral-directional stability is seen to be the most fragile. This means that the $(-i_3 pq)$ term in the yaw rate equation is the chief mechanism for inducing the jump. The following observations with regard to this flight situation are supplemented by referencing the relevant equilibrium and bifurcation surfaces, as presented in Sections 3.6.1.1 and 3.6.1.3, and as discussed there and in Sections 3.6.1.4 and 3.6.1.5.

The yaw rate inertia coupling term $(-i_3 pq)$ is destabilizing in the sense that it tries to drive r negative, and this has been observed, by the mechanism of coupling, to induce rapid changes (i.e., jumps) in the values of the other state variables. The factors most responsible for causing the jump, then, are most completely present in the term $(-i_3 pq)$. The positive elevon deflection (+2°) causes pitch down, q negative; positive aileron similarly generates negative roll rate p; with $i_3 > 0$, the coupling term, then, is also negative. Also, aircraft which are most susceptible to jump phenomena, such as aircraft B, are members of the class of so-called high-performance aircraft. Their geometry is characterized by thin, stubby wings,

which means low aspect ratio, and, critically, low I_x. The relatively lower values of I_x makes i_1, i_2 and i_3 larger, thereby enhancing greatly the (destabilizing) effect of the yaw rate inertial coupling term. Another effect is that the roll damping term, which involves C_{ℓ_p}, is related directly to wing size. As this and similar terms grow smaller, the system's ability to dissipate energy diminishes.

The sequence in which the magnitudes (and sign) of the important force and moment terms change is also significant. The principal agent for this is, again, coupling, as will be seen following a detailed description of the history of each of the moment terms which make up the roll ($\dot{p}$) and yaw ($\dot{r}$) equations.

Five terms comprise the roll moment equation: command ($\ell_{\delta a}\delta a$), damping ($\ell_p p$), dihedral ($\ell_\beta \beta$), cross derivative ($\ell_r r$), and inertia coupling ($-i_1 qr$). Of these terms, for the flight condition under discussion, the damping, inertia and cross derivative terms are seen as "stabilizing"; that is, balancing the moments due to the command and the dihedral term. In this condition, the dihedral effect is destabilizing - the rolling moment generated by the command deflection, δa, is enhanced by the dihedral term. In the context here, "destabilizing" terms - after transients have decayed, at $t \simeq 2$ seconds - are negative, and the "stabilizing" ones are positive. Refer again to Figs. 3.24 to 3.27.

For the $\delta a = 3.7°$ case (stable), after transient decay at about $t = 2.0$ sec., the stabilizing terms, which contribute the greatest to the value of the A-term, and include the I-term, in roll (Fig. 3.24), achieve a balance with the destabilizing terms (the dihedral term in A and the C-term. In the yaw axis, the critical I-term is destabilizing, but, for

AD-A051 850 SCIENTIFIC SYSTEMS INC CAMBRIDGE MA F/6 1/3
GLOBAL STABILITY AND CONTROL ANALYSIS OF AIRCRAFT AT HIGH ANGLE--ETC(U)
JUN 77 R K MEHRA, W C KESSEL, J V CARROLL N00014-76-C-0780
UNCLASSIFIED SSI-TR-77-1 ONR-CR215-248-1 NL

2 OF 3
AD
A051850

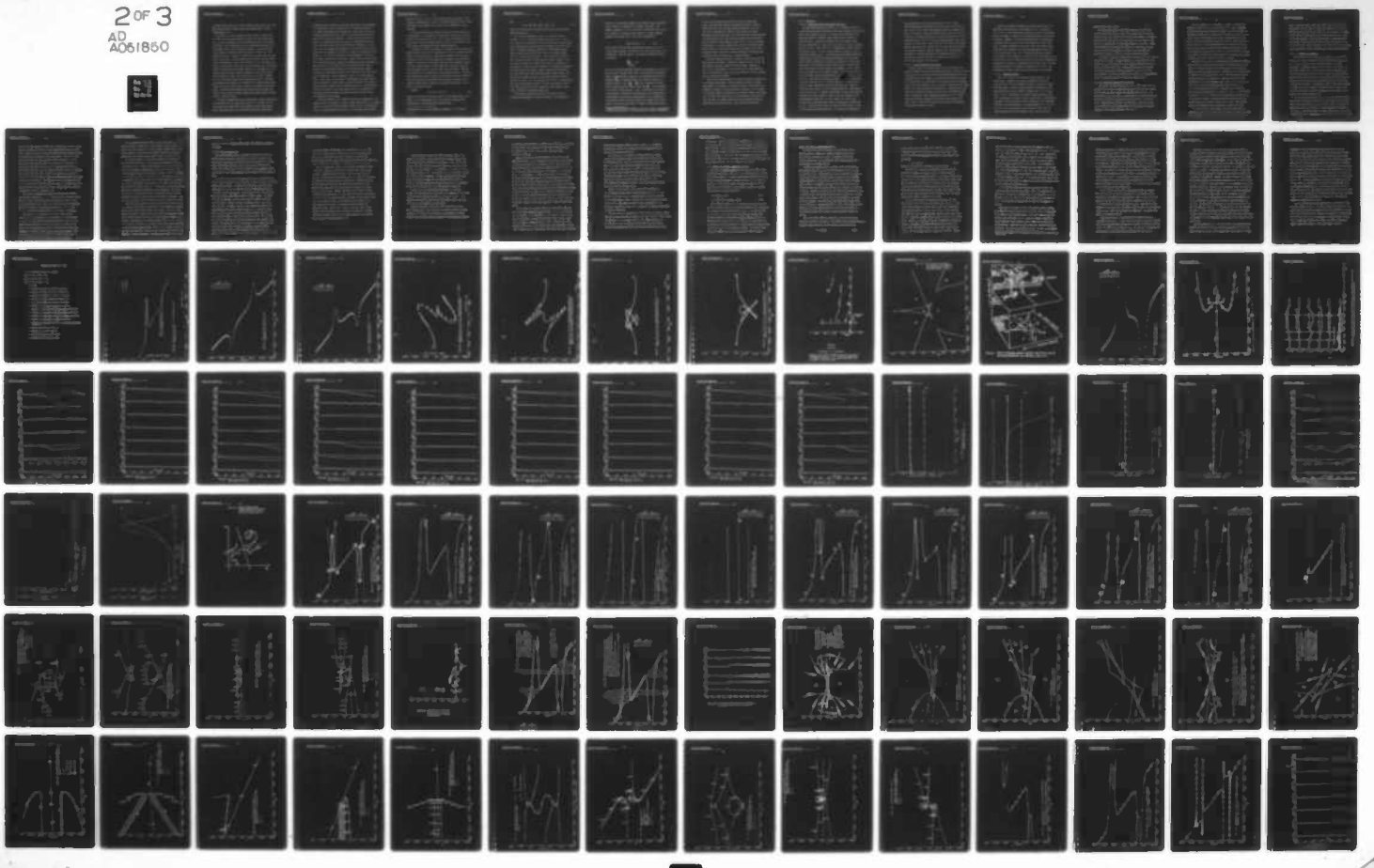

the stable control setting, it is seen to begin to decay (Fig. 3.26). This decay again maintains a balance among the yaw moment terms, so that $\dot{r}$ rapidly damps to 0.0.

For the $\delta a = 3.8°$ case (unstable), shown in Figs. 3.25 (roll) and 3.27 (yaw), δa, by directly affecting p in the yaw I-term, causes enough of an increase in magnitude of this (destabilizing) term so as to disrupt the balance. Fig.3.27 shows this critical I-term failing to decay at all (until after 15 sec, after the jump has occurred). As a result of this, $\dot{r}$ goes negative, starting just after the I-term, at about 9 sec. This changes the sign of r, which is a coupling "agent" into the roll axis (and also the pitch axis). The most direct effect in the roll axis as a result of this jump condition is seen in the I-term, Fig. 3.25. The effect on $\dot{p}$, however, is quite small (recall that I for roll is blown up in the figures). Figure 3.23 shows that the p history reflects this. The behavior of $\dot{r}$, as induced by the yaw I-term, is most noticeable in the yaw and pitch axis, as the histories of q and r (and α and β) in Fig. 3.23 show. Although the roll I-term plays no major role in inducing the jump, it nonetheless may be useful as an indicator, or a detector, of an incipient jump (A more "natural" indicator, vehicle kinetic energy, is introduced and discussed below). The terms mostly affected by the jump are seen to undergo transitions to new, and much different, steady state values following the jump, as Figs. 3.25 and 3.27 show.

It should be emphasized here that these greatly divergent results arise from a difference in the value of δa of only 0.1°. One value, $\delta a = 3.7°$, lies barely on the stable side of the bifurcation locus in the control space, while the value $\delta a = 3.8°$ lies barely outside the stable region.

An analogy to this situation of the control state being in the neighborhood of the bifurcation line is illustrated by the "Catastrophe Machine" of E.C. Zeeman (See Reference [4] of Chapter II). The machine consists of a cardboard disk pivoted about its center, with two rubber bands fixed to a point on the disk near its perimeter. The other end of one of these is fixed to the mounting board and the "machine" is operated by moving the other rubber band, whose free end location may be considered as a control point. The angle formed by the fixed point, the pivot of the disk and the common point of attachment to the disk, is a measure of the behavior of the machine. It is not hard to visualize that many movements of the control point cause a smooth rotation of the disk. However, when the control point is at a bifurcation point, the disk will suddenly swing with large amplitude. Near this point, on the stable side of the bifurcation point, there is basically a balance between "stabilizing" and "destabilizing" moments produced by the rubber bands attached to the fixed point and to the control point, respectively. This is analogous to the $\delta a = 3.7°$ case described above. At this point, on the verge of a catastrophe, only a minor disturbance is necessary to induce a jump. The balance between the two roughly equal and opposite moments, near the bifurcation point, is a precarious one. The value of δa which is just large enough to force r to go negative (in this particular flight regime), as dictated by the yaw I-term, will be that value which causes a jump.

The above discussion is not intended to minimize the importance of the dihedral term on roll behavior. Indeed, a common simplification is to neglect totally one of the roll rate jump-indicator terms, $(-i_l qr)$. Runs made first with $i_l = 0$, and then with both i_l and $\ell_r = 0$, both show a jump occurring

near $\delta a = 4°$ ($\delta_e = 2°$, $\delta r = 0°$), same initial conditions as before.* This justifies the simplification. Again, the principal importance of the r-terms with regard to roll behavior lies in their role as indicators of a jump condition.

A study was also done on the effect of adding the gravity terms to the system equations. A run made with the same control history and initial conditions as the one depicted in Fig. (3.14), except for the addition of the gravity terms, shows very similar behavior, as Fig. (3.28) indicates. This result agrees with observations made by Schy and Hannah [9].

A question now arises as to whether or not there may exist a more general dynamic indicator of incipient jump conditions. This is an important concern, insofar as the time history of a jump situation manifests only very subtle differences, prior to the jump, compared to a neighboring non-jump control setting. If the pilot had a reliable, real-time, on-board dynamic indicator of incipient jump conditions, he would then have a much better chance of taking the proper action to return to stable control settings. Providing such information to an autopilot obviously has similar benefits. The studies done with aircraft B seem to indicate that monitoring the rate of change of total vehicle kinematic energy might very well play an important role in creating a general control strategy for avoiding jump phenomena. In any event, it adds useful insight.

Consider

$$E = \frac{1}{2} m V^2 + \frac{1}{2} I \bar{\omega} \cdot \bar{\omega} \qquad (3.32)$$

where E is the vehicle total kinetic energy, m is the vehicle mass, V the velocity, I the inertia tensor, and $\bar{\omega}$ is the vehicle angular velocity, coordinatized in a body-fixed frame consistent with I.

---

*A run with only $i_1 = 0$ still produces a jump for $\delta e = 2°$, δa near $4°$, $\delta r = 0°$.

Then

$$\dot{E} = mV\,(\alpha\dot{\alpha} + \beta\dot{\beta}) + I_x p\dot{p} + I_y q\dot{q} + I_z r\dot{r} \qquad (3.33)$$

where $\dot{E}$ is the time rate of change of E and the other terms have been identified elsewhere.

Eq. (3.33) was computed for the $\delta a = 3.7°$ and $3.8°$ runs with aircraft B, $\delta e = 2°$, and the preliminary results (see Figs. 3.29 and 3.30) show that, for stable δa (3.7°), $\dot{E}$ is positive and increases during the transient period, but then decreases and changes sign shortly thereafter, then decays negatively towards zero. For the jump situation, however, there is an inflection point in $\dot{E}$ as it decreases towards zero, and it again starts increasing. This inflection point occurs in time just before the point that yaw rate goes negative (about 4.5 sec.). The resultant buildup in E because of $\dot{E}$'s failure to go negative in a jump situation, until the jump is completed, is interpreted as imparting the vehicle with enough energy to jump the energy barrier separating the current state from a new equilibrium state of higher energy. Once the jump has occurred, there is a higher level of energy, and $\dot{E}$ does decay to the origin. Fig. 3.30 shows this for the $\delta a = 3.8°$ jump setting. The jump is well underway at about t = 15 sec. (see also Fig. (3.23) for a time history of this case), where $\dot{E}$ is a local maximum. Thereafter, $\dot{E}$ falls off in magnitude towards zero.

The connection between the behavior of the vehicle's kinetic energy and jump phenomena is not mere coincidence. The equilibrium

values of any of the state variables, for aircraft B, may be interpreted as local extrema of a potential,* or Liapunov, function $\underline{\Phi}$. For example, if equations (3.8-3.12) are solved for equilibrium values of the state variables, the algebraic system reduces to a scalar, polynomial equation of ninth order for $\bar{p}$, in the form (see Appendix B)

$$f_p(\bar{p}, \delta a, \delta e, \delta_e r) = 0 \qquad (3.34)$$

after $\bar{q}$, $\bar{r}$, $\bar{\alpha}$, and $\bar{\beta}$ have been eliminated using equations (3.8-3.11) [A fifth order polynomial in $\bar{p}$ results if the $(-i_1 qr)$ term in Eq. (3.12) is neglected]. From this equation, the Liapunov or potential function is defined as

$$\left.\frac{\partial \underline{\Phi}}{\partial \bar{p}}\right|_{p=\bar{p}} = -f_p$$

Thus, $\underline{\Phi}$ may be easily generated numerically by integrating $(-f_p)$ over p, with the control variables fixed. $\underline{\Phi}(p)$ will typically have maxima and minima. The extrema of $\underline{\Phi}$ correspond to the equilibrium points, and the expression $\frac{\partial^2 \underline{\Phi}}{\partial \bar{p}^2}$ will determine whether the extremum in question is a maximum or minimum. Since $\frac{\partial \underline{\Phi}}{\partial \bar{p}^2} = -\frac{\partial f}{\partial \bar{p}}$, this is equivalent to saying that the minima of $\underline{\Phi}$ (stable points) occur where $\frac{\partial f}{\partial \bar{p}} < 0$, and conversely for the maxima (unstable points). This is consistent with the results of linearization, which require the eigenvalues of the Jacobian matrix to have negative real parts for stable behavior in the neighborhood of an equilibrium solution. $\underline{\Phi}$ changes shape as the controls vary, and the point(s) in the control space where the number of extrema of $\underline{\Phi}$ changes

*A potential function can be defined for the case in which the equilibrium equations can be reduced to a single equation, as is shown in Appendix B.

(as one or more extrema become inflection points) are bifurcation points, and their locus generates the bifurcation surface. A system state which is at a local minimum of Φ which disappears in this way (as, say, δa increases) then "jumps" to a surviving local minimum. The family of local minima of Φ, in the state space are called "attractors". For fixed controls, the initial conditions determine which equilibrium state is attained by the system as is seen in Fig. 3.31 for a representative situation. As initial conditions vary over the p-q space (controls fixed) in Fig. 3.31, the solution may or may not diverge. The x's are equilibrium points, [extrema of a Liapunov (potential) function Φ (p,q)]. S means the point is a stable node, U, unstable saddles.

From this viewpoint, Φ is seen to generate a potential energy field, with "barriers" and "sinks". Changing the controls, say δa, is then seen as changing the potential energy field of the system. Referring to Fig. (3.31), if the solution is in the vicinity of S_1 and δa changes so that U_1 moved toward S_1, then a jump occurs for that δa at which U_1 merges with S_1, cancelling the extrema.

Notice that the sum of potential and kinetic energies (or Hamiltonian) of the system stays constant. When the equilibrium state is unstable corresponding to a maximum of the potential function, any disturbance will generate an exchange of kinetic and potential energies, viz., an increase in the kinetic energy and a decrease in the potential energy of the system. Fig. 3.30 shows this increase in kinetic energy during a jump condition. After the jump, the exchange between kinetic and potential energies is completed and the system settles to a new stable equilibrium point.

(3.6.2) Aircraft H.

(3.6.2.1) Equilibrium Surface and Nonlinear Root Locus.

The equilibrium surface for aircraft H is a 3-dimensional surface in an eight dimensional space consisting of five state variables (p,q,r,α,β) and three control variables $(\delta a,\delta e,\delta r)$. We present here projections of the equilibrium surface on different planes formed by pairs of state and control variables. Following the approach taken for aircraft A and B, first the equilibrium roll rate $\bar{p}$ versus δa curves are shown for different values of $(\delta e,\delta r)$. (Figs. 3.32-3.42). A comparison with similar figures for aircraft B (Figs. 3.3 and 3.4) reveals that for aircraft H, up to 9 equilibrium points may exist. A linearized stability analysis around each equilibrium point reveals that unstable equilibrium points may have one or more complex eigenvalues with real parts in addition to positive real eigenvalues. Points denoted by letter L have one pair of complex eigenvalues with positive real part whereas points denoted by E have in addition a real eigenvalue in the right half plane. Interestingly enough, in most of the cases, only one equilibrium point is stable (see Figs. 3.32 to 3.41) for a fixed value of the control variable. However, an examination of the root locus plot (Fig. 3.47) shows stability is generally lost by a pair of complex eigenvalues crossing the imaginary axis. Based on the discussions in Chapter II, this indicates possibility of Hopf Bifurcations to limit cycles. A complete representation of limit cycles requires a minimum of two state dimensions chosen to span the eigenspace of the purely imaginary eigenvalues. For this reason, limit cycles, which are nothing but equilibrium orbits cannot be represented on figures such as 3.33. In the next four sections, we would show limit cycles in terms of time histories and phase plane plots. We complete our discussion of

the equilibrium plots here by referring to Figs. 3.43-3.46, which show the remaining state variables (q,r,α,β) versus δa for $\delta e = \delta r = 0°$ and to Figs. 3.59-3.63 which show equilibrium states with respect to δe and δr. The effect of neglecting different terms in Eqs.(3.8)-(3.12) for aircraft H on the equilibrium surface can be seen from Figs. 3.64-3.66. A comparison of Figs. 3.69, 3.65 and the corresponding figure with ($-i_1 qr$) neglected (not shown here) reveals that there is virtually no difference between these three cases. However, Fig. 3.66 shows that neglecting all the nonlinear aerodynamic terms for aircraft H has a serious effect, particularly on the minor branches of the equilibrium surface. It is interesting to note that for $|\delta a| < 10°$ the shape of the $\bar{p}$ vs. δa curve is quite similar in all the cases.

(3.6.2.2) Hopf Bifurcation to Limit Cycles

Figures 3.48 and 3.49 show the projection of limit cycles on the p-axis for different values of δa obtained by solutions to Eqs.(3.8)-(3.12). A comparison of the two figures shows the hysteresis phenomena, which is a consequence of the finite domains of attraction surrounding limit cycles. It is seen from Fig. 3.48 that when δa is decreased from zero to negative values, limit cycles appear at $\delta a \approx -12°$ when the equilibrium point changes from an S to L-type (representing the crossing of a complex pair of eigenvalues into the right half plane). The limit cycle first grows and then decays in amplitude, finally disappearing around $\delta a \approx -30°$. A stable limit cycle generally disappears by collision with an unstable limit cycle. Figs. 3.48 and 3.49 only show the stable limit cycles obtained by solving the equations of motion.

When δa is increased from negative to positive values, Figs. 3.49 shows that limit cycles exist for δa values up to -2°. In fact for $\delta a = -2°$, $\delta e = 2°$, the state portrait consists of at least 5 equilibrium points (one stable, 4 unstable) and 2 equilibrium orbits or limit cycles (1 stable, 1 unstable). The stable equilibrium point is surrounded by an unstable limit cycle which in trun is surrounded by a stable limit cycle. Therefore, depending on the initial state, the aircraft trajectories may either converge to the stable equilibrium point (Fig. 3.48) or to the limit cycle (Fig. 3.49). Actual phase plane plots showing this phenomena will be presented in section 3.6.2.5. The existence of two stable limit cycles for a particular value of δa will also be demonstrated. To complete our discussion of Hopf Bifurcation, we show in Fig. 3.50 time history plots where δa is increased in steps from -10° to -20°. The development and growth of limit cycles is seen clearly in this figure.

(3.6.2.3) Bifurcation Surface

Figs. 3.51, 3.52 and 3.53 show the bifurcation surface in the control space. Compared to the Butterfly bifurcation surface for aircraft B (Fig. 3.10), the bifurcation surface for aircraft H is much more complicated. A three or higher dimensional visualization of the equilibrium surface can be obtained by combining Figs. 3.51-3.53 with Figs. 3.32-3.42. The presence of an umbilic (possibly parabolic type [14]) is indicated by the shape of curves around N and N'. These regions correspond to the case where two distinct eigenvalues of the linearized system go to zero simultaneously. The dotted branches (I,I', J,J', K,K', L and L') on Fig. 3.51a represent (δa, δe) points at which a pair of complex eigenvalues crosses the imaginary axis, resulting in Hopf

Bifurcations to limit cycles.

The bifurcation branches (solid lines) separate each plane into a group of individual regions. Each point (corresponding to a specific control setting) in any specific region has the same number of equilibrium solutions as any other point in the same region, and the number of such solutions is indicated by the number which appears in the region. Catastrophic behavior can occur when the controls are varied so as to cross one of the bifurcation branches to a region with a fewer number of equilibrium solutions, as some of the stable solutions disappear.

The bifurcation behavior around M and M' (see also Fig. 3.42) in Fig. 3.51a requires further study. A proper representation of this behavior would require the use of two behavior or state variables corresponding to the case of an umbilic catastrophe. Further computations are also needed to obtain the limit cycle bifurcation boundaries in the ($\delta e, \delta r$) and ($\delta a, \delta r$) planes. Both the above computations, however, are straightforward and are not expected to present any additional complications.

(3.6.2.4) Qualitative Dynamics for Aircraft H

Dynamically, the added complexity of the aircraft H model vis-a-vis aircraft A and B tends to produce more periodic motions and even tighter coupling than the simpler models which describe these aircraft. As a consequence of this, one expects to observe some of the phenomena which are oscillatory in nature, and which have not been observed in aircraft A and B. These would include limit cycle phenomena, buffeting and wing rock, in addition to the phenomena which have characterized the high-α behavior of the aircraft discussed in Sec. 3.6.1.

The basic maneuver to be investigated is similar to the maneuver applied to aircraft B; i.e., a pitch down ($\delta e = 2°$), with a commanded aileron deflection near the stability surface. For this condition, the equilibrium surface plot of (steady state) roll rate $\bar{p}$ vs δa (Fig. [3.33]) shows the usual linear behavior in the small control deflection region which is one of five possible solutions for small δa. While this plot has most of the traits of the corresponding one for aircraft B (Fig. [3.4]), there are extra curves for high $|\delta a|$ which reflect the increased order of the equilibrium equation for $\bar{p}$. The $\delta e = 0°$ plot shows this even more convincingly, as these "extra curves" have moved to the small $|\delta a|$ region, providing nine possible solutions for $\bar{p}$ (Fig. [3.32]).

Returning to Fig. [3.33], a linearized stability analysis at selected points along the equilibrium reveals whether the equilibrium point has stable (S), unstable because of real positive roots (U), or unstable because of right-half complex roots (L), eigenvalues. The L surfaces were not present in earlier studies (Sec. 3.6.1), and they indicate regions of possible limit cycles. Refer also to the root locus plot of the eigenvalues with $\bar{p}$ as the parameter, given in Sec. 3.6.2.2 (Fig. [3.47]). In Fig. [3.33], the main equilibrium branch starting from ($\bar{p} = 0$, $\delta a = 0$) becomes unstable around $|\delta a| \approx 14°$, when a pair of complex roots crosses the imaginary axis (see also Fig. [3.47]). If the aircraft is excited at $\delta a = -12°$, there are five possible equilibrium points, but all of them are unstable. The Hopf Bifurcation Theorem predicts the possible existence of a family of stable limit cycles. Results which confirm these predictions will be presented in following sections.

If δa starts from 0° and increases, the solution will begin to approach the limits of the linear region of steady state solutions. Just prior to the jump, at stable $\delta a \approx \pm 12°$, $p \approx \pm 120°$/sec. (Fig. [3.33]),

there is observed a small region where stable limit cycle behavior is experienced. At this point, one expects oscillations in all axes to develop, somewhat like pre-stall buffeting. As δa increases to a jump setting, the equilibrium states jump to limit cycle solutions. Here, if $|\delta a|$ were decreased, there would again result a hysteresis effect, culminating in an autorotational limit cycle when $|\delta a|$ decreases to 0.0°. On the other hand, a further increase in $|\delta a|$ would result in the equilibrium solutions entering a region characterized by stable equilibrium points.

(3.6.2.5) Numerical Verification

The verification of the limit cycles, predicted in the previous section as a result of analysis of the equilibrium surface plots (e.g., Fig. [3.33]), is done first by solving the equations of motion numerically for different values of δa from -12° to -40°, and $\delta e = 2°$. The results shown in Fig. [3.50] are again in general agreement with the equilibrium plot for this case (Fig. [3.32]). The significance of these results is that the family of limit cycle oscillations shown are believed to be the first case of five-dimensional limit cycles shown to exist for an aircraft. The appearance, growth, decay, and extinction of these limit cycles is typical of Hopf Bifurcations; and this has also been conjectured to play an important role in the onset of turbulence (see Ruelle and Takens [12].

As in the case of aircraft B (Sec. 3.6.1), time history runs were made to study the behavior of aircraft H in the vicinity of its "inner" jump control setting for $\delta e = 2°$ viz. $\delta a \approx 12°$. Refer to the roll rate equilibrium plot (Fig. [3.33]) for a global perspective of behavior in this region. Time history plots for aileron values equal to 8,10,11,12, 14 and 16° are shown, respectively, in Figs. [3.67 - 3.72]). For $\delta a = 8,10$

and 11°, the time response is linear, and the steady state values for each value of δa behave as indicated by the corresponding equilibrium surface plots. There is, however, a noticeable tendency towards increasing oscillatory response as δa increases in this linear region. At $\delta a = 12°$, just beyond the bifurcation value, the jump is quite obvious at t = 3 sec., and the post jump trajectory grows to a limit cycle. This behavior is quite accurately predicted by Fig. [3.33], since Hopf Bifurcations to limit cycles occur when a pair of complex eigenvalues crosses the imaginary axis from the left half plane. The final two figures in the sequence (Fig. [3.71,3.72]) show that the limit cycle amplitude decreases and finally vanishes with increasing δa. This behavior is also in agreement with Fig. [3.33], as there one notices the stable (S) region of the upper equilibrium branch which exists for high values of $|\delta a|$. Except where noted, gravity is neglected in these and subsequent runs.

The hysteresis phenomenon was adequately discussed and verified for the simpler models of Sec. 3.6.1, and thus will not be repeated here. There is a clear hysteresis situation for aircraft H as well, setting up an autorotational state. Figs. [3.73] and [3.74] show the hysteresis behavior of aircraft H, with multiple solutions for $a = 11.2°$ and $\delta e = 2°$. The initial conditions for Fig. [3.73] are p = -80 deg/sec, q = -8.1 deg/sec, r = 2.5 deg/sec, $\alpha = -2.5°$, $\beta = 3.80°$; and for Fig. [3.74], p = -310 deg/sec, q = -23.69 deg/sec, r = -38.56 deg/sec, $\alpha = 6.92°$, $\beta = 6.14°$. For both cases δa was set to 11.2 °at t = 2 sec., from an initial setting of 6° (Fig. [3.73]) and 13.5 (Fig. [3.74]). This is not an autorotational situation, but the figures do show great differences in behavior. There is nearly limit cycle behavior in Fig. [3.73], with much less severe amplitude and frequency than is seen in Fig. [3.74], where limit cycle behavior is very much evident.

The distinguishing characteristic of the aircraft H model, with its nonlinear aerodynamic coefficients, is the existence of limit cycles in the motion, over large portions of the flight regime. BACTM provides a systematic approach for predicting the existence of limit cycle behavior, exhibited by time histories such as shown in Figs. [3.50] and [3.74].

As further validation, a "finer grid" study of the response of aircraft H was conducted for $\delta e = 2°$ and δa in the neighborhood of the bifurcation point $\delta a = 12°$. A family of plots for $\delta a = 11.4$, 11.46, 11.48, 11.5 and 11.6° is presented, respectively, in Figs. [3.75] to [3.79]. The initial conditions for these runs are $p(0) = -80.$ deg., $q(0) = -8.1$(deg/sec., $r(0) = 2.5$ deg/sec, $\alpha(0) = -2.5°$, $\beta(0) = 3.8°$. From these plots, it can be deduced that the critical value of δa at which damping of an oscillatory mode is zero lies between 11.46 and 11.48°. For values of δa just short of the critical value (Figs. [3.69, 3.75 3.76]), there is excitation of steady amplitude and frequency oscillations of very low damping. The case $\delta a =$ 11.46 (Fig. [3.76]) was run for 64 sec., much longer than the aircraft characteristic times, and there is only a mild decay in amplitude. Therefore this value for δa is the critical value, for all practical purposes.

Once the jump has occurred, for $\delta a = 11.48°$ and 11.50° cases, there is no question that growth to a limit cycle is the predominant phenomenon. Again, the state space plots of Sec. 3.6.2.6 (Figs. [3.87] and [3.88]) amplify this result. Observe also that the limit cycle magnitude is greater for the smaller value of δa. Fig. [3.80] also shows this tendency, as it presents a time history for 4 different values of δa, 13.5, 12., 11.4 and 11.2°, with $\delta e = 2°$ and $\delta r = 0°$, as usual and the state initial conditions on the post-jump equilibrium branch. Figs.[3.87] and [3.88], plotting p vs. the other state variables, runs for 72 sec., by which time the limit cycle amplitude is clearly established. The time history shown in Fig. [3.80]

runs for t = 32 sec., stopping shortly before this steady state amplitude is reached.

(3.6.2.6) Physical Explanation

The distinguishing feature of the model for aircraft H is that the added nonlinear aerodynamic terms enhance the overall nonlinearity and, specifically, cause limit cycle behavior over large regions of the control space. Even though, physically, limit cycles are very different from equilibrium points compared to the non-oscillatory jump phenomena observed for aircraft B, their sudden appearance may be thought of as an oscillatory jump.

As before, the roll and yaw moment equation will be examined as being typical of the remaining state variables. For aircraft H, there are four extra moment-generating terms: the pitch cross derivative, ($\ell_q q$), and three terms linear in β, r and δa, with the coefficient being proportional to α, ($\ell_{r\alpha} r\alpha$), ($\ell_{\beta\alpha} \alpha\beta$), and ($\ell_{\alpha\delta a} \delta a$). The inclusion of such terms obviously makes the aircraft H model more realistic in high-α regions. The added terms are all nonlinear, and they tend to make the behavior generally more oscillatory. However, the basic conclusions of Sec. 3.6.1 remain valid here also. As before, yaw rate is the variable most sensitive to the mechanisms which create a jump situation; i.e., i_3, which is large when I_x is small (as it is for high performance aircraft) and p and q, which respond directly to the control settings δa and δe. For δe fixed at a pitch down setting (2°), and for increasing δa, the yaw moment term ($-i_3 pq$), will eventually force the secular part of r to remain below zero (see Fig. [3.77]). Thus, as before, an imbalance between the aerodynamic and inertia moment terms, produced by the large values of δa and i_3 in the latter, causes the jump to occur. Figs. 3.83 to 3.86 show the

roll and yaw moment time histories for a non-jump ($\delta a = 10°$) and jump ($\delta a = 11.6°$) control setting. See Section (3.6.1.6) for definitions of the A, C, I and N terms; and Figs. 3.68 and 3.79 for the state variable time histories. The time history initial conditions for these runs are $p = -80°/sec$, $q = -8.1°/sec$, $r = 2.5°/sec$, $\alpha = -2.5°$, $\beta = 3.8°$.

Fig. 3.79 shows that, for $\delta a = 11.6°$, the jump is underway by about $t = 6.0$ sec. However, the roll I-term's behavior (Fig. 3.84) is seen to begin to diverge from the stable ($\delta a = 10°$, Fig. 3.83) I-term by 5.0 sec. As explained for the aircraft B case, this term is not involved in producing the jump, but seems to indicate well, if magnified enough, the presence of an incipient jump. Note also, particularly in the stable $\dot{r}$ plot, Fig. 3.85, that the nonlinear (N) terms play a noticeable role in the motion. Further, note that the yaw I-term is greater in magnitude than the control (C) -term. The yaw I-term for the unstable δa, 11.6°, Fig. 3.86, begins to diverge in behavior from the stable I-term, Fig. 3.85, at about 5.0 sec. As was observed with aircraft B, this term's behavior for aircraft H is similarly the main catalyst for inducing the jump. This is clear in Fig. 3.86 as the I-term's growth preceeds that of the other terms. As before, this causes r to assume consistently negative values, and the coupling effect in pitch and the other variables is obvious from Fig. 3.79.

A study was made to compare the effect of gravity terms on the dynamics of aircraft H. Time history plots for dynamics without, and with, gravity terms are presented, respectively, in Figs. [3.81], and [3.82]. The initial conditions for both runs at $\delta a = 2°$ are p = 0.40 deg/sec., q = -2.80 deg/sec., r = -.16 deg/sec., $\alpha = -2.35°$, $\beta = 0.18°$. The elevator setting is $\delta e = 2°$ throughout. As for the aircraft B study, the results are quite comparable, the most noticeable difference here being the smoothing of peaks near the jump region when gravity is included. The jump consequently does not occur until $\delta a = 14°$, slightly higher than the critical value of δa when gravity is neglected.

A limit cycle is a self-sustained oscillation in a dynamic system. The amplitude of this oscillation is not dependent on the initial conditions of the problem, as is the case for linear systems, but it depends on the nonlinear nature of the system model itself. See Figs. [3.74] and [3.77] for examples of limit cycles.

Hopf has shown that a limit cycle always exists under certain mild conditions when a pair of roots of the linearized system is purely imaginary. The Liapunov Center Theorem is one consequence of Hopf's results, and the Liapunov stability analysis of the equilibrium solutions

for aircraft H have shown that the conditions are present for bifurcations to limit cycles. Time histories of several flight conditions (see, for example, Figs. [3.77], [3.78], [3.81], and [3.82]) have verified this behavior.

Phase plane plots of the state variable p (roll rate) vs. the remaining variables (q,r,α,β) demonstrate the evolution of limit cycles. An entire set of such plots is presented in Figs. [3.87] and [3.88]. These plots represent a run made with aircraft H with $\delta e = 2°$, $\delta r = 0°$, $\delta a = 11.46°$, and initial conditions p = -310 deg/sec., q = -23.7 deg/sec., r = -38.6 deg/sec., $\alpha = 6.92°$, and $\beta = 6.14°$. Due to scaling within the plot algorithm, portions of the large amplitude limit cycles have been cut. The initial conditions place the equilibrium state on the "outer" solution branch of Fig. [3.33]. A very similar time history, also on this equilibrium branch, but with time as the independent variable is given in Sec. 3.6.2.5, Fig. [3.74]. The major differences are that in Fig. [3.74], the control settings are $\delta a = 13.5°$, and then 11.2° for 30 sec., whereas in Figs. [3.87] and [3.88], $\delta a = 11.46°$ is used for 72 seconds to allow the limit cycle amplitude to reach a steady state value.

If the above run is repeated, except that the initial conditions are on the "inner" equlibrium solution branch - i.e., p = -80 deg/sec., q = -8.1 deg/sec., r = 2.5 deg/sec., $\alpha = -.25°$ and $\beta = 3.8°$, the solution is "attracted" to a completely different region, as Fig. [3.89] (p vs. q) shows, in comparison to Fig. [3.87]. Figure [3.76] is the companion plot to Fig. [3.89], showing time as the independent variable. A more complete series of time history runs, varying the intial conditions,

would define the barriers between attractor regions in, for example, the p-q plane. However, the equilibrium surfaces themselves perform this function far more efficiently.

Fig. [3.90] shows how a change in elevator setting to a value outside of the "Butterfly" region of the bifurcation surface affects the subsequent motion. The run is the same one as that which generated Fig. [3.88], except that the initial conditions were right on the Fig. [3. 8] limit cycle, and, at t = 8 sec., δe was changed to -2°. As can be seen, there is very erratic behavior (plots of the other state variables are similar, due to coupling) in the course of transition from the limit cycle to a stable, steady state solution. The equilibrium surface predicts the results, but not the transient behavior very much in evidence in Fig. [3.90].

Finally, runs were made from the same initial conditions as the runs started from the "inner" equilibrium branch $\delta_e = 2°$, $r = 0°$; however, δa was set to 10.6°, a non-jump value, for one run, and then to 13.5°, which forces a jump. Plots of p vs. β for both cases are shown in Fig. [3.91], which shows the effect of the "disappearance" of an "attractor" equilibrium solution, as it merges with an unstable equilibrium solution for changing δa.

As with aircraft B, the behavior of kinetic energy of aircraft H under jump and non-jump conditions was studied, and Figs. 3.92 and 3.93 show $\dot{E}$ and E vs. time for $\delta a = 10°$ (no jump) and $\delta a = 11.6°$ (jump) settings of a run with $\delta e = 2°$, $\delta r = 0°$, and zero initial conditions. The results indicate large exhanges of kinetic and potential energy typical of limit

cycle motions. Note the smoothness of the (decaying) oscillations of $\dot{E}$ in the stable case, Fig.[3.92], as opposed to the behavior of $\dot{E}$ in Fig.[3.93]. Table 6 and Fig. [3.79] also show non-sinusoidal inflections in $\dot{E}$ at 6.5 and 7.5 seconds, hinting of a jump, which does occur at about 8 seconds. Unlike aircraft B, E, the energy, does not asymptotically approach a new, higher value. This is due to the limit cycle nature of the jump state. The time history of the $\delta a = 10°$ run is shown in Fig. [3.68].

(3.7) Control and Stability Augmentation (A/C B)

The effect of feedback controls on the bifurcation behavior may be studied by using Eqs. (3.26)-(3.31). It is seen from Fig. 2.9 that large positive values of c_3 produce unique stable equilibrium solutions. Consider a negative feedback on δa from roll rate viz. $\delta a = -K_1 p + K_2$ where $K_1 > 0$. This has the effect of changing all the f's, but for simplicity, let us concentrate on the change in f_5' and f_1'. The new values, denoted by f_1' and f_5' would be:

$$f_1' = 326.7K_1 - 21.64 \tag{3.34}$$

$$f_5' = 11752.78\ \delta e + 23015K_1 - 1525.9 \tag{3.35}$$

Thus, negative feedback ($K_1 > 0$) increases the values of f_1' and f_5' and by a proper choice of K_1, both can be made positive. The effect on c_3 is seen from the last term in Eq. (3.16). It is seen that for $K_1 = 0$ and $\delta e > .13$ rad, this term is negative and increases with δe. The net-effect is a decrease in c_3 which eventually results in unstable behavior for ($\delta a = 0$, $\bar{p} = 0$). With $K_1 > 0$, this problem can be avoided and c_3 can be increased to a value for which the stable region around ($\delta a = 0$, $\bar{p} = 0$) is considerably enlarged. The effect of more complicated feedback laws can also be studied in similar fashion.

Control and Stability Augmentation (A/C H).

Bifurcation and equilibrium surfaces can be of great help in deriving stability augmentation systems or feedback control laws, which need not necessarily be linear. An example involving the aircraft H model will now be considered. More detailed analysis will be presented in forthcoming reports.

A combat-type maneuver of basic interest is the rolling pullout. This maneuver typically calls for coordinated deflections of all three controls ($\delta a, \delta e, \delta r$). Lateral response is often enhanced by the addition of the aileron-rudder-interconnect (ARI) and stability-axis yaw damper command augmentation systems [11,15]. The ARI system causes the rudder (δr) to deflect in conjunction with roll control inputs (δa) so as to eliminate adverse yaw due to these surfaces, and to improve roll response in general. Typically, the ARI gain(s) are scheduled with angle-of-attack. In implementation, more and more rudder deflection results from a lateral control stick movement, and less and less aileron deflection, as angle-of-attack increases. The stability axis yaw damper deflects the rudder (δr) in response to a signal proportional to ($r-p\alpha$). The purpose of this feedback is to reduce sideslip excursions during rolling maneuvers at high angles-of-attack, and to improve lateral-directional damping in general.

Equivalent lateral stability augmentors can be derived from the bifurcation surfaces for aircraft H. The example given here shows results for relatively small deflections of δe. The ARI law may be written as

$$\delta r = k(\delta e)\delta a \qquad (3.36)$$

In Eq. (3.36), while δr is linear in δa, the gain k is actually a parameter varying with δe setting, as will be seen below. This law can be rather straightforwardly extended to a more general form of the type

$$\delta r = f(\delta a, \delta e) \tag{3.37}$$

Details of this extension will appear in future reports.

The form of Eq. (3.36) may be ascertained directly from the bifurcation surface, of which Fig. [3.53] is a typical example. Fig. [3.53] shows the bifurcation surface in the $(\delta a, \delta r)$ control plane, with $\delta e = 0°$. In this figure, bifurcations in the form of jumps occur when a $(\delta a, \delta r)$ locus crosses one of the branch lines. The branches A and B are of particular interest because they are associated with lower values of equilibrium roll rate, $\bar{p}$; hence, these branches would mark the first jump encountered as $(\delta a, \delta r)$ move away from the linear (trim) region, which is centered at the origin.

If δr is fixed during a roll maneuver (δa varies), then the $(\delta a, \delta r)$ locus in Fig. [3.53] is a horizontal line. If $\delta r = 0°$, this line intersects branches A and B at $|\delta a| \simeq 11.5°$. The corresponding equilibrium plot, $\bar{p}$ vs. δa for $\delta e = \delta r = 0°$ (Fig. [3.32]), confirms that jumps will occur at these settings, when the problem starts near $\delta a = 0°$. Thus, the "non-jump" region for $\delta e = 0°$ and $\delta r = 0°$ is $|\delta a| \leq 11.5°$. However, this region can obviously be expanded by relating δa and δr so that their locus passes through the points N and N' in Fig. [3.53]. The simplest locus is a line of form (3.36), with $k = -0.152$. Fig. [3.94] shows the $\bar{p}$ vs. δa plot for this case. Notice

that the trim (basic) stability region has been expanded to $|\delta a| \leq 17°$ from $\pm$ 11.5° for the $\delta r = 0°$ case. Time histories for the $\delta r = 0°$ case and the ARI case are compared in Figs. [3.95 and 3.96], respectively. It is obvious that ARI aids not only in stability, but in performance as well. Note that ARI causes decoupling, even for the large δa values. In order to excite the instability at $\delta a = 18.5°$, it was necessary to hold that setting for much longer than the 8 sec. shown in Fig. [3.96a]. Fig. [3.96b] shows that when $\delta a = 18.5°$ for an extended time, a very mild divergence ensues.* Thus, for ARI when $\delta e = 0°$, the effective range of δa is increased upwards to $|\delta a| \simeq 36°$. It is therefore obvious, from the time histories shown, that stability augmentation control laws can rather easily be derived from the bifurcation plots.

If k is not the value which intersects the points N and N', the results are seen to be less than optimal. Fig. [3.97] shows the $\delta e = 0°$ case with k = +0.152 (the "optimum" value of k for this case is -0.152). The plot is $\overline{p}$ vs. δa. Note how the stable region for δa has shrunk to $\pm$ 8°. (Other equilibrium branches are not shown for the purposes of clarity).

When elevon is nonzero, the use of the equilibrium plots becomes more important, as well as the bifurcation plots. This is because limit cycle behavior enters the major branch. Fig. [3.98] demonstrates this, showing a pitch down case, $\delta e = 5°$. Thus, for combined longitudinal-lateral maneuvers, where elevon as well as rudder-aileron deflections become prominent, there are two kinds of stability criteria that must be considered: the first, seen already for the $\delta e = 0°$ case, is the jump in

*There is one unstable root at this value of δa, which has a time constant of 14.8 sec.

stability, indicated by the bifurcation loci; the second is the entry into a limit cycle region, which is seen to occur for magnitudes of δa which are less than values at which jumps occur. In Fig. [3.98], the jumps occur at $|\delta a| \approx 35°$, while limit cycle behavior may be expected to begin at around $\pm$ 20°. This figure, for the particular case $\delta e = 5°$, was plotted using the ARI relationship (3.36), with the "optimum" k being used (k = -0.250). As for the $\delta e = 0°$ case, the value of k is determined as the slope of the line which connects the points N and N' on the relevant bifurcation surface, Fig. [3.99]. It is worthwhile to consider the "optimum" gain k as the slope of the line which connects two points which are on loci marking the onset of limit cycle behavior. The two points would be selected so as to maximize the stable range of δa.

In Fig. [3.99], only the major bifurcation branches are plotted. Note that, for $\delta e = 5°$, the non-jump region of δa is generally quite insensitive to variations in k (the ARI gain). But it turns out for this case that the non-limit-cycle range of δa is greatest for the value of k (-0.250 here) which connects the points N and N'. More work is being completed in this area, viz., the effect of the ARI gain k on both stability ranges for δa: limit cycle and jump (roll departure). The results will appear in forthcoming reports.

Time history results for the pitch-down roll maneuver case are presented in Fig. [100a]. It can be seen that there is limit cycle behavior both at the pre-jump aileron setting of 24°, as well as the post-jump value of 40°. The jump occurs at around 17 sec., just after δa is changed to 40°. These results are consistent with the predictions of Fig. [3.98].

The studies conducted thus far show that definite improvement in performance results from doing control system design using the bifurcation surfaces. Even for the most simple situation, a control law of the form (3.36), there are significant improvements. For the above pitch-down case, the ARI $\bar{p}$ vs. δa plot, Fig. [3.98], shows that limit cycle behavior will be avoided if $|\delta a| < 18°$. If there is no ARI ($\delta r = 0°$; see Fig. [3.34]), this region is only $\pm$ 13°. In this case (and also for the $\delta e = -5°$ case, presented below), the jump stability region is not particularly sensitive to k, as Fig. [3.99] indicates. However, for smaller values of δe, as noted earlier, jump stability is particularly sensitive to k (for smaller values of δe, i.e., $|\delta e| \leq 4°$, limit cycle behavior is not predominant on the major equilibrium branches). Time histories are compared in Fig. [3.100]for the $\delta e = 5°$ case. For the same δa history, there is a noticeable improvement in response when ARI is active (Fig. [3.100a]), as opposed to no ARI ($\delta r = 0°$ Fig. [3.100b]). Note especially the reduced amplitudes for all of the δa settings, and the lack of oscillation, after transients, at $\delta a = 12°$. The rolling pullout maneuver is a combined pitch-up ($\delta e < 0°$) and roll, executed together. For the case $\delta e = -5°$, the "optimum" ARI gain k = 0.118. This gain is optimum in the sense that the rudder control is specified by Eq. 3.36, and in the sense that k has a value which is the slope of the line connecting the N-N' points in the relative bifurcation surface.

The equilibrium plot, $\bar{p}$ vs. δa, for aircraft H in a rolling pullout maneuver is given for the ARI (k = 0.118) and non-ARI (k = 0°; $\delta r = 0°$) cases in Figs. [3.101 and 3.40], respectively. As for the $\delta e = 5°$ case,

a comparison of these figures clearly shows that limit cycles are avoided over a much larger δa range ($\pm 32°$) with ARI than without ($\pm 20°$). Additionally, time history comparisons of the ARI and non-ARI systems (Fig. [3.102]),as for the 0 and 5° settings of δe, show improved response over all of the values of δa. Note particularly that $\bar{\alpha}$ does not change sign when δa moves to 30° from 12°, and longitudinal buffeting (α oscillations) is greatly reduced at this setting of δa. Furthermore, roll rate $\bar{p}$ has a lower average value at $\delta a = 30°$ for the ARI case, as can be verified by comparing the respective histories of roll angle, $\bar{\phi}$. Note further, for $\delta a = 30°$, that the frequencies of oscillation are reduced with ARI, and that there is a tendency for the oscillations to dampen out. Fig. [3.102b] shows the damping out of the variables more clearly, as δa is held to 30° for 16 sec. This tendency is not evident in the non-ARI case; indeed, $\delta a = 30°$ is a setting for possible limit cycle activity, according to Fig. [3.40]. The time history Fig. [3.102c] at $\delta a = 30°$ certainly supports the results of Fig. [3.40].

Plots of the ARI gain k versus equilibrium angle-of-attack $\bar{\alpha}$ show nonlinear behavior in the $\bar{\alpha} < 10°$ region; however, the values of k as derived from the bifurcation surfaces are in the neighborhood of the ARI gain values presented in [11]. Results of a comparison of the BACTM ARI gain with others [11,15] will be presented in a later report. At this time, it seems that BACTM is fully capable of deriving satisfactory command augmentation schemes, as the above example indicates.

Notation for Figs. 3.2 - 3.102

P,p = Equilibrium Roll rate ~ Deg/Sec

DR, δr = Rudder Angle ~ Deg

DA, δa = Aileron Angle ~ Deg

DE, δe = Elevator Angle ~ Deg

S = Stable

U = Unstable with one real positive eigenvalue

A = Unstable with two real positive eigenvalues

B = Unstable with three real positive eigenvalues

C = Unstable with four real positive eigenvalues

D = Unstable with five real positive eigenvalues

L = Unstable with one pair of complex eigenvalues

E = Unstable with one real and one pair complex eigenvalues

F = Unstable with two real and one pair complex eigenvalues

G = Unstable with three real and one pair complex eigenvalues

H = Unstable with two pairs of complex eigenvalues

I = Unstable with one real eigenvalue and two pairs of complex eigenvalues

Q = Equilibrium pitch rate ∿ deg/sec.

R = Equilibrium yaw rate ∿ deg/sec.

A = Equilibrium angle-of-attack ∿ deg.

B = Equlibrium side-slip angle ∿ deg.

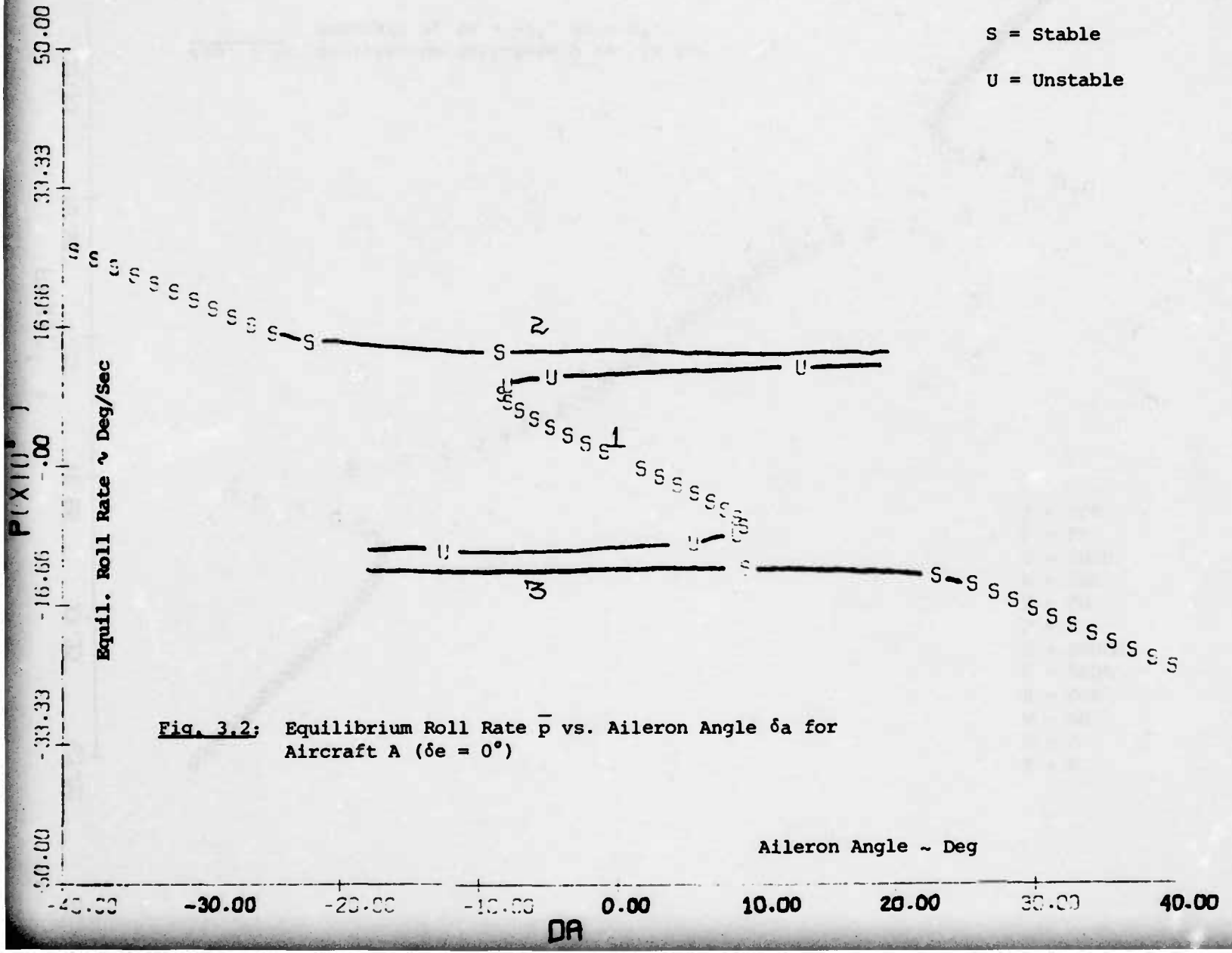

Fig. 3.2: Equilibrium Roll Rate $\bar{p}$ vs. Aileron Angle δa for Aircraft A ($\delta e = 0°$)

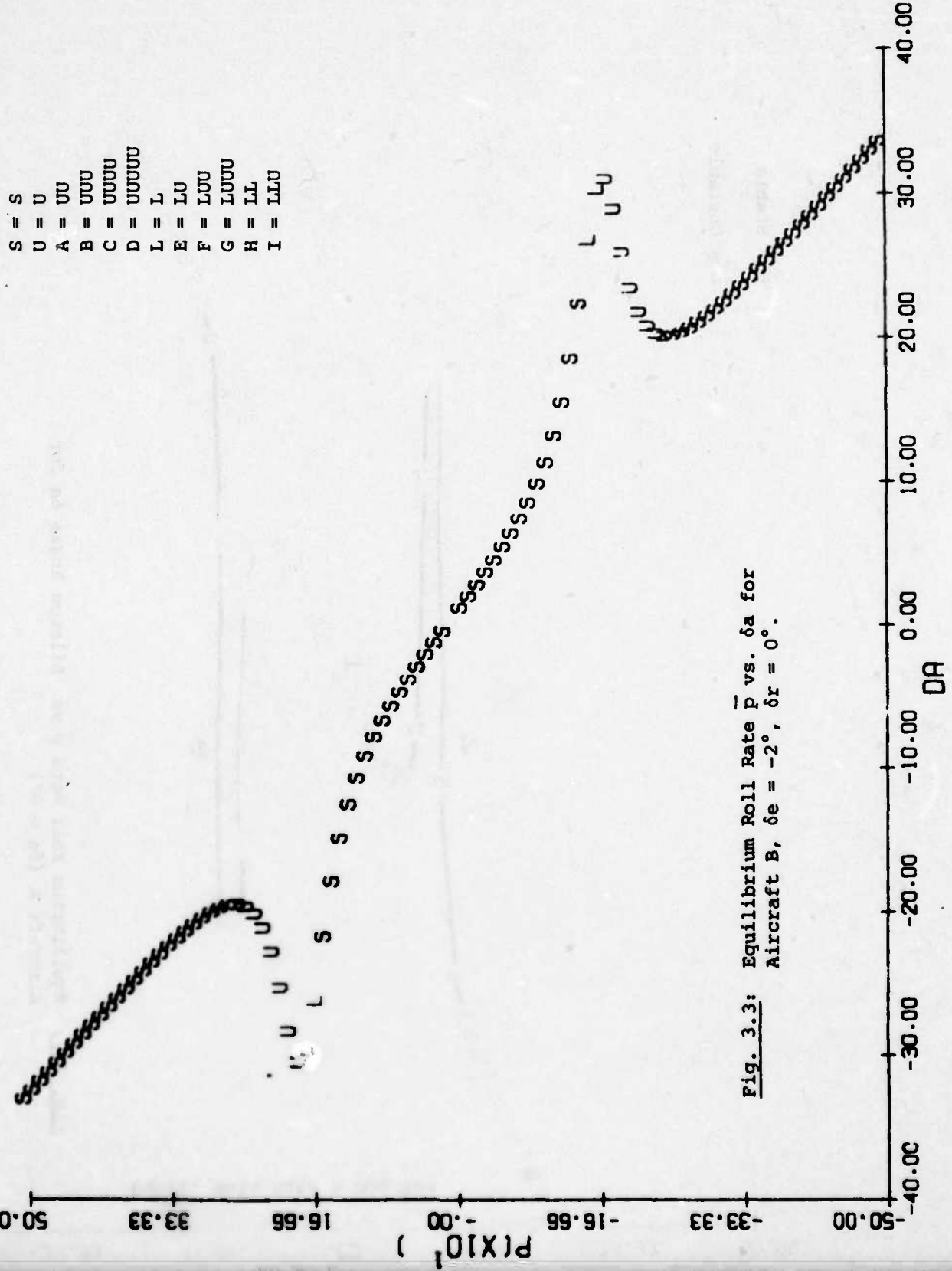

Fig. 3.3: Equilibrium Roll Rate $\bar{p}$ vs. δa for Aircraft B, $\delta e = -2°$, $\delta r = 0°$.

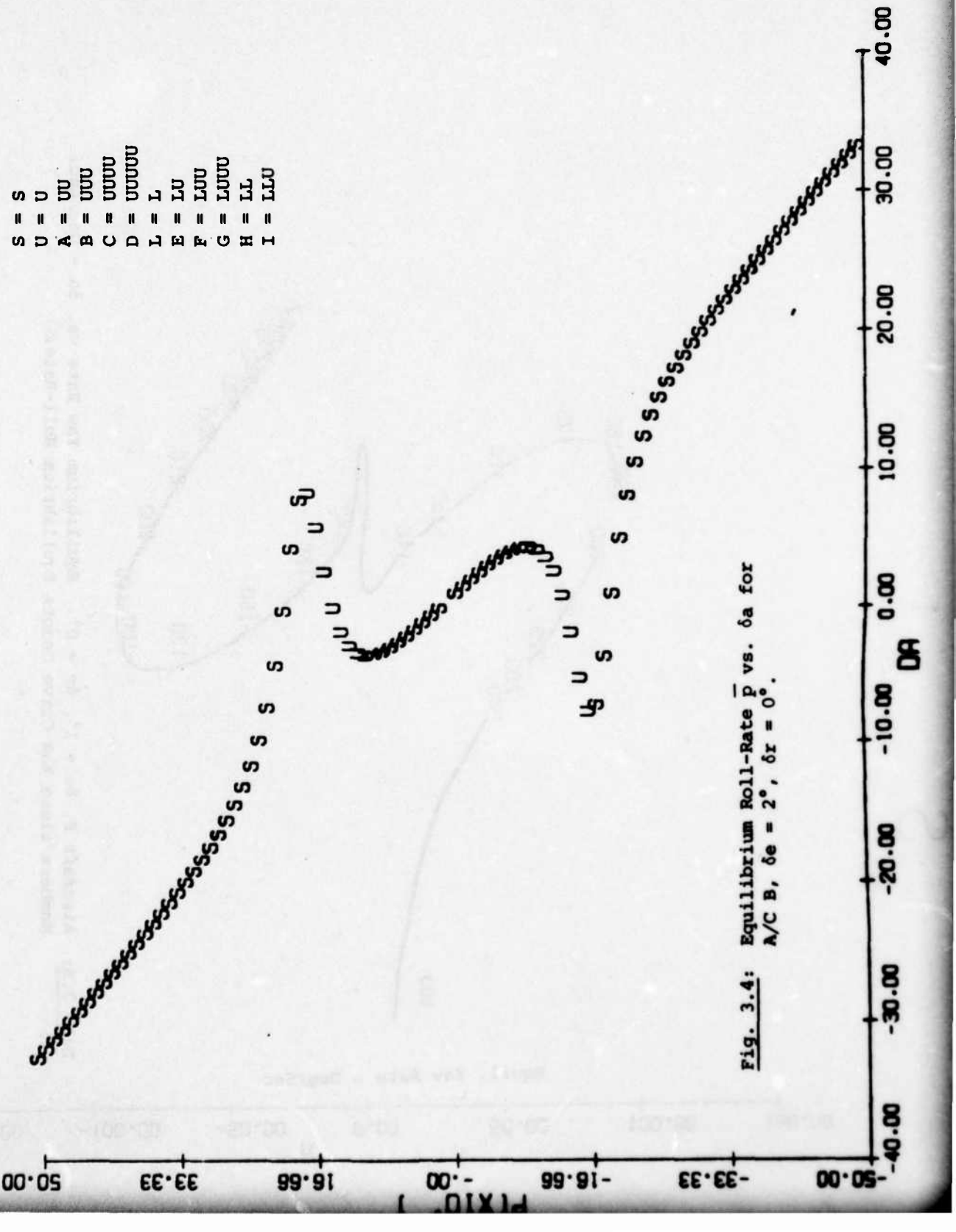

Fig. 3.4: Equilibrium Roll-Rate $\bar{p}$ vs. δa for A/C B, $\delta e = 2°$, $\delta r = 0°$.

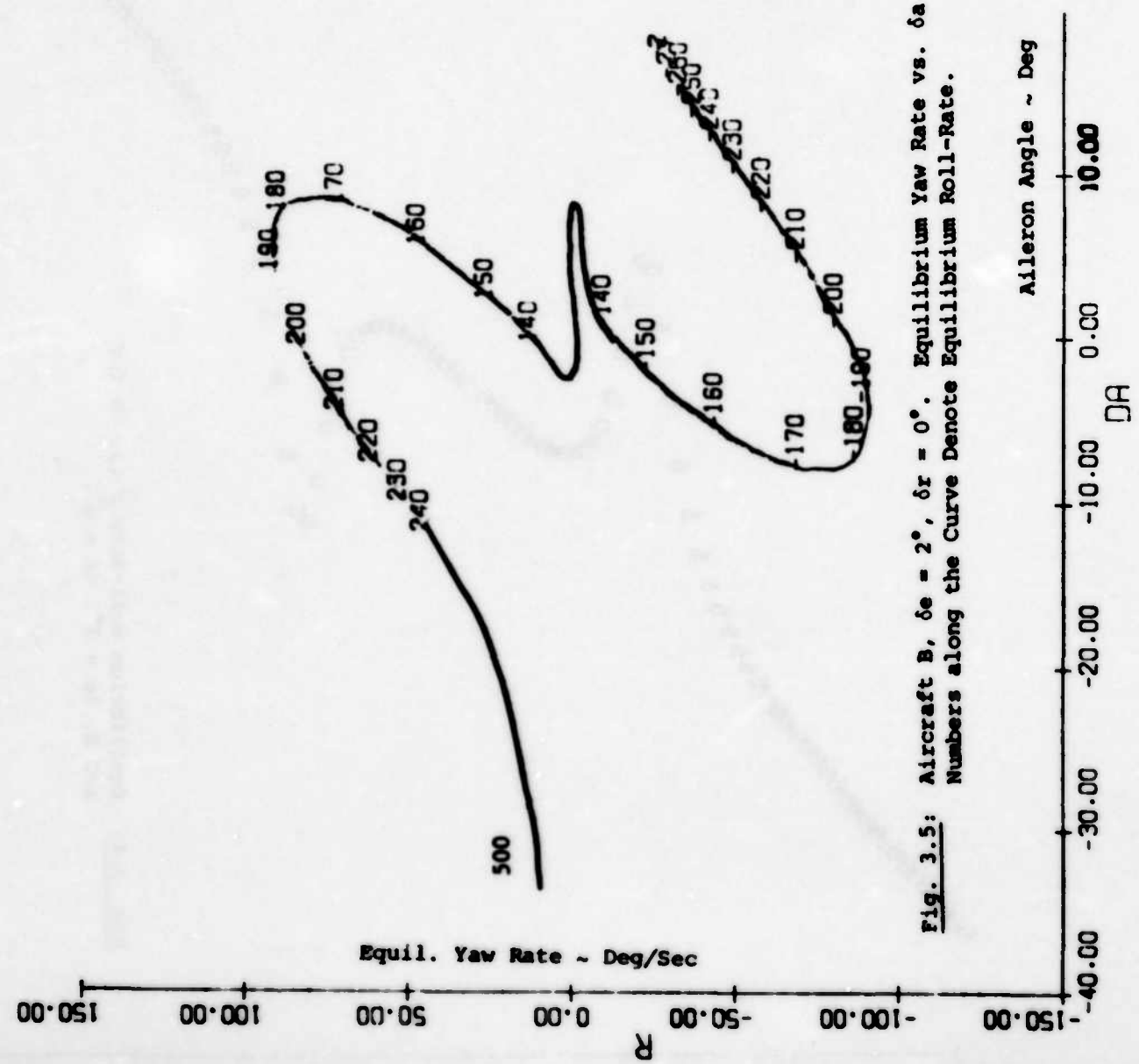

Fig. 3.5: Aircraft B, $\delta e = 2°$, $\delta r = 0°$. Equilibrium Yaw Rate vs. δa - Deg/sec. Numbers along the Curve Denote Equilibrium Roll-Rate.

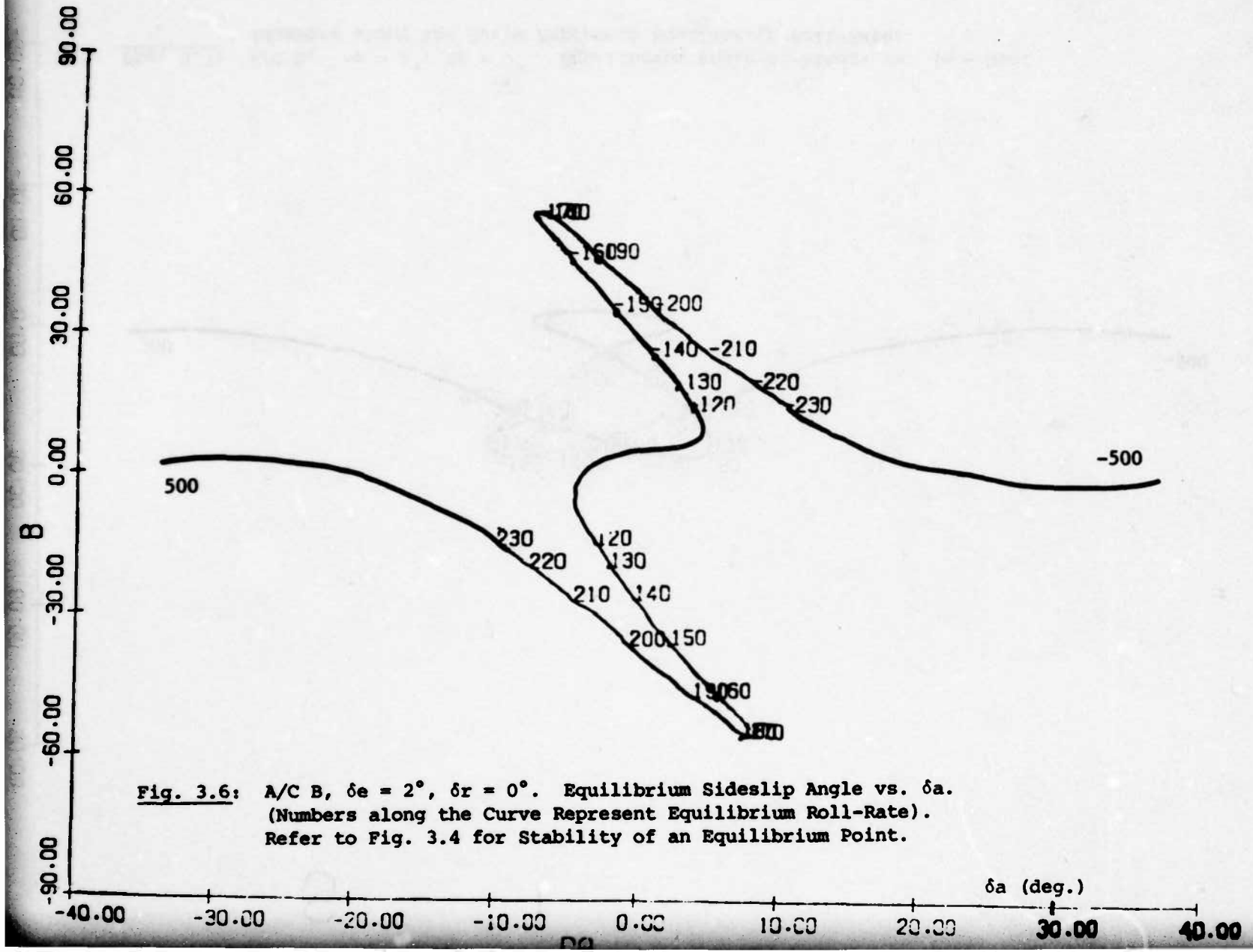

Fig. 3.6: A/C B, δe = 2°, δr = 0°. Equilibrium Sideslip Angle vs. δa. (Numbers along the Curve Represent Equilibrium Roll-Rate). Refer to Fig. 3.4 for Stability of an Equilibrium Point.

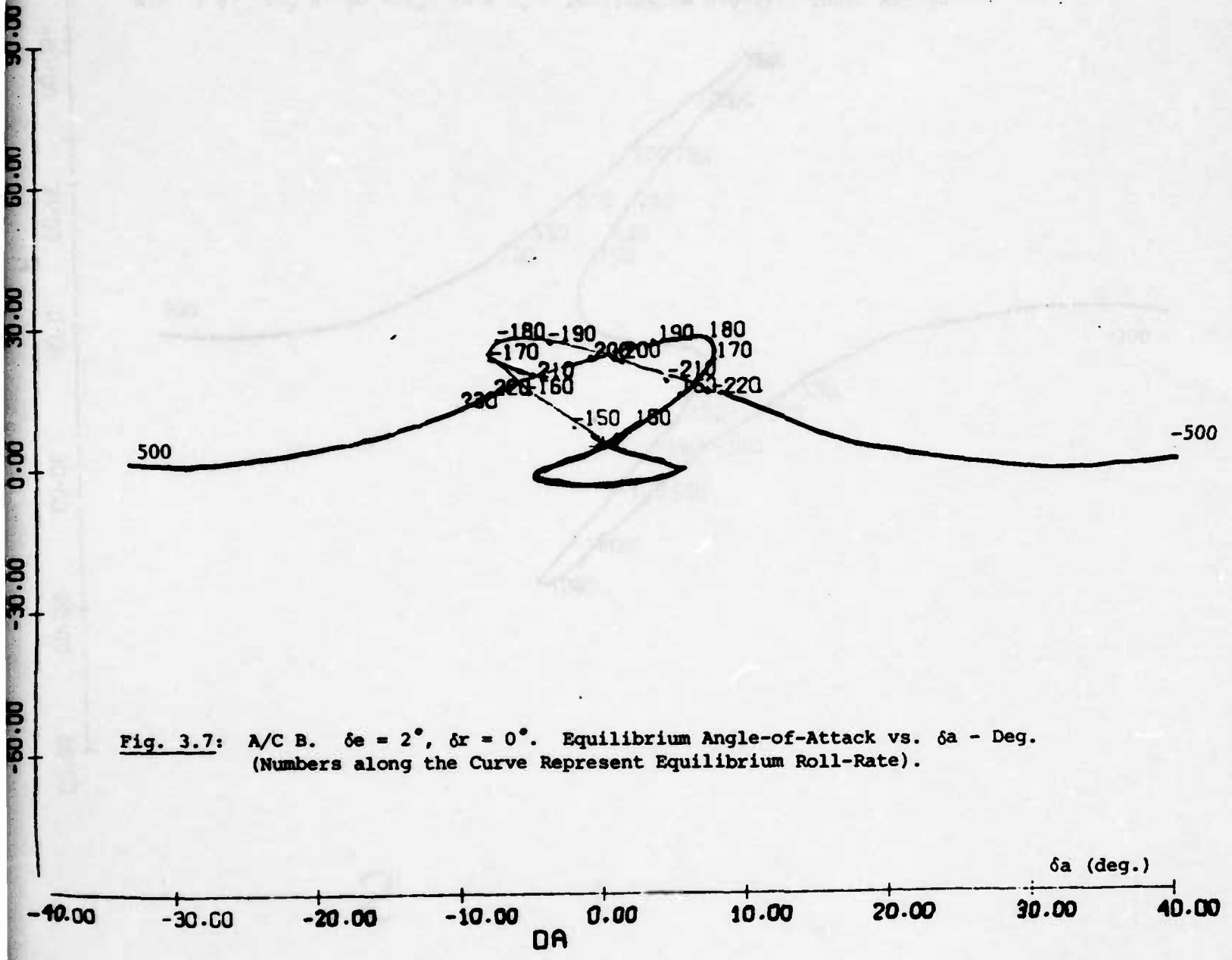

Fig. 3.7: A/C B. $\delta e = 2^\circ$, $\delta r = 0^\circ$. Equilibrium Angle-of-Attack vs. δa - Deg. (Numbers along the Curve Represent Equilibrium Roll-Rate).

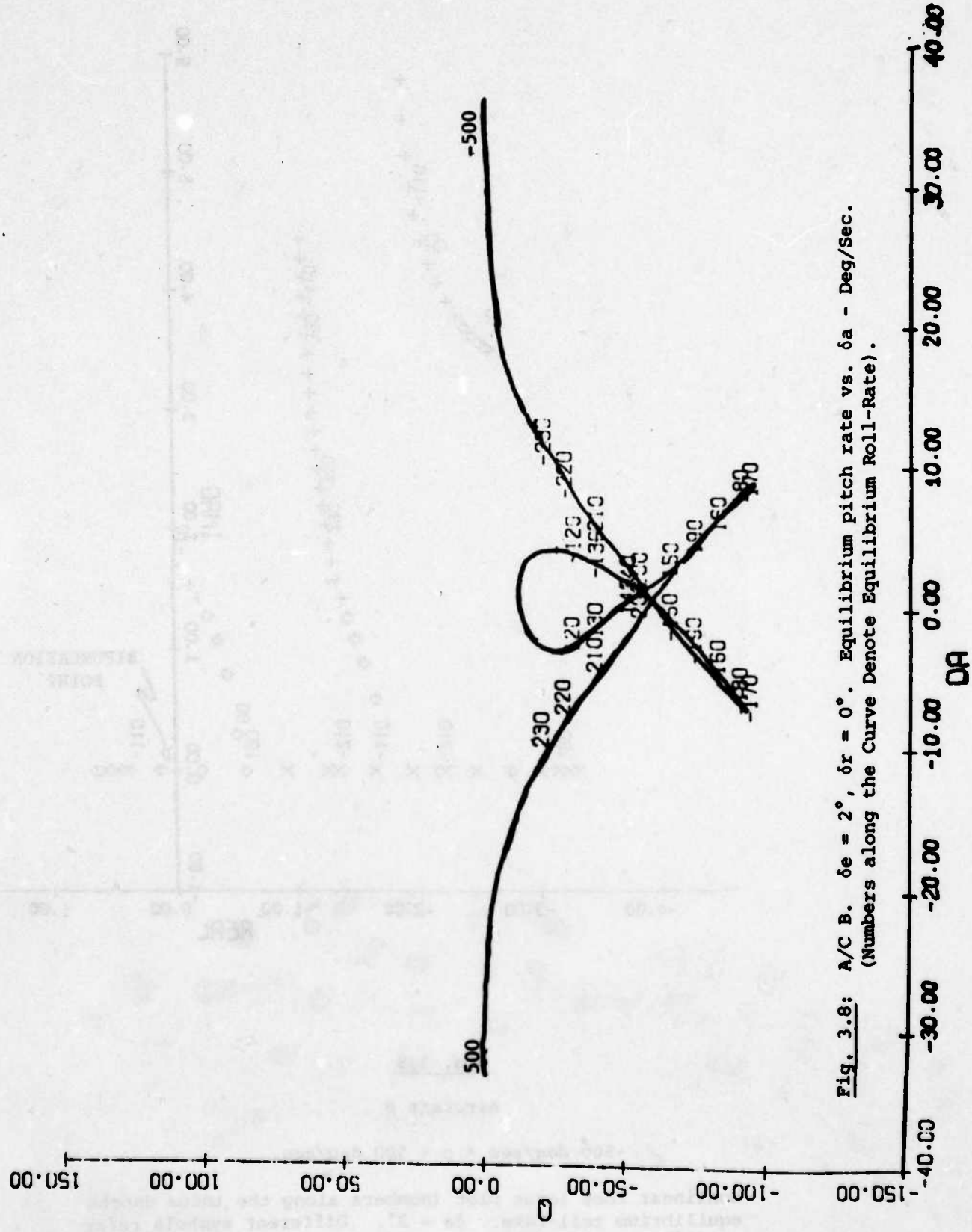

Fig. 3.8: A/C B. $\delta e = 2°$, $\delta r = 0°$. Equilibrium pitch rate vs. δa - Deg/Sec. (Numbers along the Curve Denote Equilibrium Roll-Rate).

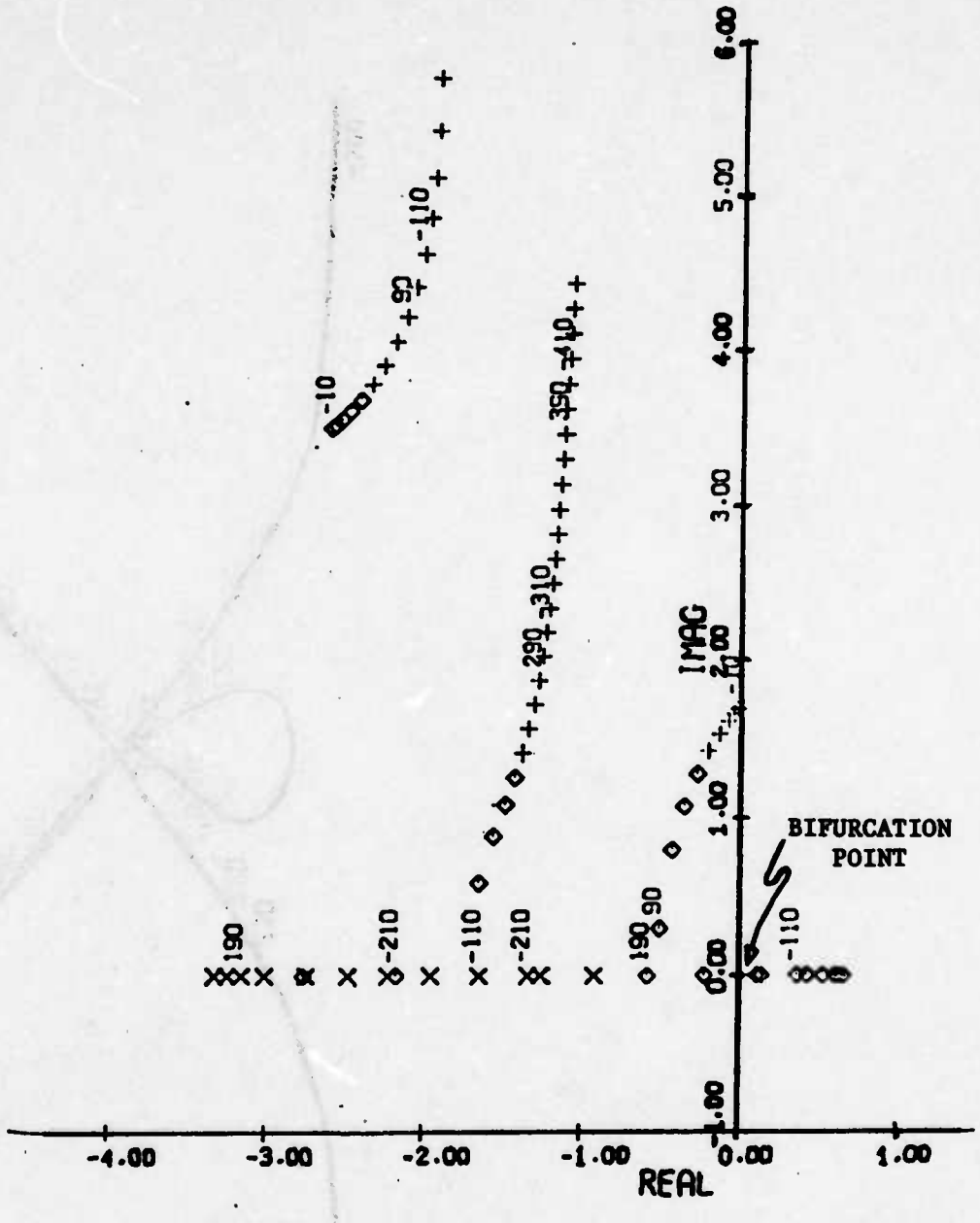

Fig. 3.9

Aircraft B

-500 deg/sec < p < 500 deg/sec.

Nonlinear root locus plot (Numbers along the locus denote equilibrium roll-rate. $\delta e = 2°$. Different symbols refer to different eigenvalues. For complex eigenvalues, only one member of the pair is shown.

Fig. 3.10: A/C B, Bifurcation Surface in (δa, δe) plane. The numbers in each region indicate number of equilibrium points; $\delta_r = 0.$

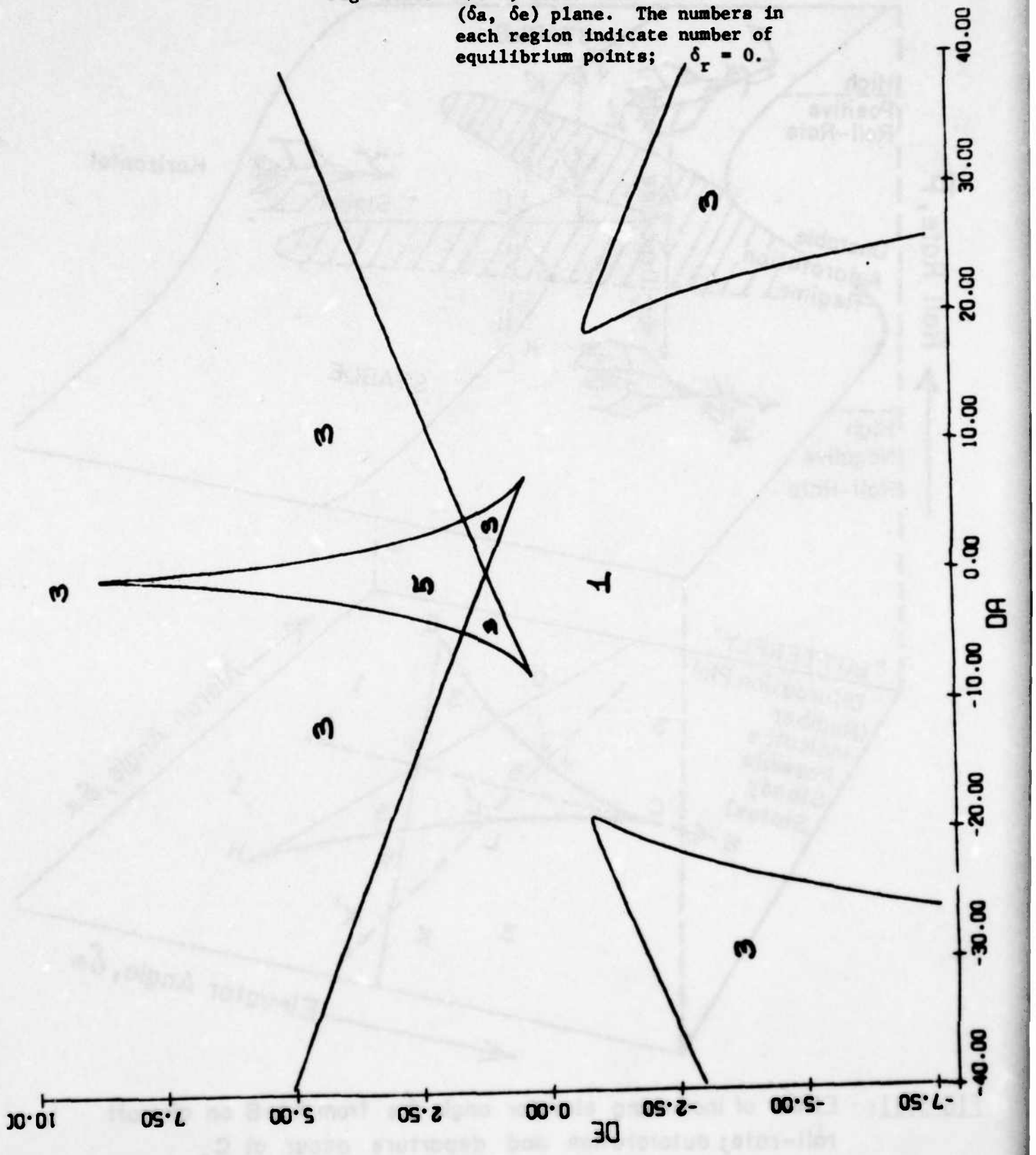

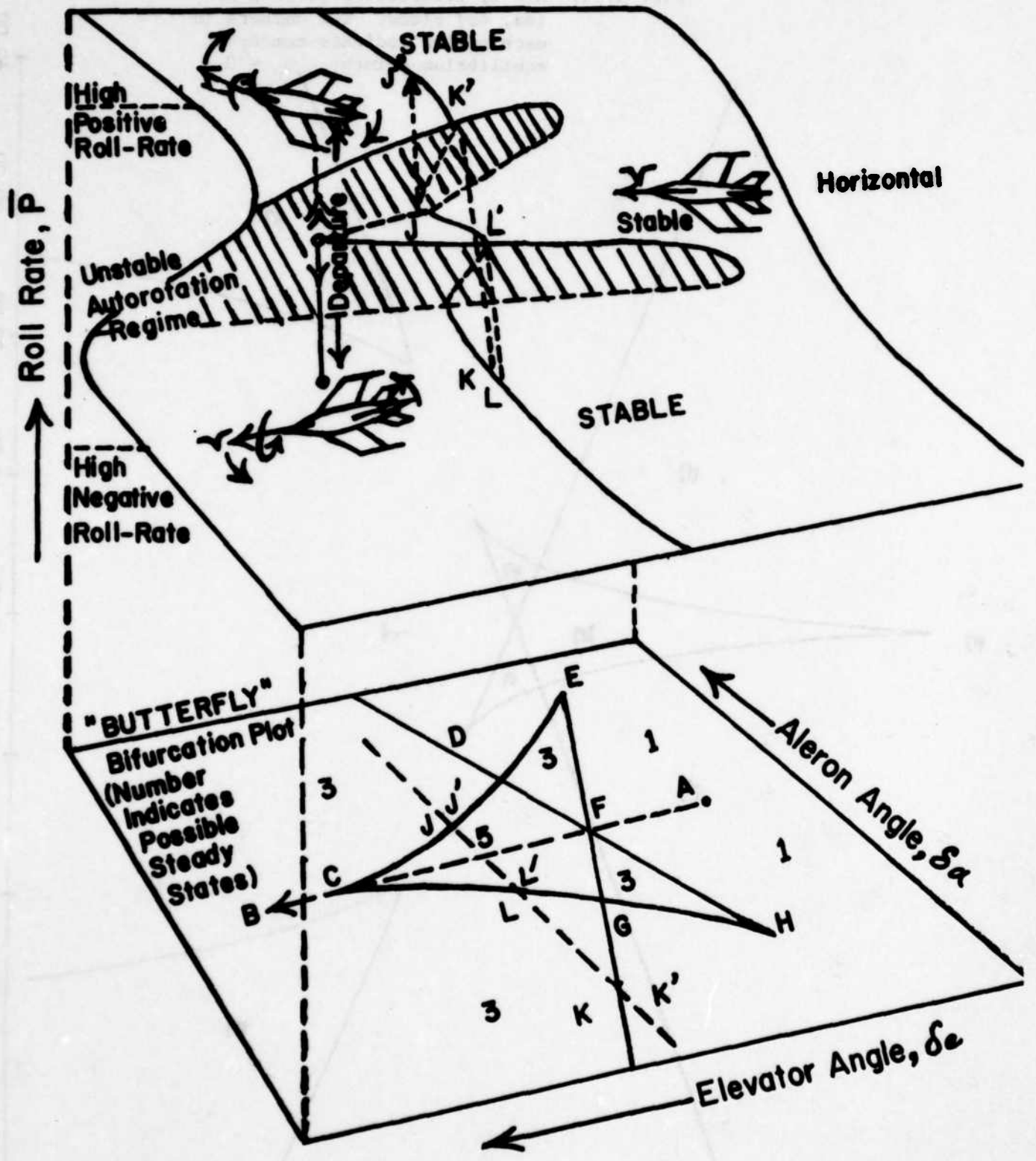

FIG 3.11: Effect of increasing elevator angle δe from A to B on aircraft roll-rate; autorotation and departure occur at C.

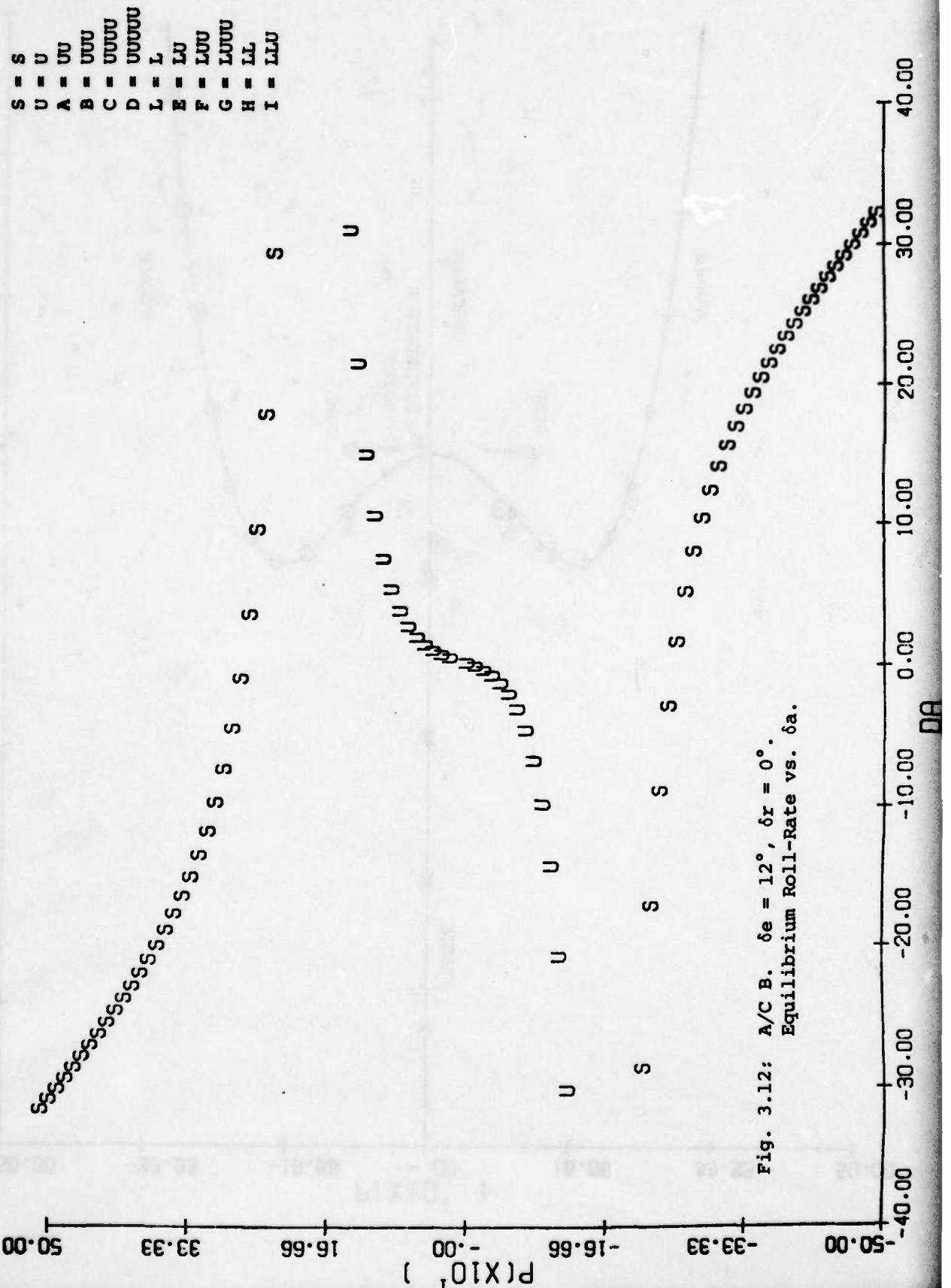

Fig. 3.12: A/C B. δe = 12°, δr = 0°.
Equilibrium Roll-Rate vs. δa.

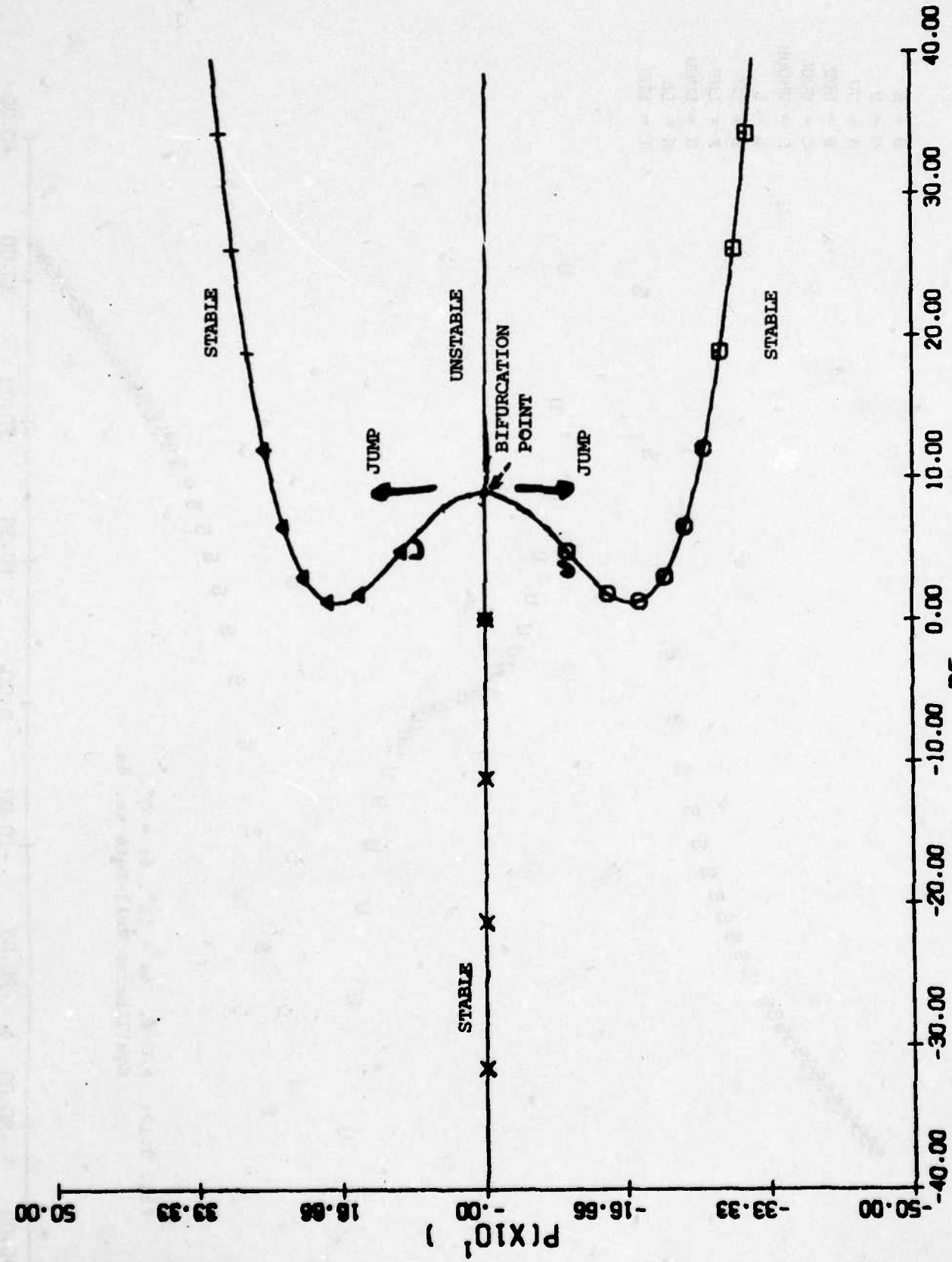

Fig. 3.13: Aircraft B, Equilibrium roll rate vs. δe; $\delta a = 0°$, $\delta r = 0°$.

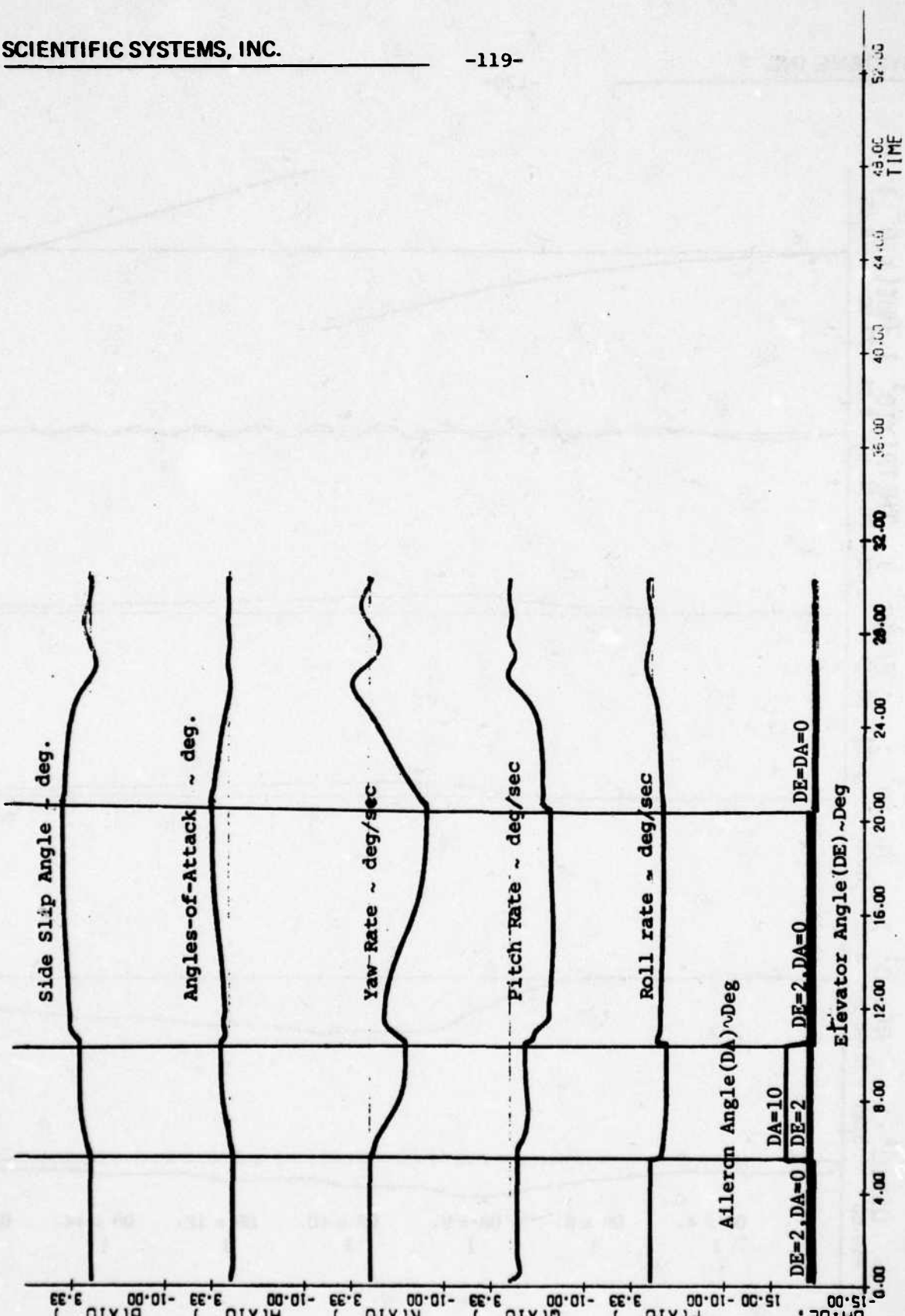

Fig. 3.14: A/C B; Time history plots showing hysteresis and jump behaviour; vertical lines indicate the times at which δa or δe are changed discontinuously.

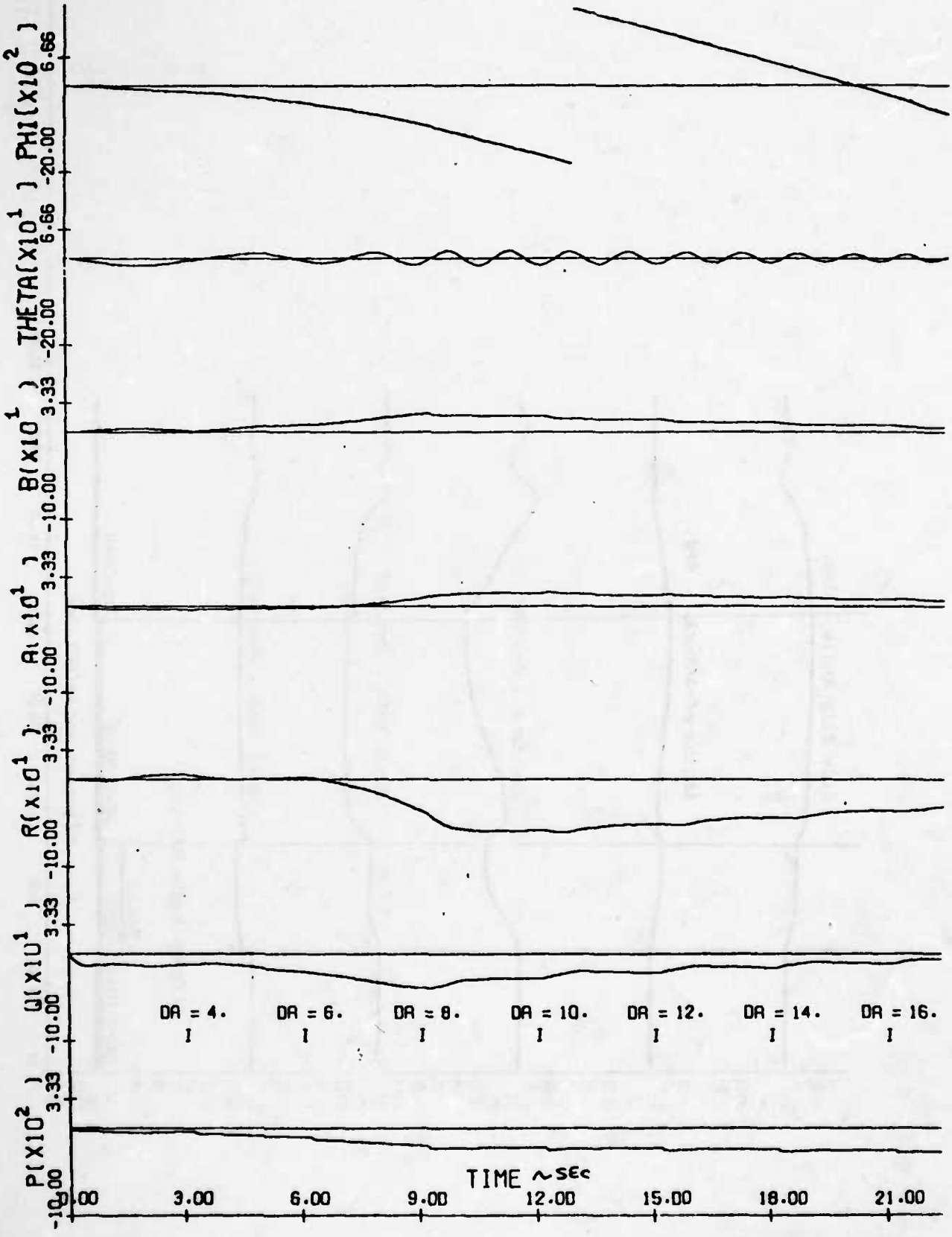

Fig. 3.15: A/C B $\delta e = 2°$, $\delta r = 0°$.
Time history for $\delta a = 2°, 4°, 6°, 8°, 10°, 12°, 14°, 16°$.

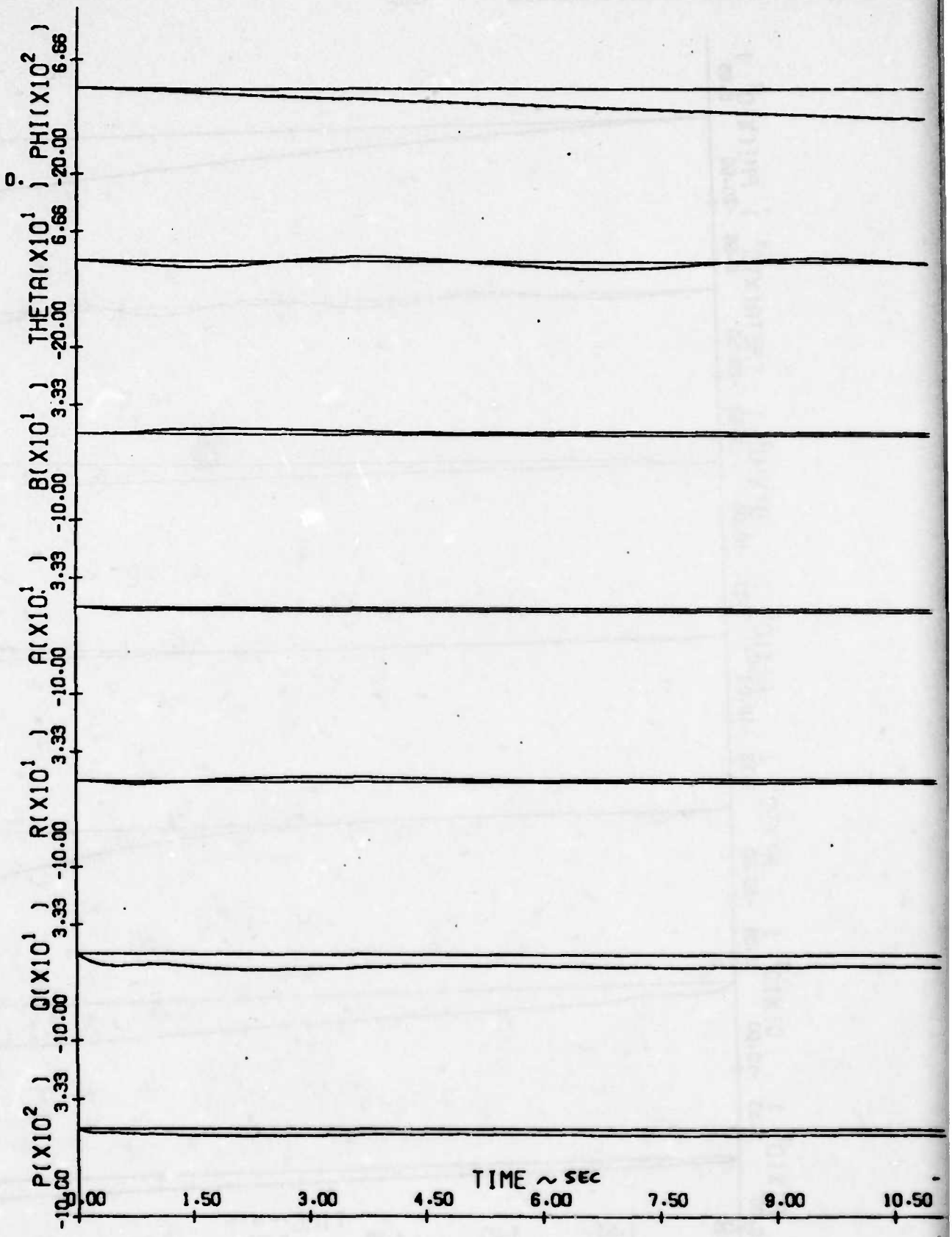

Fig. 3.16: A/C B $\delta e = 2°$, $\delta r = 0°$.
Time history for $\delta a = 3°$.

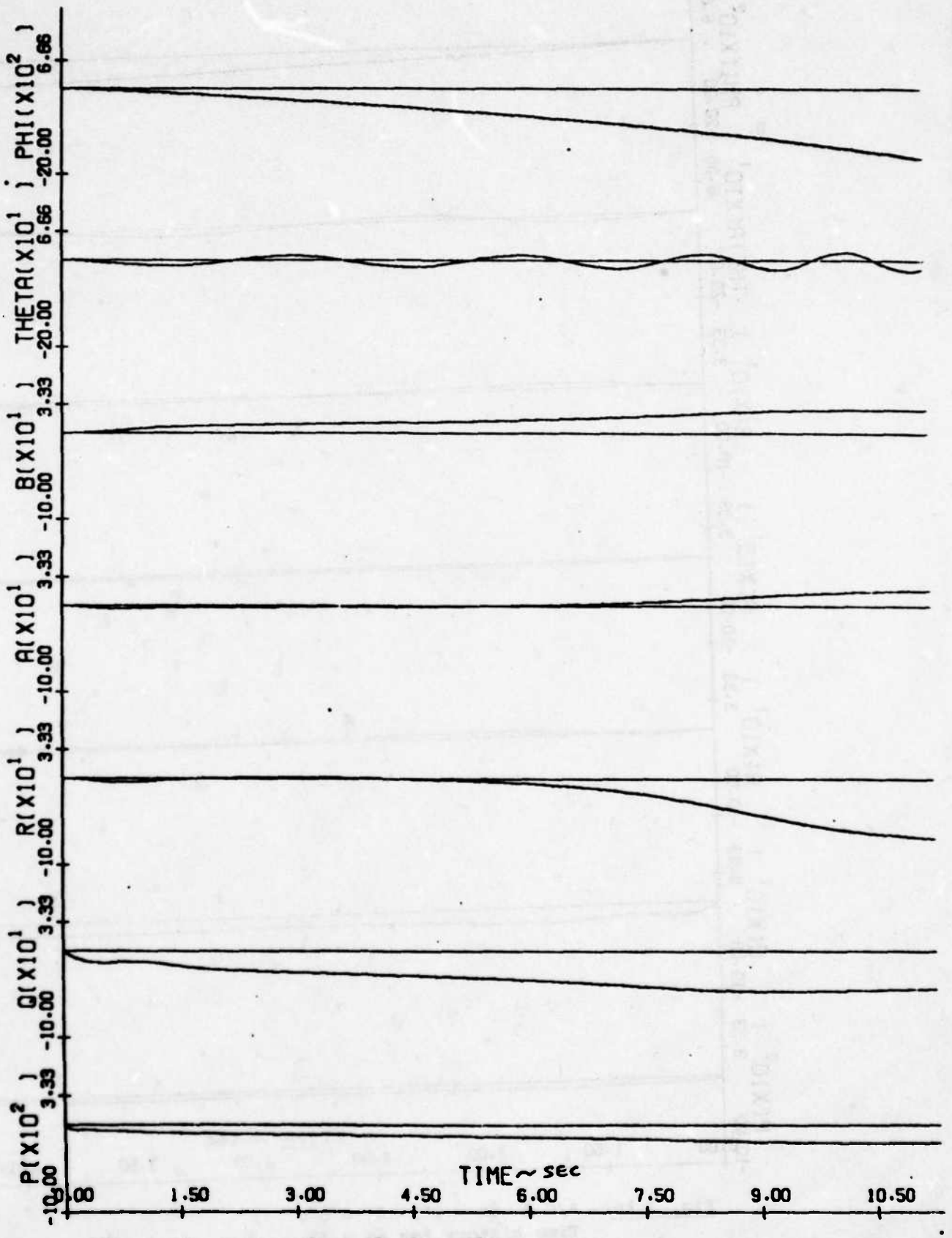

Fig. 3.17: A/C B $\delta e = 2°$, $\delta r = 0°$.
Time history for $\delta a = 4°$.

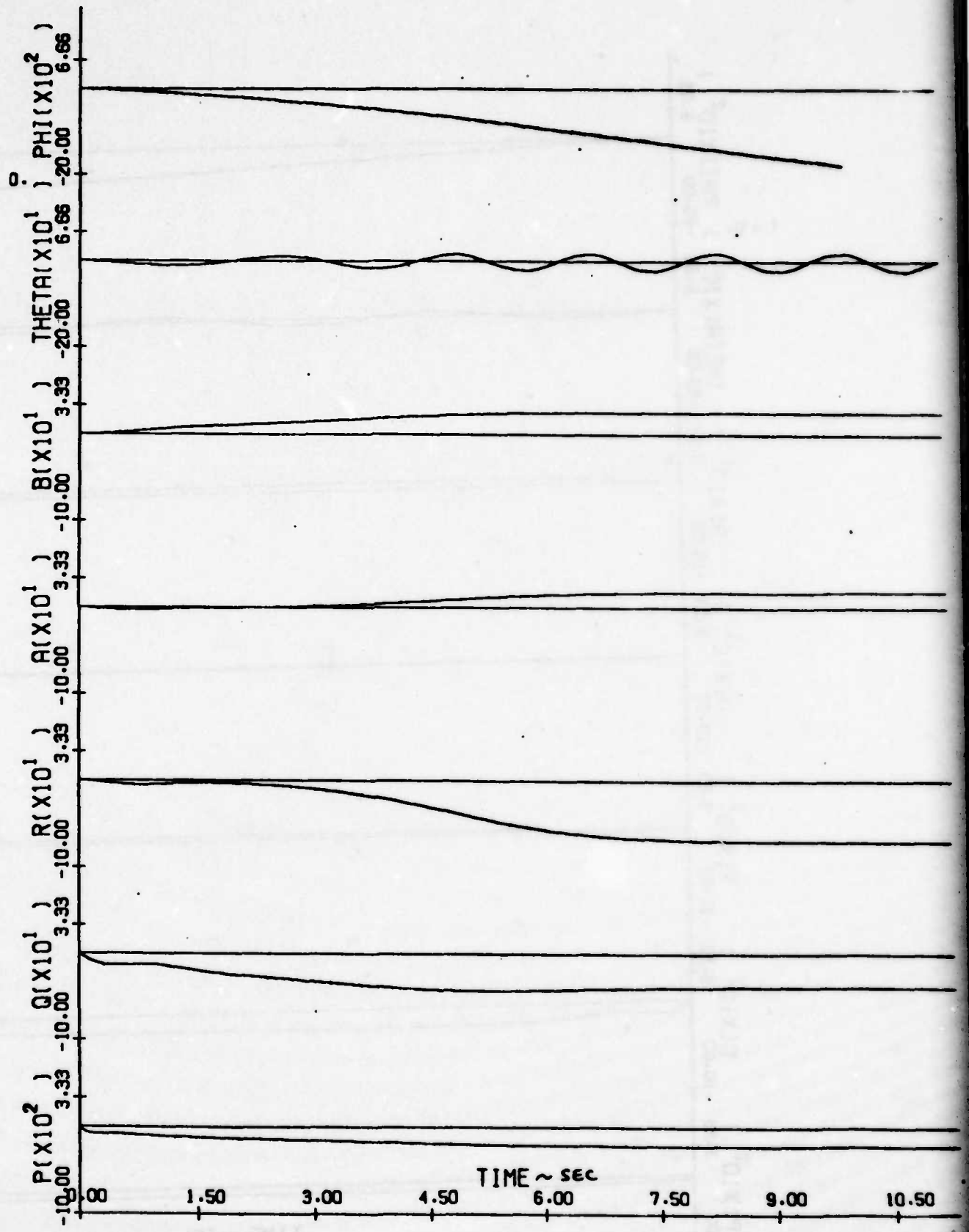

Fig. 3.18: A/C B $\delta e = 2°$, $\delta r = 0°$.
Time history for $\delta a = 5°$.

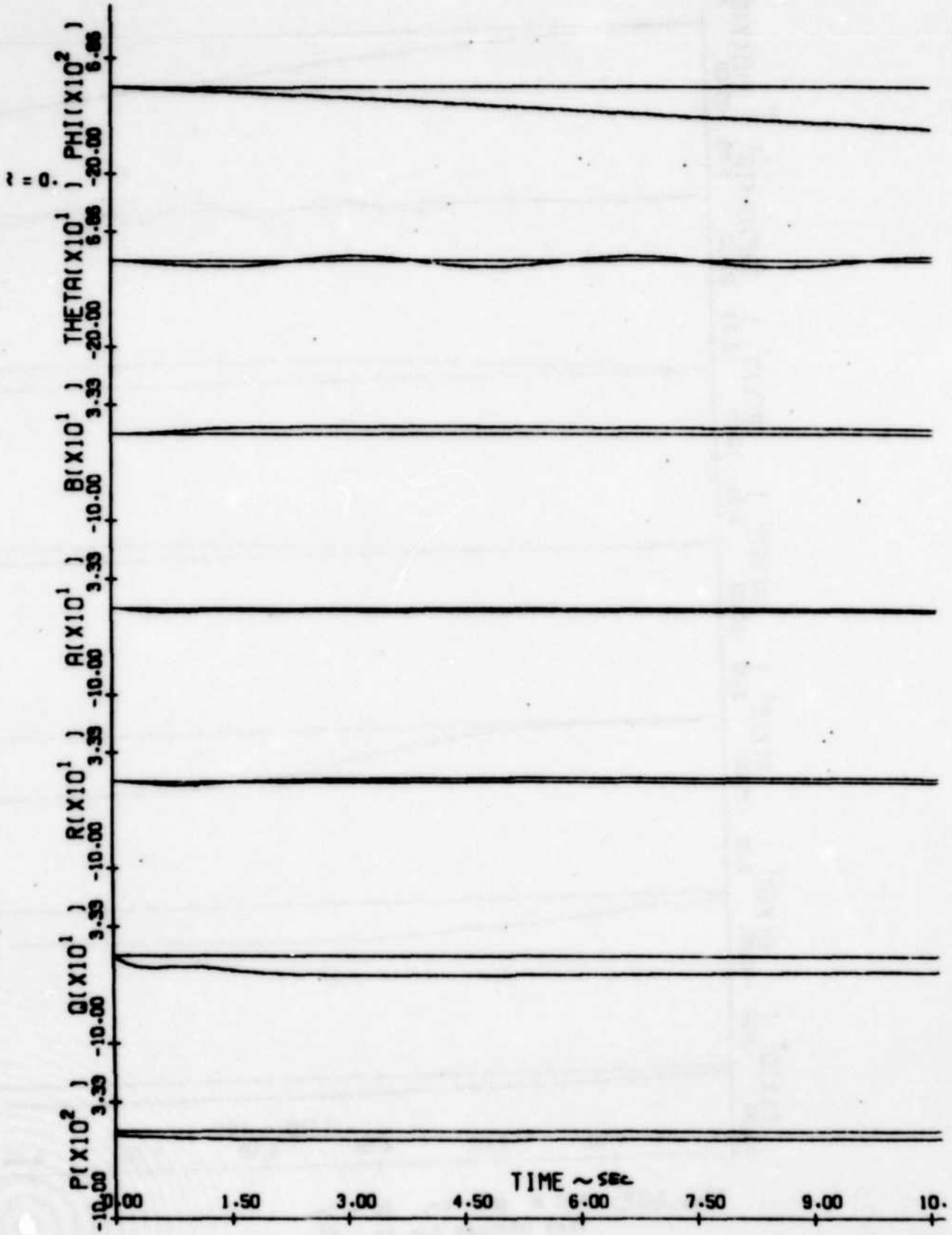

Fig. 3.19: A/C B $\delta e = 2°$, $\delta r = 0°$.
Time history for $\delta a = 3.6°$.

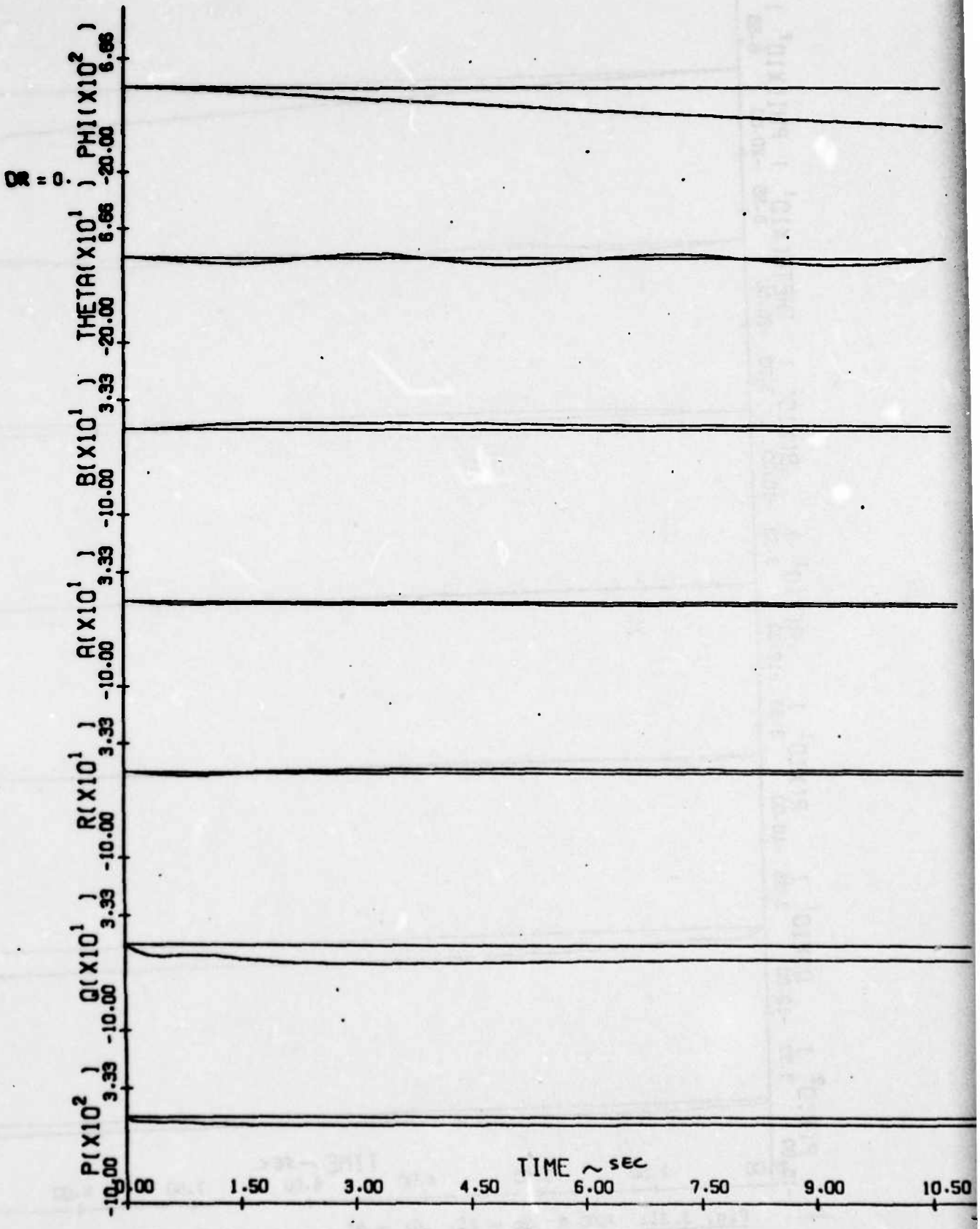

Fig. 3.20: A/C B $\delta e = 2°$, $\delta r = 0°$.
Time history for $\delta a = 3.7°$.

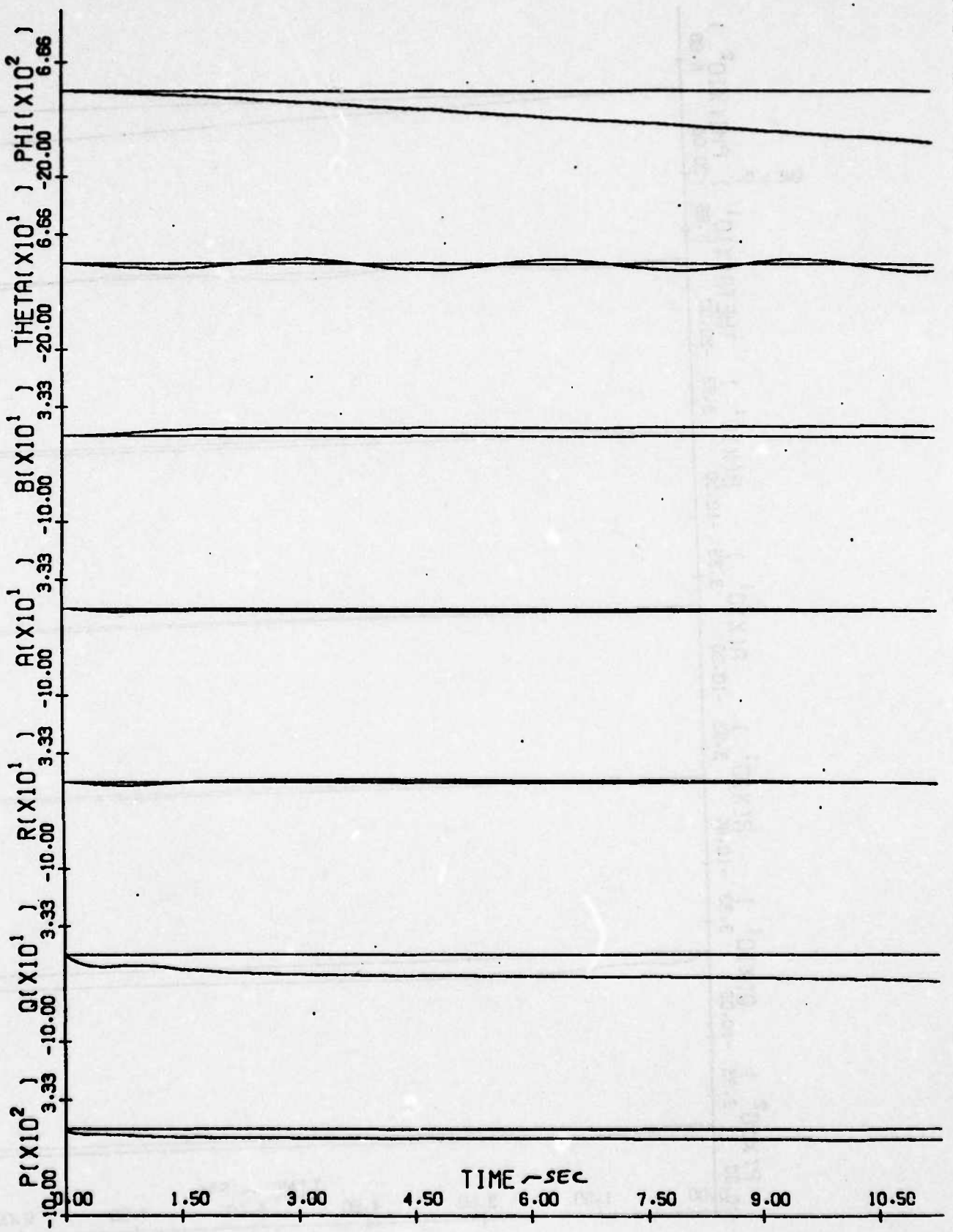

Fig. 3.21: A/C B $\delta e = 2°$, $\delta r = 0°$.
Time history for $\delta a = 3.8°$.

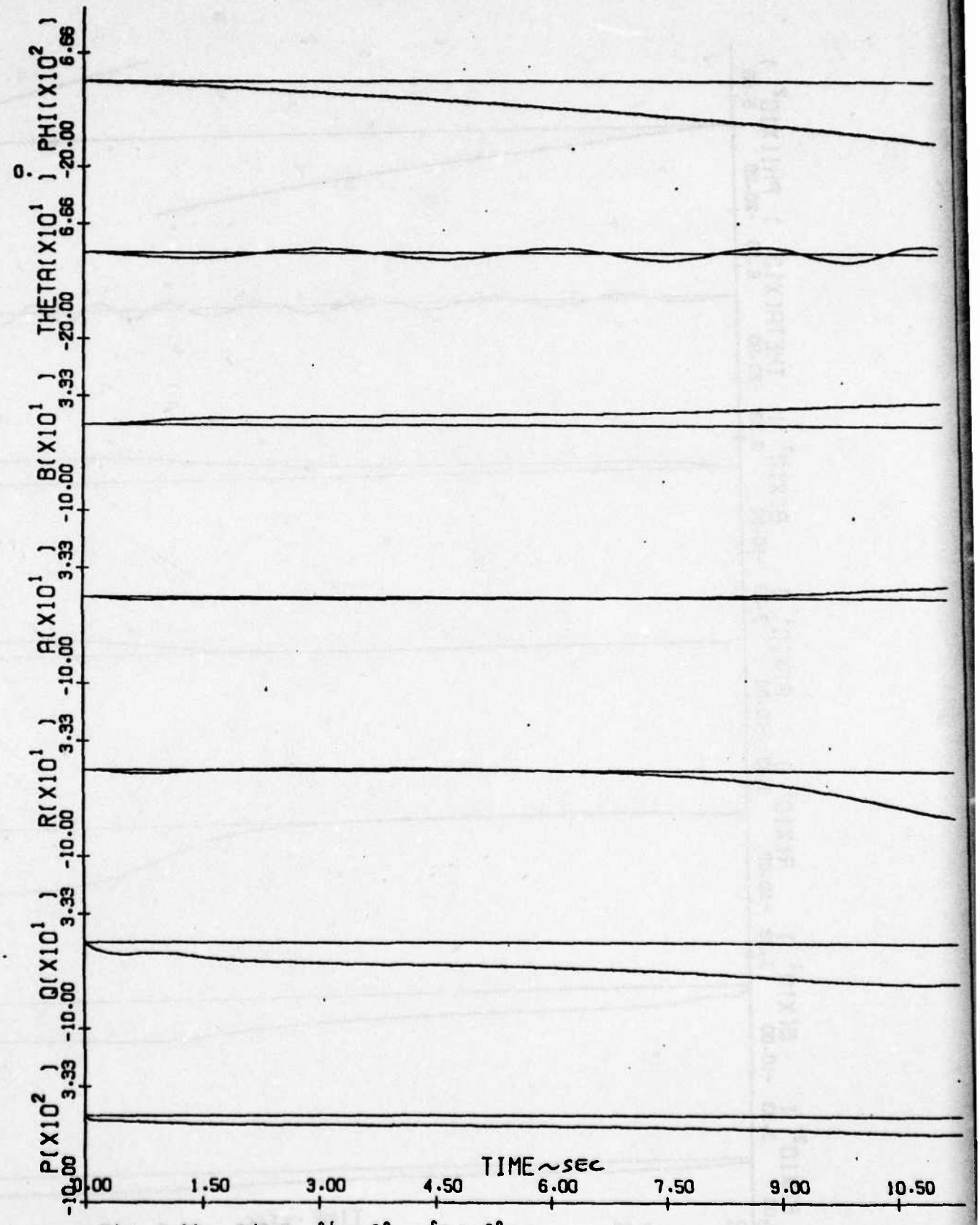

Fig. 3.22: A/C B δé = 2°, δr = 0°.
Time history for δa = 3.9°.

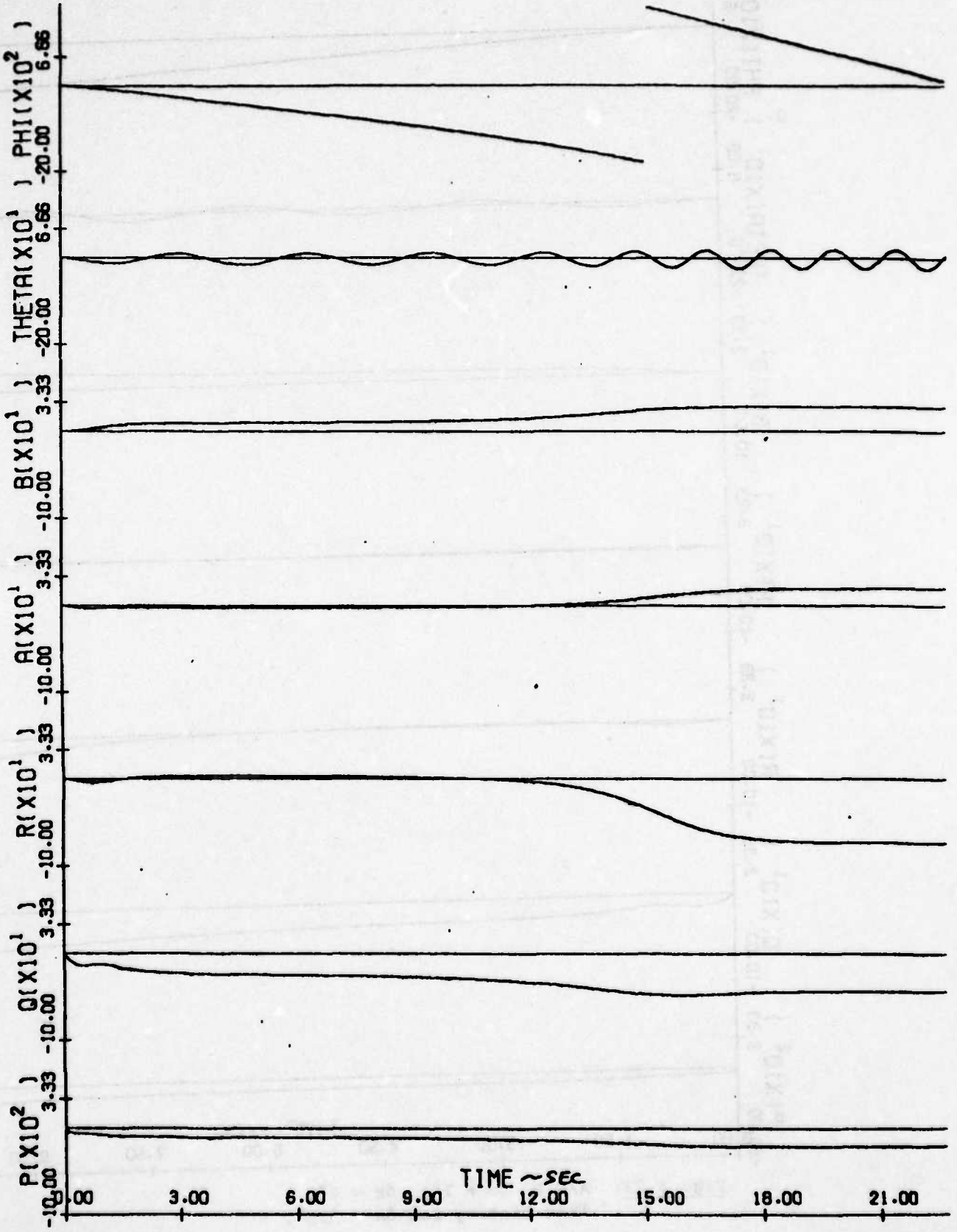

Fig. 3.23: A/C B $\delta e = 2°$, $\delta r = 0°$.
Time history for $\delta a = 3.8°$.

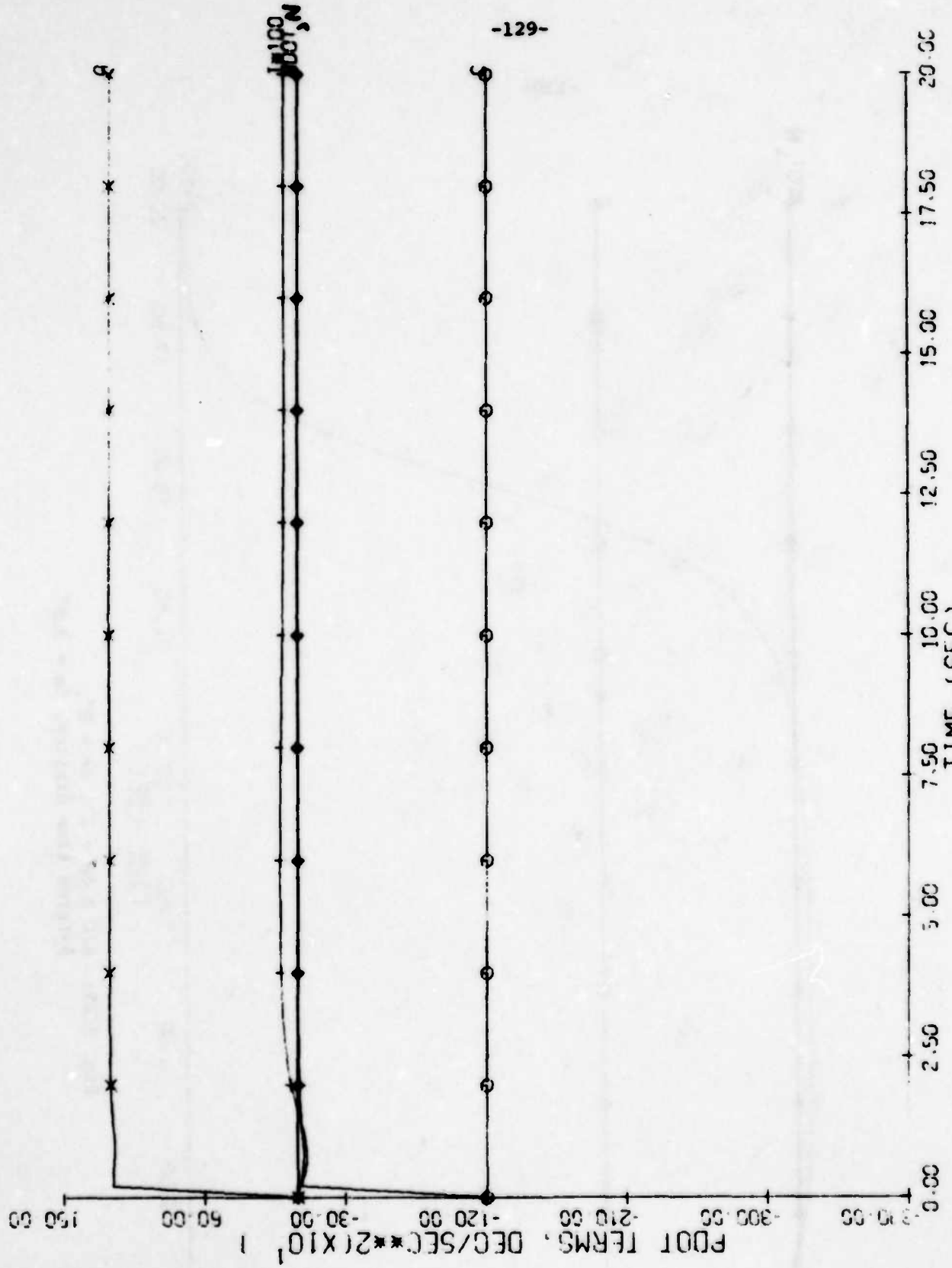

Fig. 3.24: A/C B $\delta e = 2°$, $\delta r = 0°$; $\dot{p}$-terms time history, $\delta a = 3.7°$

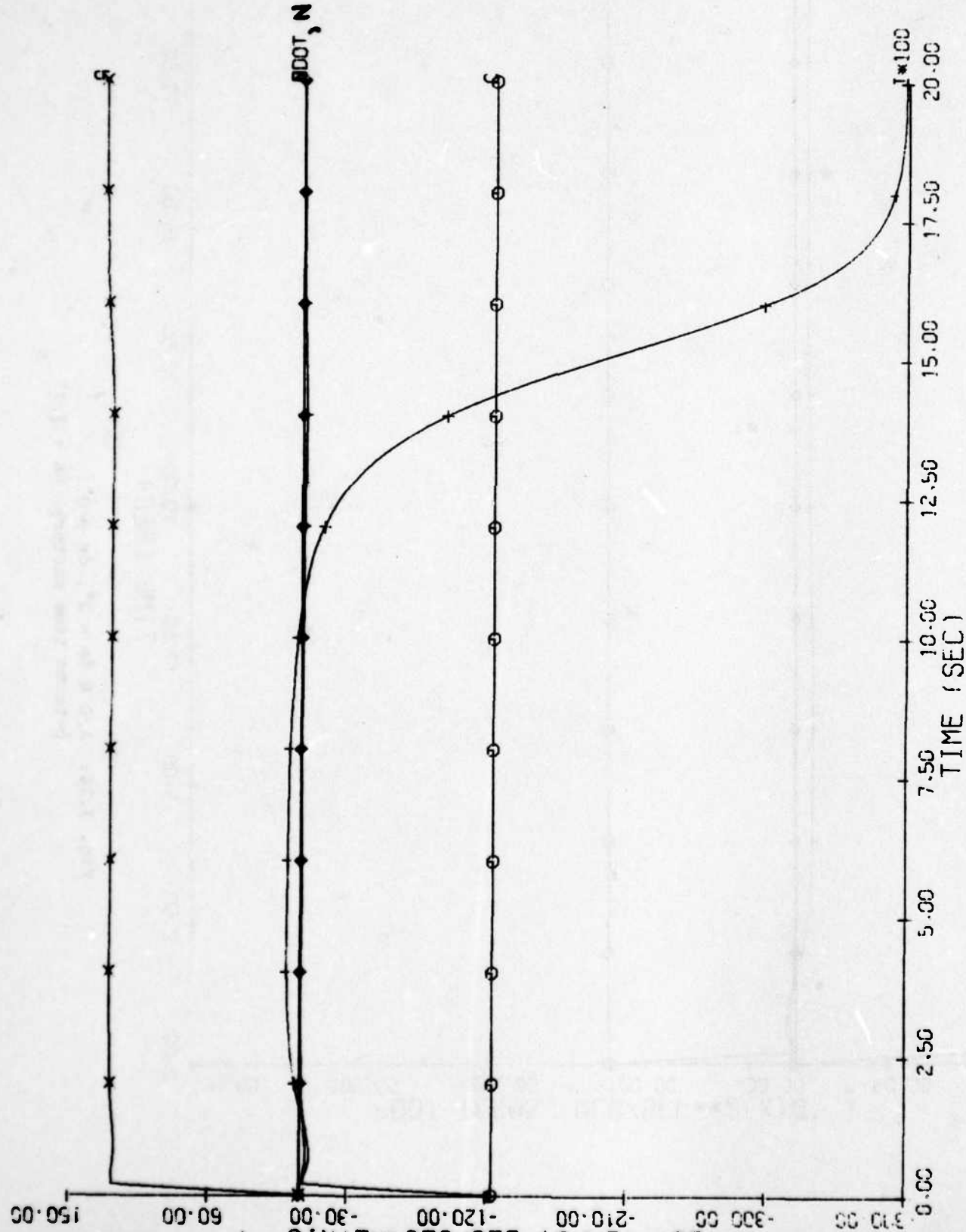

Fig. 3.25: A/C B $\delta e = 2°$, $\delta r = 0°$;
$\dot{p}$-terms time history, $\delta a = 3.8°$

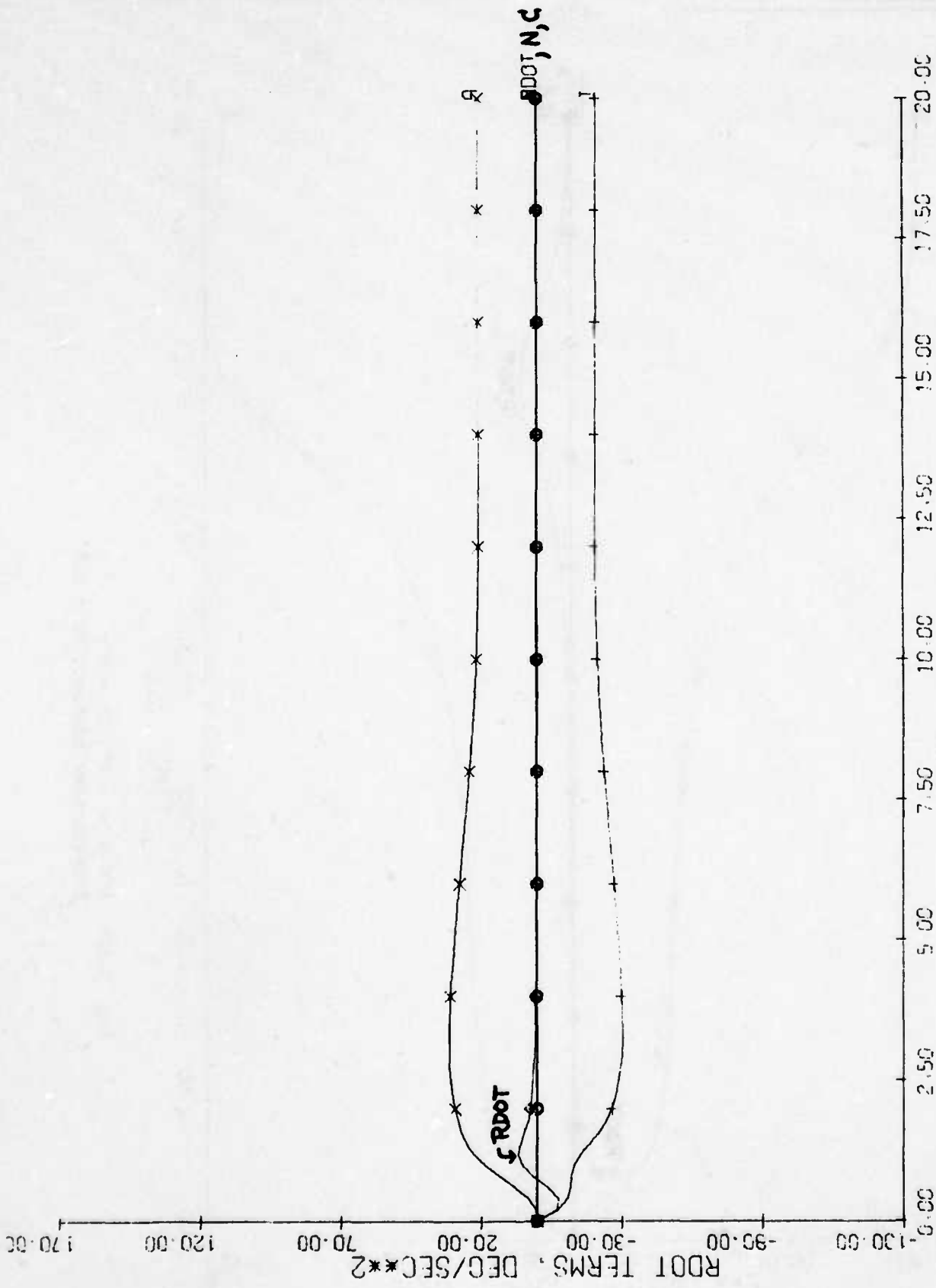

Fig. 3.26: A/C B $\delta e = 2°$; $\delta r = 0°$; $\dot{r}$-terms time history, $\delta a = 3.7°$

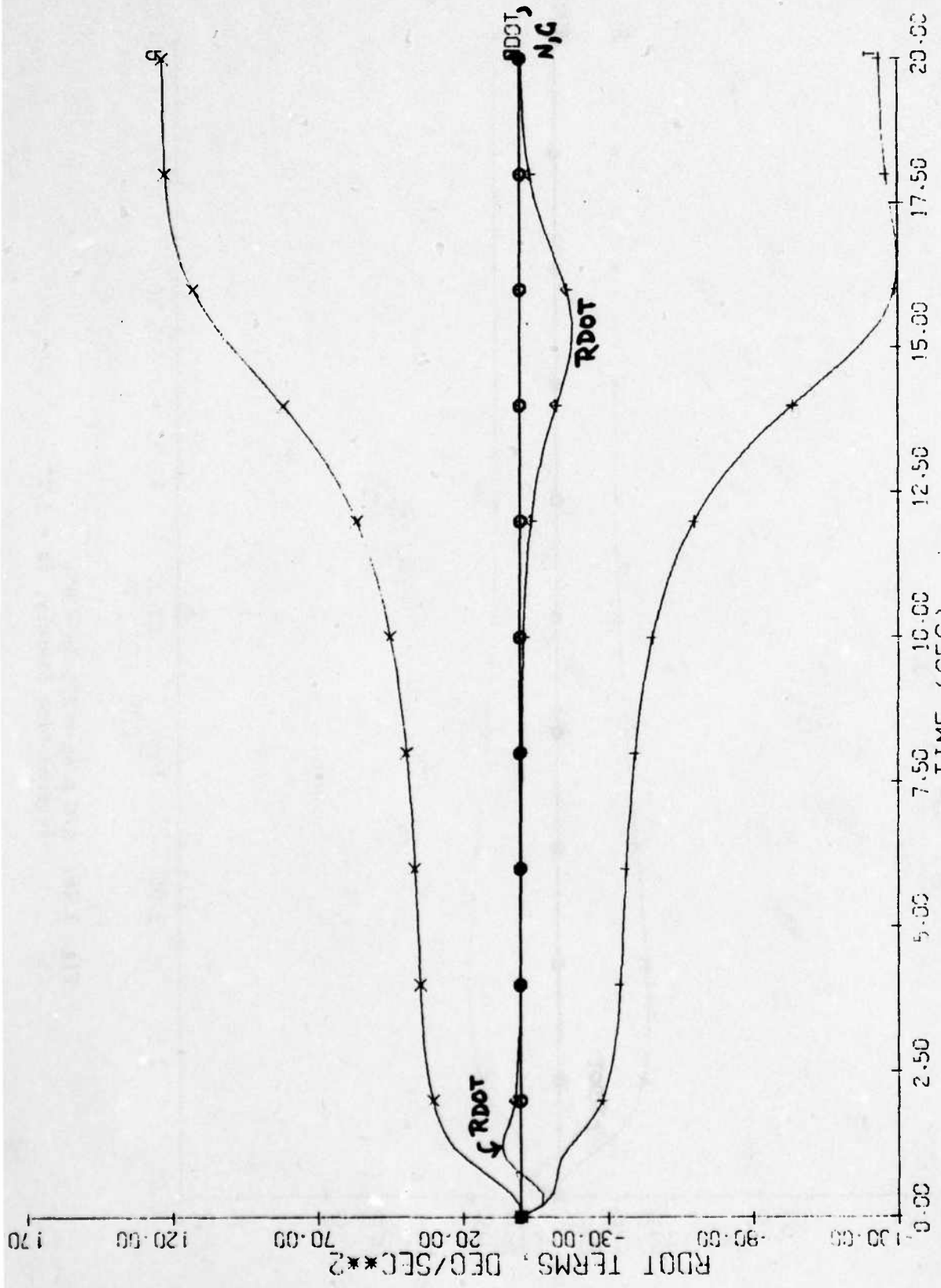

Fig. 3.27: A/C B $\delta e = 2°$, $\delta r = 0°$;
ṙ-terms time history, $\delta a = 3.8°$

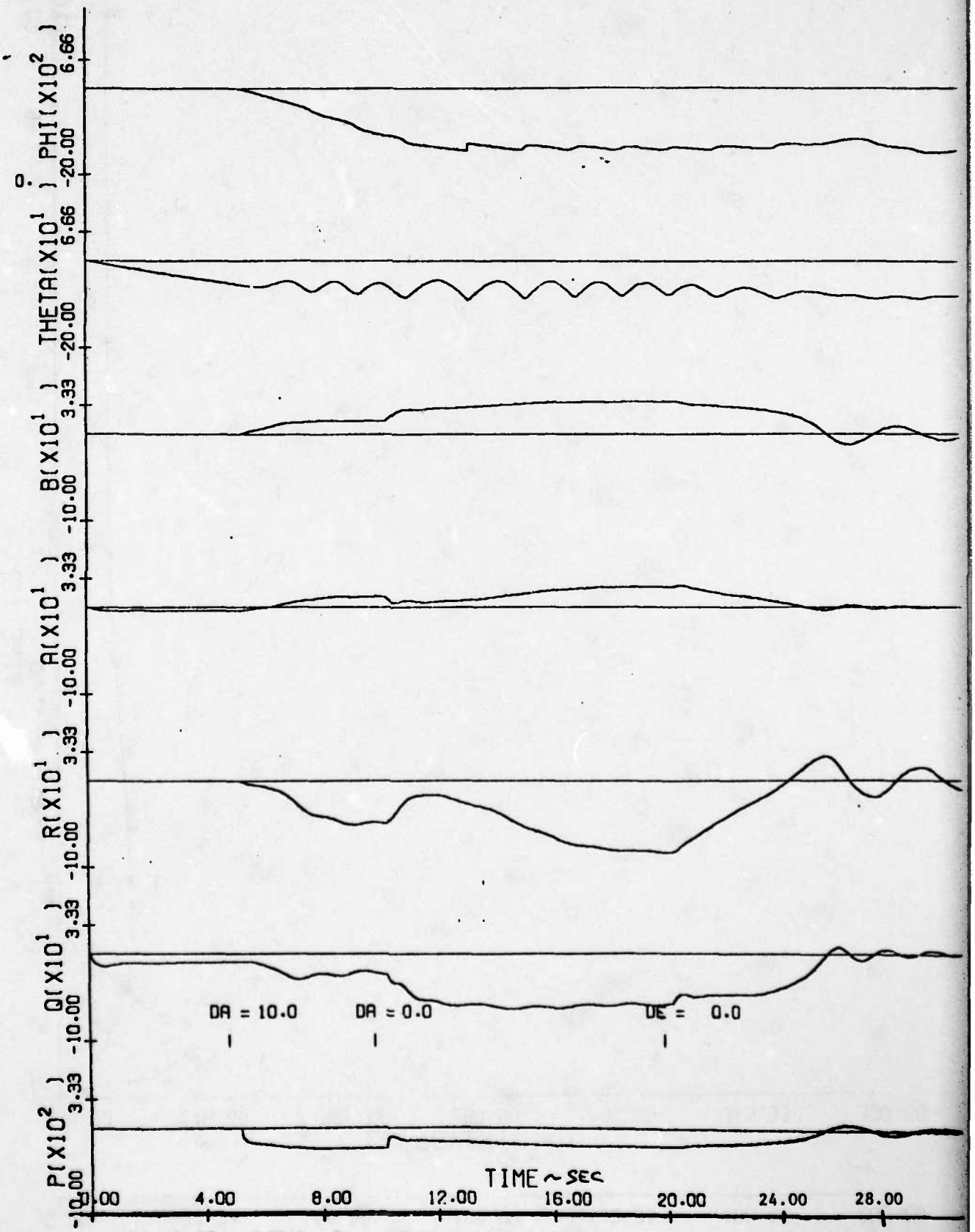

Fig. 3.28: A/C B $\delta r = 0°$.
Time history for $\delta a = 0°$; $\delta e = 2°$;
gravity terms included (see Fig. 3.14).

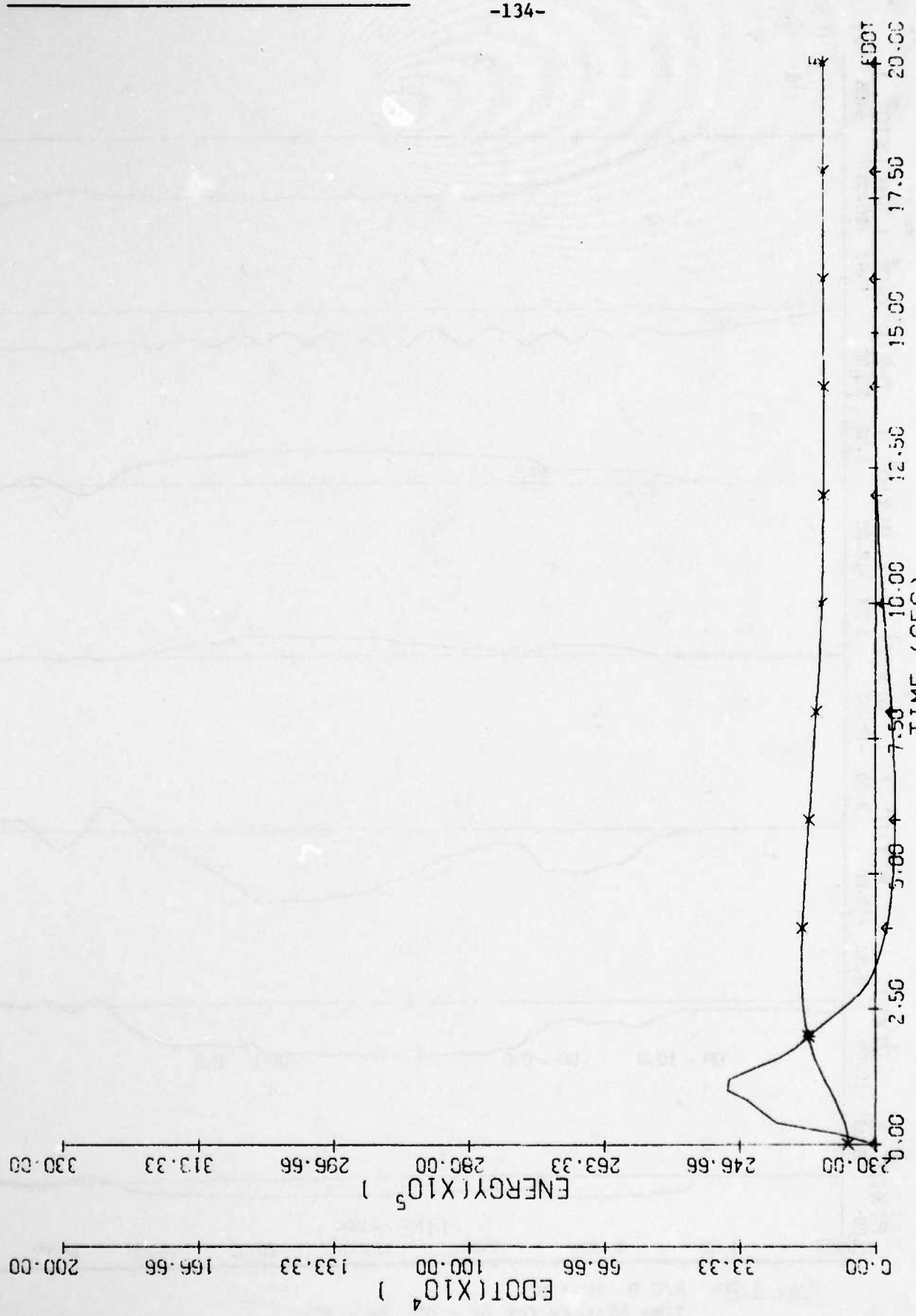

Fig. 3.29: A/C, B $\delta e = 2°$, $\delta r = 0°$;
E, Ė histories for $\delta a = 3.7°$

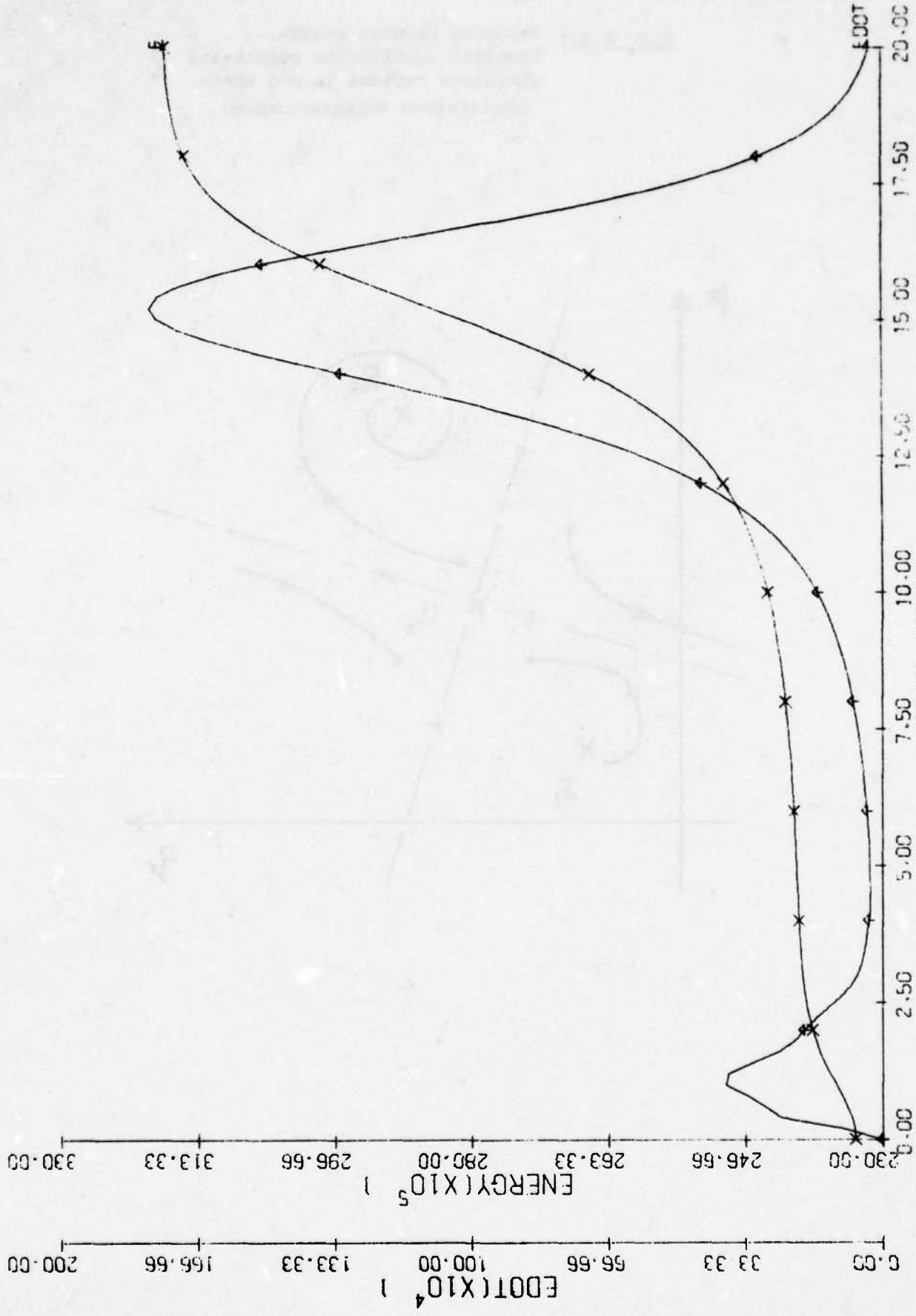

Fig. 3.30: A/C, B $\delta e = 2°$, $\delta r = 0°$; E, Ė histories for $\delta a = 3.8°$

Fig. 3.31: Relation between stable, unstable equilibrium points and attractor regions in p-q space. (Qualitative Representation).

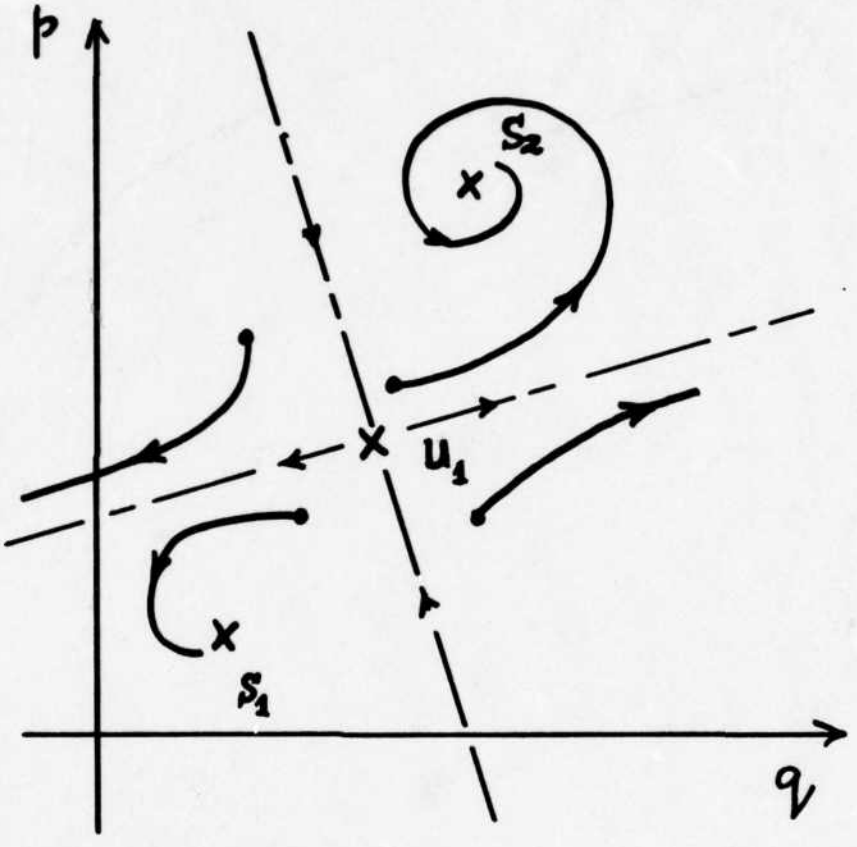

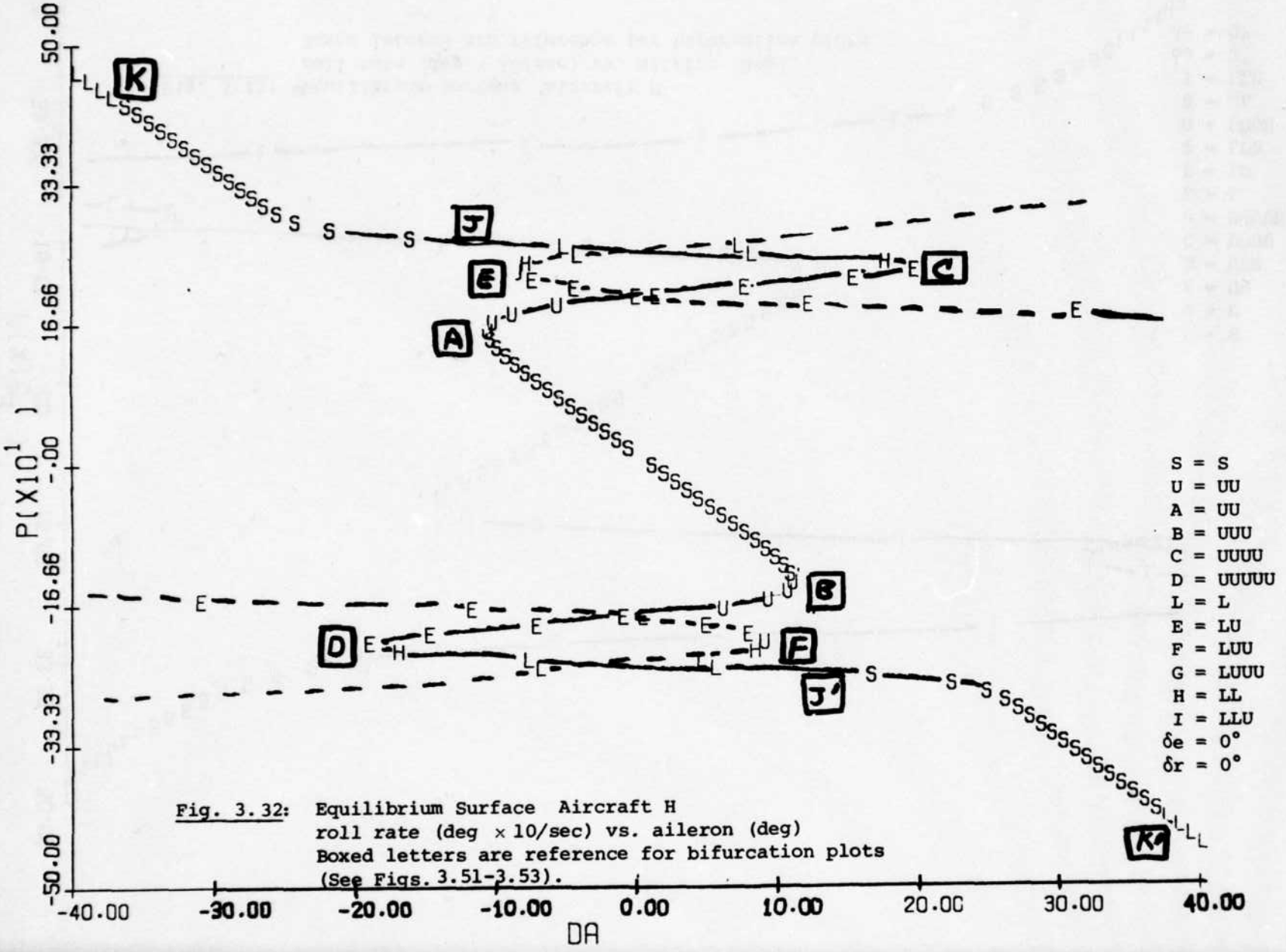

Fig. 3.32: Equilibrium Surface Aircraft H
roll rate (deg × 10/sec) vs. aileron (deg)
Boxed letters are reference for bifurcation plots
(See Figs. 3.51-3.53).

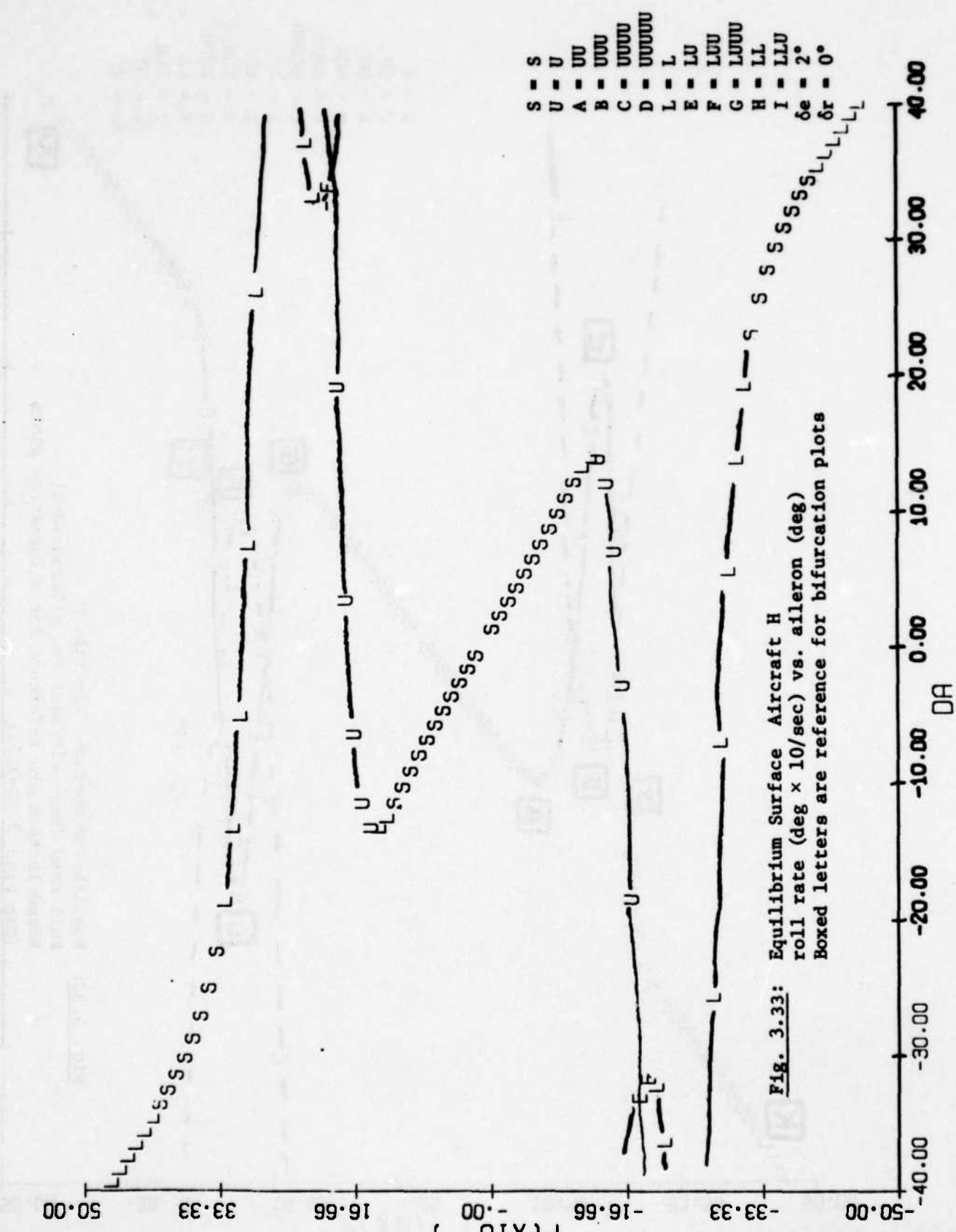

Fig. 3.33: Equilibrium Surface Aircraft H
roll rate (deg × 10/sec) vs. aileron (deg)
Boxed letters are reference for bifurcation plots

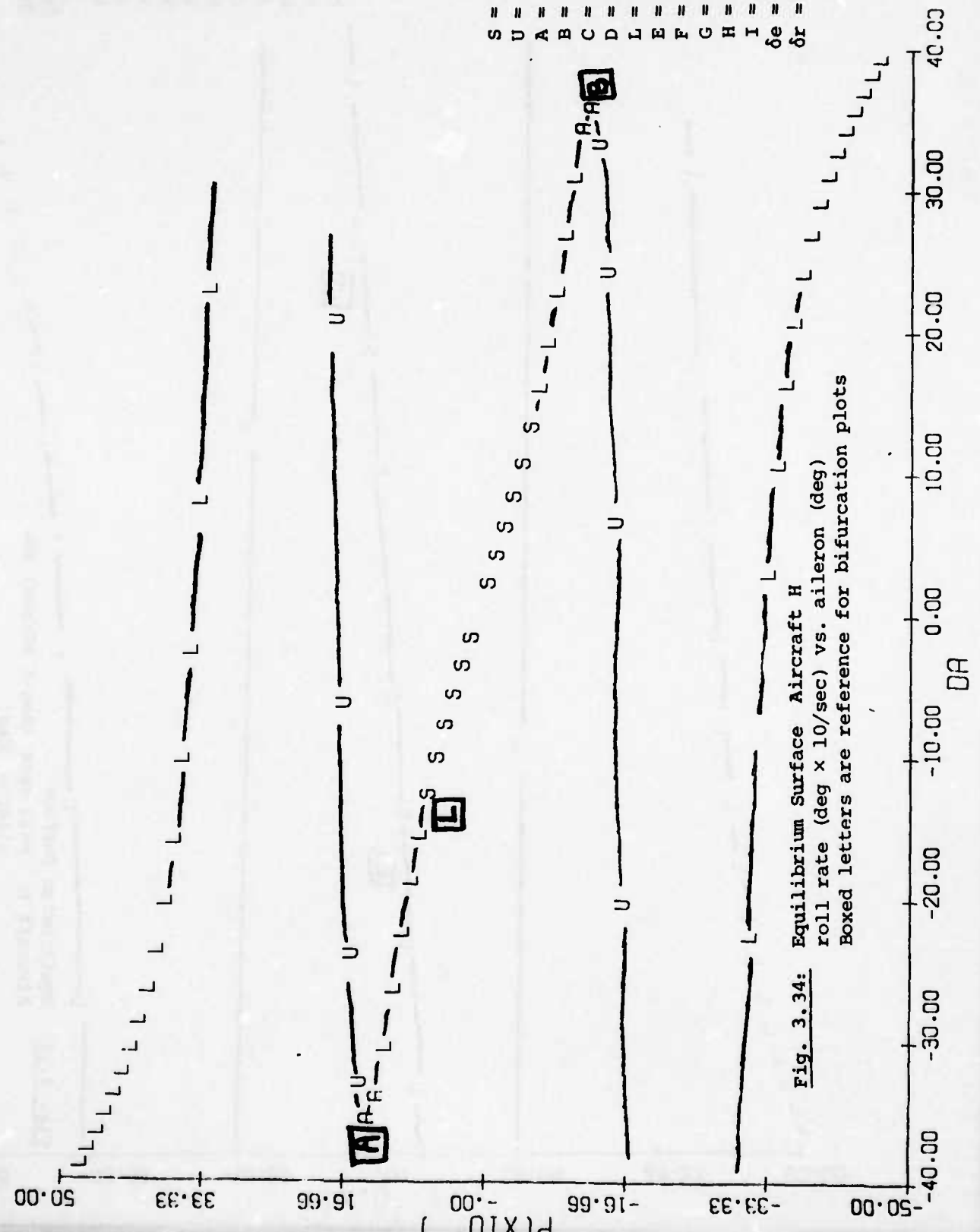

Fig. 3.34: Equilibrium Surface Aircraft H
roll rate (deg × 10/sec) vs. aileron (deg)
Boxed letters are reference for bifurcation plots

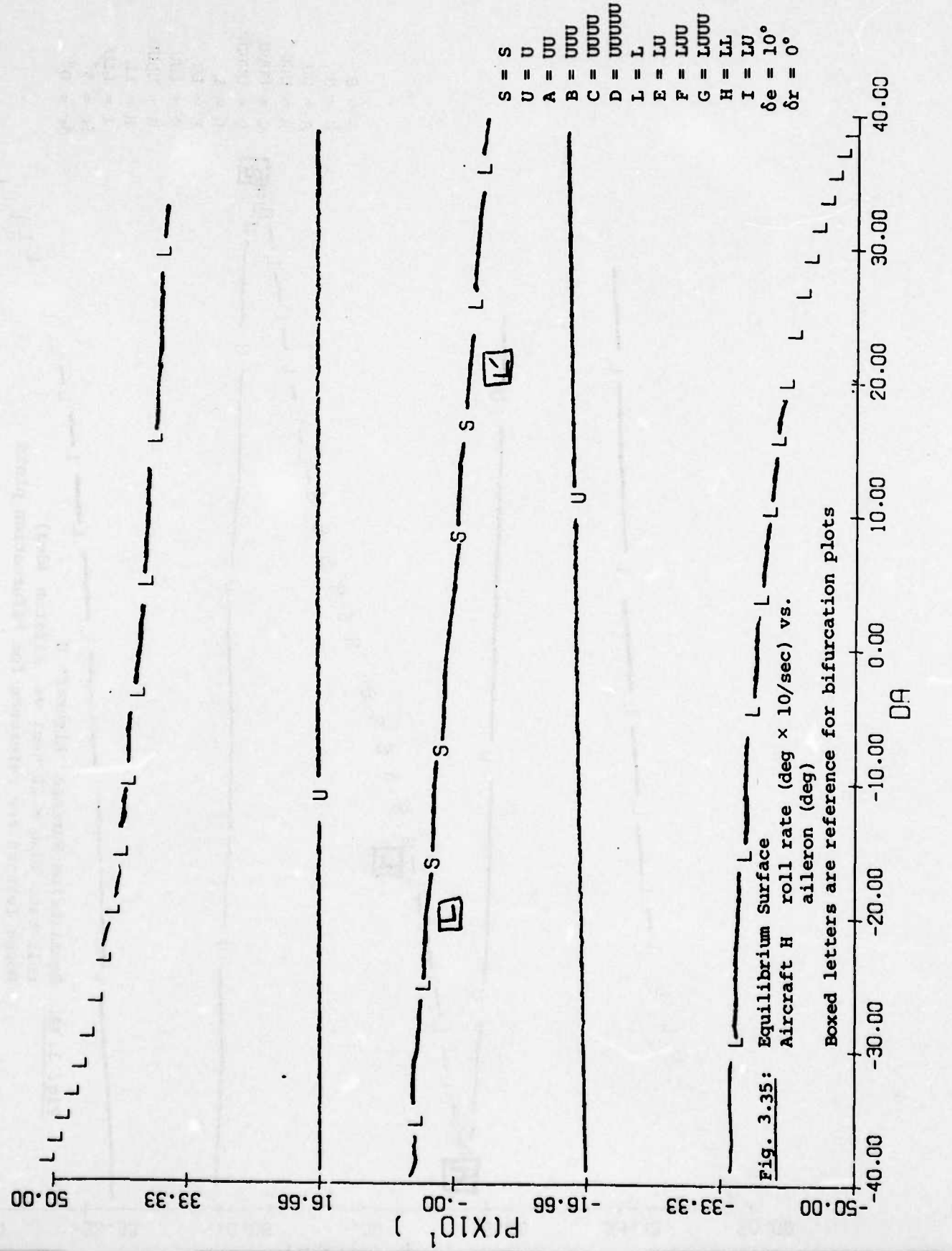

Fig. 3.35: Equilibrium Surface
Aircraft H roll rate (deg × 10/sec) vs. aileron (deg)
Boxed letters are reference for bifurcation plots

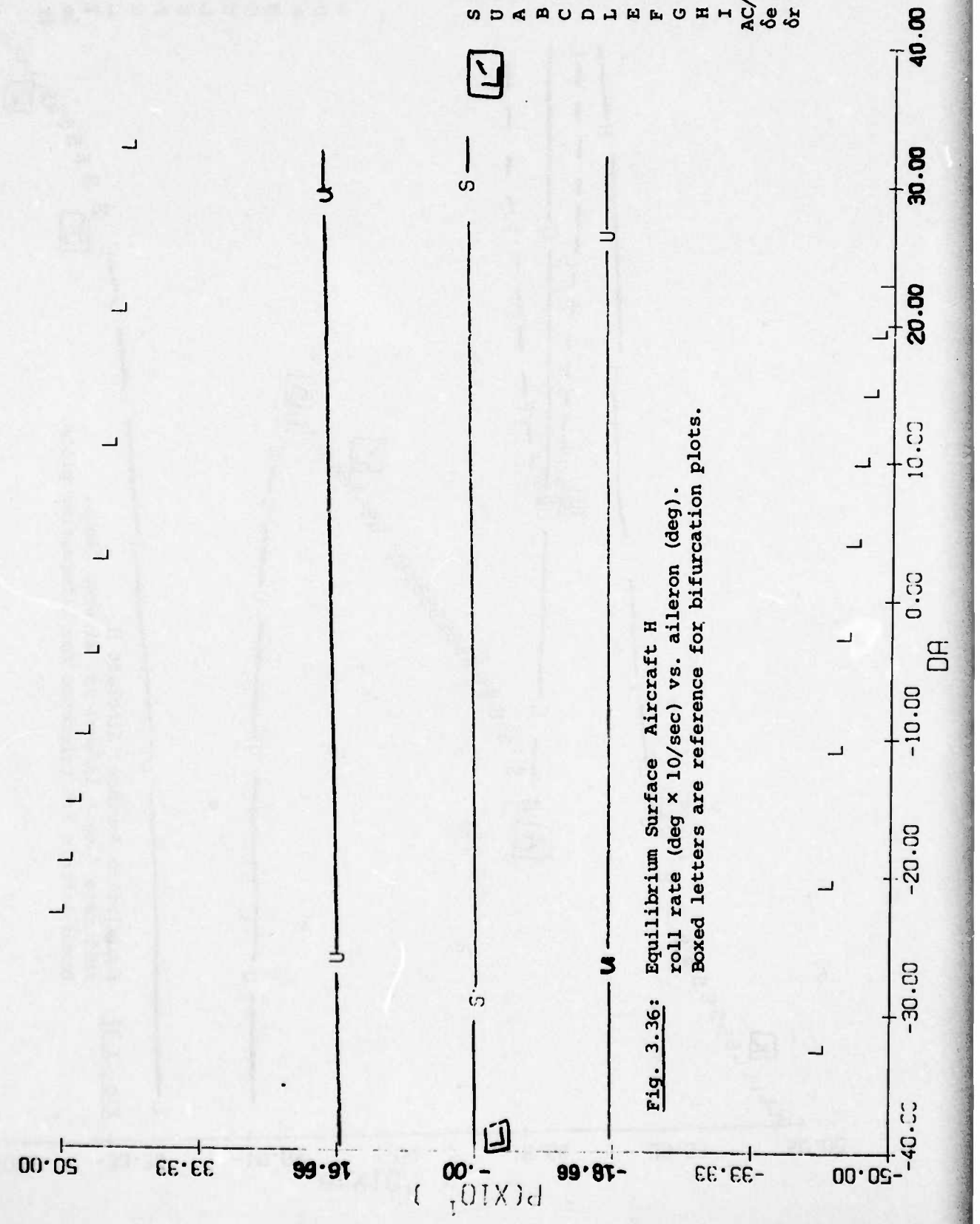

Fig. 3.36: Equilibrium Surface Aircraft H
roll rate (deg x 10/sec) vs. aileron (deg).
Boxed letters are reference for bifurcation plots.

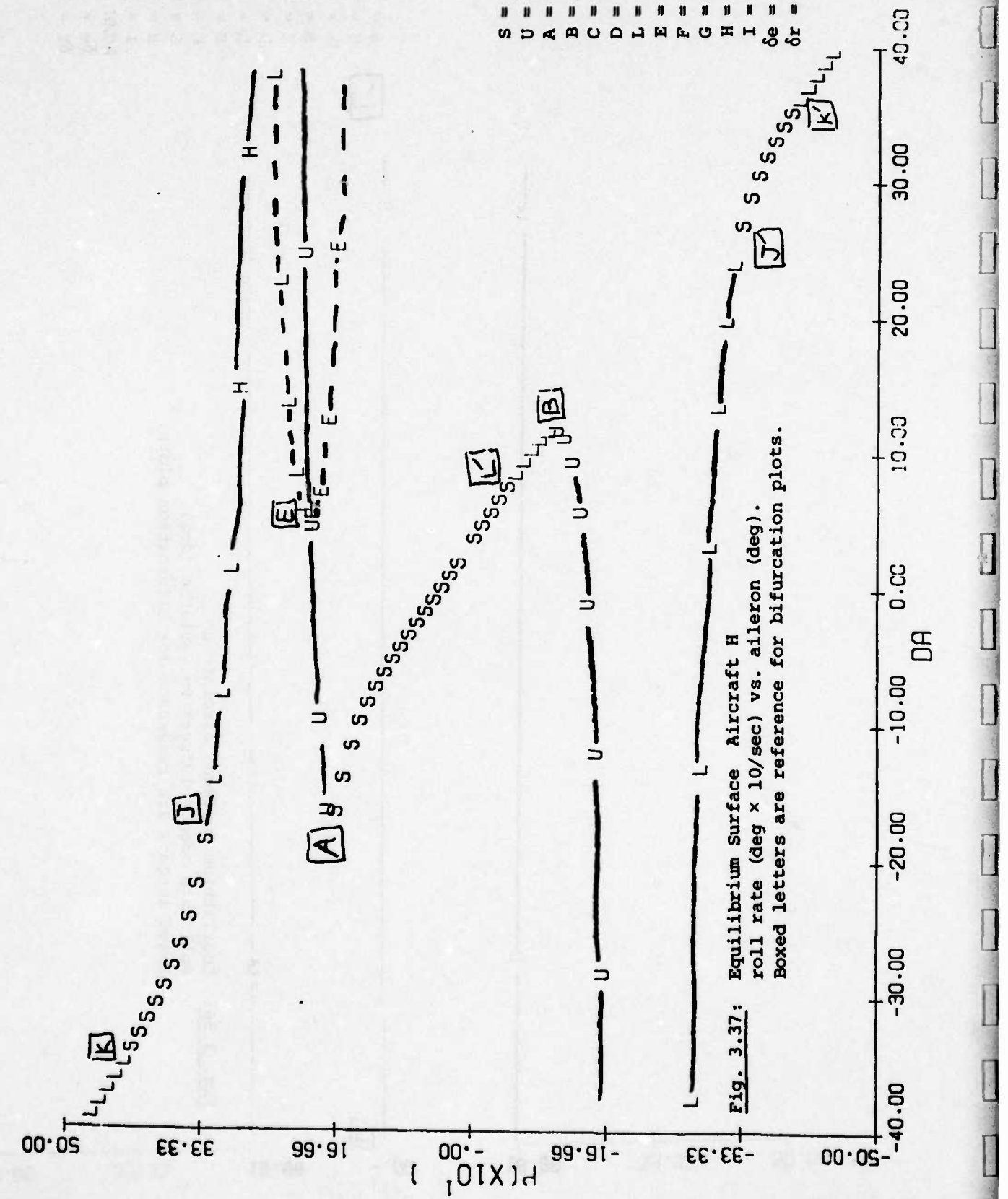

Fig. 3.37: Equilibrium Surface Aircraft H
roll rate (deg × 10/sec) vs. aileron (deg).
Boxed letters are reference for bifurcation plots.

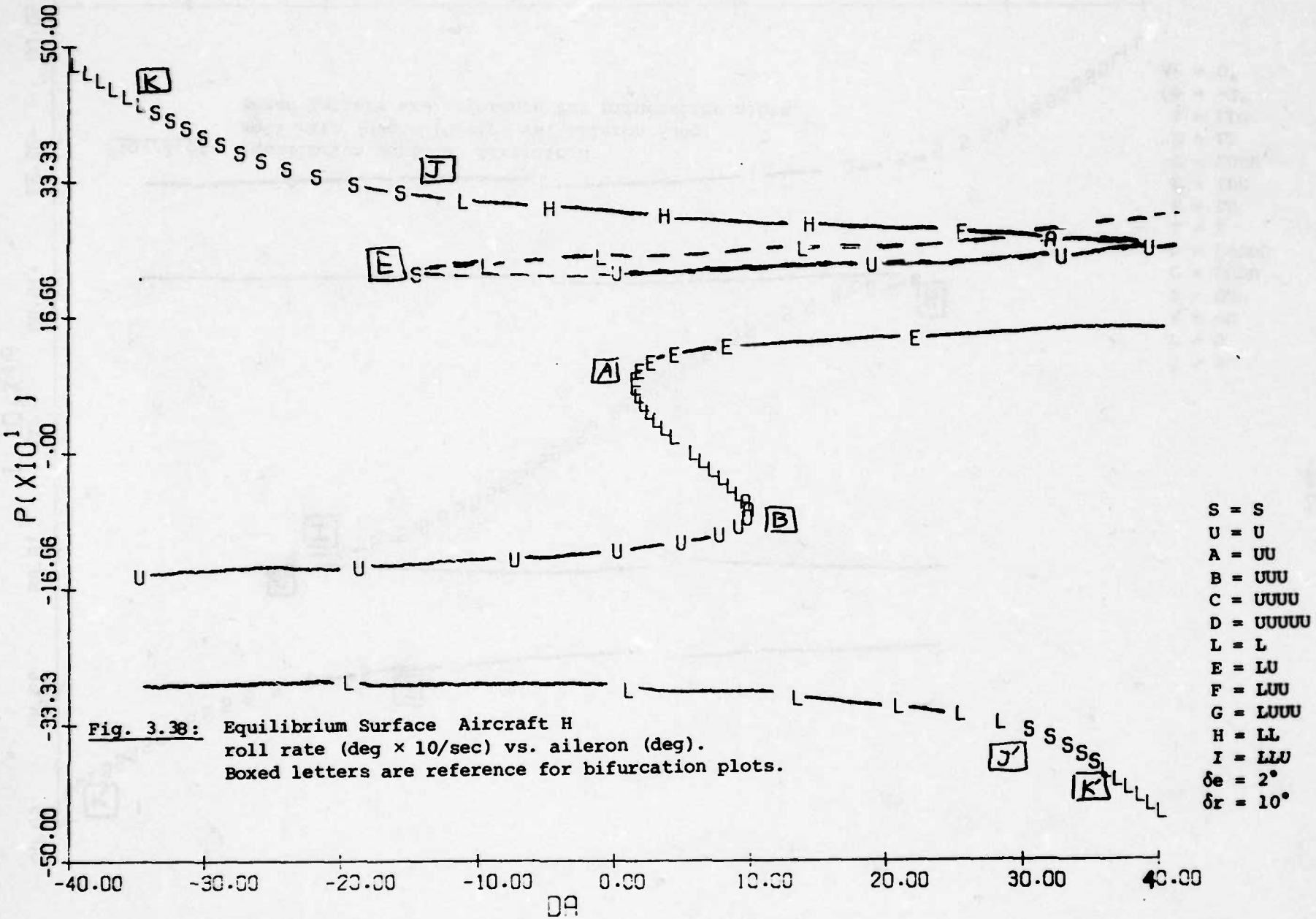

Fig. 3.38: Equilibrium Surface Aircraft H
roll rate (deg × 10/sec) vs. aileron (deg).
Boxed letters are reference for bifurcation plots.

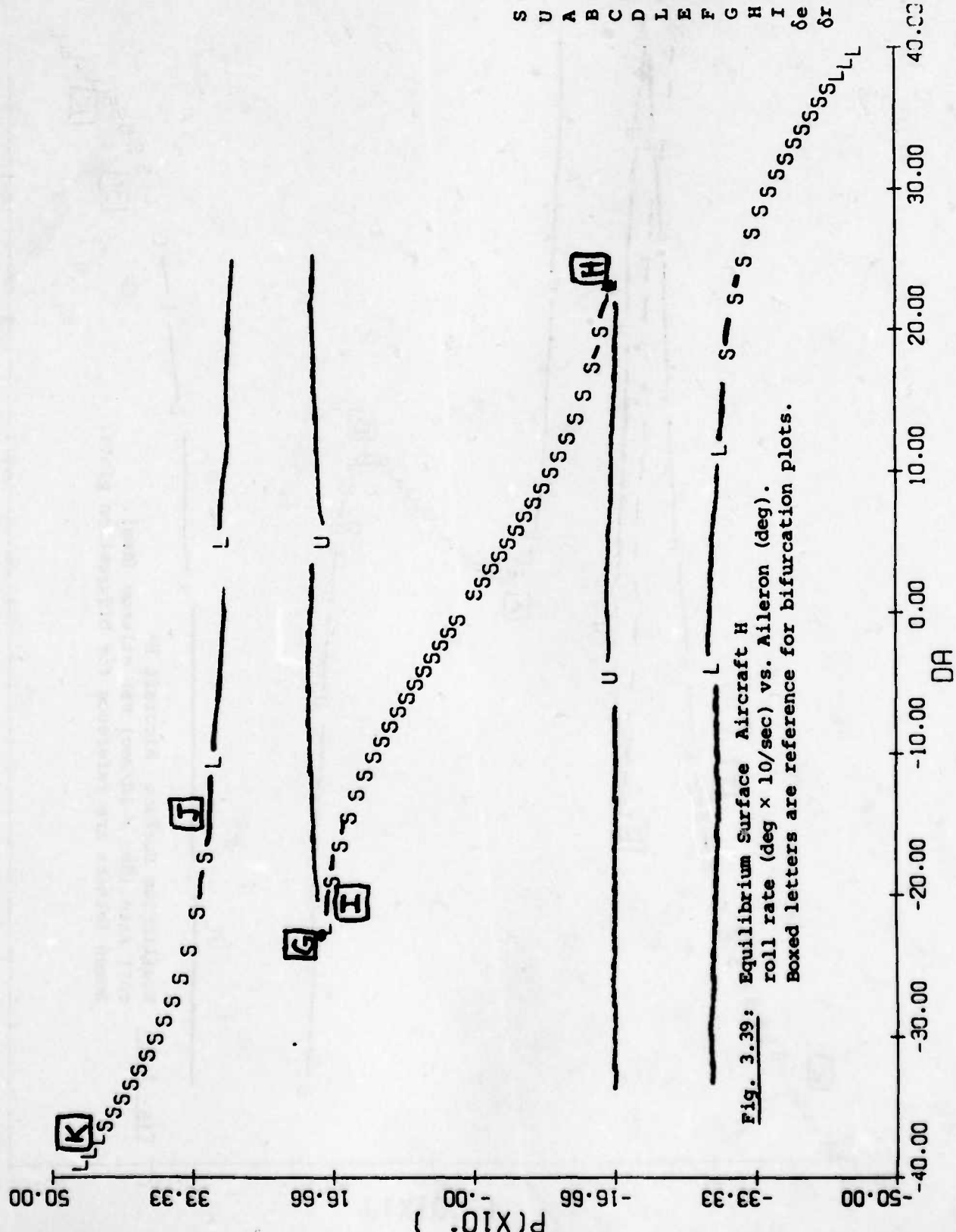

Fig. 3.39: Equilibrium Surface Aircraft H
roll rate (deg × 10/sec) vs. Aileron (deg).
Boxed letters are reference for bifurcation plots.

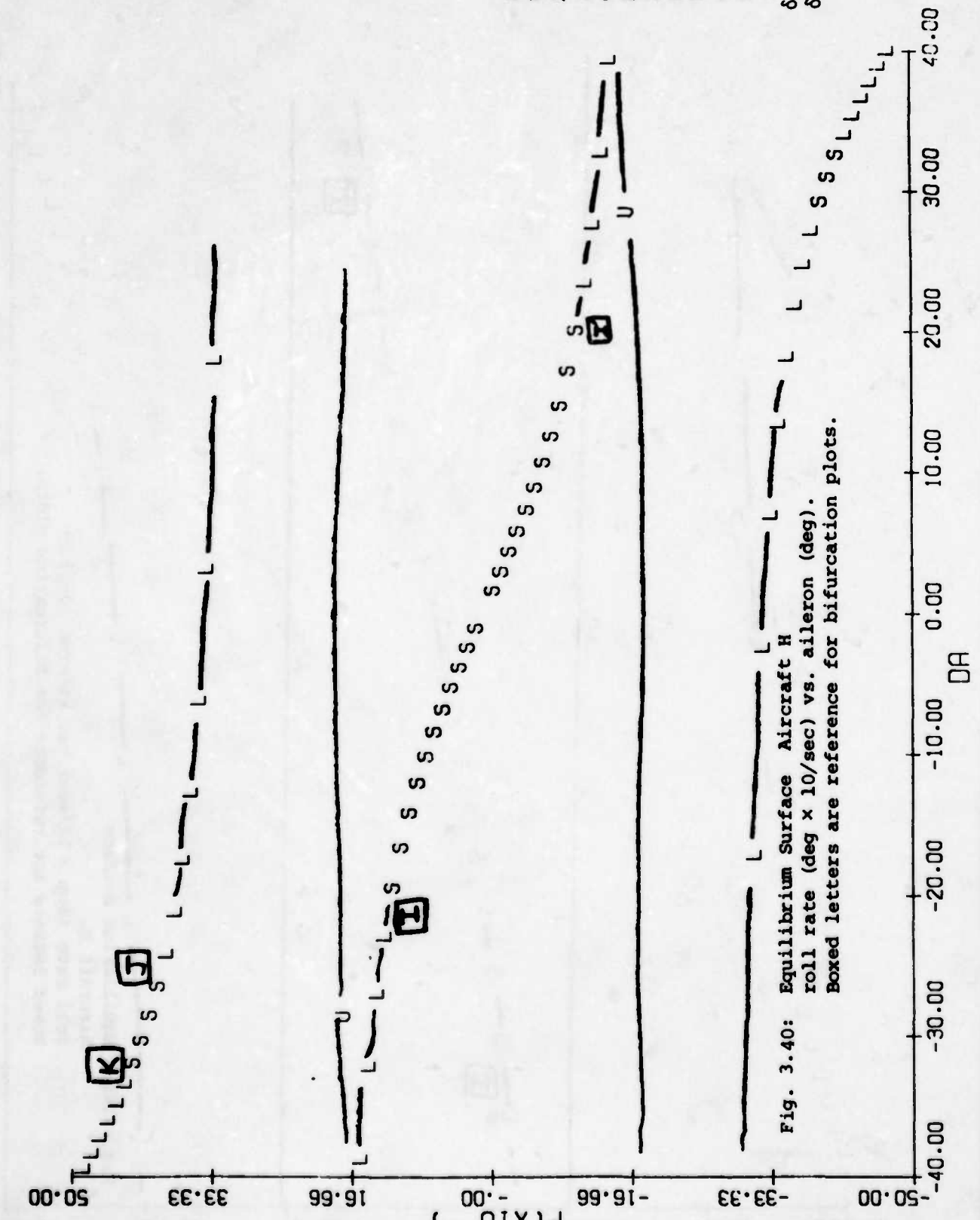

Fig. 3.40: Equilibrium Surface Aircraft H
roll rate (deg × 10/sec) vs. aileron (deg).
Boxed letters are reference for bifurcation plots.

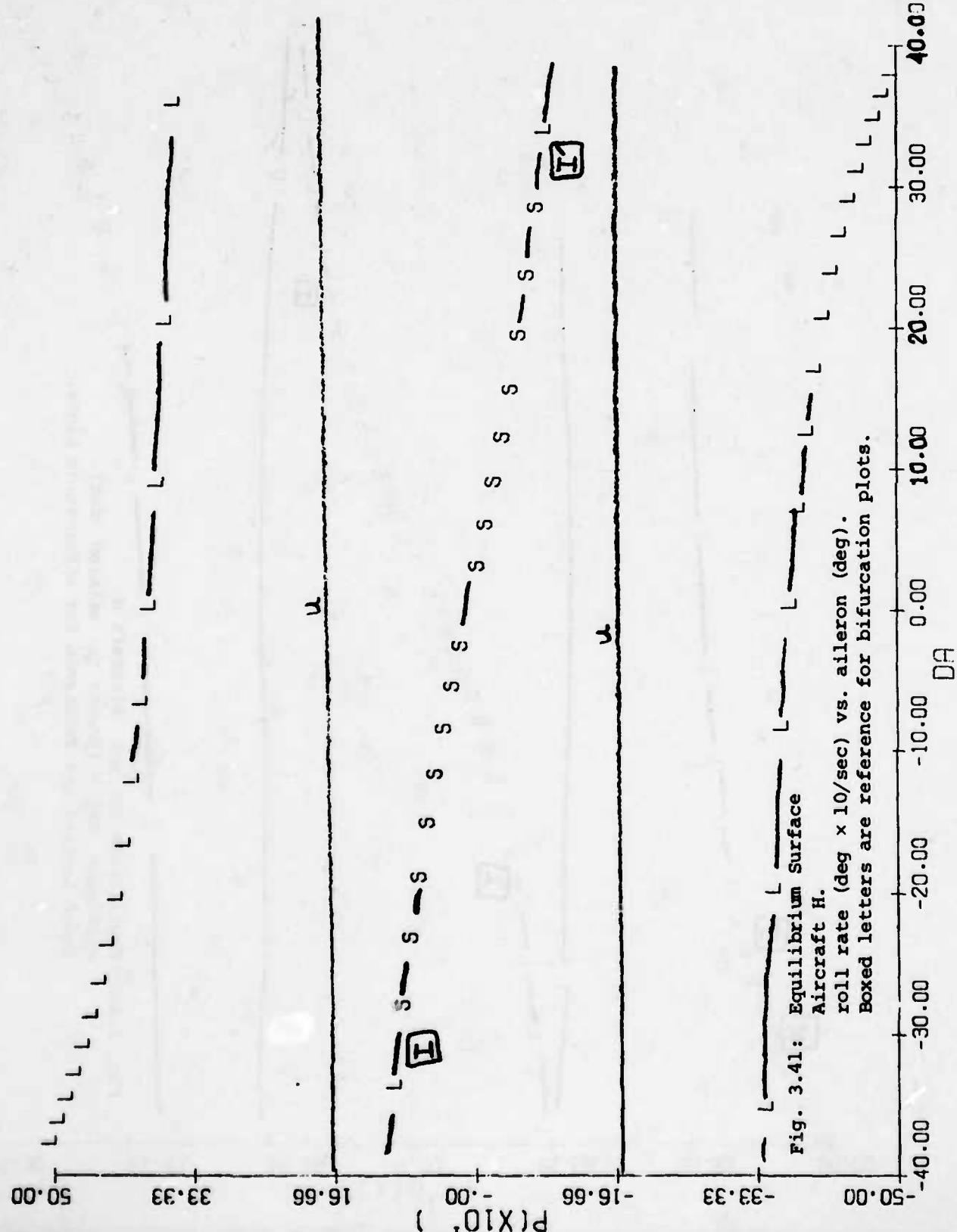

Fig. 3.41: Equilibrium Surface
Aircraft H.
roll rate (deg × 10/sec) vs. aileron (deg).
Boxed letters are reference for bifurcation plots.

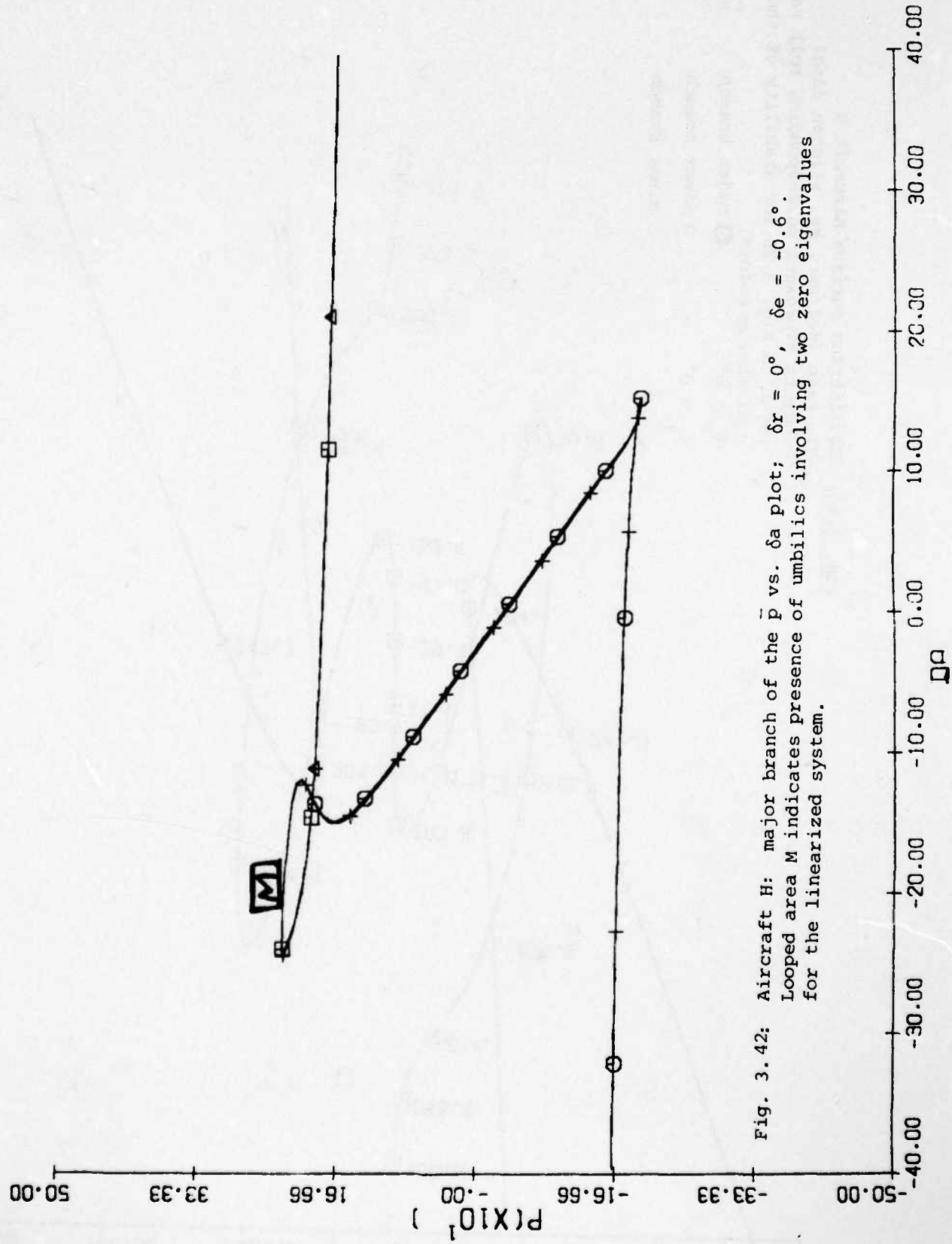

Fig. 3.42: Aircraft H: major branch of the $\tilde{p}$ vs. δa plot; $\delta r = 0°$, $\delta e = -0.6°$. Looped area M indicates presence of umbilics involving two zero eigenvalues for the linearized system.

Fig. 3.43: Equilibrium Surface Aircraft H
Yaw rate (deg/sec) vs. aileron (deg)
(numbers represent corresponding roll rate - refer to Fig. 3.26 for stability of the equilibrium points)
$\delta_e = 0°$ ☐ major branch
$\delta_r = 0°$ O minor branch
Δ minor branch

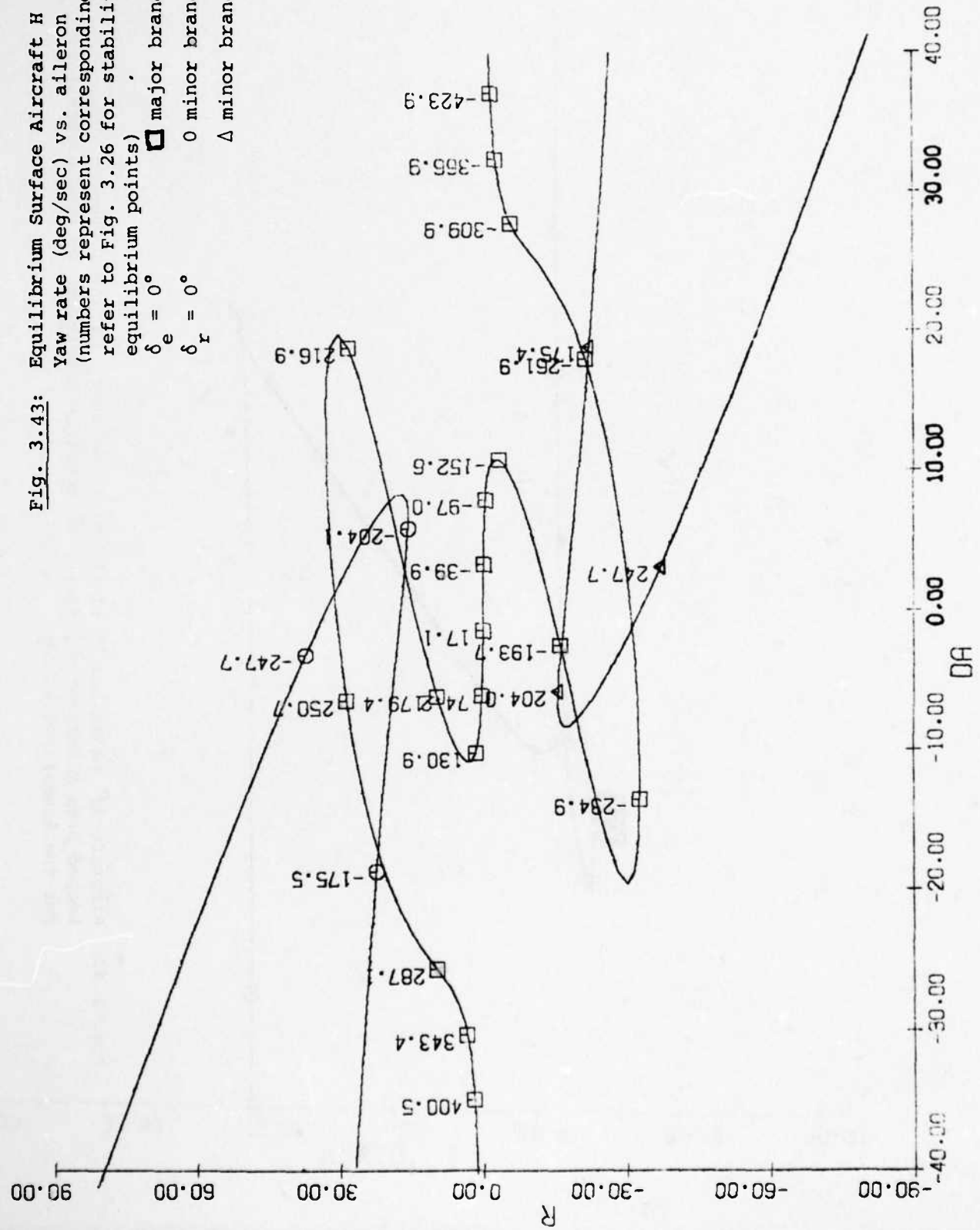

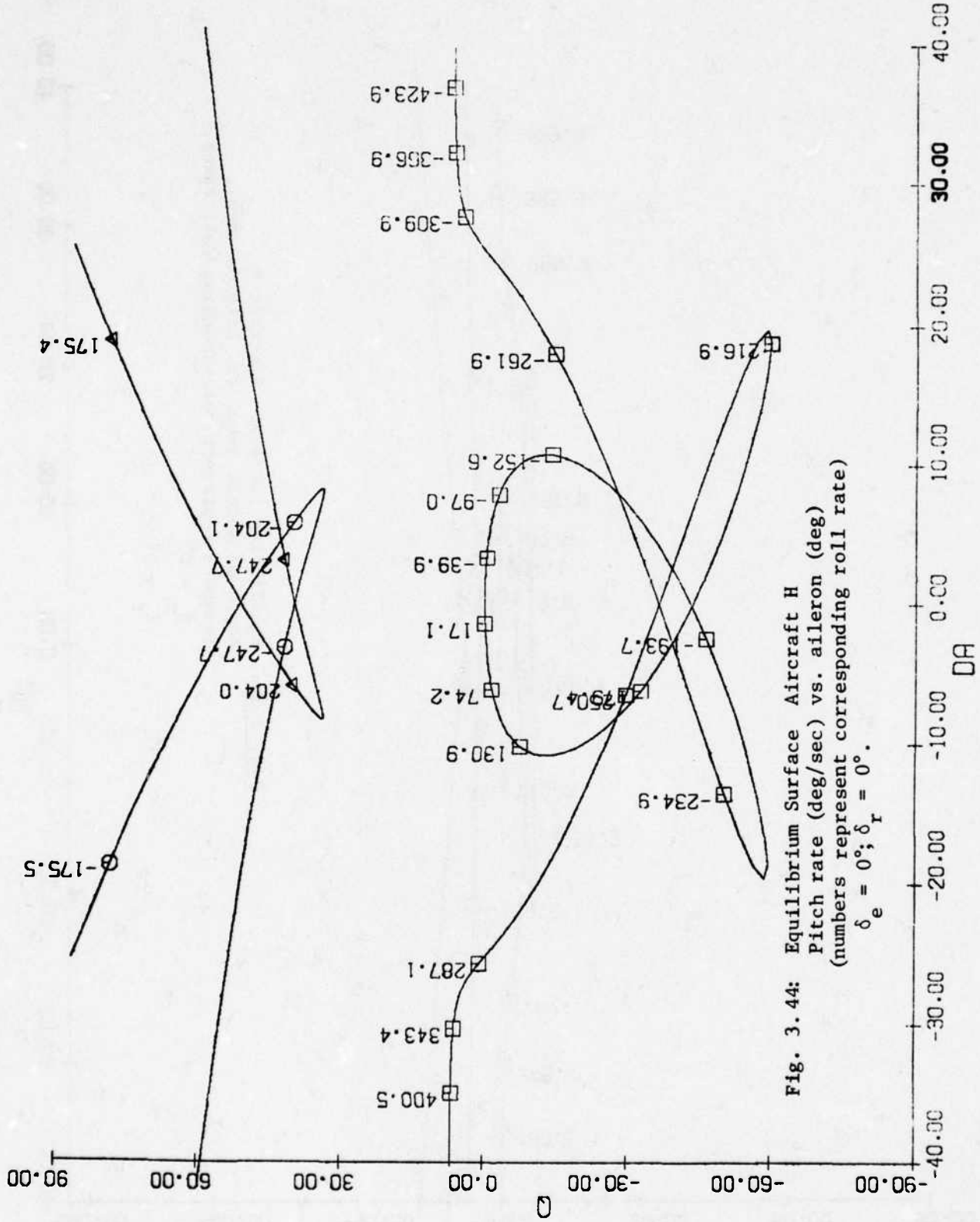

Fig. 3.44: Equilibrium Surface Aircraft H
Pitch rate (deg/sec) vs. aileron (deg)
(numbers represent corresponding roll rate)
$\delta_e = 0°; \delta_r = 0°$.

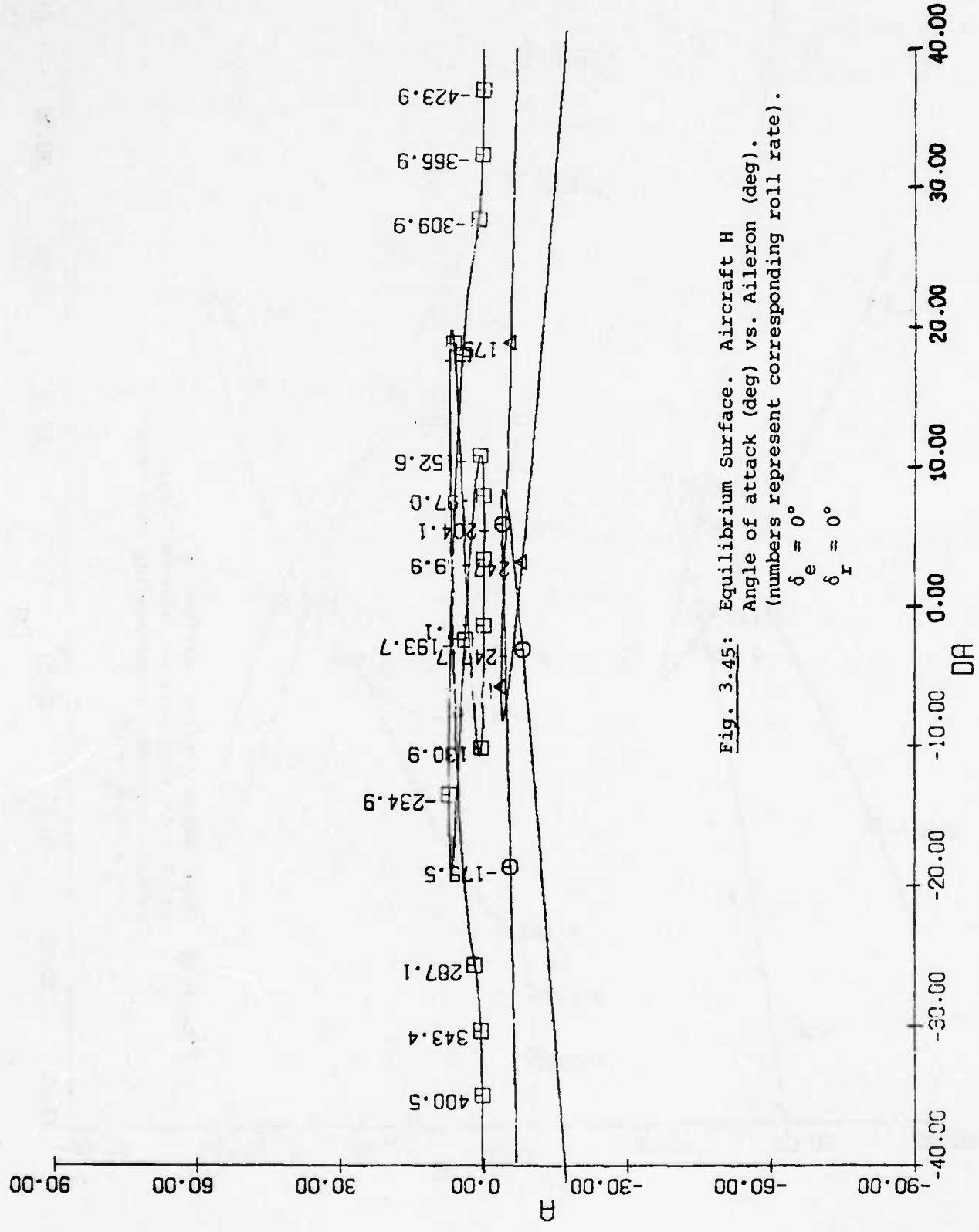

Fig. 3.45: Equilibrium Surface. Aircraft H
Angle of attack (deg) vs. Aileron (deg).
(numbers represent corresponding roll rate).
$\delta_e = 0°$
$\delta_r = 0°$

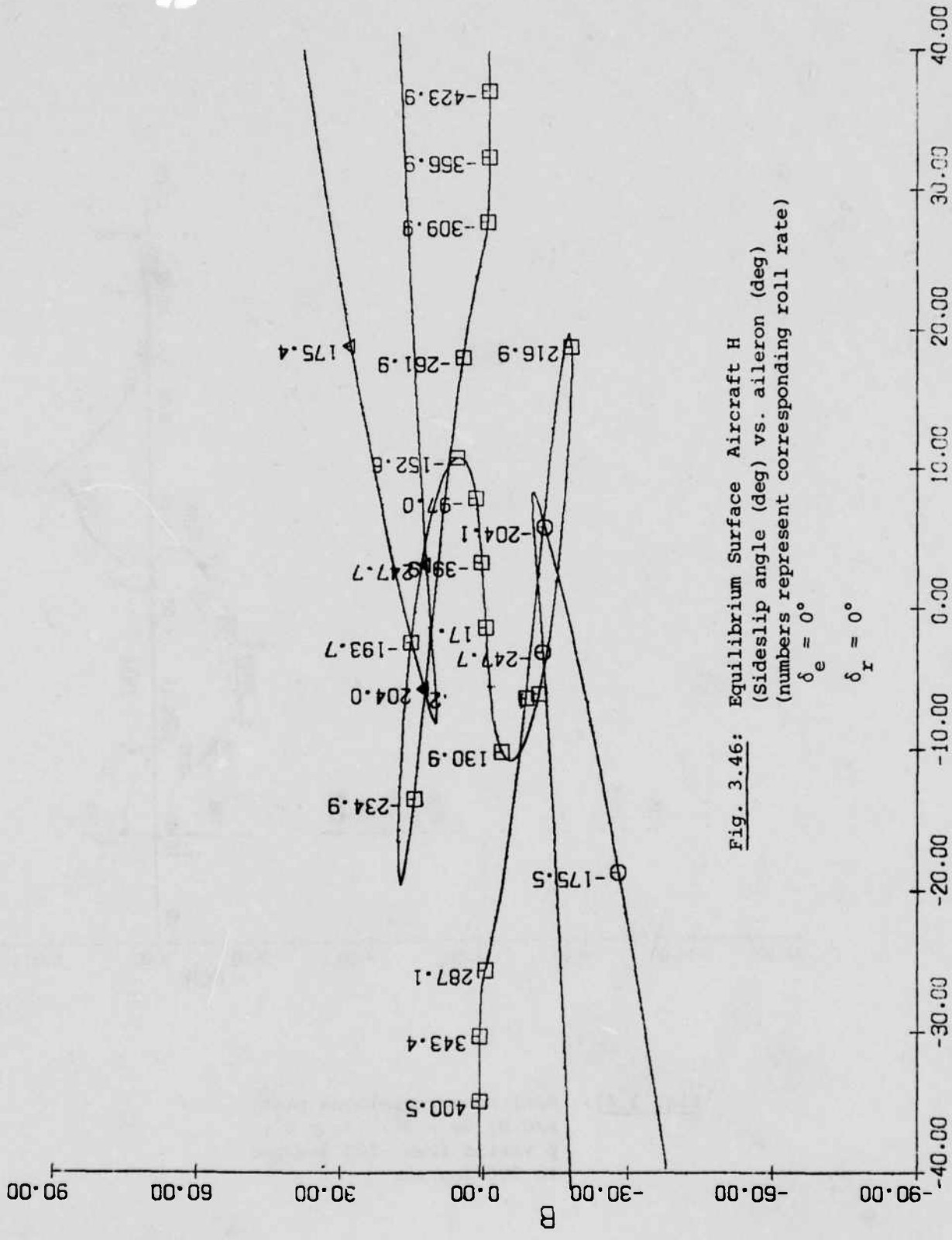

Fig. 3.46: Equilibrium Surface Aircraft H
(Sideslip angle (deg) vs. aileron (deg)
(numbers represent corresponding roll rate)
$\delta_e = 0°$
$\delta_r = 0°$

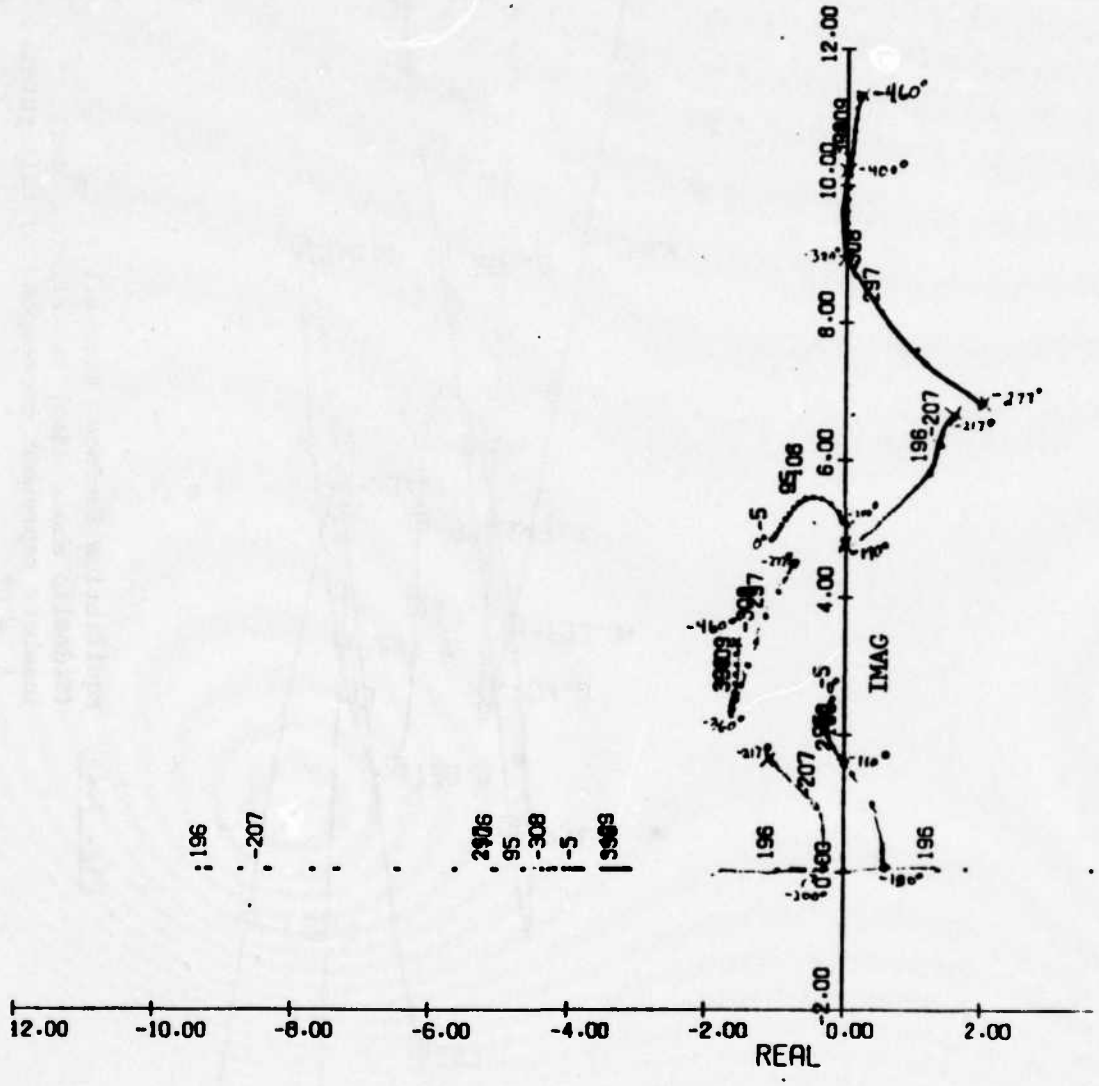

Fig. 3.47: Nonlinear root-locus plot, A/C H; $\delta e = 2°$; $\delta r = 0°$; $\bar{p}$ varied from -500 deg/sec to 500 deg/sec.

A = UU
B = UUU
C = UUUU
D = UUUUU
L = L
E = LU
F = LUU
G = LUUU
H = LL
I = LLU

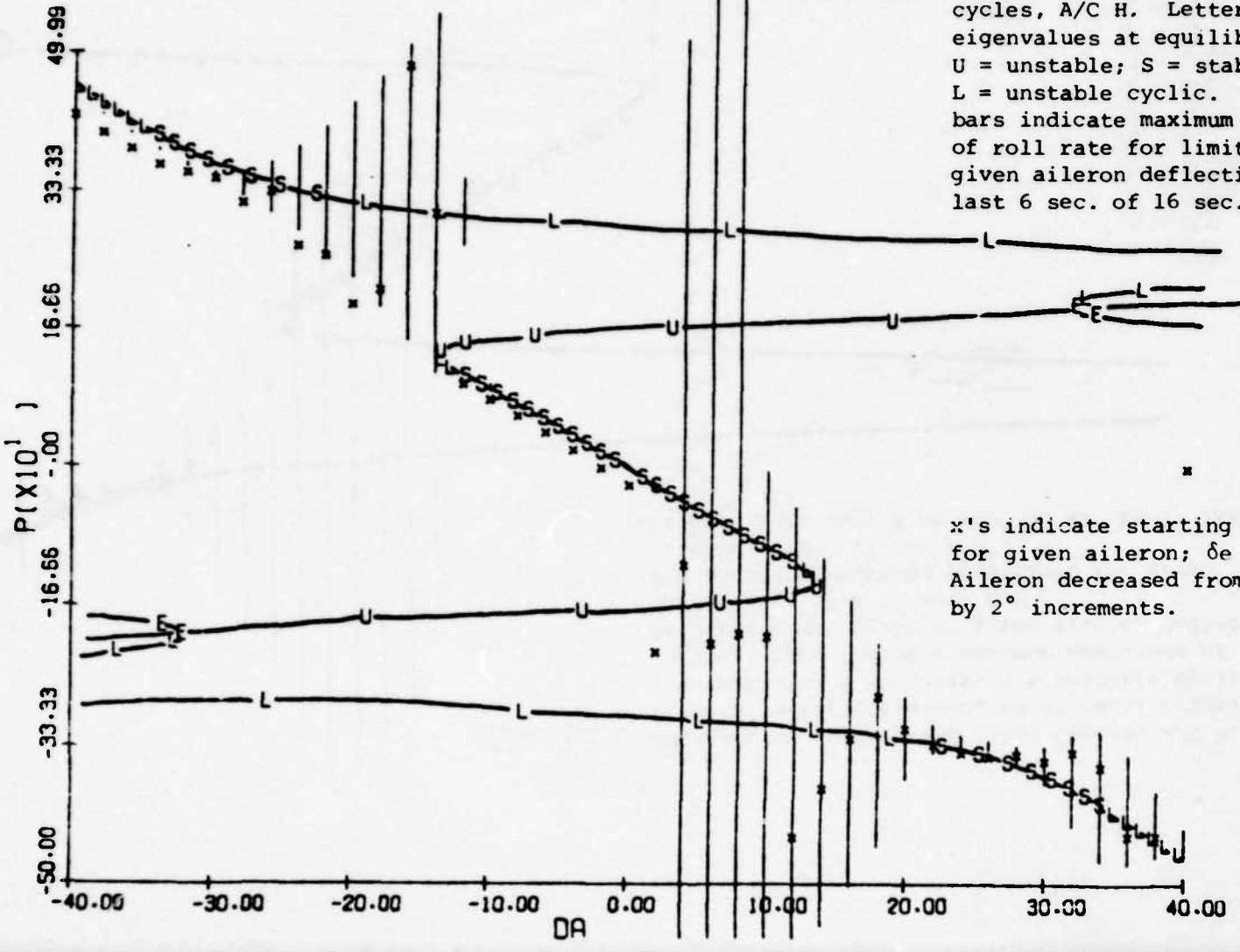

Fig. 3.48: Equilibrium surface and limit cycles, A/C H. Letters indicate eigenvalues at equilibrium: U = unstable; S = stable; L = unstable cyclic. Vertical bars indicate maximum magnitude of roll rate for limit cycle at given aileron deflection over last 6 sec. of 16 sec. run.

x's indicate starting conditions for given aileron; $\delta e = 2°$, $\delta r = 0°$. Aileron decreased from 40° to -40° by 2° increments.

Fig. 3.49: Equilibrium Surface and Limit Cycles, A/C H.
Letters indicate eigenvalues at equilibrium:
U = unstable; S = stable; L = unstable cyclic.
Vertical bars indicate maximum magnitude of roll rate for limit cycle at given aileron deflection over last 6 sec. of a 16 sec. run.
x's indicate starting conditions for given aileron. $\delta e = 2°$, $\delta r = 0°$.
Aileron increased from -40° to 40° by 2° increments.

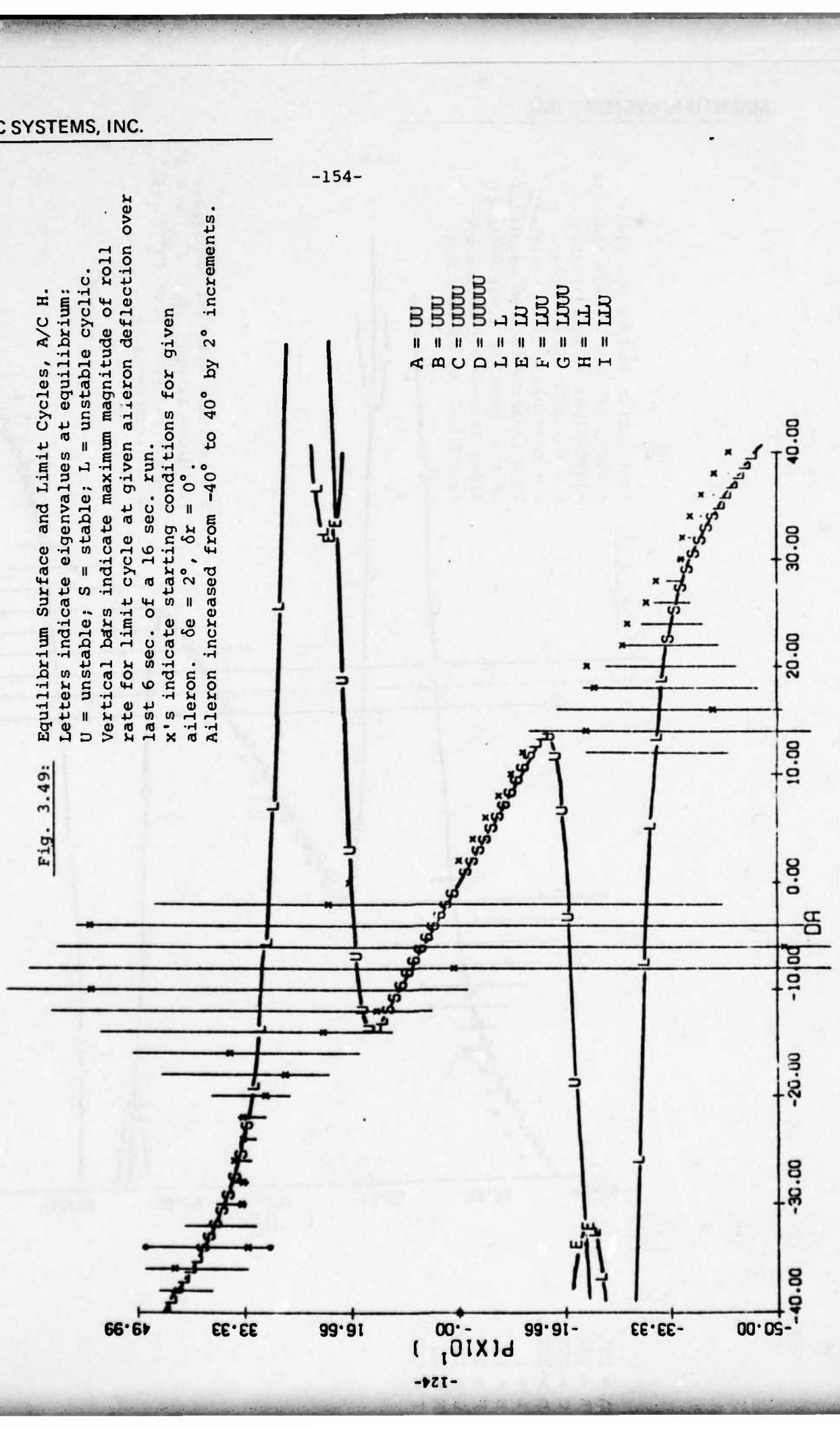

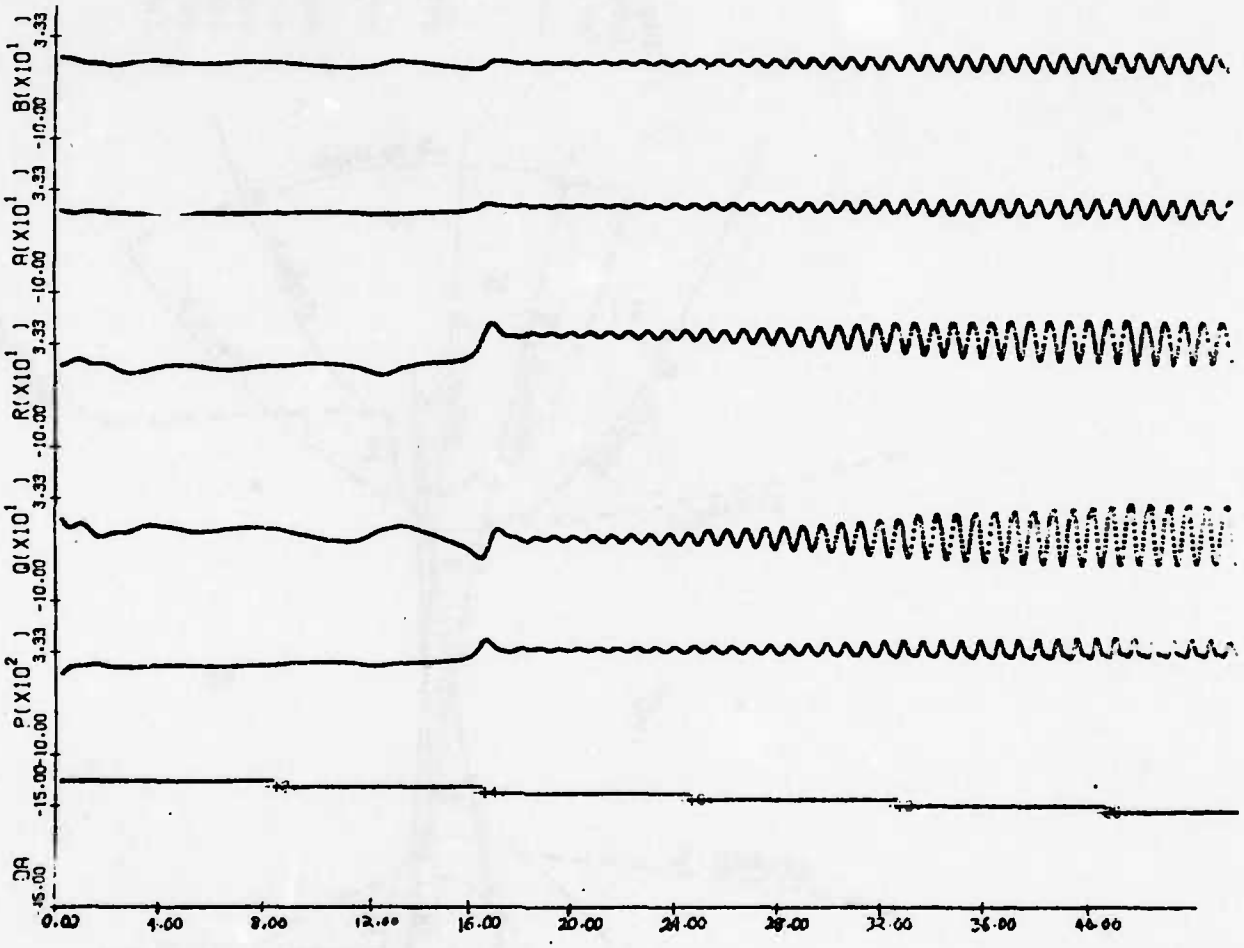

Fig. 3.50: Time history plots showing the development of an expanding limit cycle for Aircraft H.

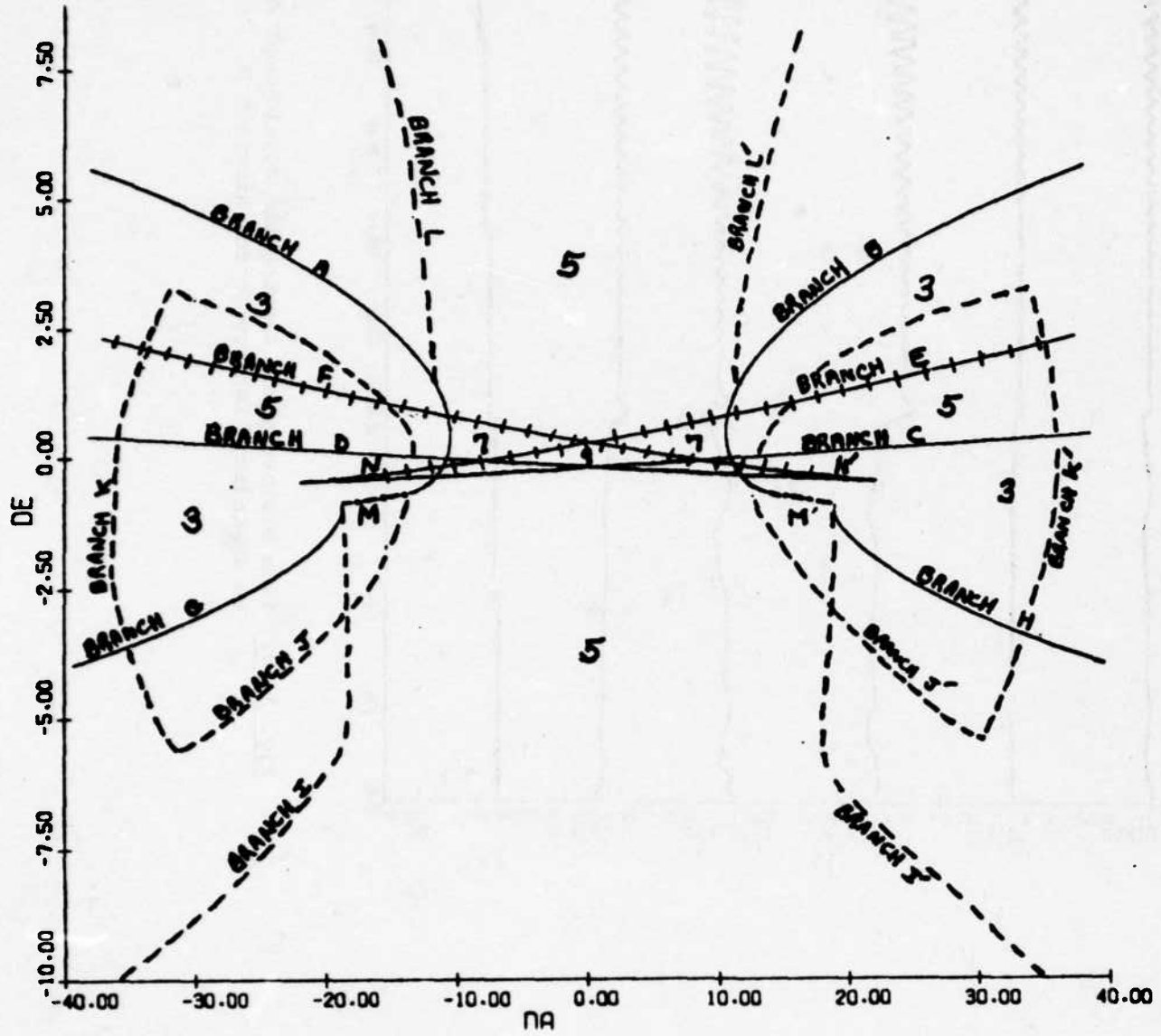

Fig. 3.51a: Bifurcation locus in (δa,δe) plane; (units,deg.) A/C H; δr = 0°.

——zero eigenvalue of linearized system (major branch).

╫zero eigenvalue (minor branch)

---purely imaginary eigenvalue.

Numbers indicate number of equilibrium solutions in regions demarcated by solid lines; branch letters refer to letters on Figs. 3.26 and 3.36.

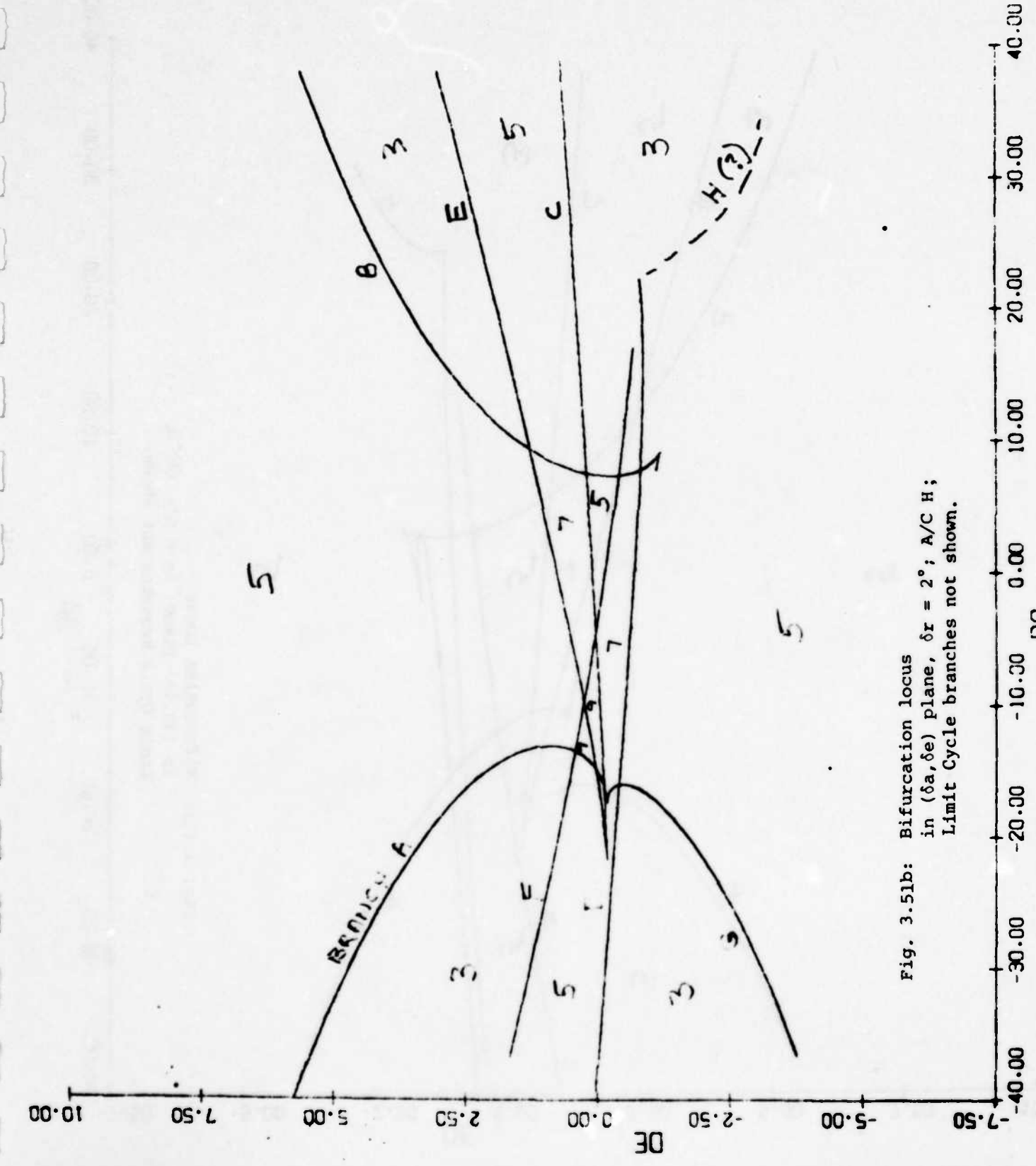

Fig. 3.51b: Bifurcation locus in (δa,δe) plane, δr = 2°; A/C H; Limit Cycle branches not shown.

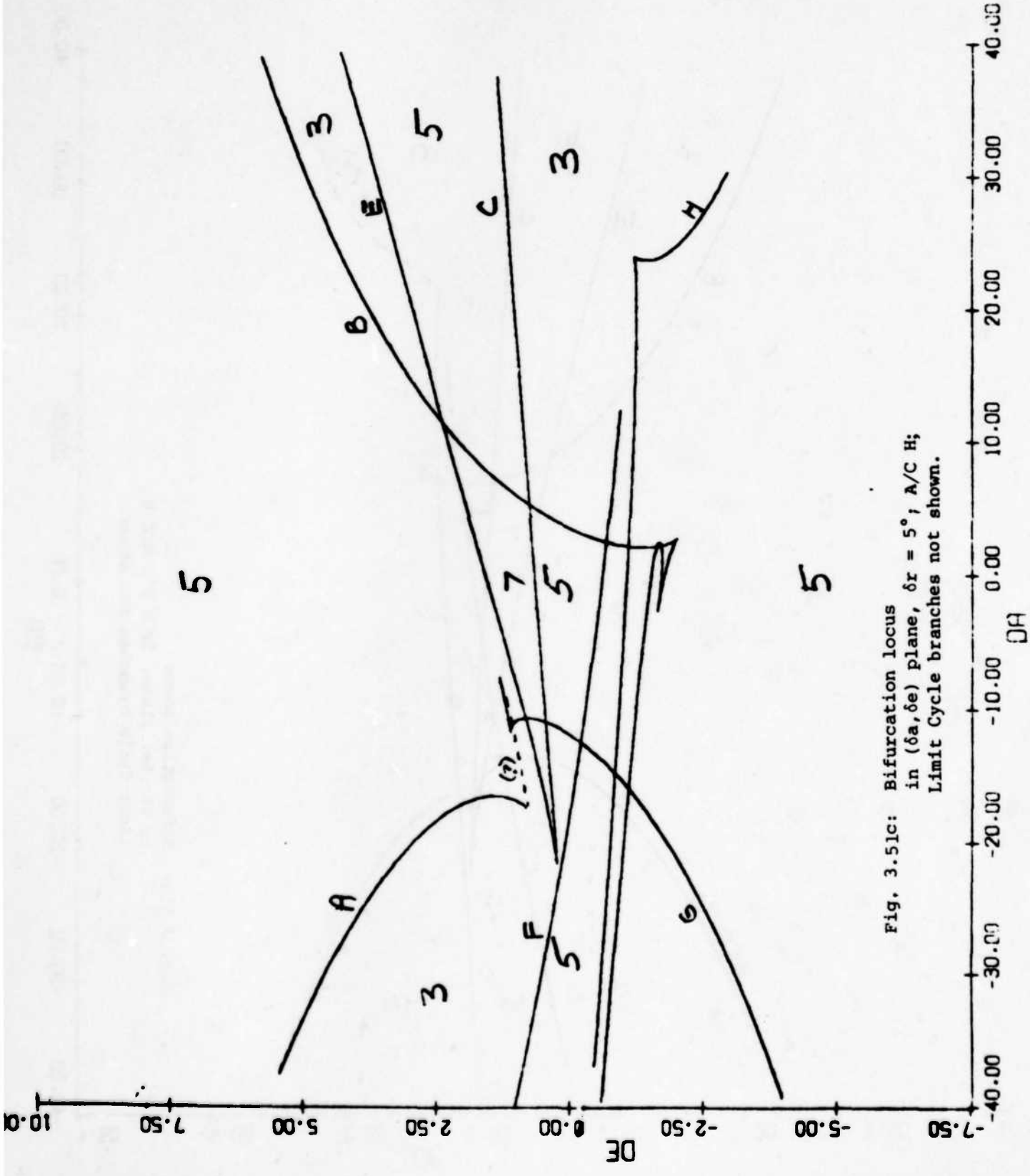

Fig. 3.51c: Bifurcation locus in ($\delta a, \delta e$) plane, $\delta r = 5°$; A/C H; Limit Cycle branches not shown.

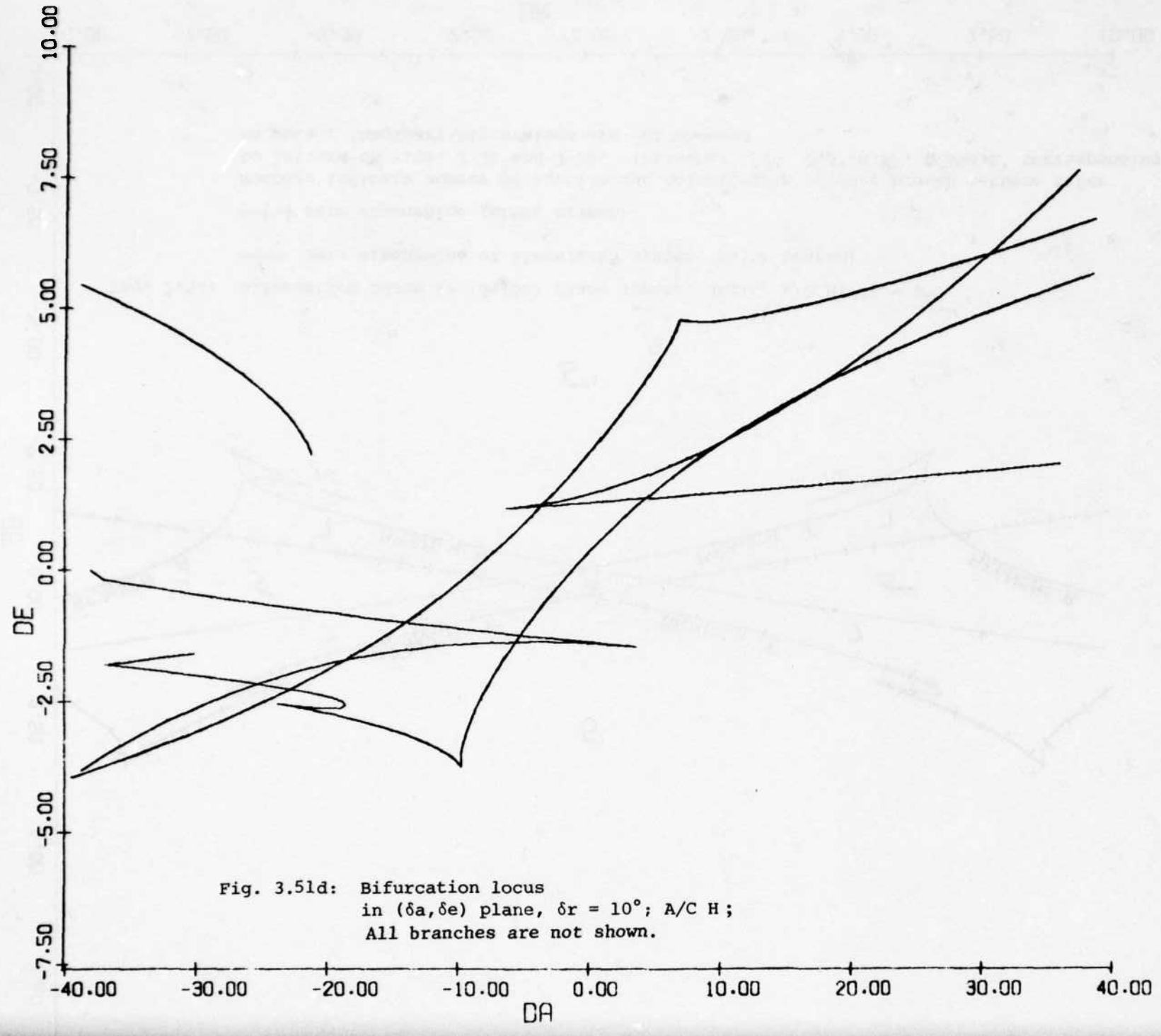

Fig. 3.51d: Bifurcation locus in ($\delta a, \delta e$) plane, $\delta r = 10°$; A/C H; All branches are not shown.

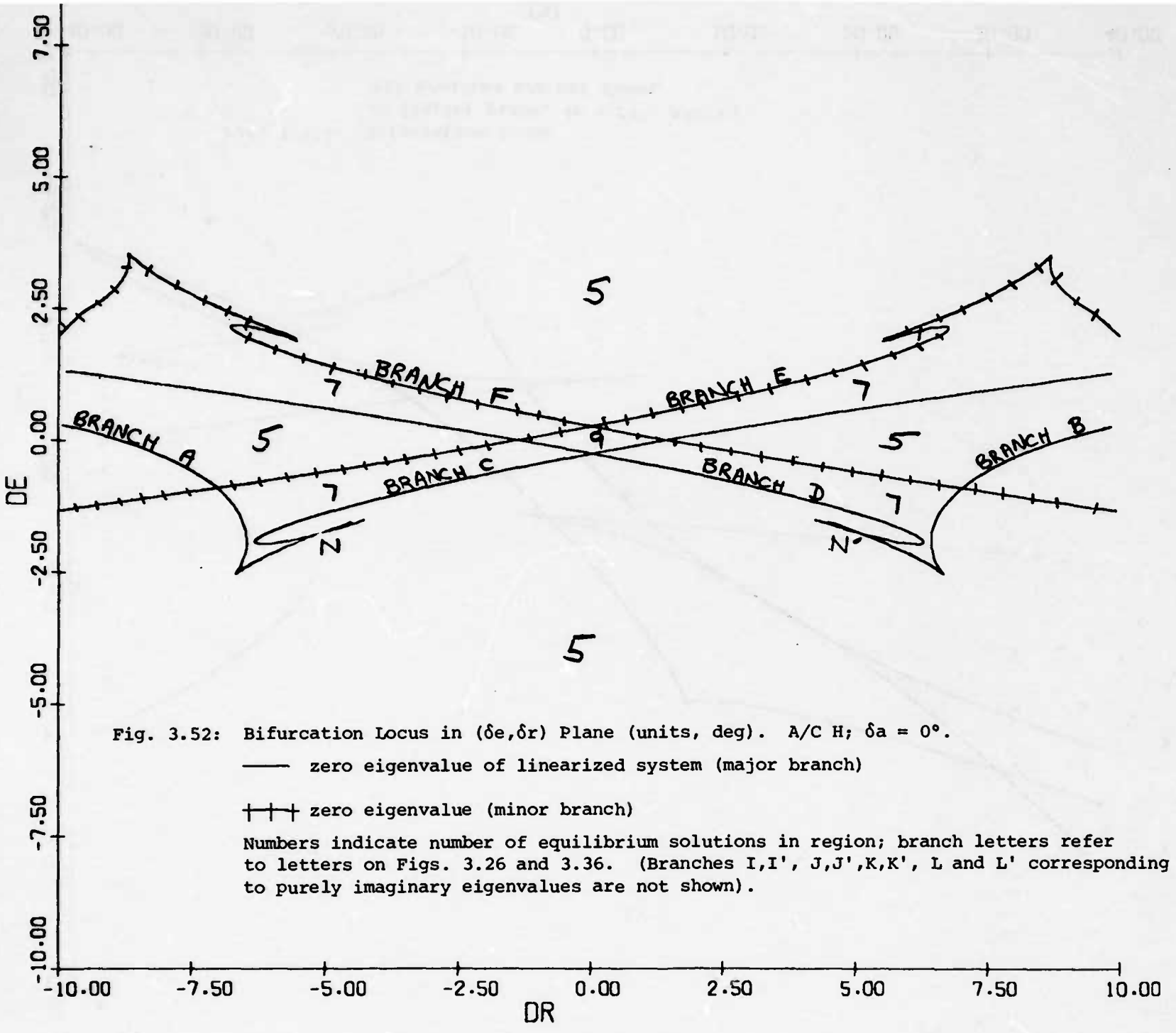

Fig. 3.52: Bifurcation Locus in ($\delta e, \delta r$) Plane (units, deg). A/C H; $\delta a = 0°$.

—— zero eigenvalue of linearized system (major branch)

+++ zero eigenvalue (minor branch)

Numbers indicate number of equilibrium solutions in region; branch letters refer to letters on Figs. 3.26 and 3.36. (Branches I,I', J,J',K,K', L and L' corresponding to purely imaginary eigenvalues are not shown).

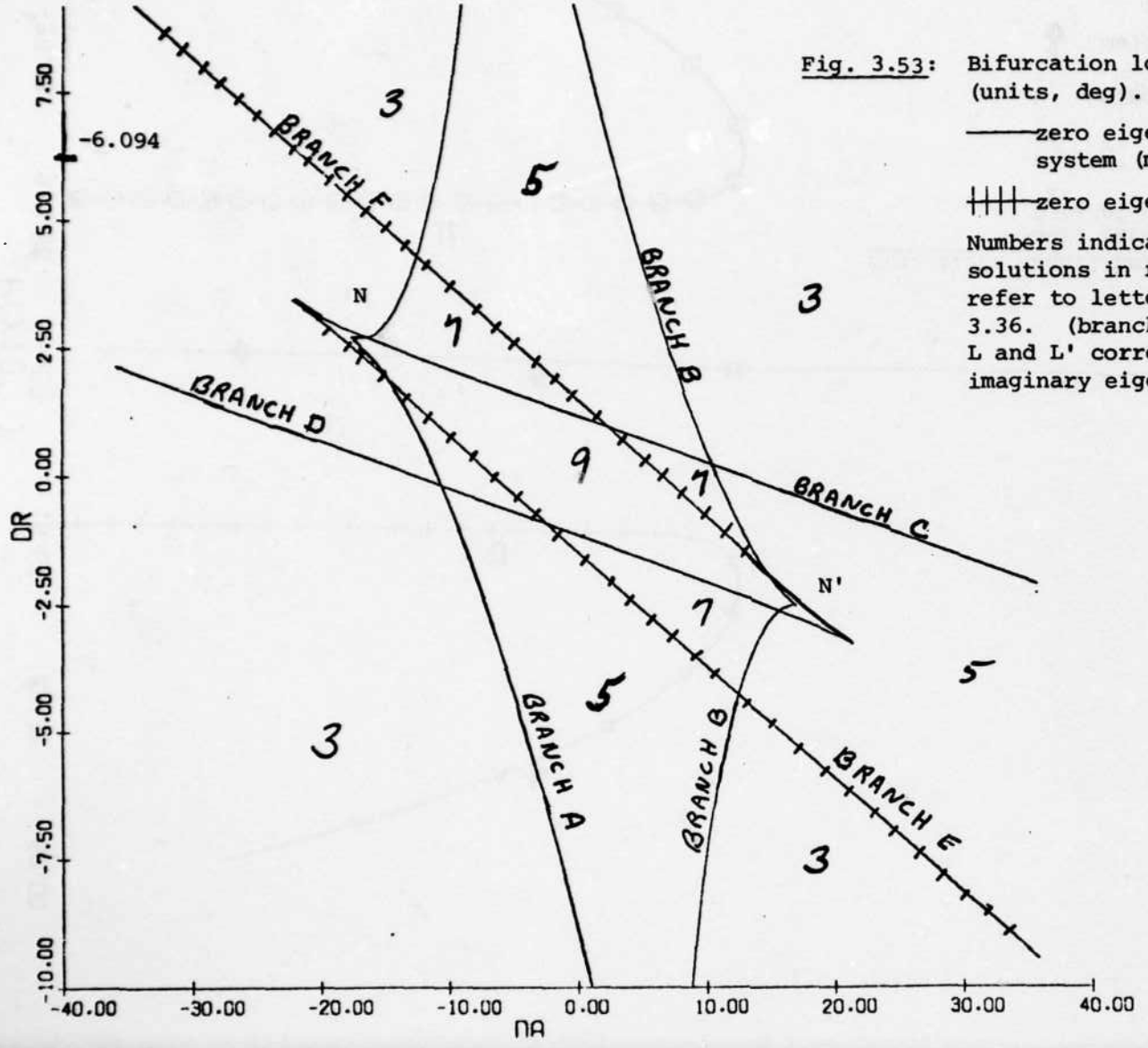

Fig. 3.53: Bifurcation locus in ($\delta a, \delta r$) plane (units, deg). A/C H; $\delta e = 0°$.

——— zero eigenvalue of linearized system (major branch).

++++ zero eigenvalue (minor branch)

Numbers indicate number of equilibrium solutions in region; branch letters refer to letters on Figs. 3.26 and 3.36. (branches I,I', J,J', K,K', L and L' corresponding to purely imaginary eigenvalues are not shown.)

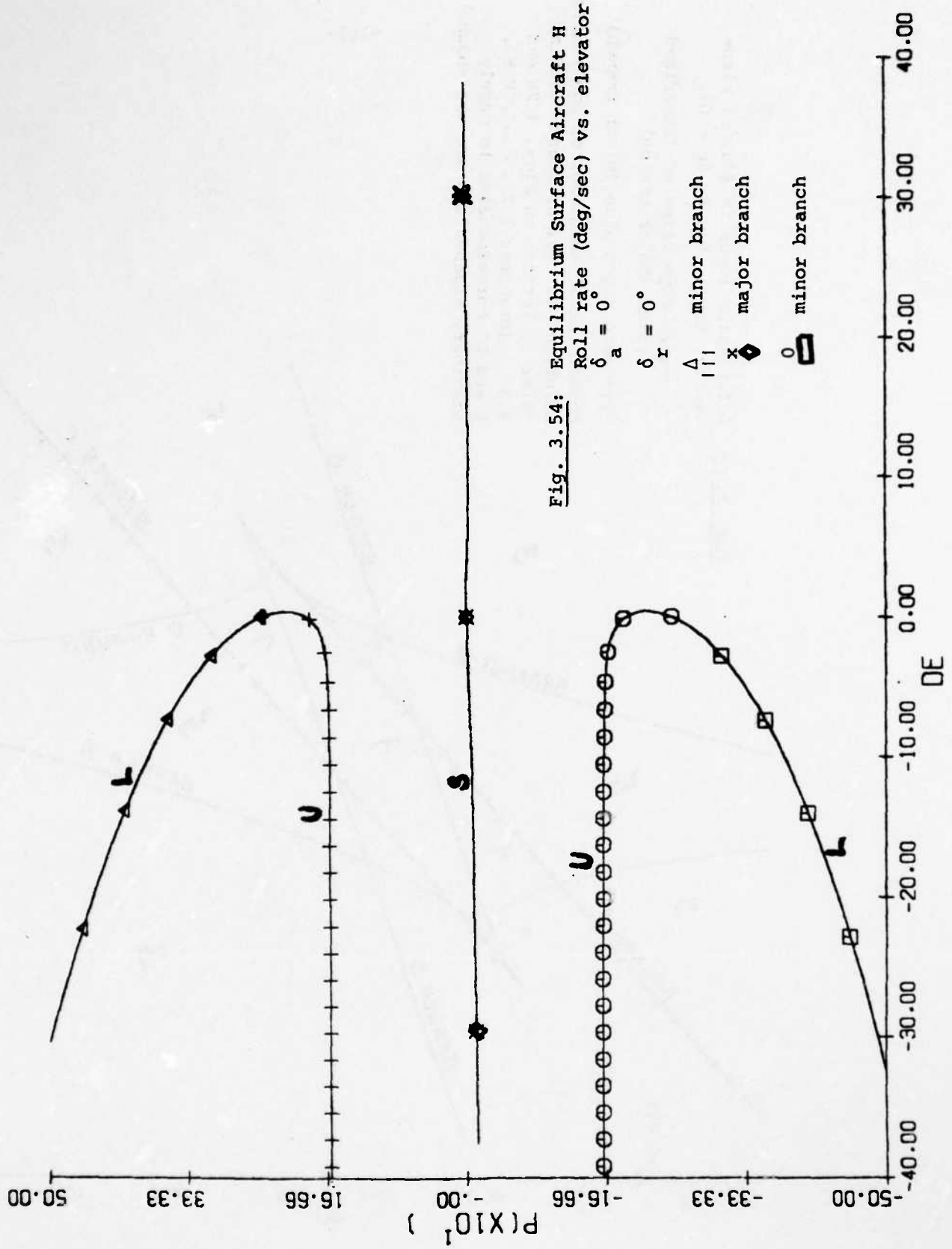
Equilibrium Surface Aircraft H
Roll rate (deg/sec) vs. elevator (deg)
δa = 0°
δr = 0°
minor branch
major branch
minor branch
P(X10¹)
DE
50.00
33.33
16.66
-.00
-16.66
-33.33
-50.00
40.00
30.00
20.00
10.00
0.00
-10.00
-20.00
-30.00
-40.00
U
L
S
U
L

Fig. 3.54:

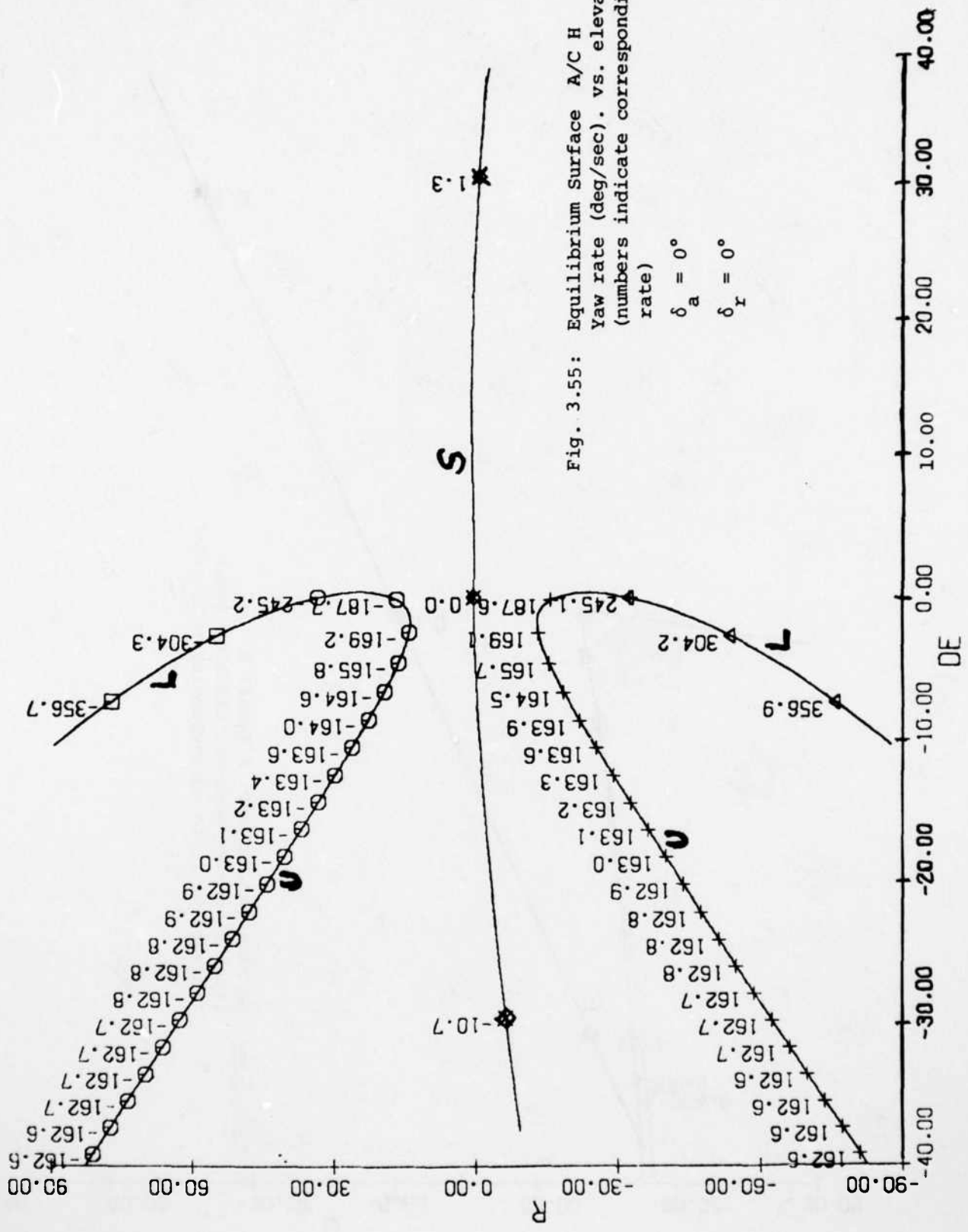
Fig. 3.55: Equilibrium Surface A/C H
Yaw rate (deg/sec). vs. elevator (deg)
(numbers indicate corresponding roll rate)
δ_a = 0°
δ_r = 0°
DE
R
40.00
30.00
20.00
10.00
0.00
-10.00
-20.00
-30.00
-40.00
90.00
60.00
30.00
0.00
-30.00
-60.00
-90.00
S
U
F
1.3
-10.7
0.0
-187.3
-245.2
-304.3
-356.7
187.6
245.1
304.2
356.9
-169.2
-165.8
-164.6
-164.0
-163.6
-163.4
-163.2
-163.1
-163.0
-162.9
-162.9
-162.8
-162.8
-162.8
-162.7
-162.7
-162.7
-162.7
-162.6
-162.6
169.1
165.7
164.5
163.9
163.6
163.3
163.2
163.1
163.0
162.9
162.8
162.8
162.8
162.7
162.7
162.7
162.6
162.6
162.6

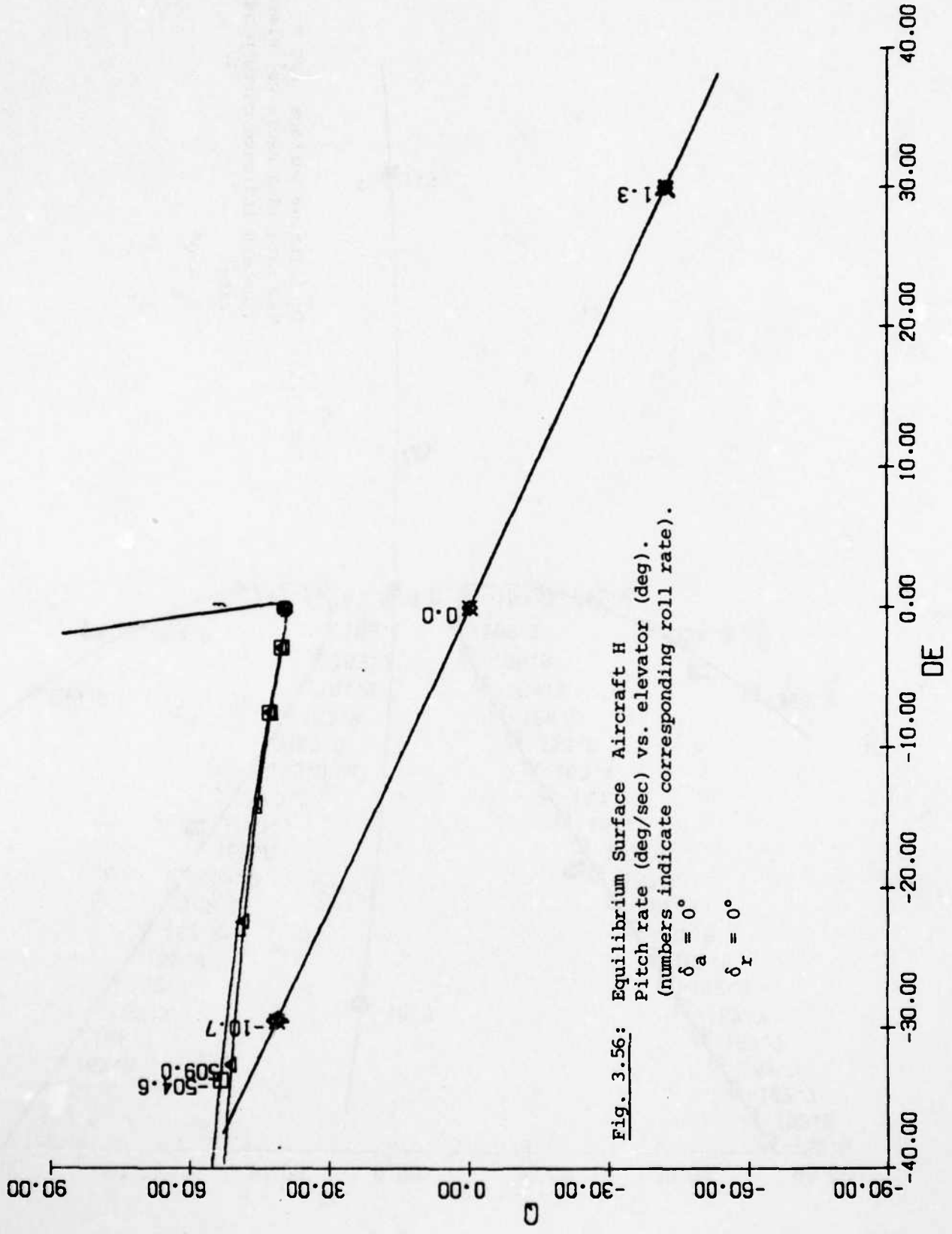

Fig. 3.56: Equilibrium Surface Aircraft H
Pitch rate (deg/sec) vs. elevator (deg).
(numbers indicate corresponding roll rate).
$\delta_a = 0°$
$\delta_r = 0°$

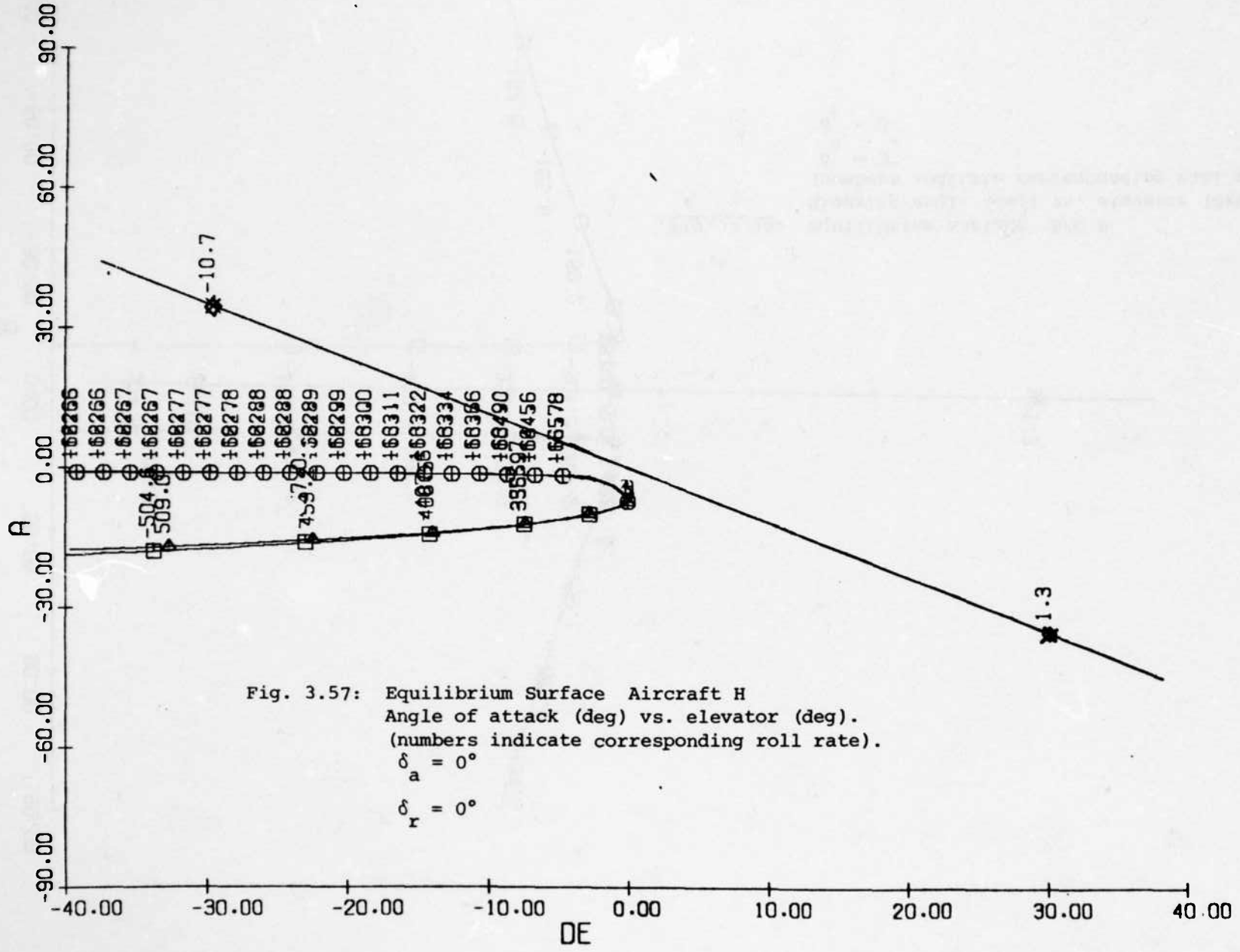

Fig. 3.57: Equilibrium Surface Aircraft H
Angle of attack (deg) vs. elevator (deg).
(numbers indicate corresponding roll rate).
$\delta_a = 0°$
$\delta_r = 0°$

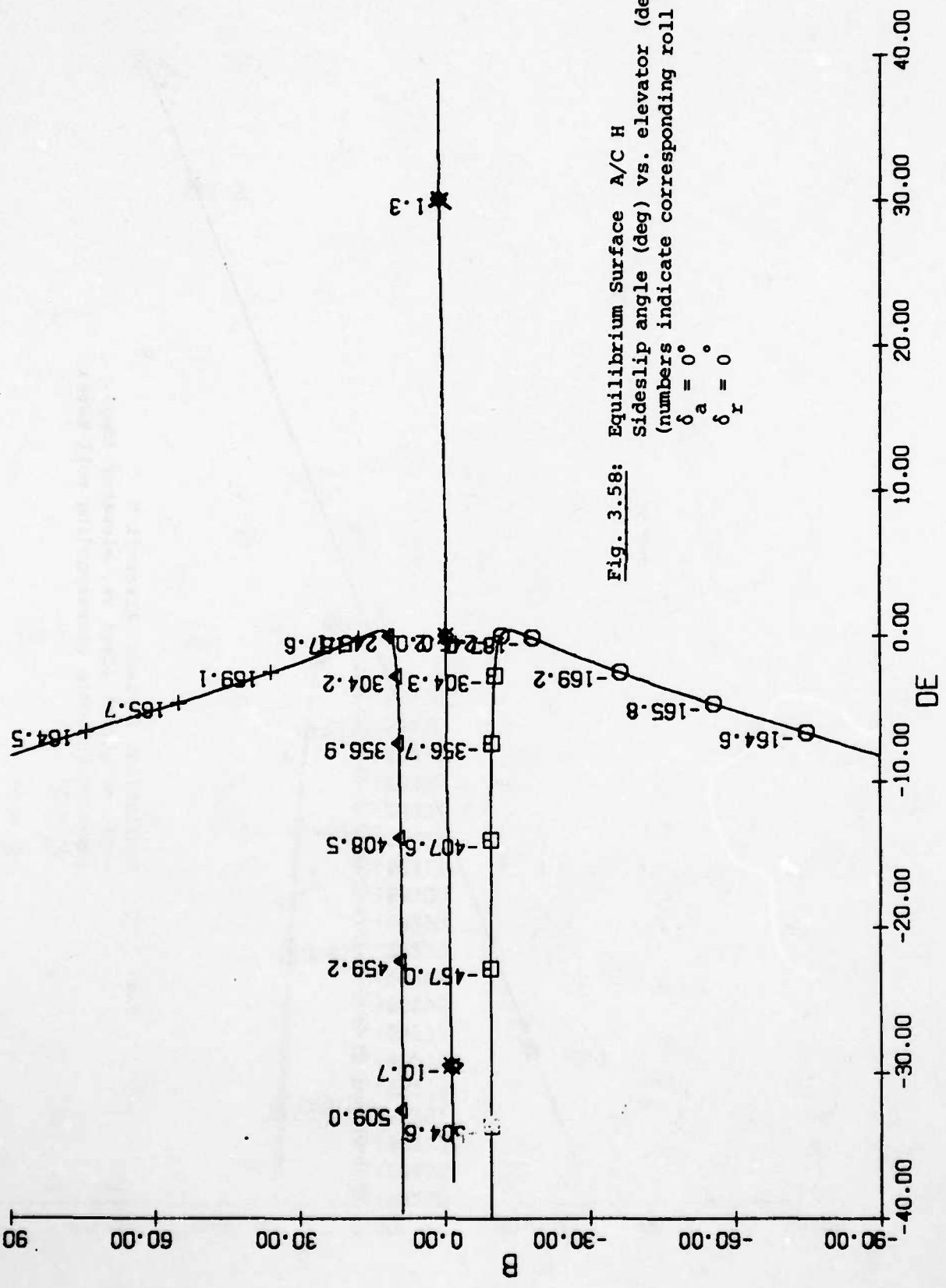
Equilibrium Surface A/C H
Sideslip angle (deg) vs. elevator (deg)
(numbers indicate corresponding roll rate).
$\delta_a = 0°$
$\delta_r = 0$
1.3
-10.7
-304.6
509.0
-457.0
459.2
-407.6
408.5
-356.7
356.9
-304.3
304.2
-252.0
252.6
-164.5
-165.7
-159.1
-159.2
-165.8
-164.6
40.00
30.00
20.00
10.00
0.00
-10.00
-20.00
-30.00
-40.00
δE
90.00
60.00
30.00
0.00
-30.00
-60.00
-90.00
β

Fig. 3.58:

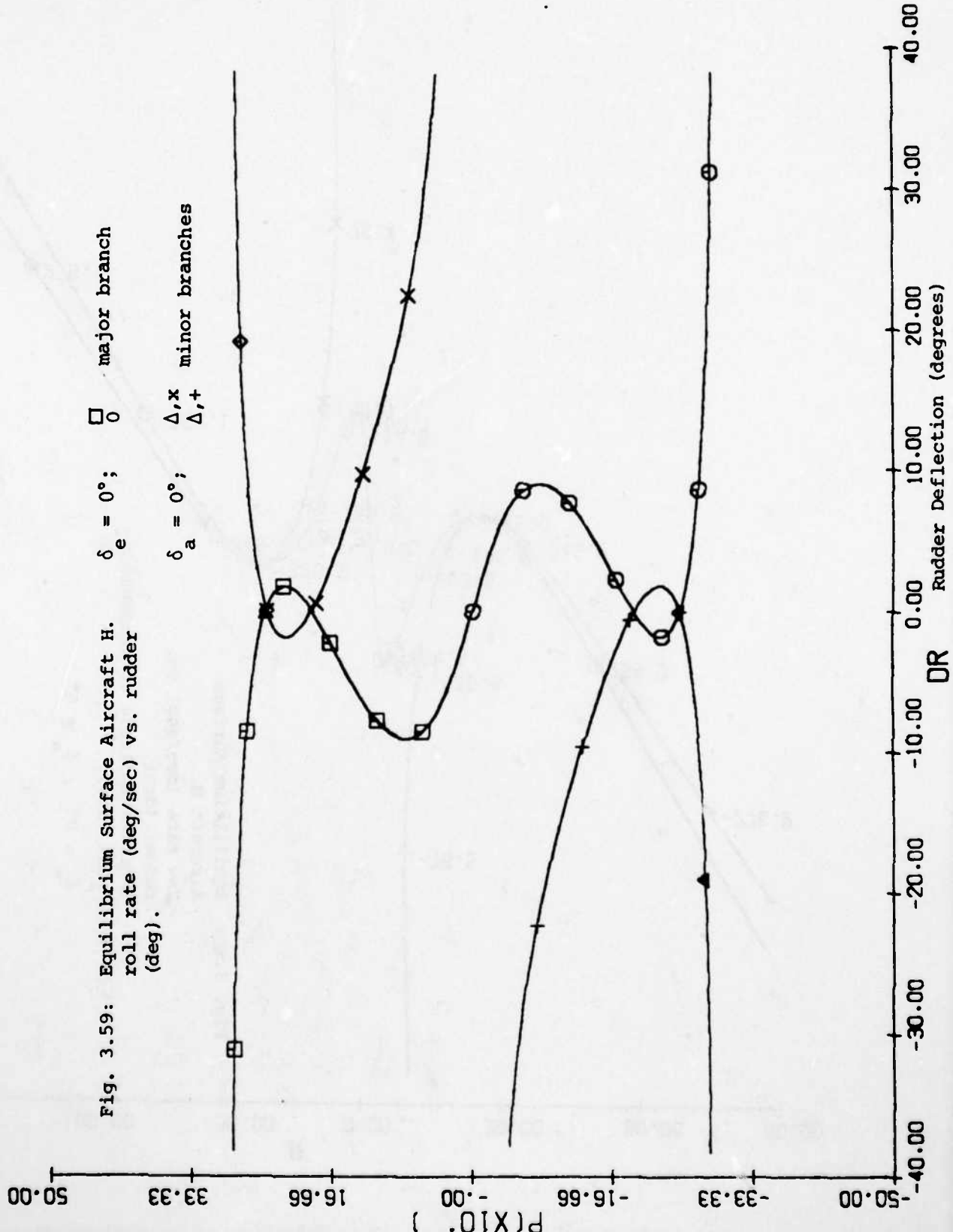

Fig. 3.59: Equilibrium Surface Aircraft H. roll rate (deg/sec) vs. rudder (deg).

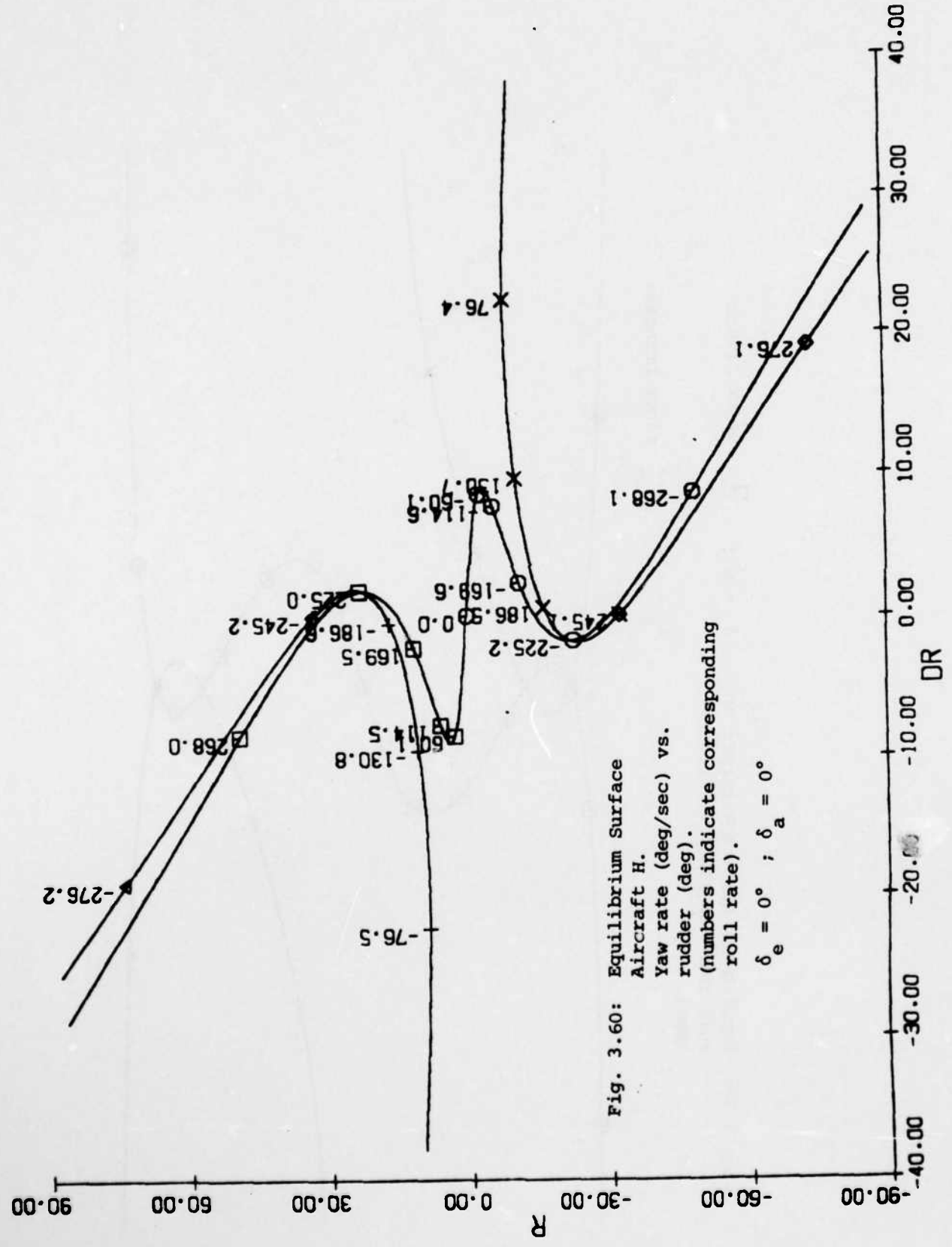

Fig. 3.60: Equilibrium Surface
Aircraft H.
Yaw rate (deg/sec) vs.
rudder (deg).
(numbers indicate corresponding
roll rate).
$\delta_e = 0°$; $\delta_a = 0°$

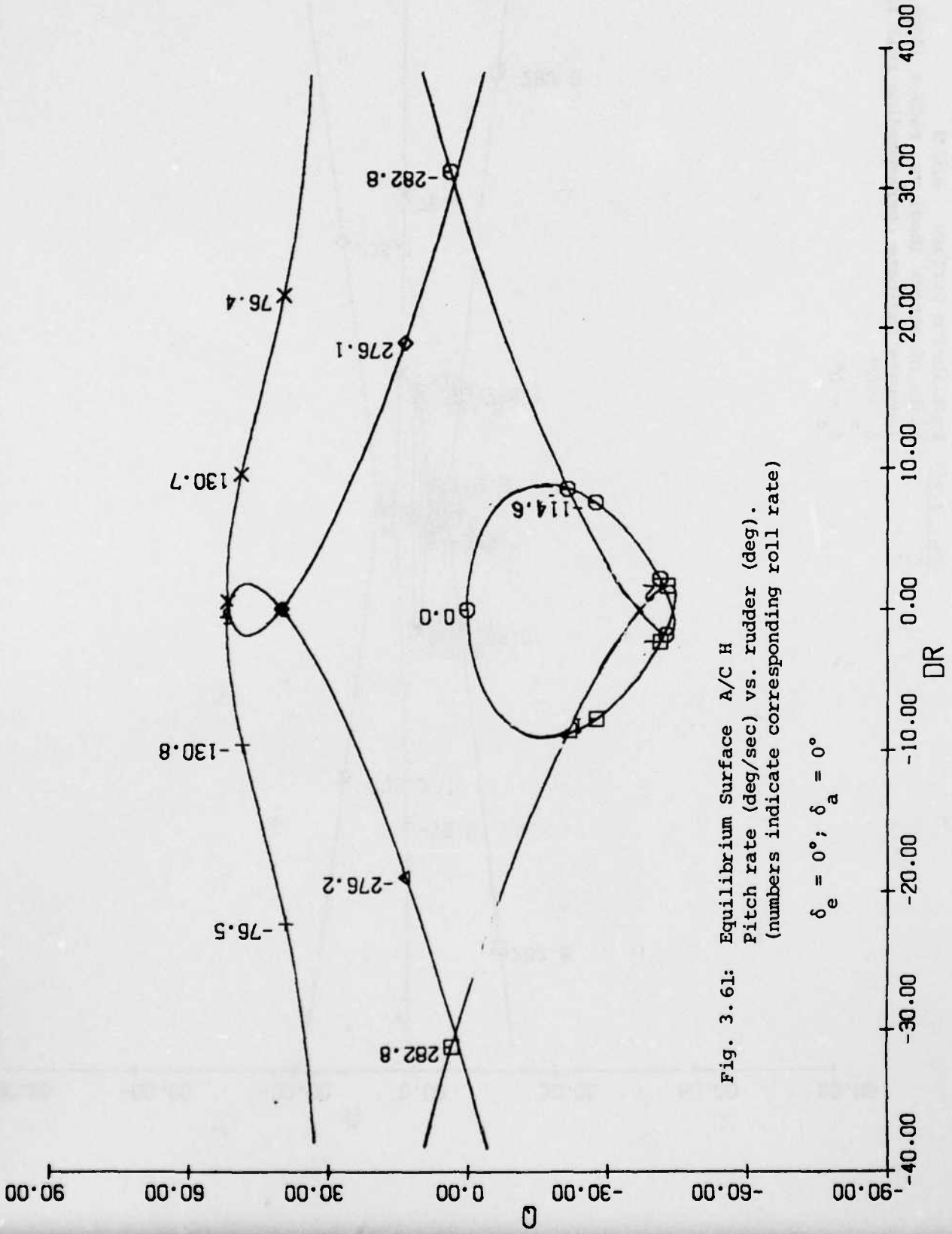

Fig. 3.61: Equilibrium Surface A/C H
Pitch rate (deg/sec) vs. rudder (deg).
(numbers indicate corresponding roll rate)

$\delta_e = 0°$; $\delta_a = 0°$

(numbers indicate corresponding roll rate)
$\delta_e = 0°$
$\delta_a = 0°$
-282.8
76.4
276.1
-276.2
-76.5
282.8
DR
P
40.00
30.00
20.00
10.00
0.00
-10.00
-20.00
-30.00
-40.00
90.00
60.00
30.00
0.00
-30.00
-60.00
-90.00

Fig. 3.63: Equilibrium Surface A/C H

Sideslip angle (deg) vs. Rudder (deg)
(numbers indicate corresponding roll rate)
$\delta_e = 0^o$
$\delta_a = 0^o$

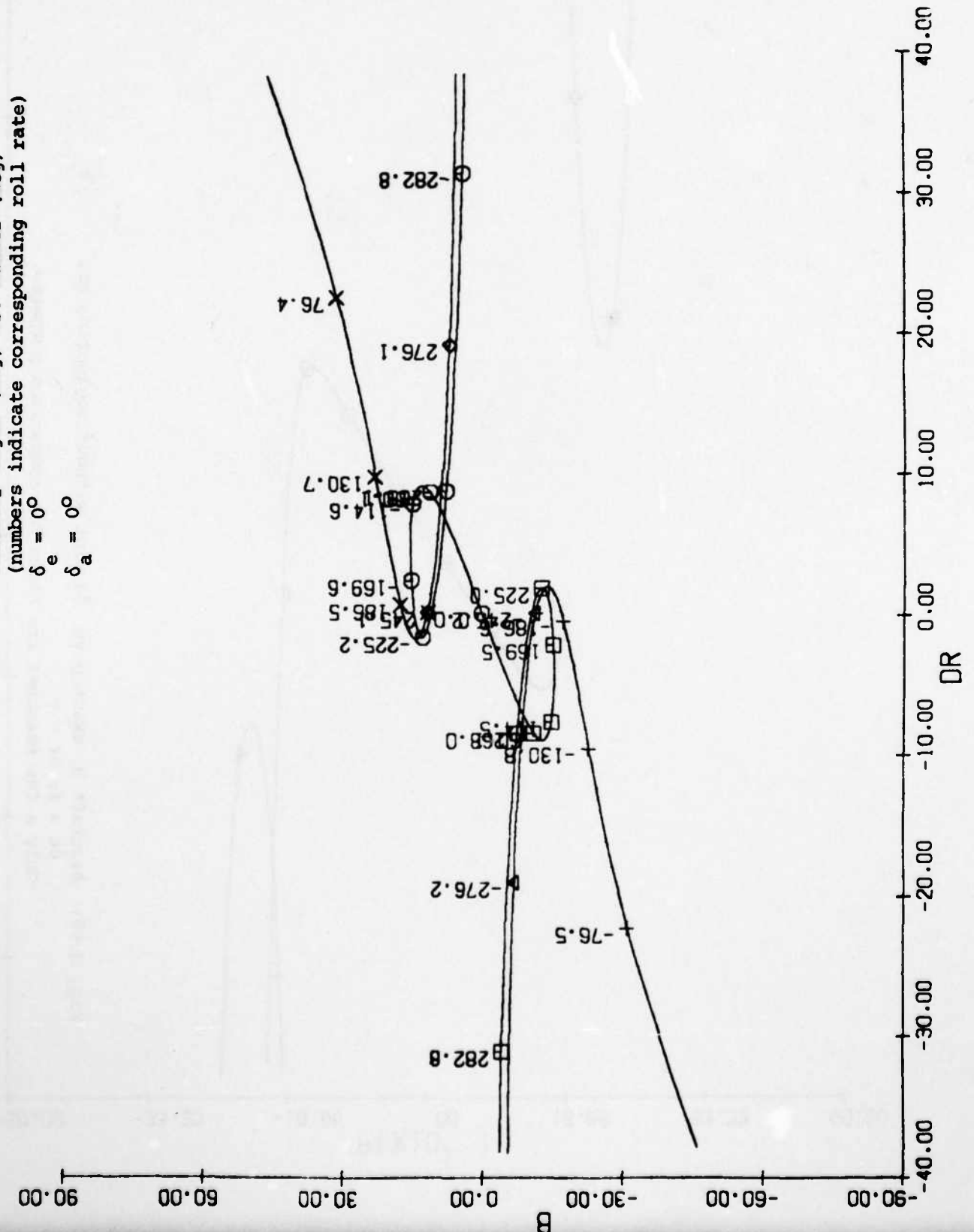

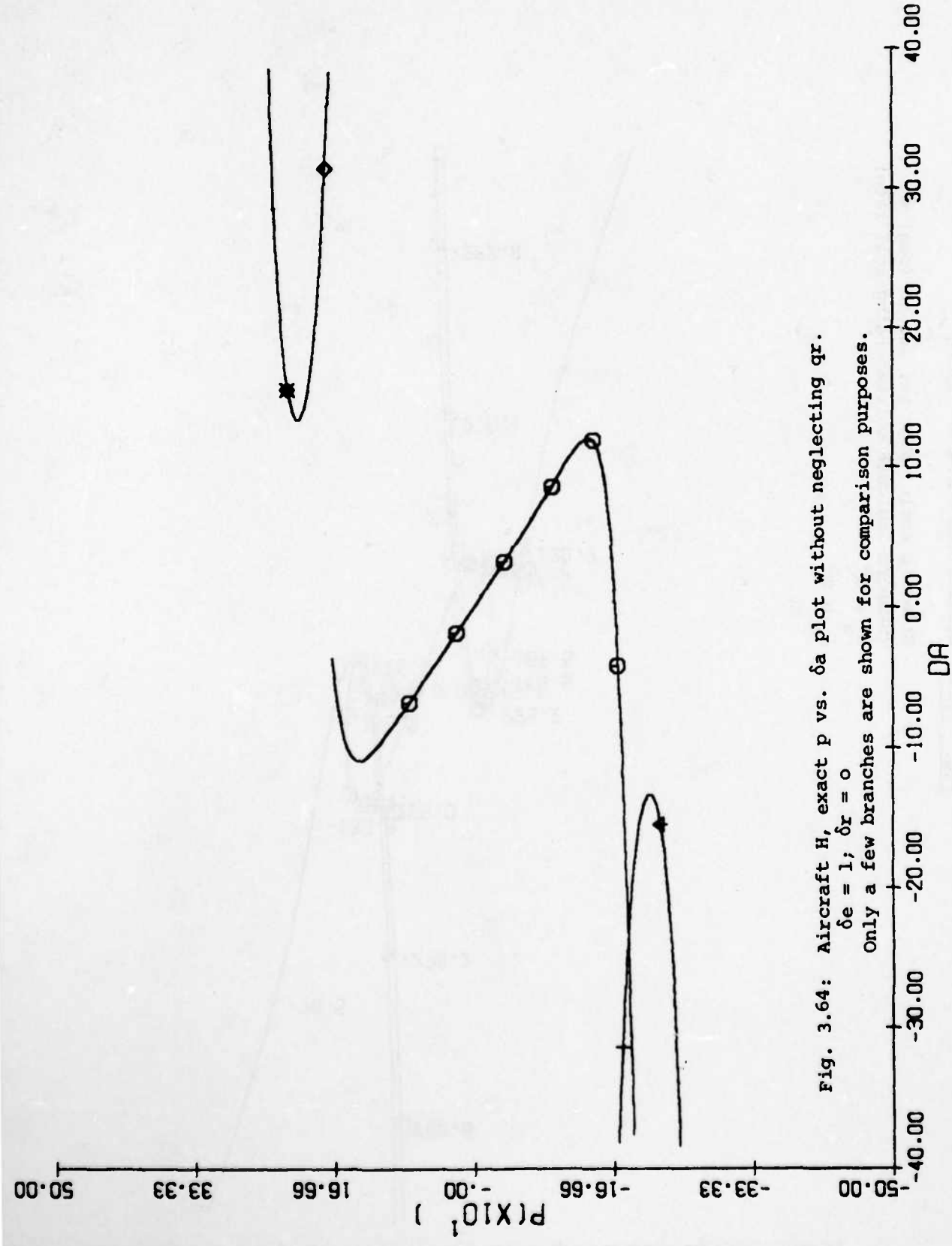

Fig. 3.64: Aircraft H, exact p vs. δa plot without neglecting qr.
δe = 1; δr = 0
Only a few branches are shown for comparison purposes.

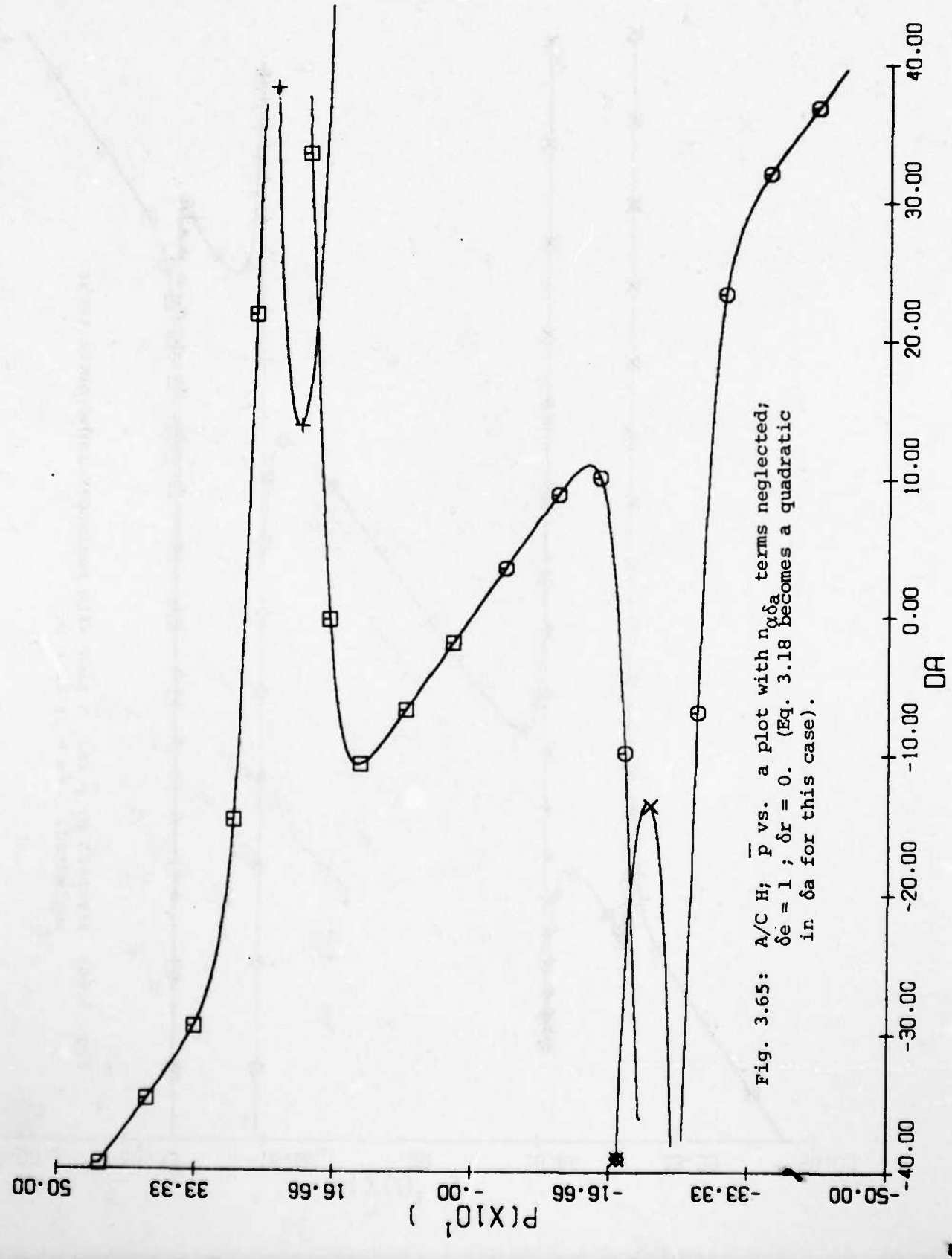

Fig. 3.65: A/C H; $\bar{P}$ vs. a plot with $n_{\alpha\delta a}$ terms neglected; $\delta e = 1$; $\delta r = 0$. (Eq. 3.18 becomes a quadratic in δa for this case).

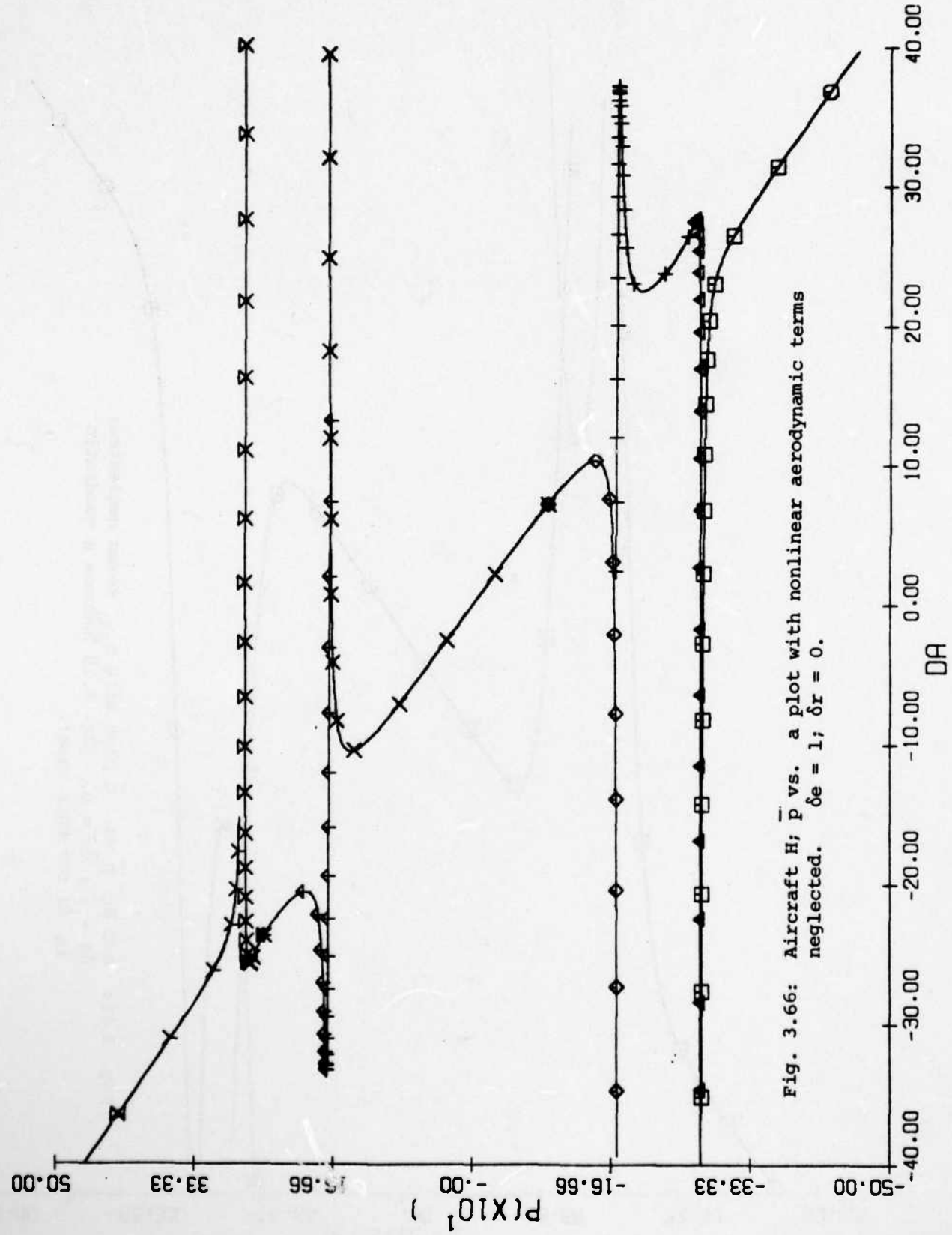

Fig. 3.66: Aircraft H; $\bar{p}$ vs. a plot with nonlinear aerodynamic terms neglected. $\delta e = 1$; $\delta r = 0$.

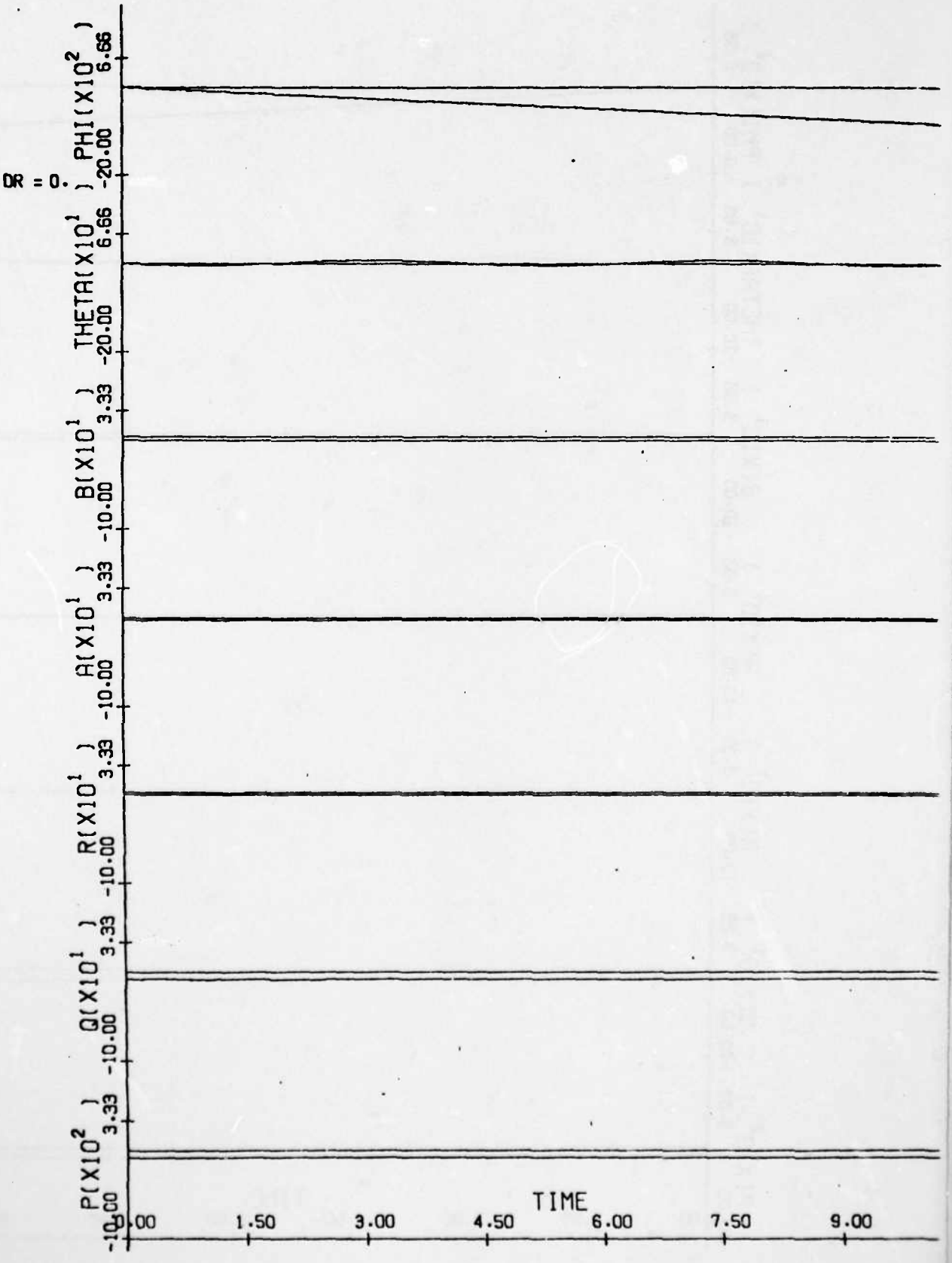

Fig. 3.67: A/C H $\delta e = 2°$, $\delta r = 0°$.
Time history for $\delta a = 8°$.

AD-A051 850 SCIENTIFIC SYSTEMS INC CAMBRIDGE MA F/G 1/3
GLOBAL STABILITY AND CONTROL ANALYSIS OF AIRCRAFT AT HIGH ANGLE--ETC(U)
JUN 77 R K MEHRA, W C KESSEL, J V CARROLL N00014-76-C-0780
UNCLASSIFIED SSI-TR-77-1 ONR-CR215-248-1 NL

3 OF 3
AD
A051850

END
DATE
FILMED
4-78
DDC

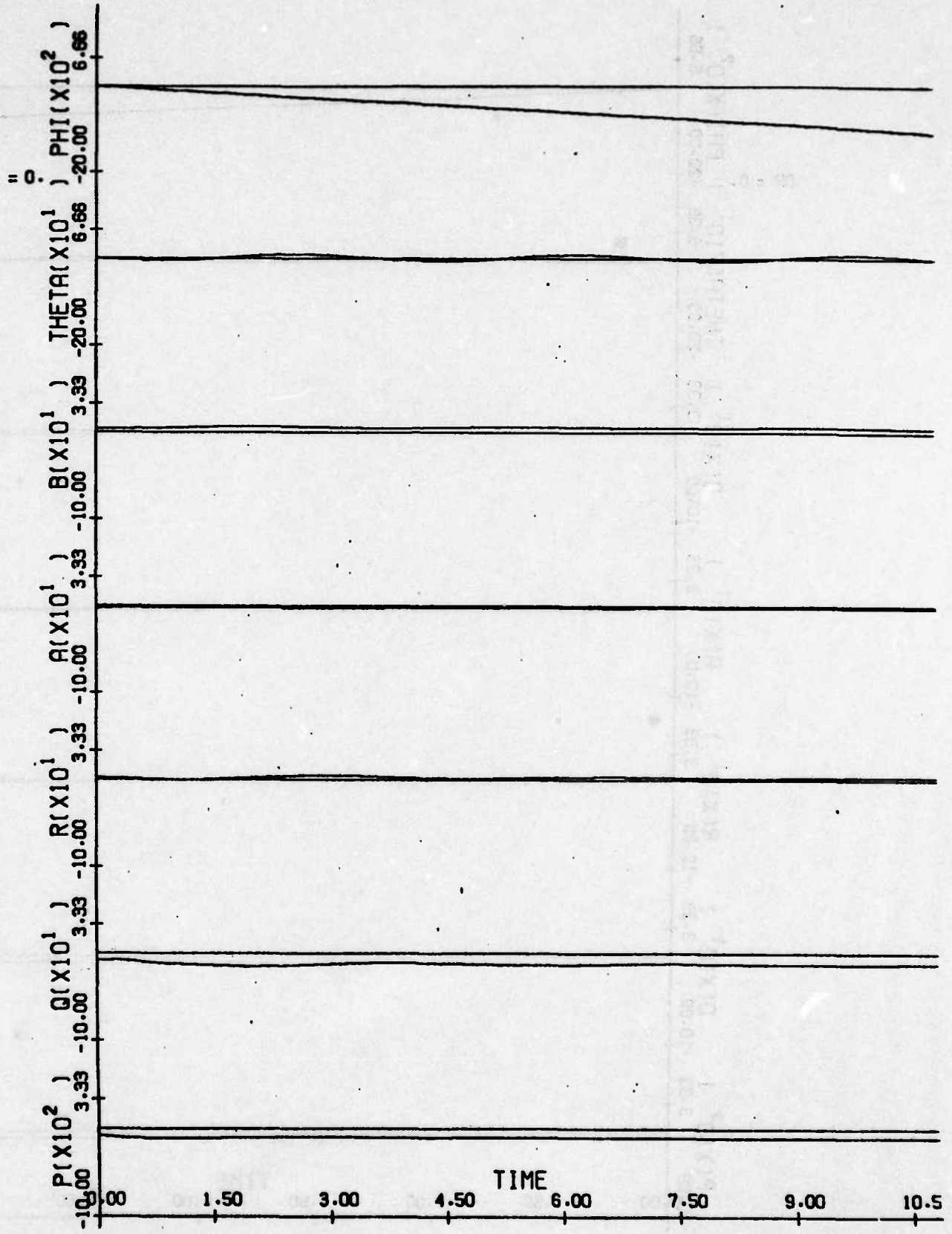

Fig. 3.68 A/C H $\delta e = 2°$, $\delta r = 0°$.
Time history for $\delta a = 10°$.

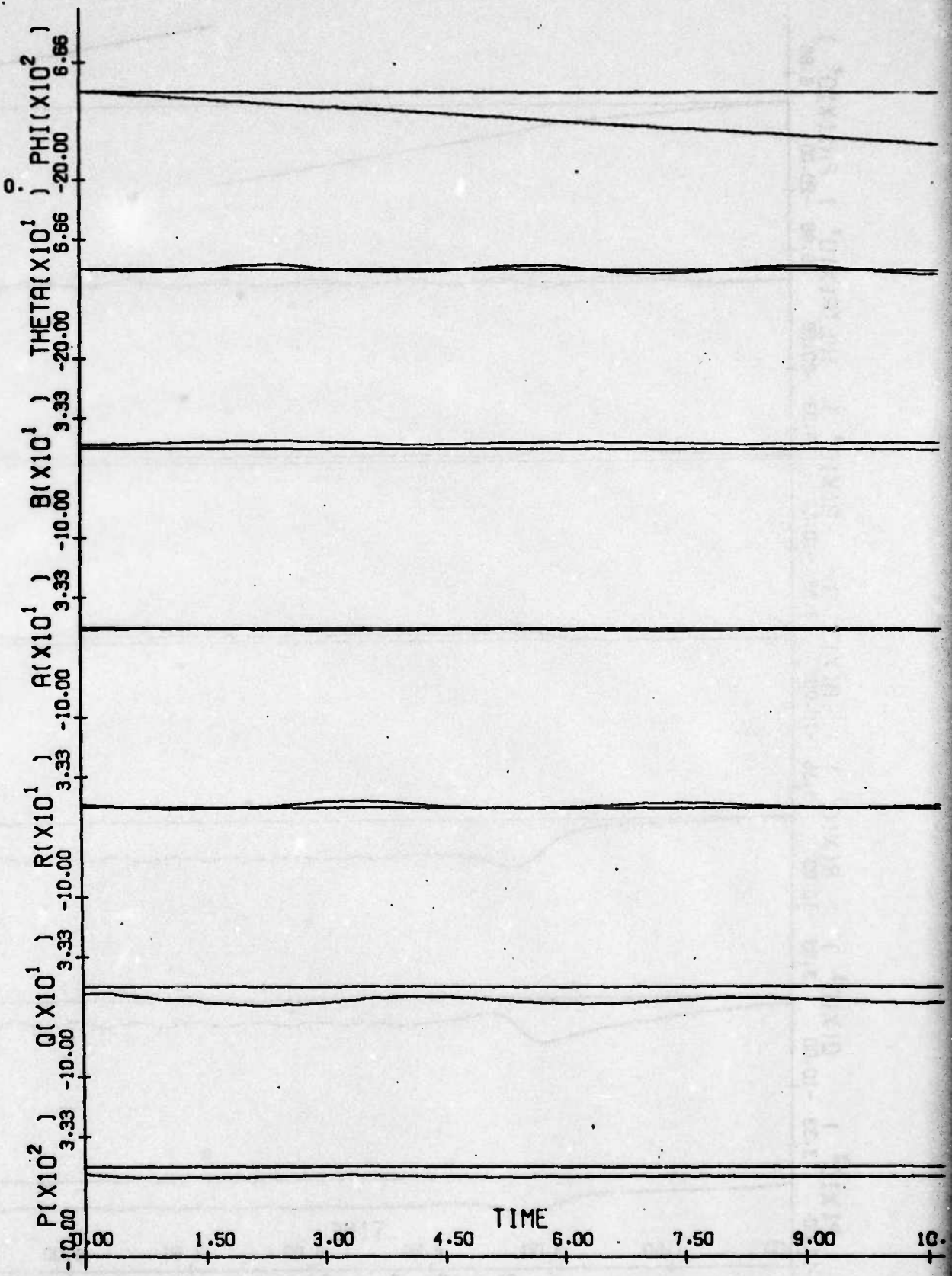

Fig. 3.69: A/C H $\delta e = 2°$, $\delta r = 0°$.
Time history for $\delta a = 11.0°$.

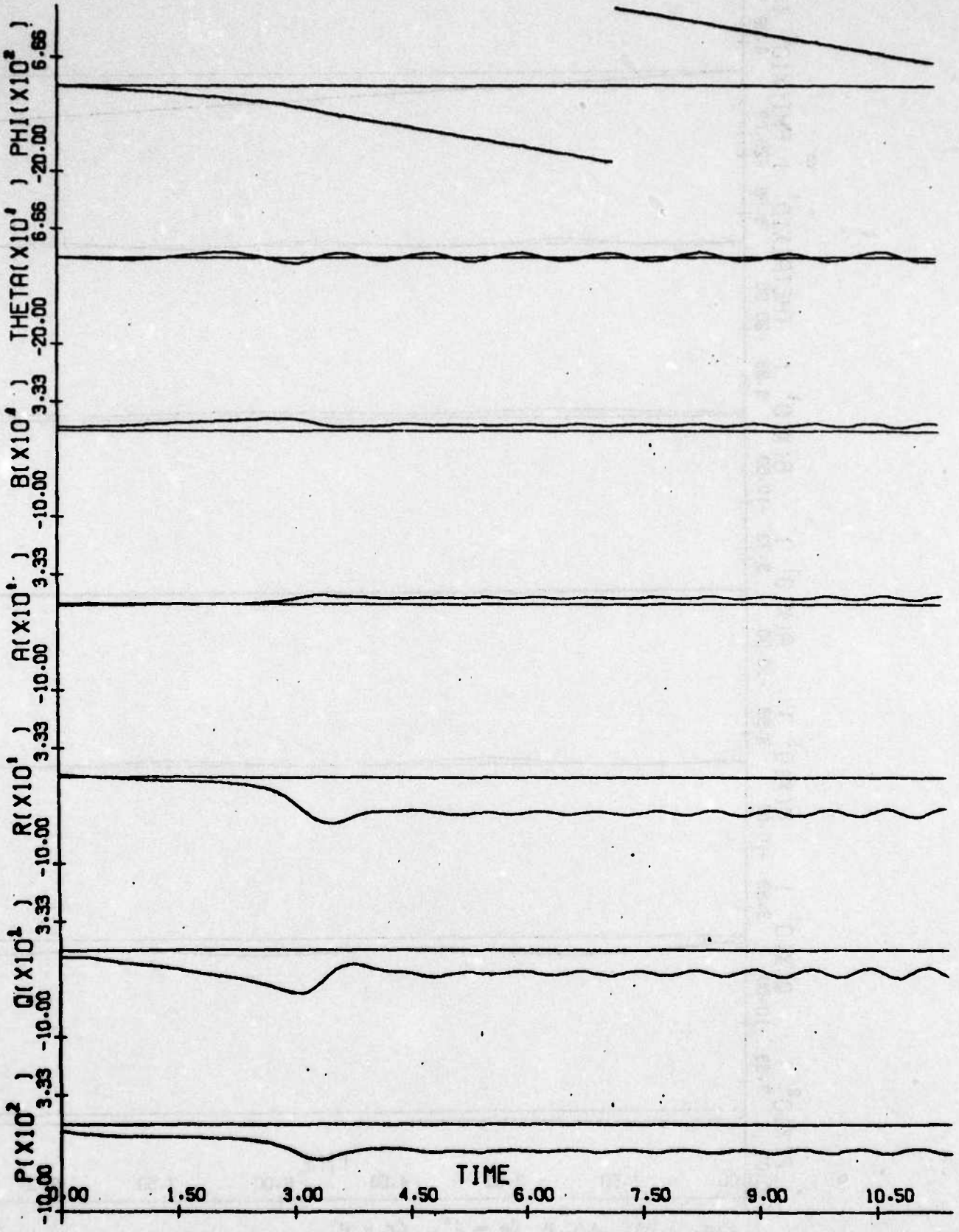

Fig. 3.70: A/C H. $\overline{\delta e = 2^\circ}$, $\delta r = 0^\circ$.
Time history for $\delta a = 12^\circ$.

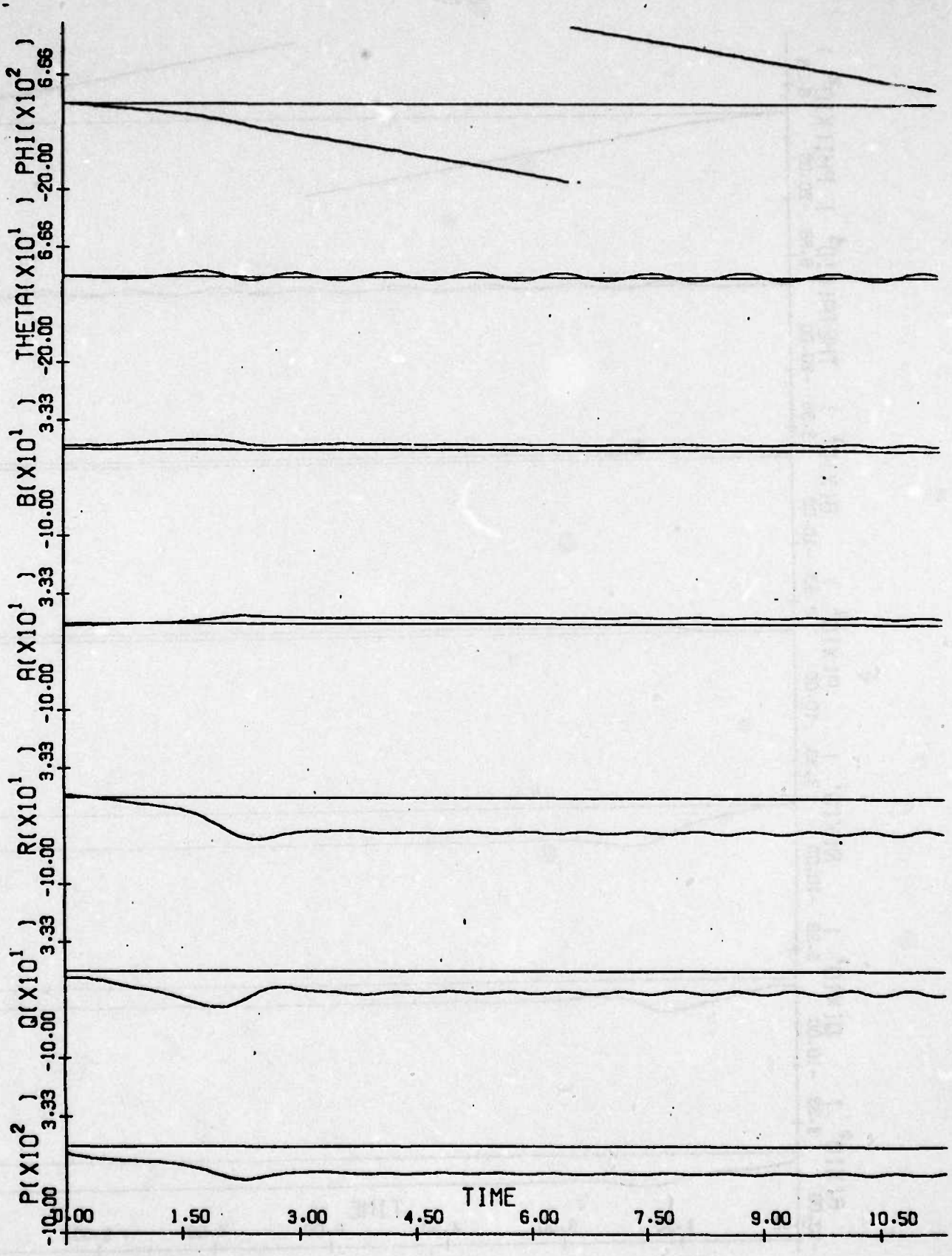

Fig. 3.71: A/C H $\delta e = 2°$, $\delta r = 0°$.
Time history for $\delta a = 14°$.

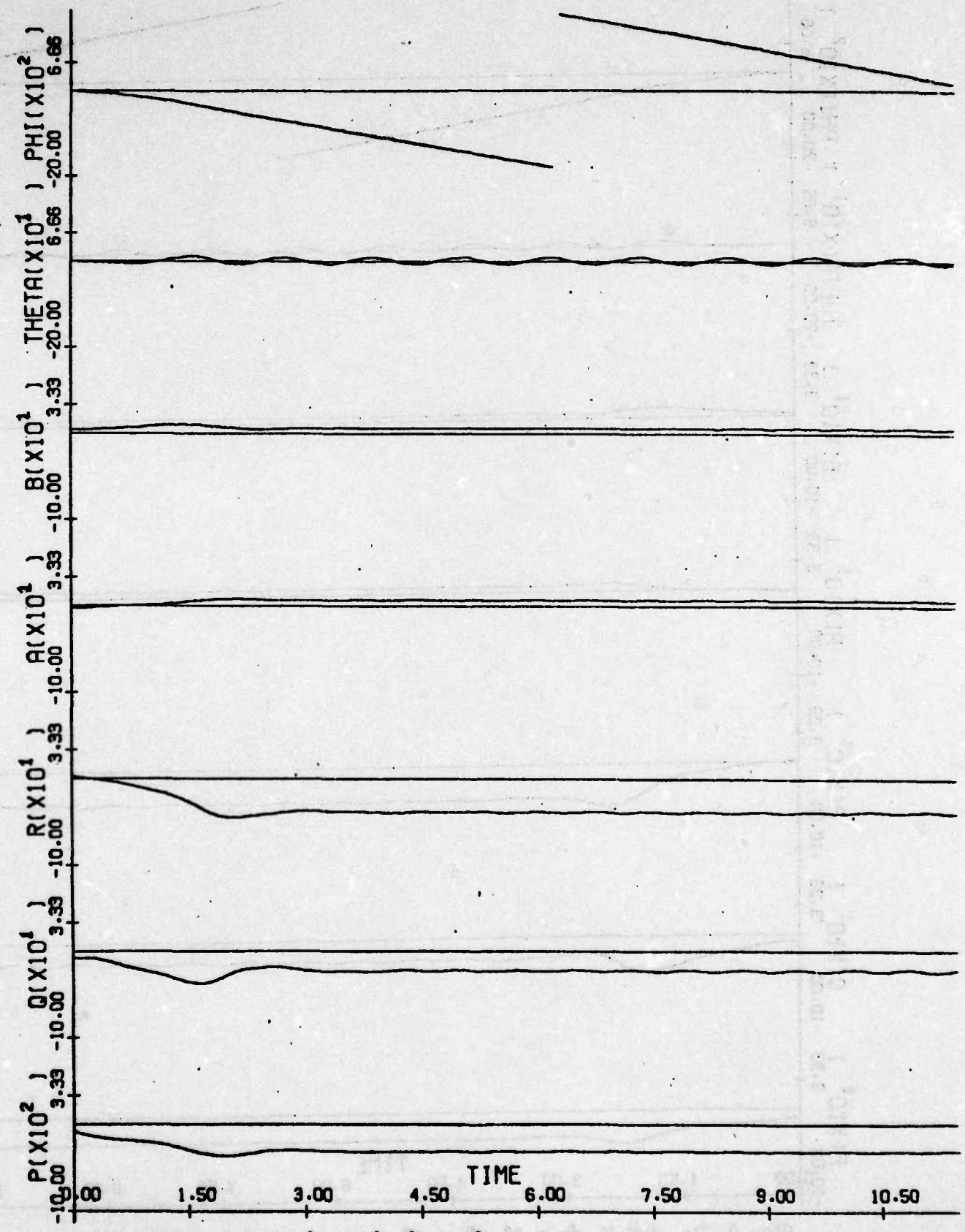

Fig. 3.72: A/C H $\delta e = 2°$, $\delta r = 0°$.
Time history for $\delta a = 16°$.

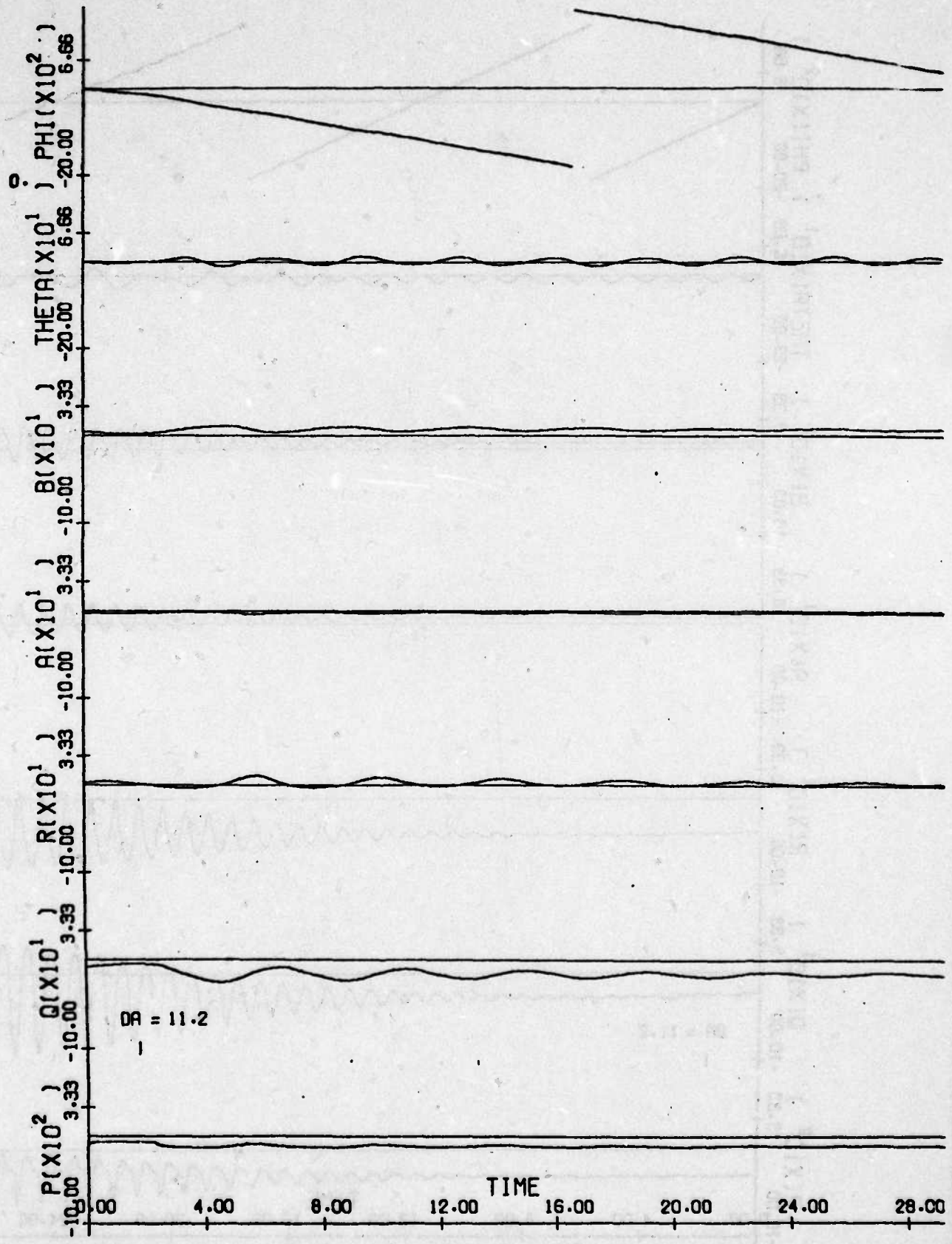

Fig. 3.73: A/C H $\delta e = 2°$, $\delta r = 0°$.
Time history with initial conditions on linear equilibrium branch; $\delta a = 6$, $11.2°$.

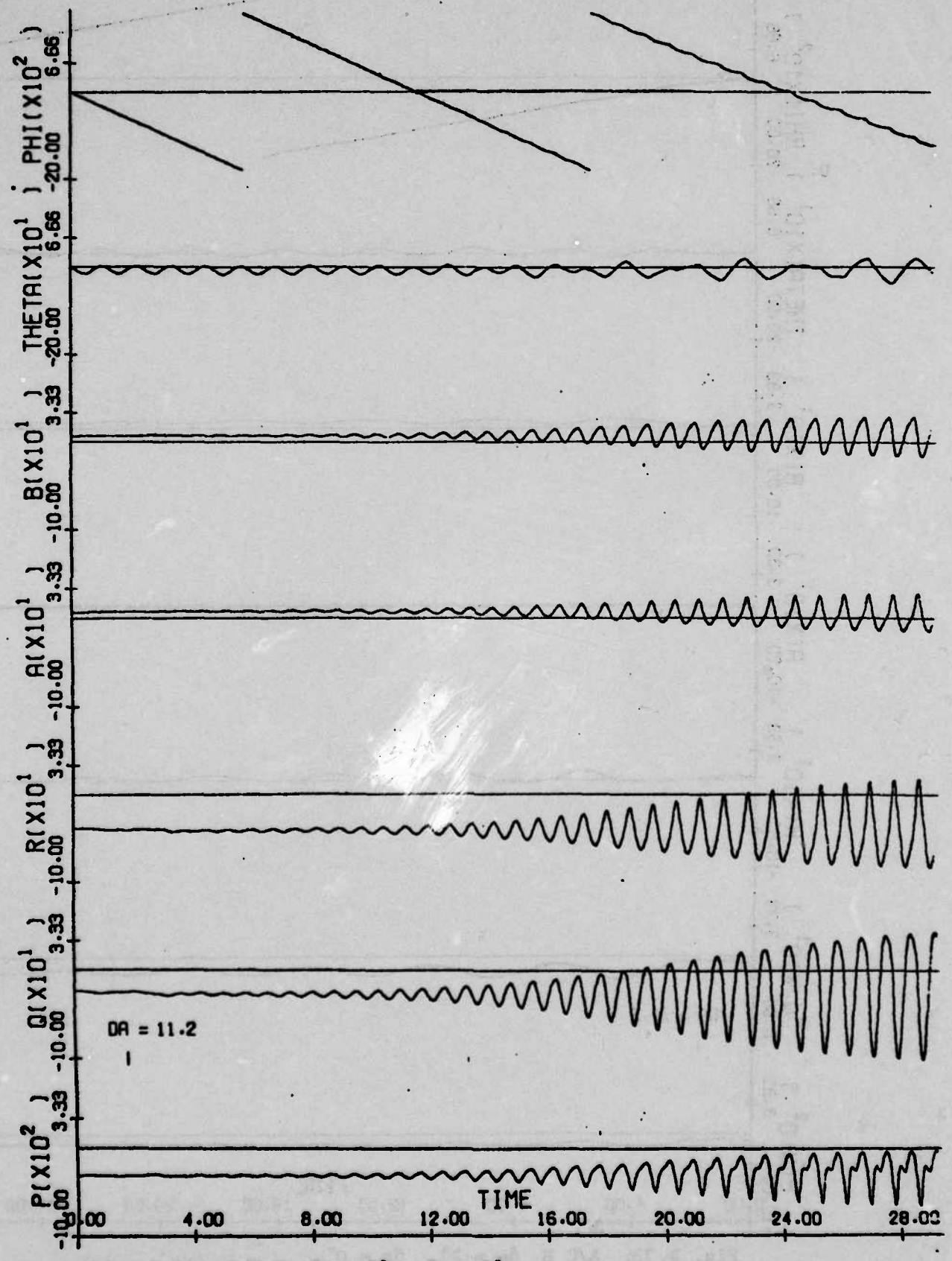

Fig. 3.74: A/C H $\delta e = 2°$, $\delta r = 0°$.
Time history with initial conditions on outer equilibrium branch; $\delta a = 13.5°$, $11.2°$.

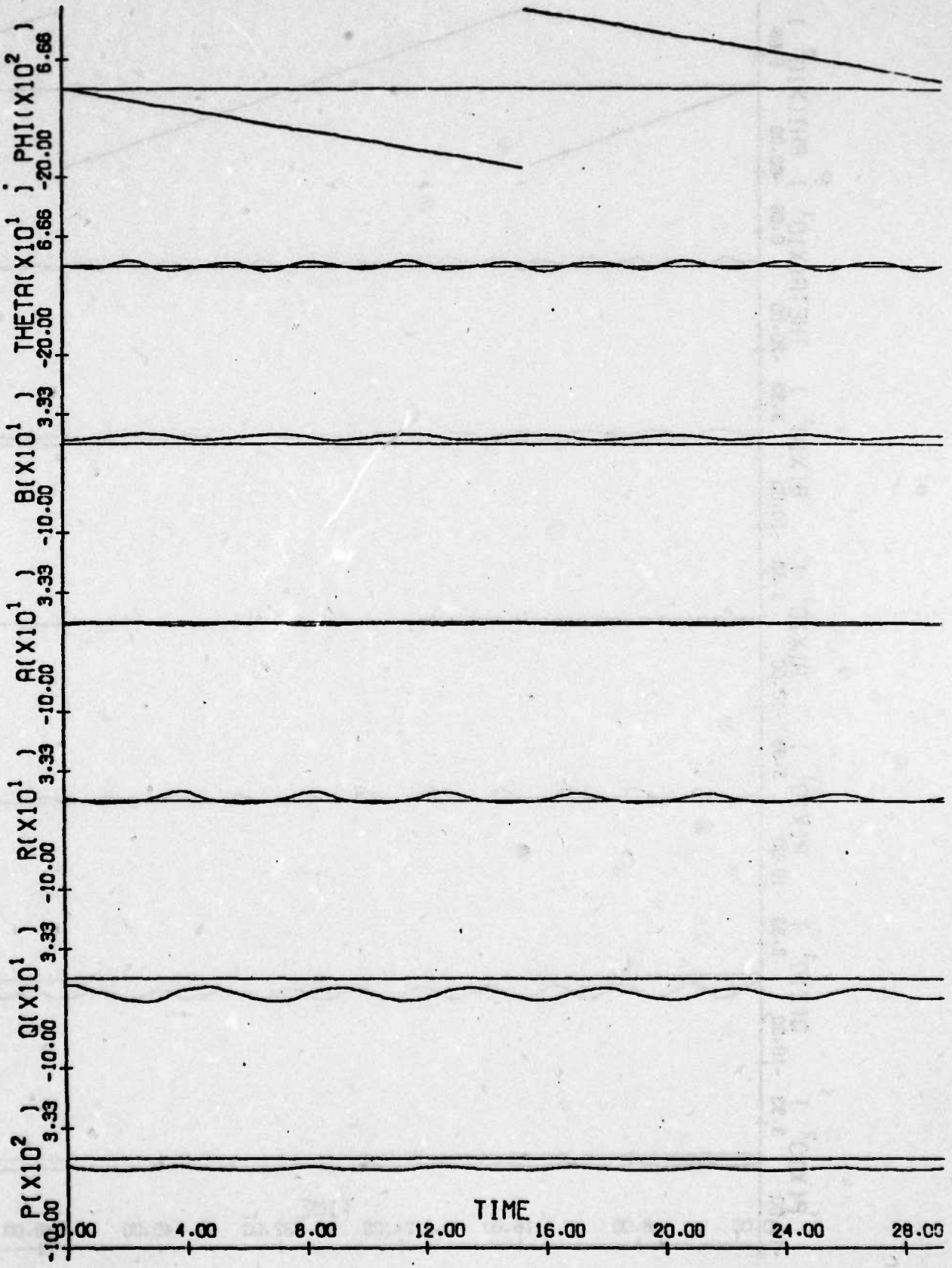

Fig. 3.75: A/C H $\delta e = 2°$; $\delta r = 0°$.
Time history for $\delta a = 11.4°$.

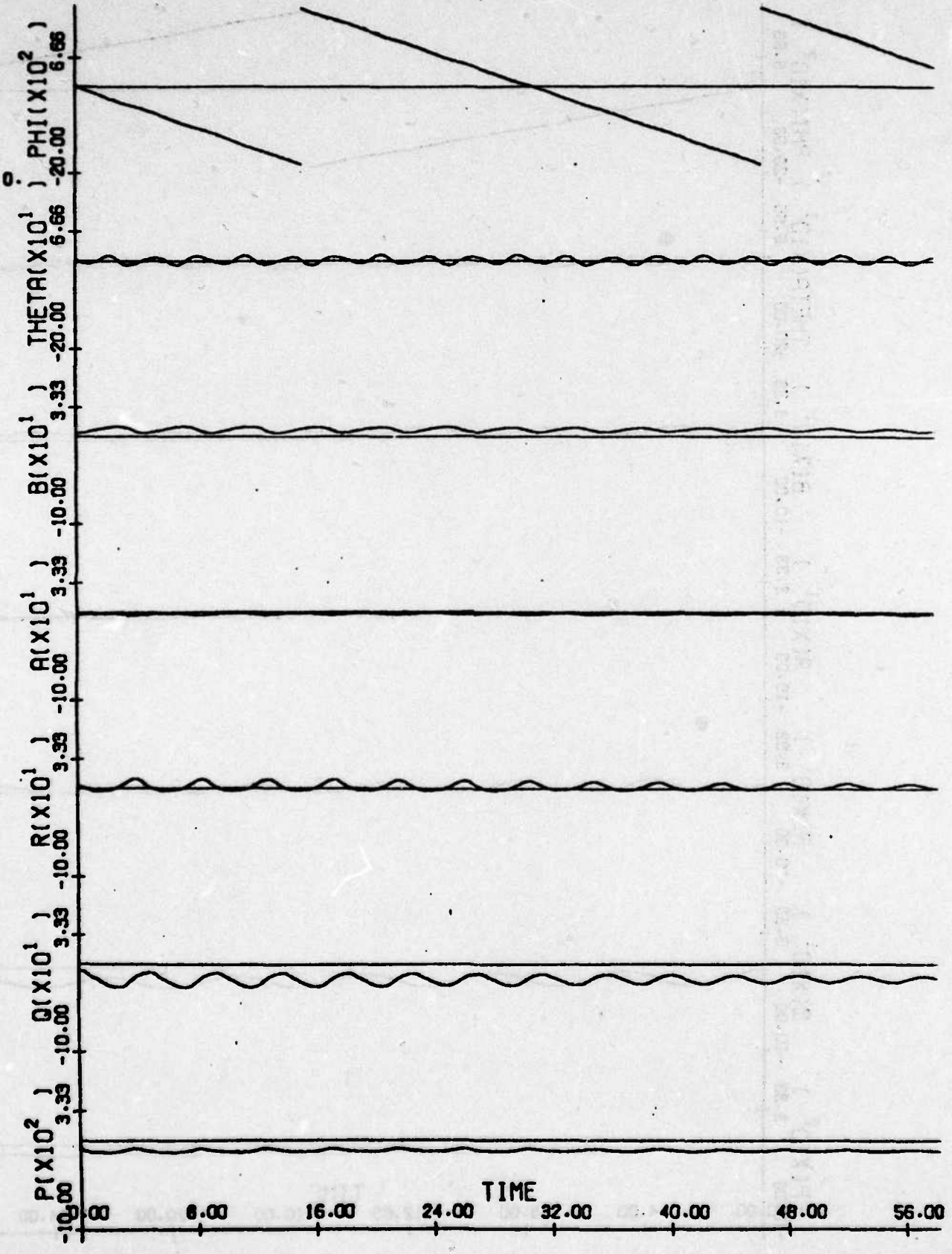

Fig. 3.76: A/C H $\delta e = 2°$; $\delta r = 0°$.
Time history for $\delta a = 11.46°$.

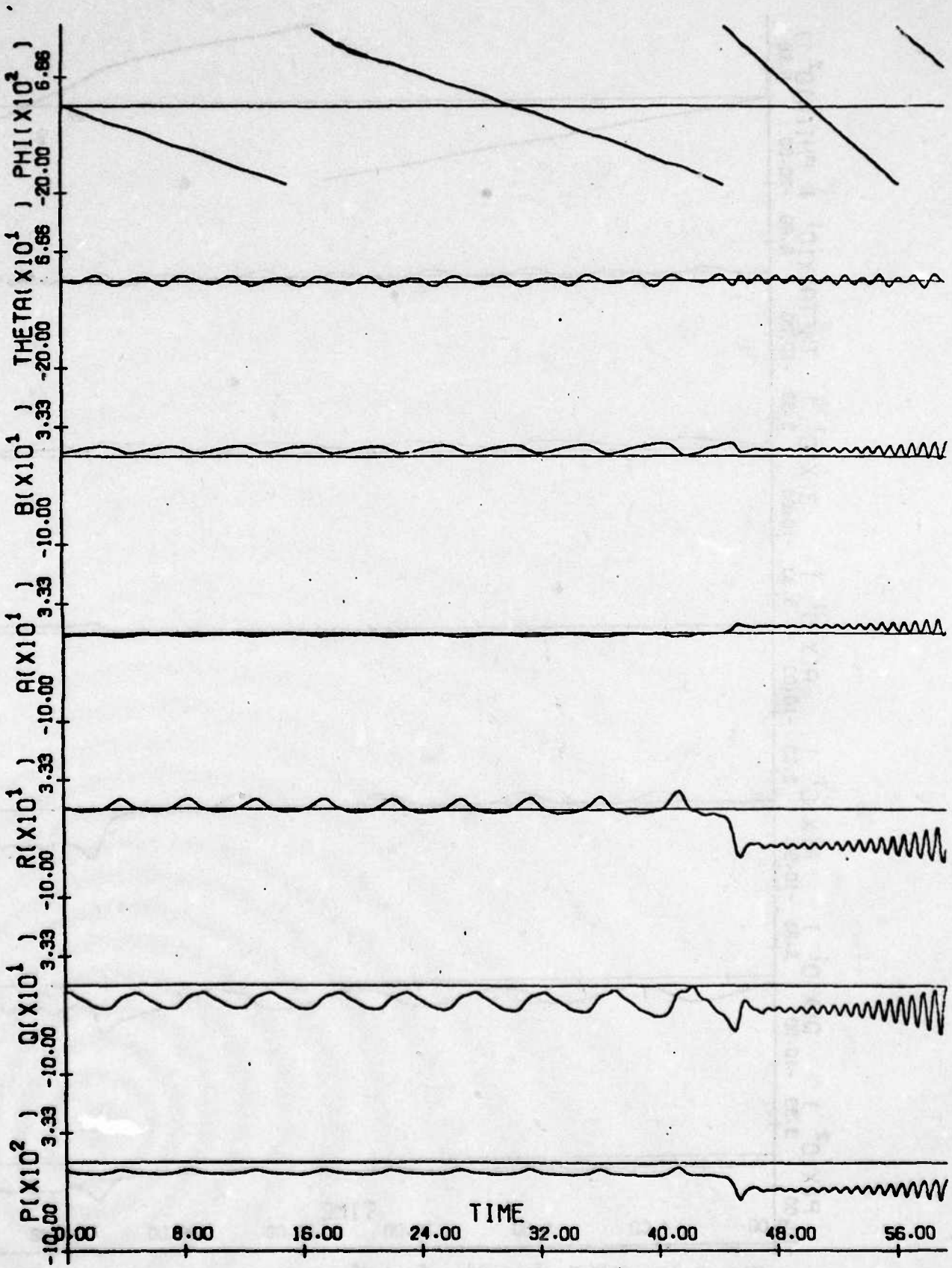

Fig. 3.77: A/C H $\delta e = 2°$; $\delta r = 0°$.
Time history for $\delta a = 11.48°$.

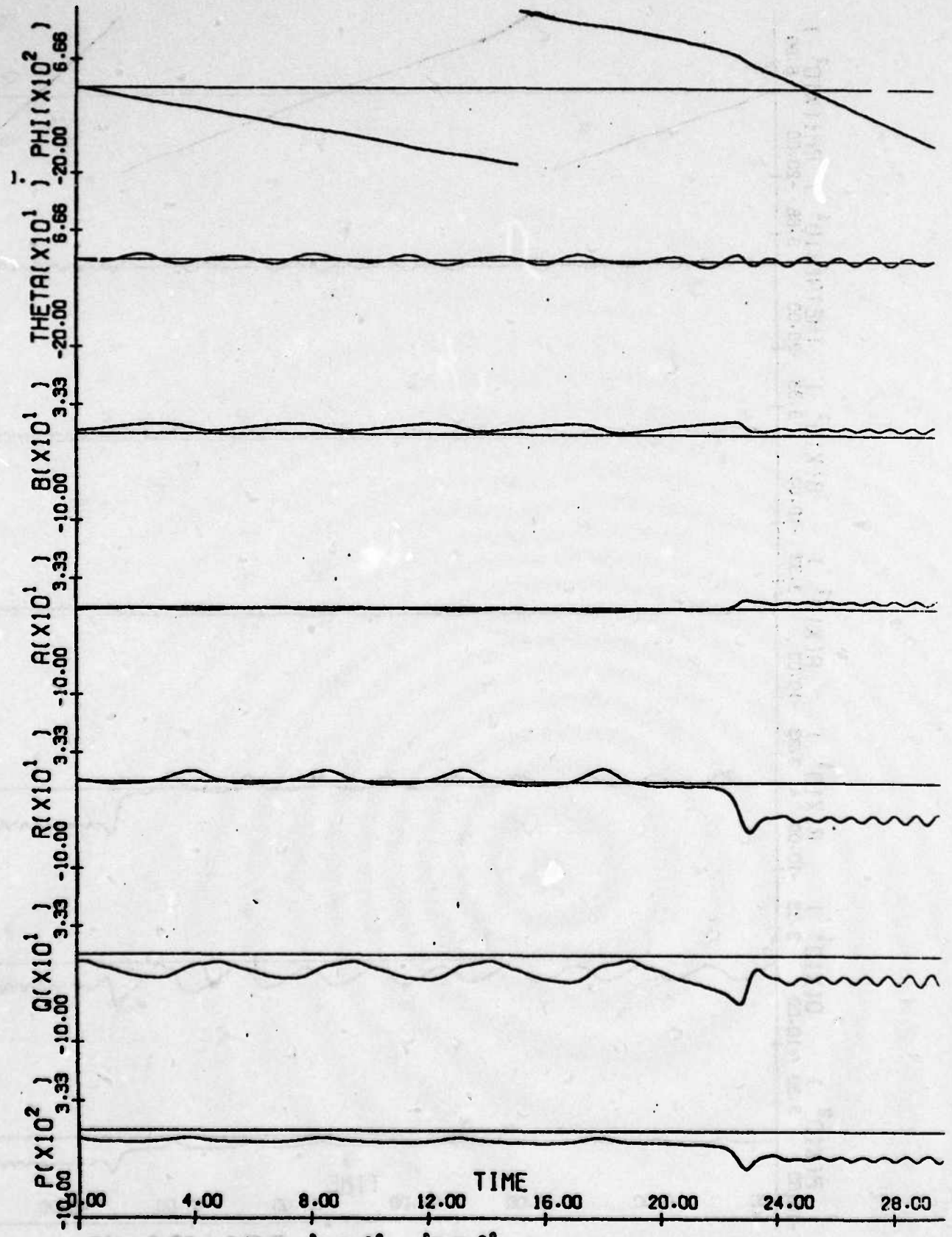

Fig. 3.78: A/C H, $\delta_e = 2°$. $\delta_r = 0°$.
Time history for $\alpha = 11.5°$.

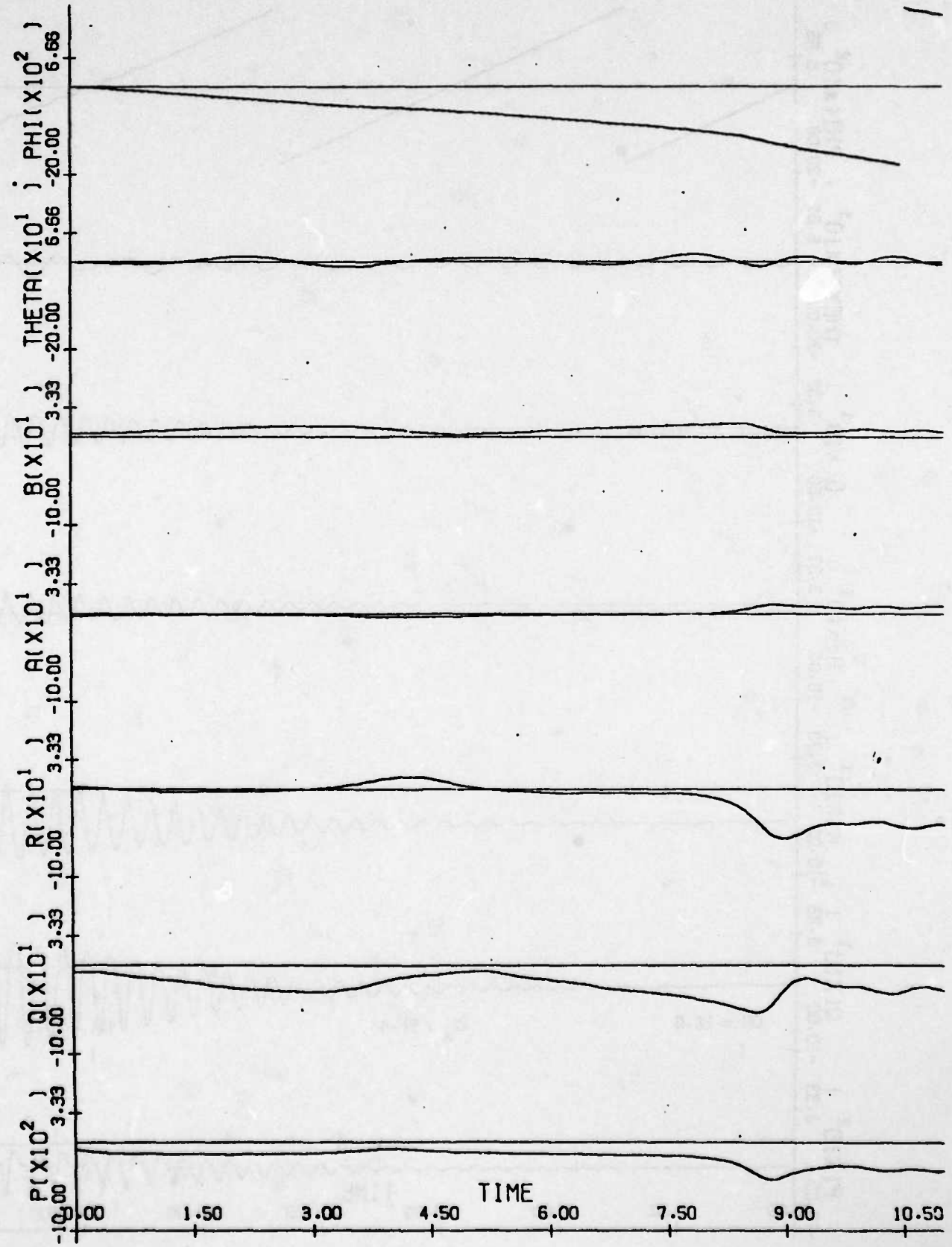

Fig. 3.79: A/C H $\delta e = 2°$; $\delta r = 0°$.
Time histories for $\delta a = 11.6°$

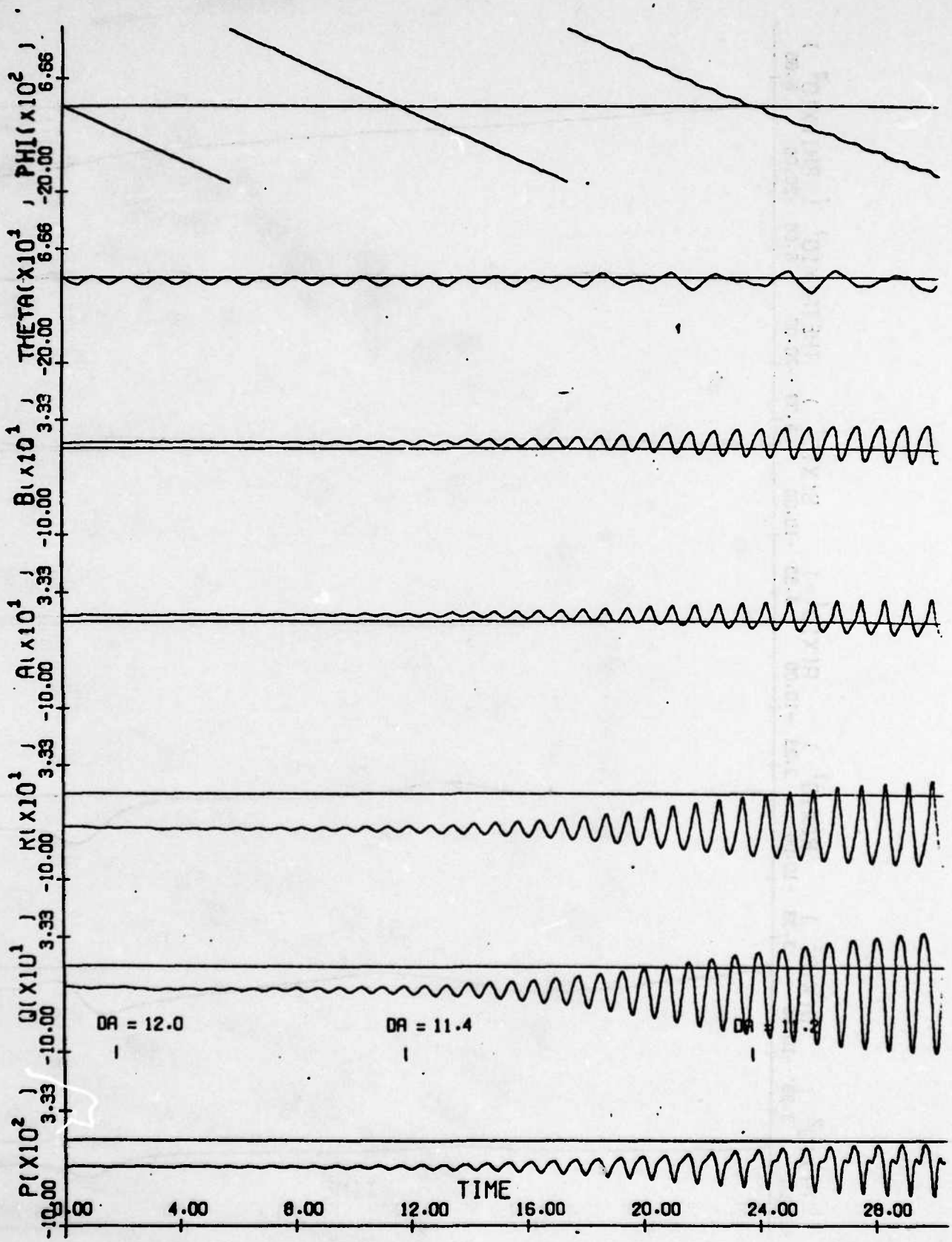

Fig. 3.80: A/C H $\delta e = 2°$, $\delta r = 0°$.
Time history for $\delta a = 0°$, 12°, 11.4°, 11.2°

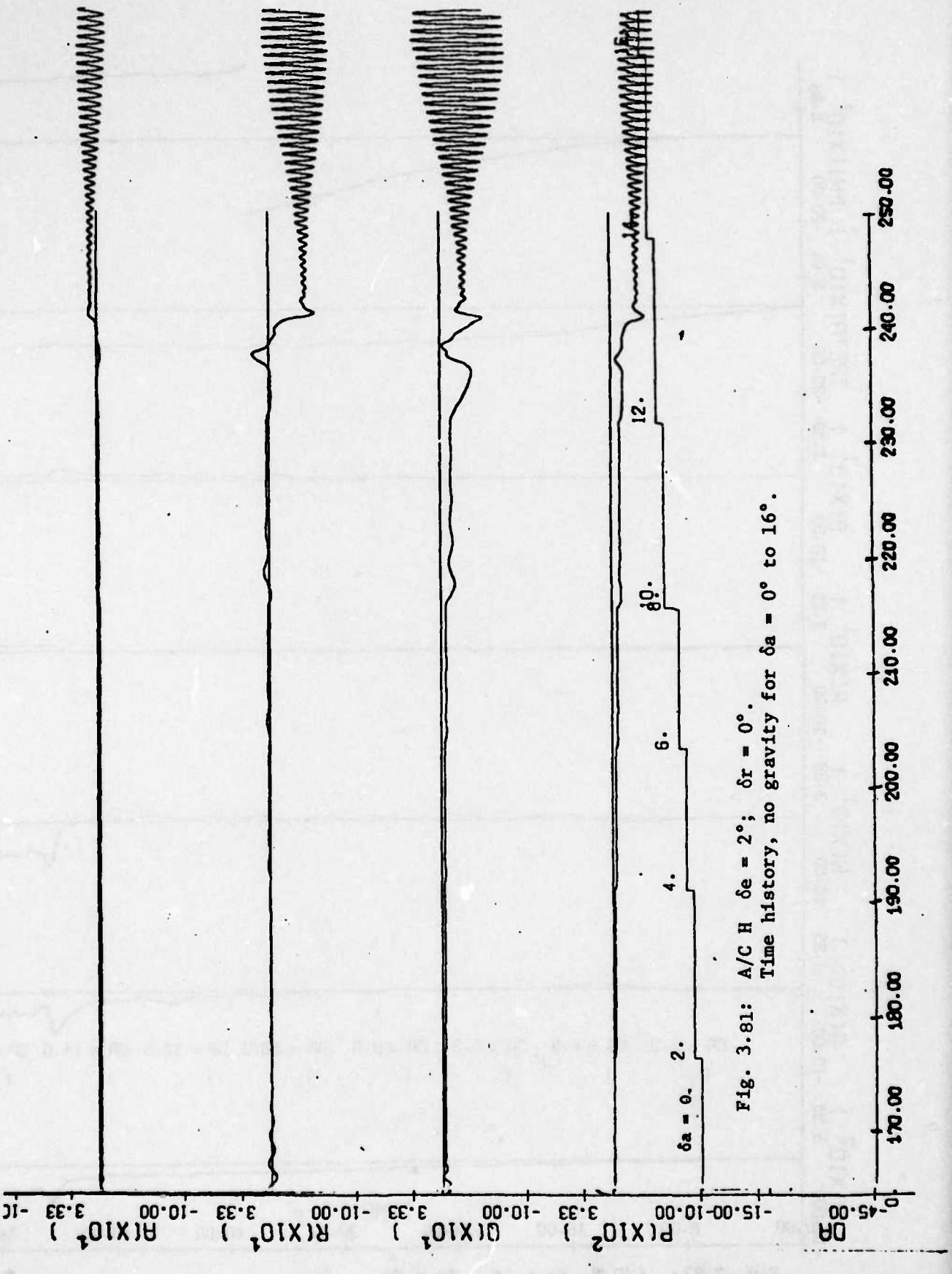

Fig. 3.81: A/C H δe = 2°; δr = 0°.
Time history, no gravity for δa = 0° to 16°.

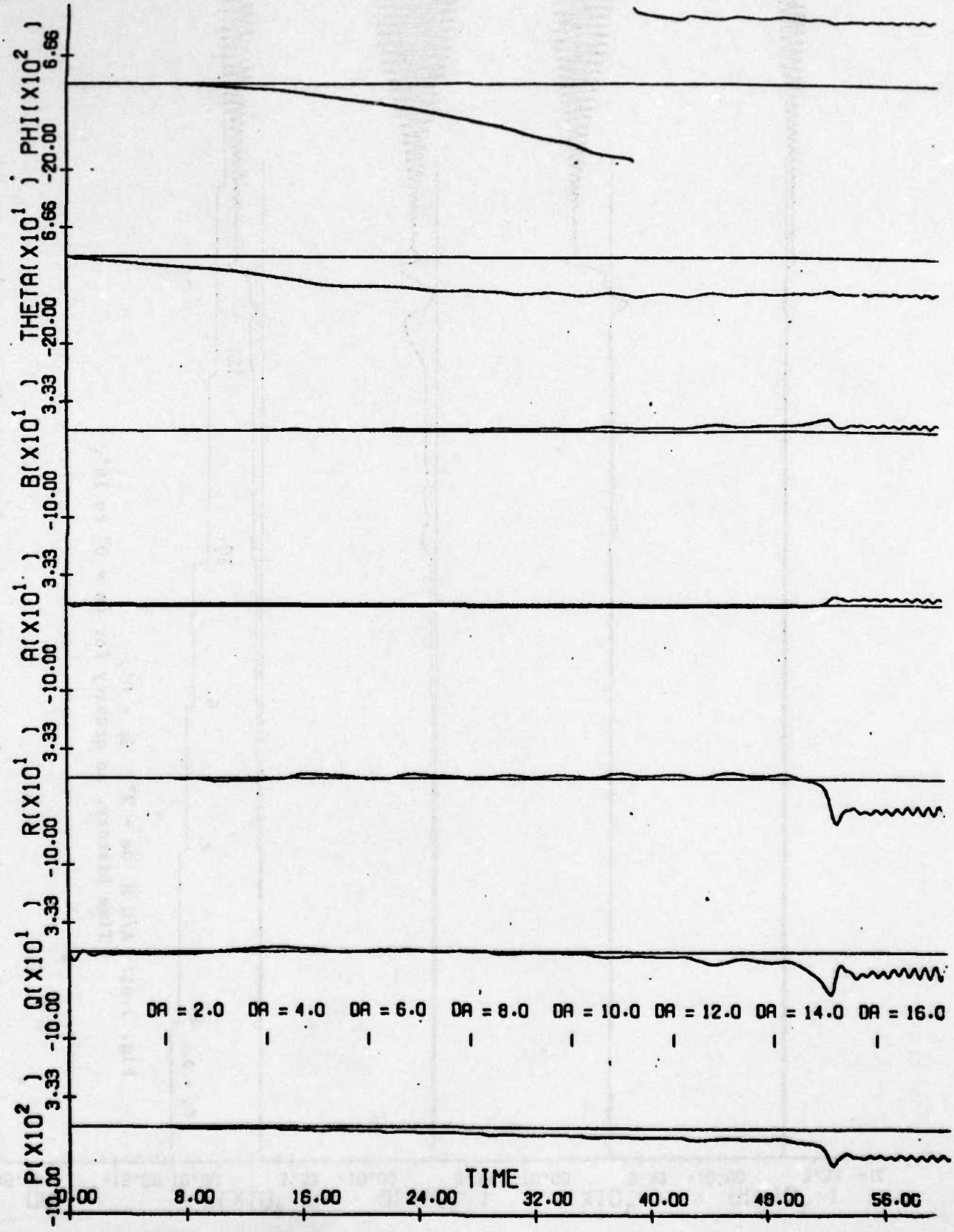

Fig. 3.82: A/C H $\delta e = 2°$, $\delta r = 0°$.
Time history for $\delta a = 0°$ to $16°$; gravity terms included.

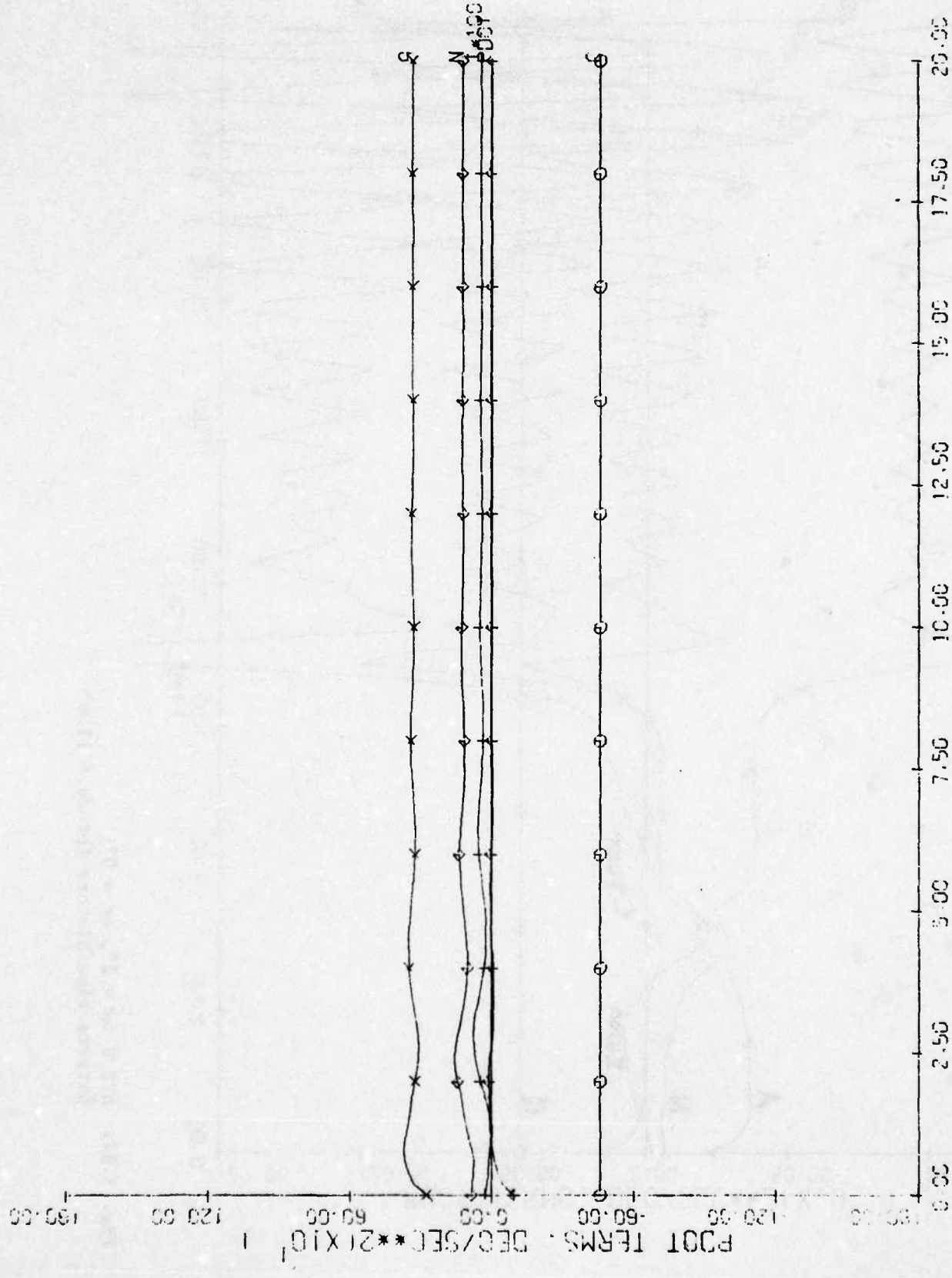

Fig. 3.83: A/C H $\delta e = 2°$, $\delta r = 0°$;
$\dot{p}$-terms time history for $\delta a = 10°$

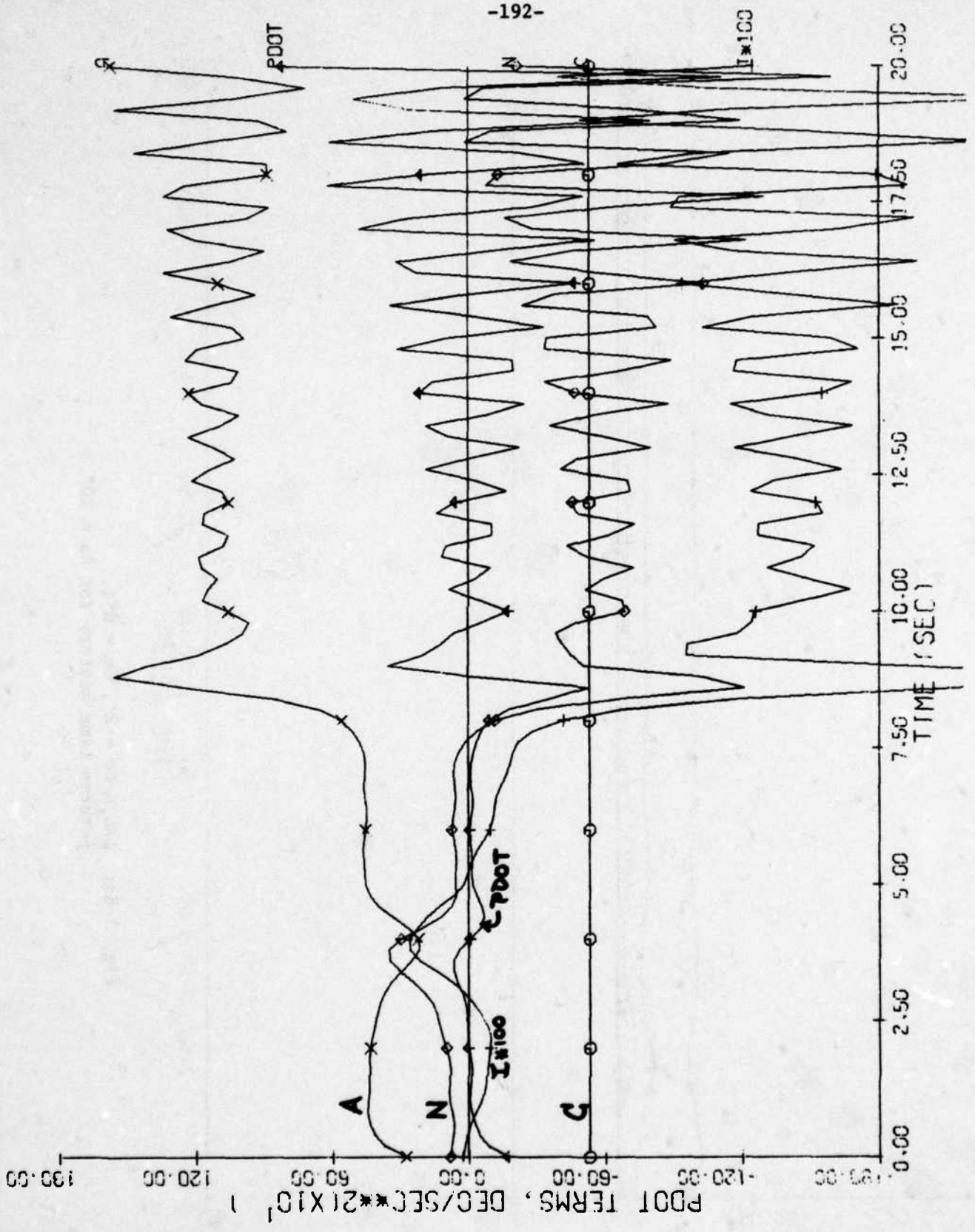

Fig. 3.84: A/C H $\delta e = 2°$, $\delta r = 0°$;
$\dot{p}$-terms time history for $\delta a = 11.6°$

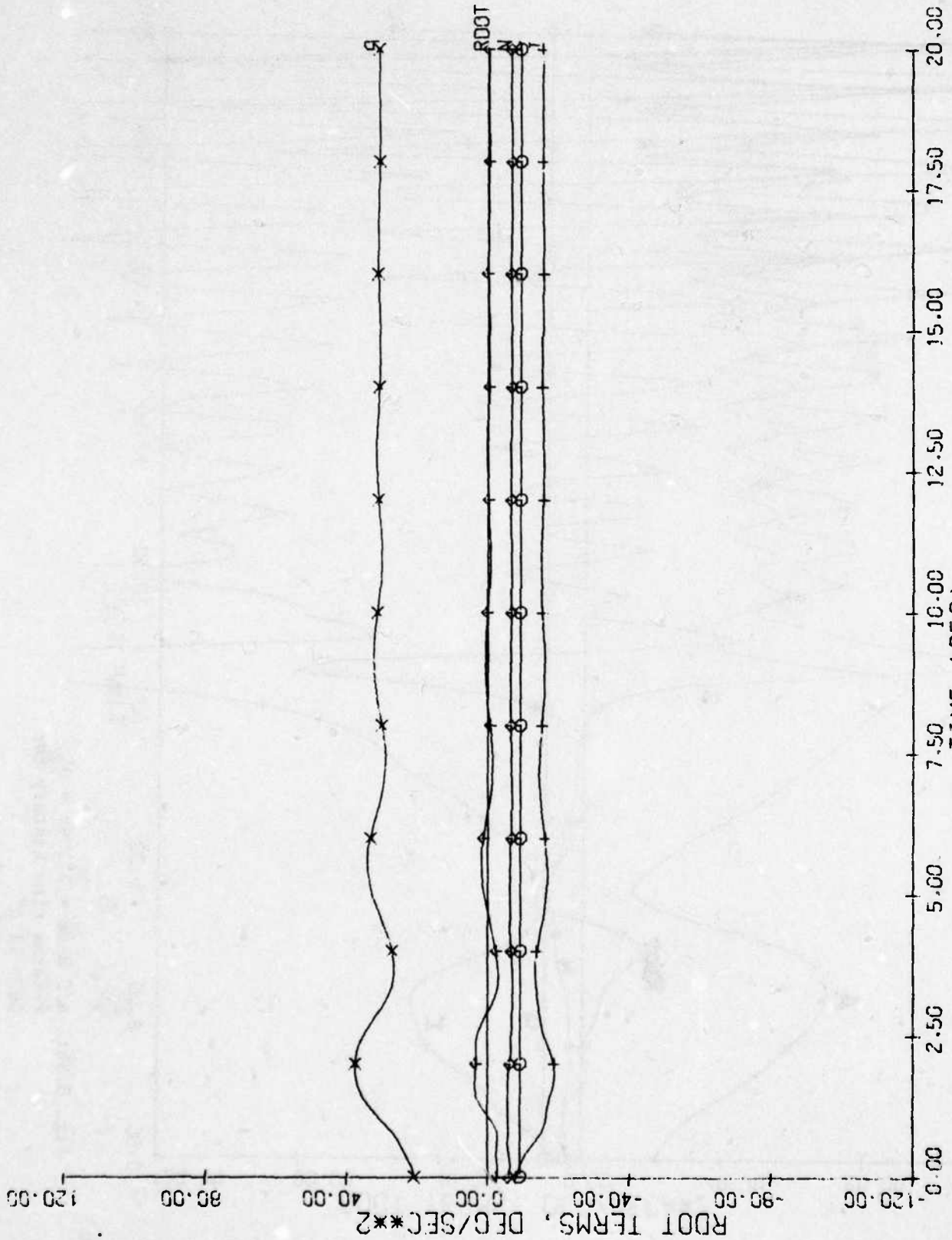

Fig. 3.85: A/C H $\delta e = 2°$, $\delta r = 0°$; $\dot{r}$-terms time history for $\delta a = 10°$

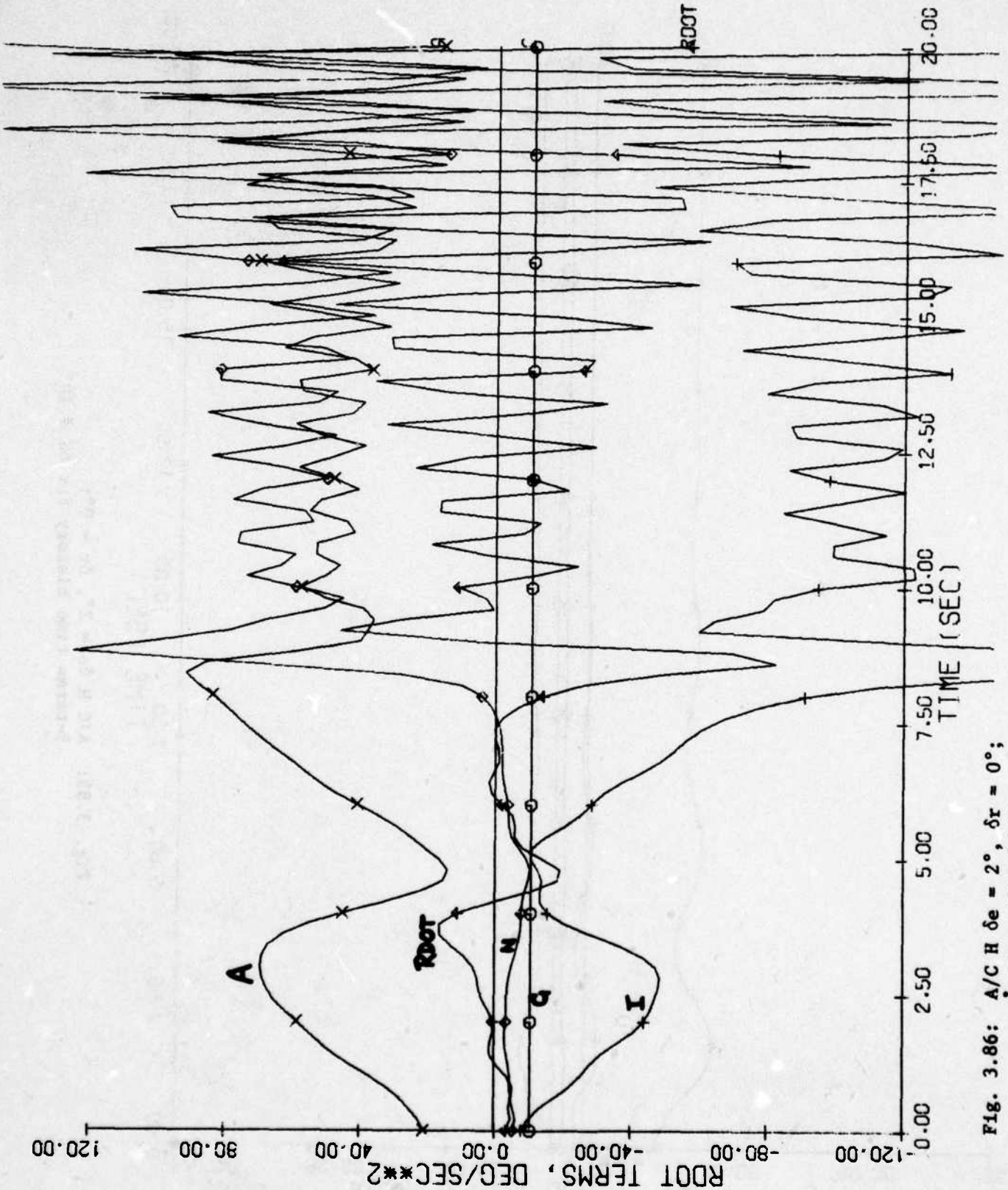

Fig. 3.86: A/C H $\delta e = 2°$, $\delta r = 0°$; $\dot{r}$-terms time history for $\delta a = 11.6°$

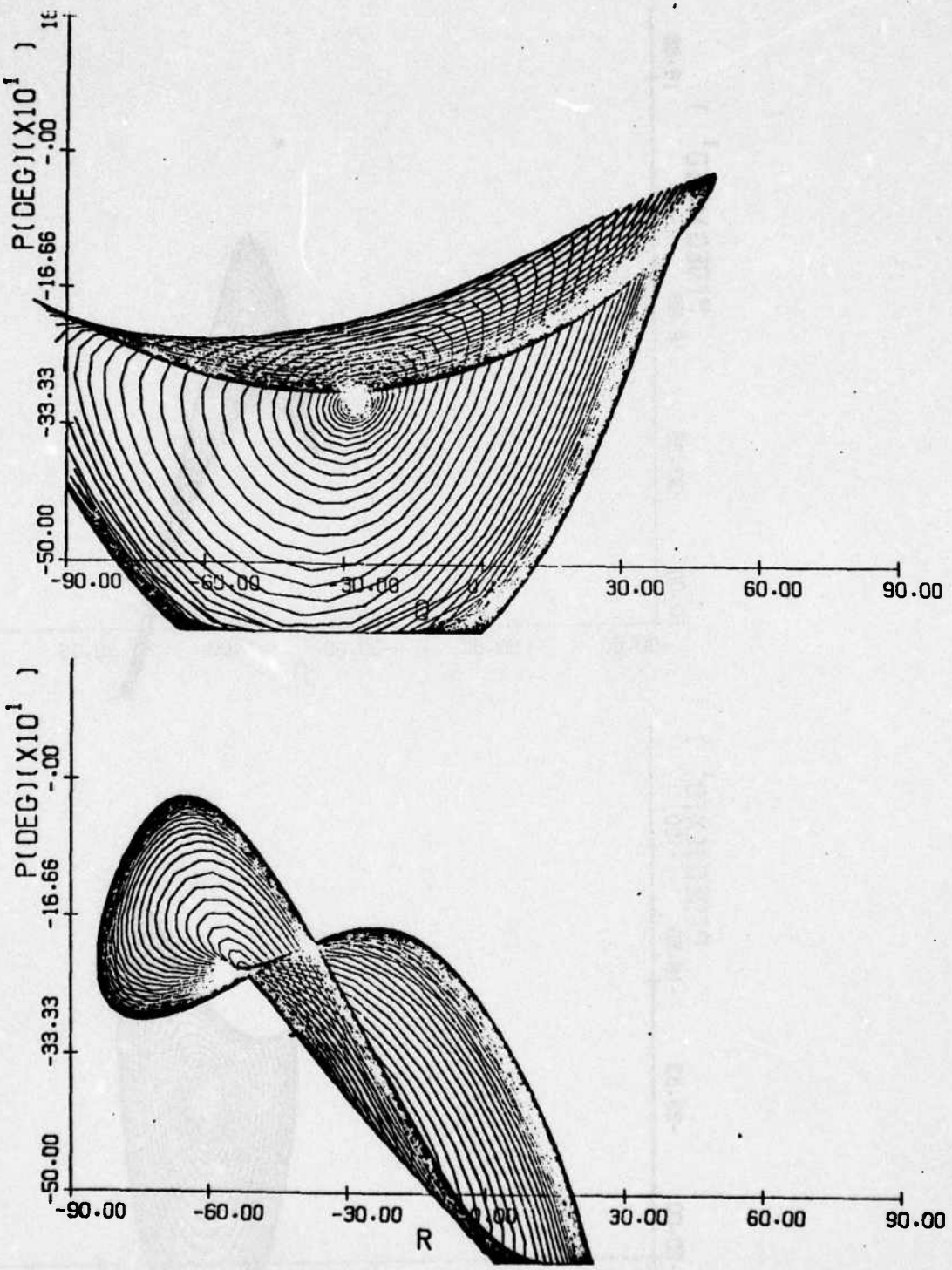

Fig. 3.87: A/C H $\delta e = 2°$, $\delta r = 0°$, $\delta a = 11.46°$. Phase plots, p vs. q and p vs. r, for initial conditions on outer equilibrium branch, showing limit cycle (t_f = 72 sec).

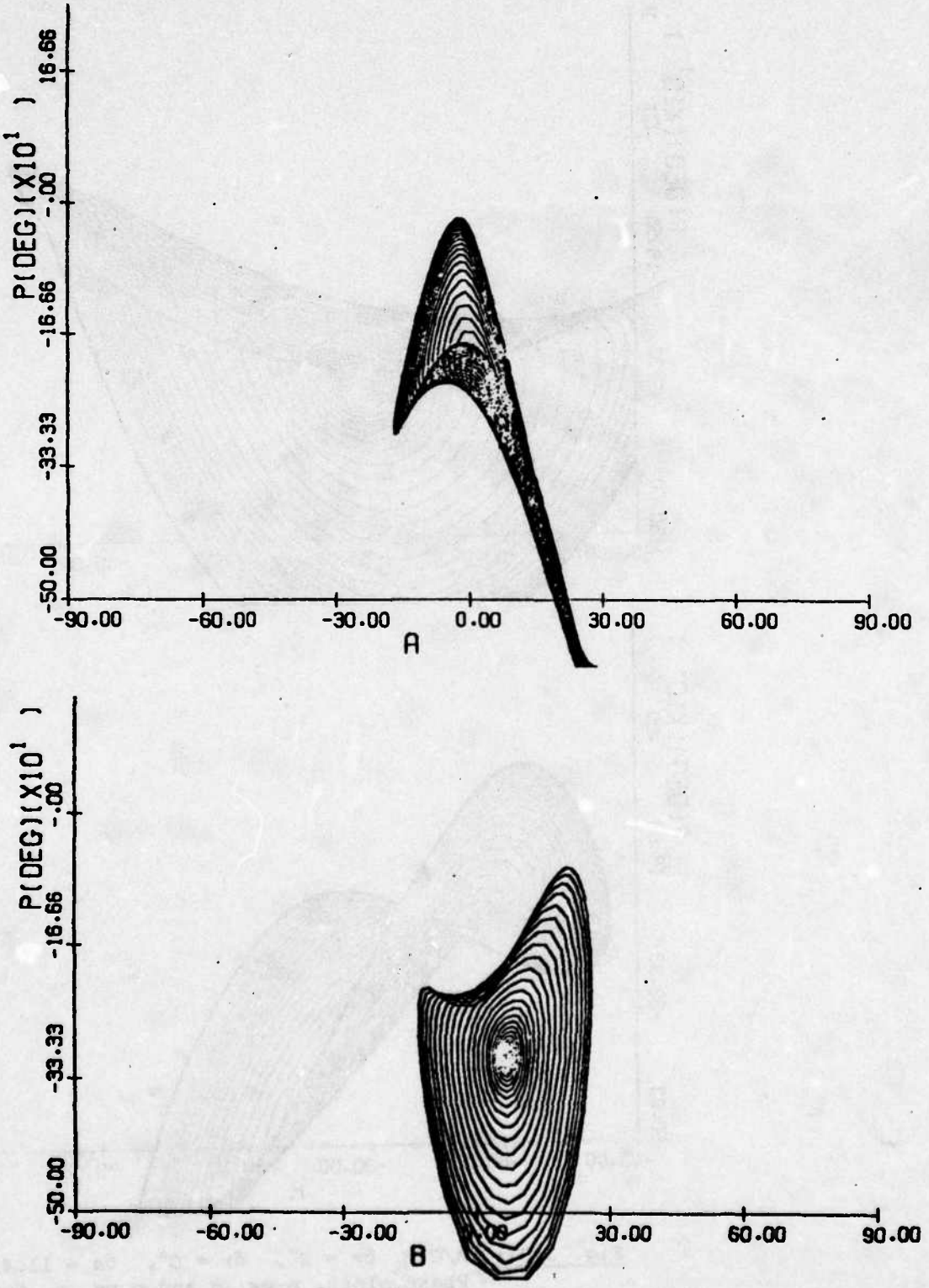

Fig. 3.88: A/C H $\delta e = 2°$, $\delta r = 0°$, $\delta a = 11.4°$. Phase plots, p vs. α and p vs. β, for initial conditions on outer equilibrium branch, showing limit cycle (t_f = 72 sec).

Fig. 3.89: A/C H $\delta e = 2^{\circ}$, $\delta r = 0^{\circ}$, $\delta a = 11.46^{\circ}$
Phase plot, p vs q, for initial conditions on linear equilibrium branch (t_f = 25 sec)

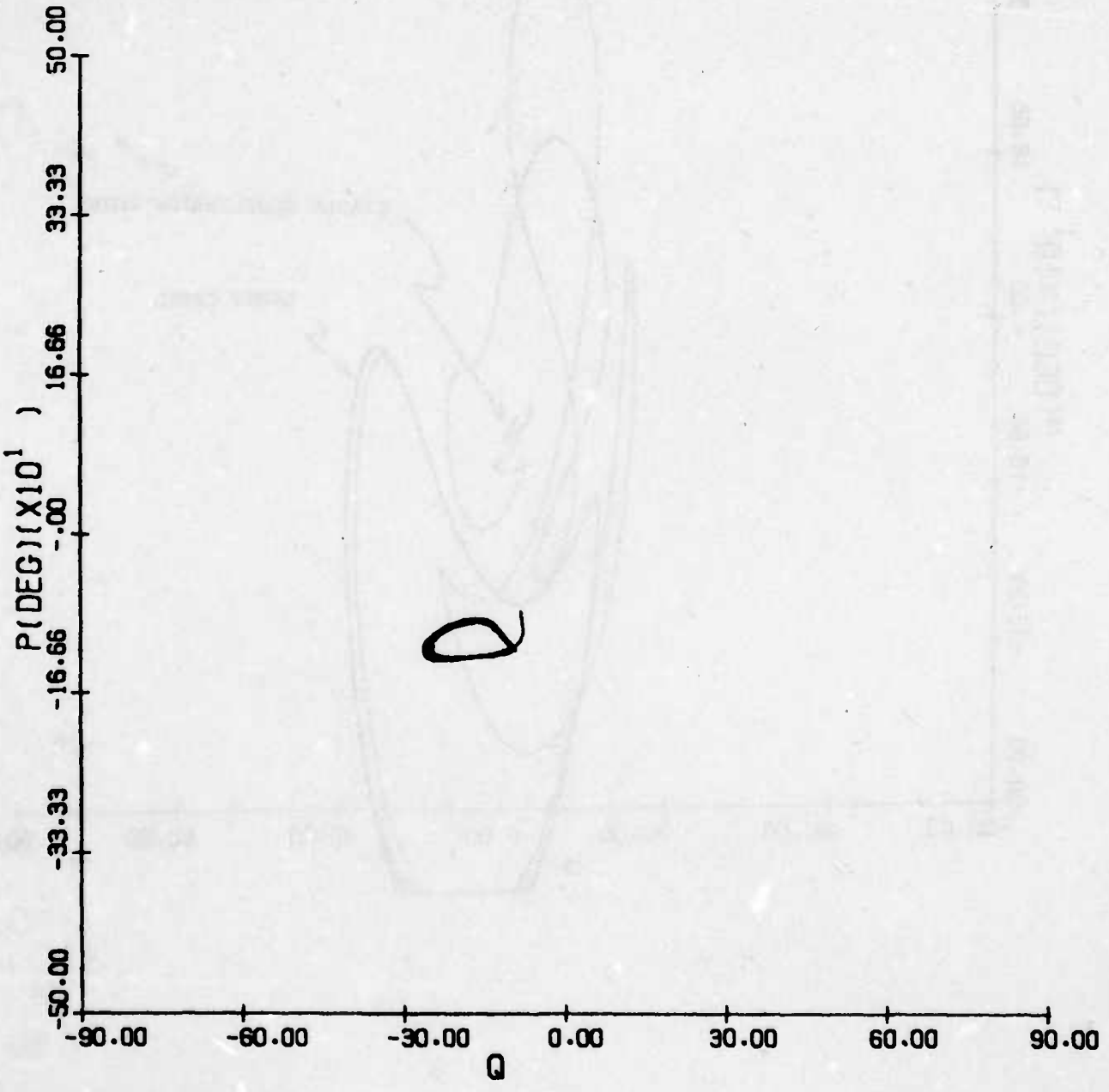

Fig. 3.90: A/C H $\delta r = 0^{\circ}$, $\delta a = 11.46^{\circ}$ Phase plot, p vs β, initial conditions on outer equilibrium branch, t_f = 64 sec; $\delta e = 2^{\circ}$, then -2° at t = 8 sec.

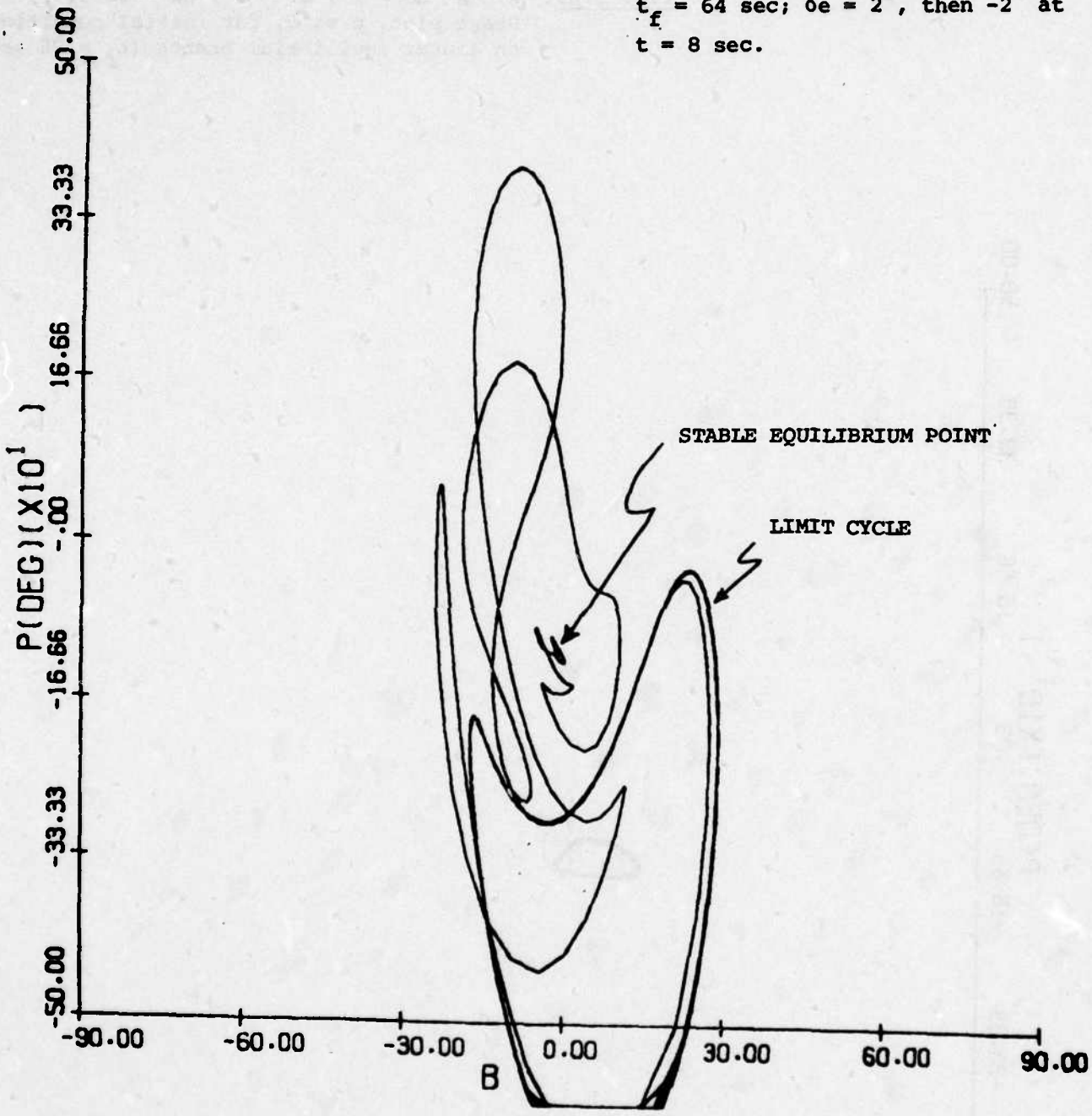

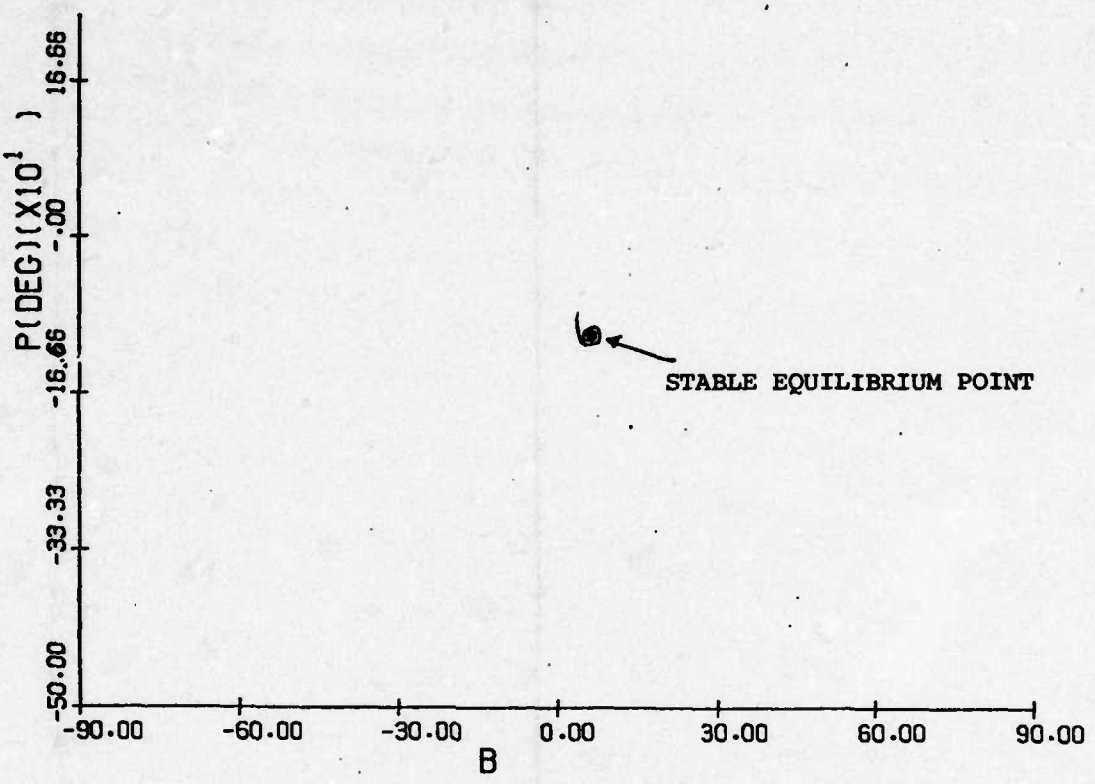

Fig. 3.81(a)

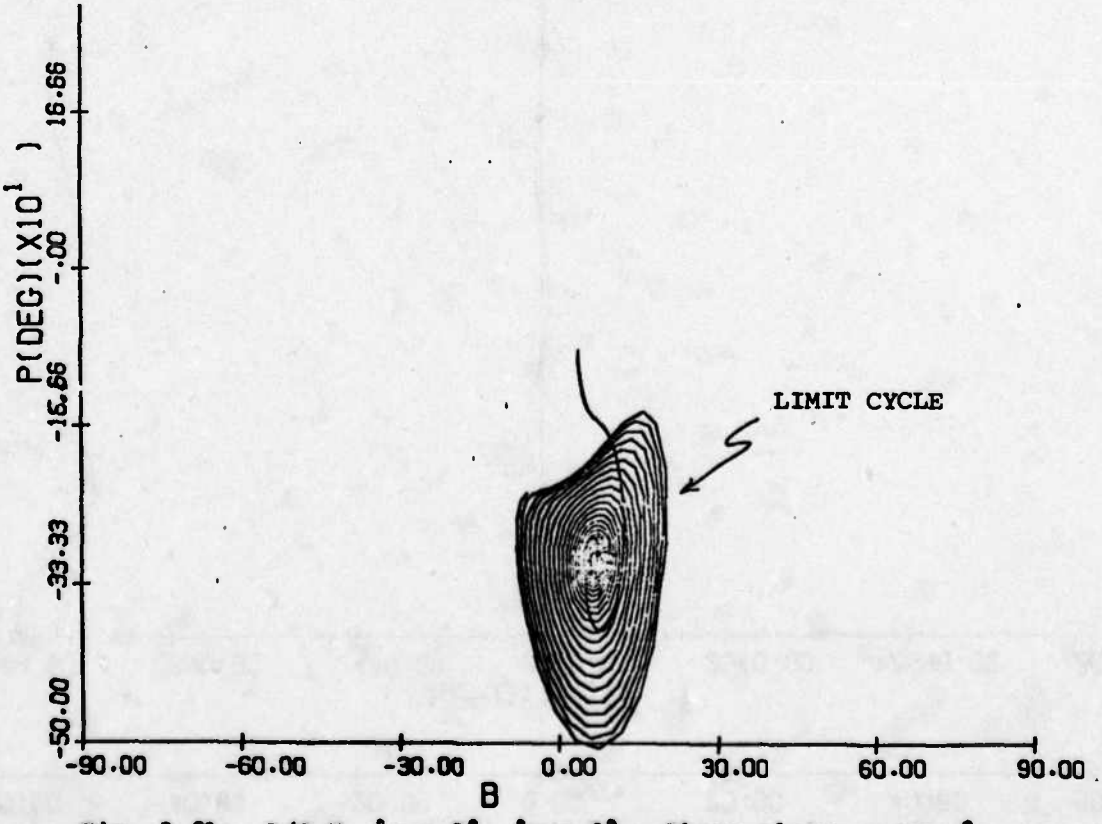

Fig. 3.91: A/C H $\delta e = 2°$, $\delta r = 0°$. Phase plots, p vs. β, for initial conditions on linear equilibrium branch, $t_f = 64$ sec; for (a) $\delta a = 10.6°$. (b) $\delta a = 13.5°$.

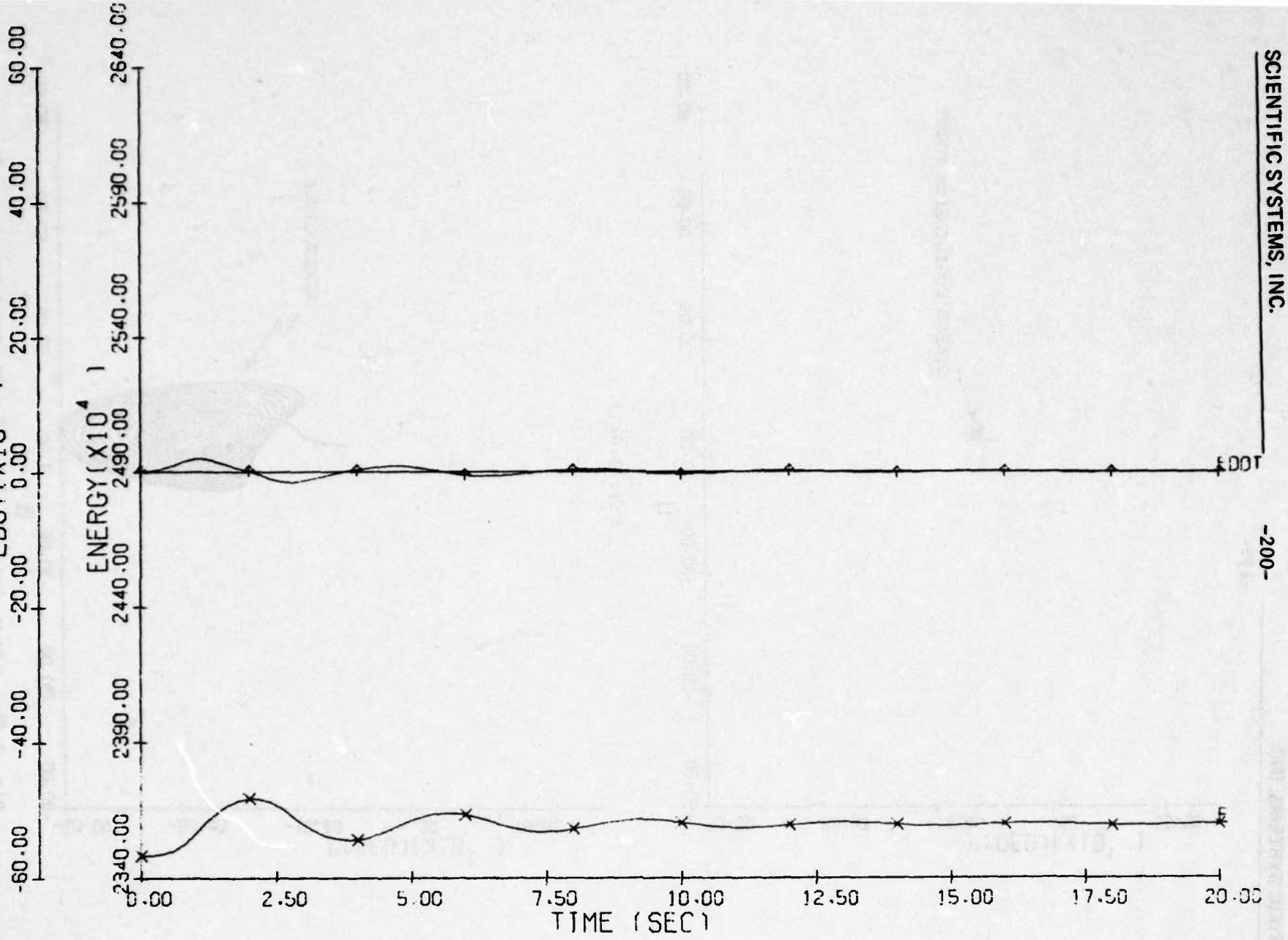

Fig. 3.92: A/C H $\delta e = 2°$, $\delta r = 0°$;
E, $\dot{E}$ histories for $\delta a = 10°$

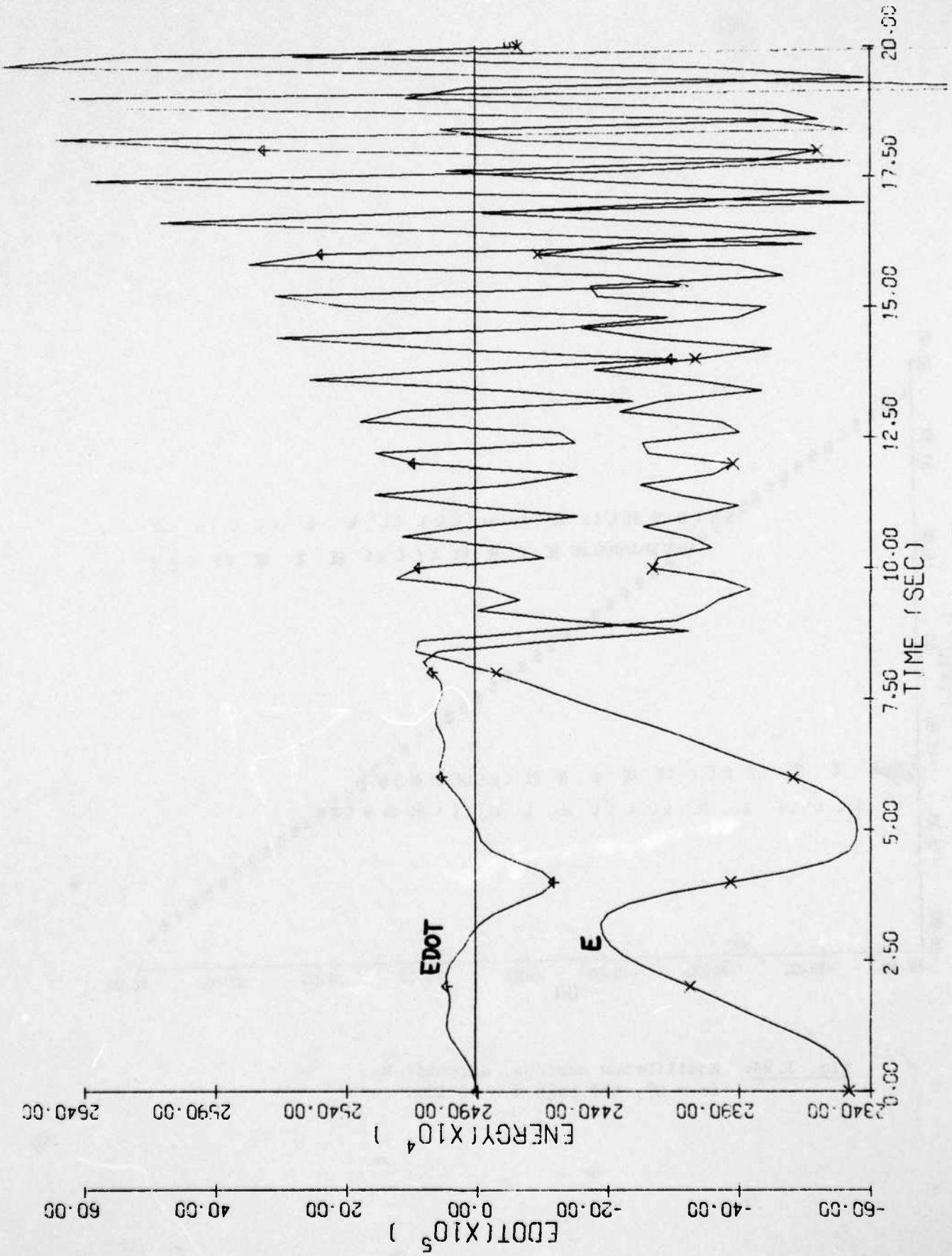

Fig. 3.93: A/C H $\delta e = 2°$, $\delta r = 0°$;
E, $\dot{E}$ histories for $\delta a = 11.6°$

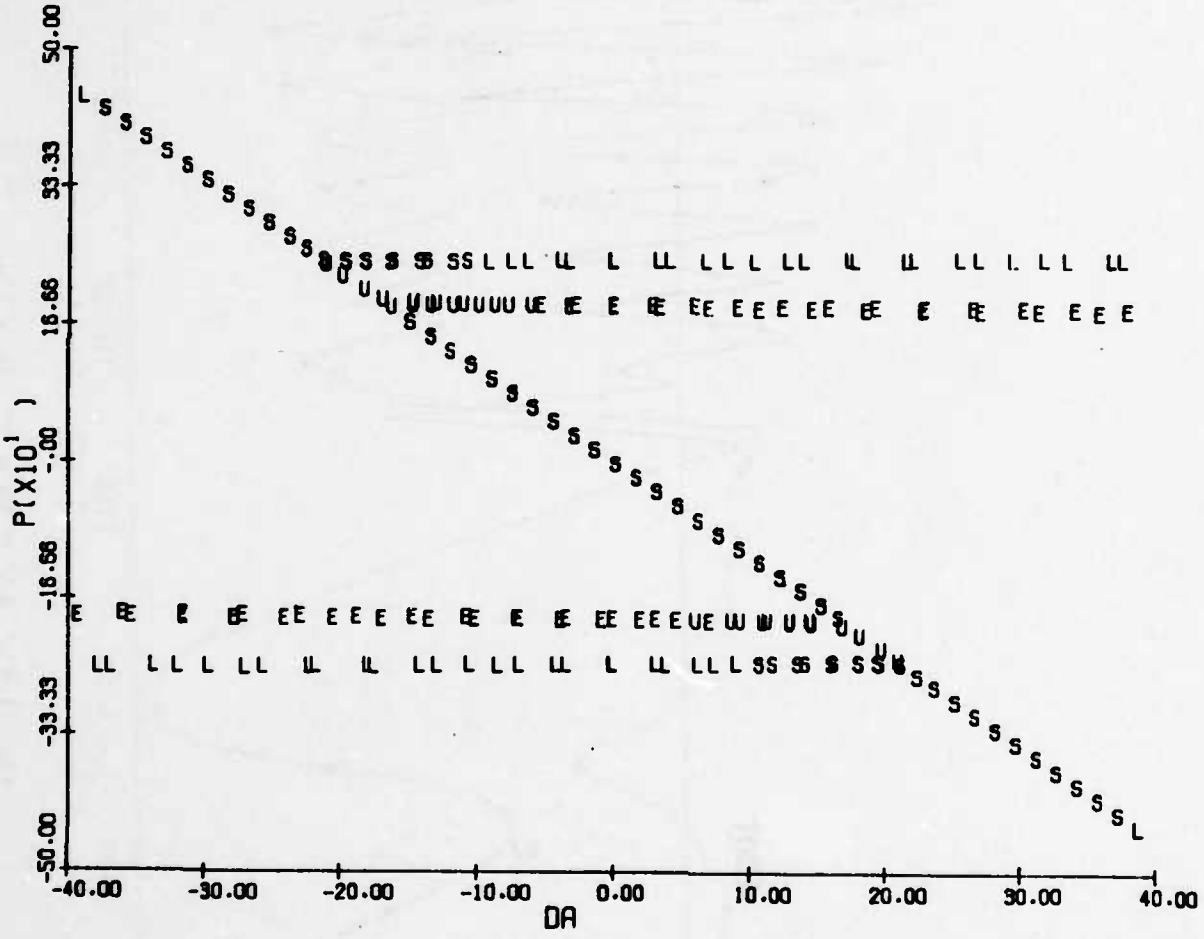

Fig. 3.94: Equilibrium surface, aircraft H;
$\delta e = 0°$, ARI gain $k = -0.152$.

SCIENTIFIC SYSTEMS, INC.

Fig. 3.95: Time history, aircraft H;
$\delta e = 0°$, no ARI ($\delta r = 0°$).

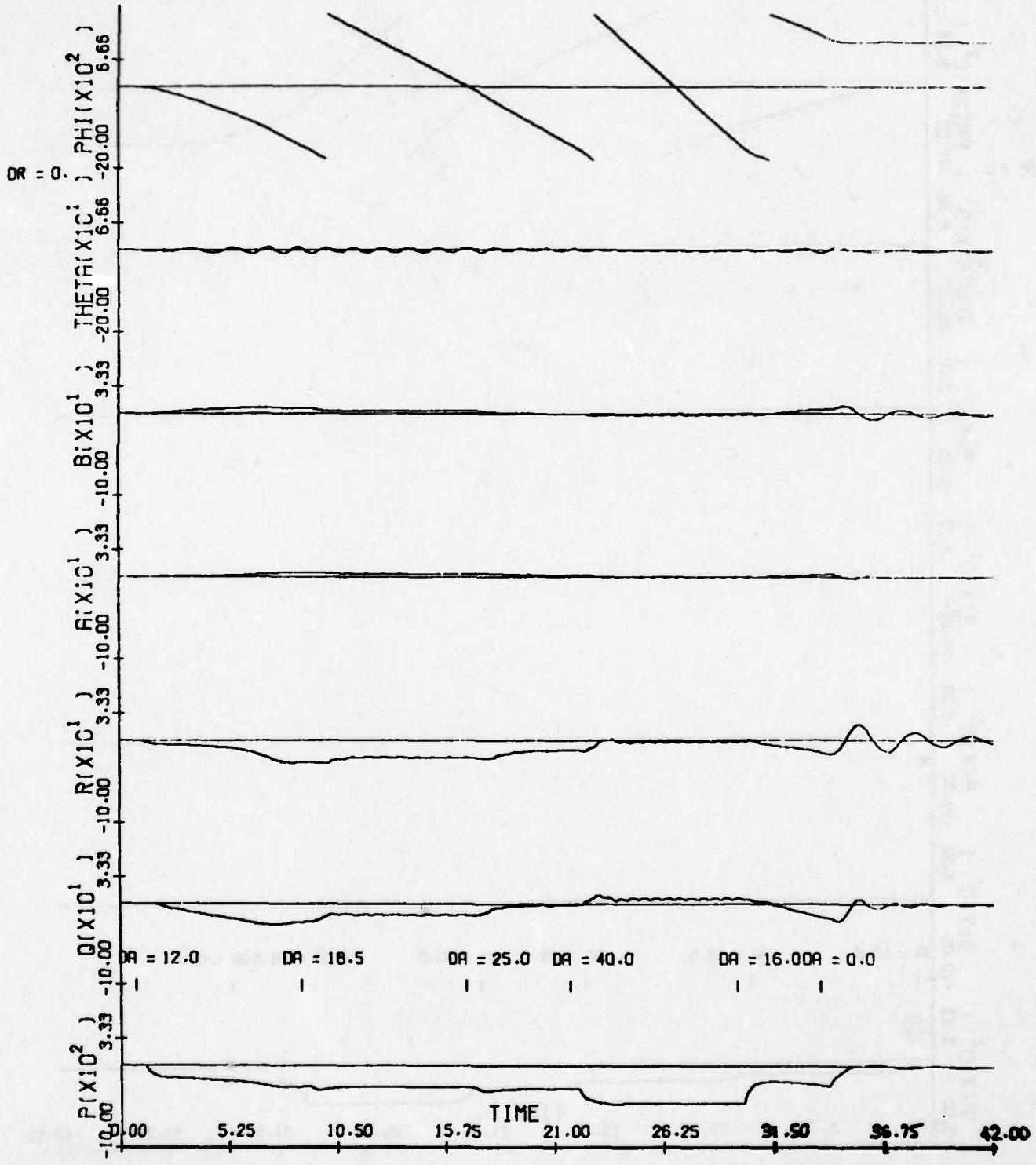

SCIENTIFIC SYSTEMS, INC.

Fig. 3.96: Time history, aircraft H;
$\delta e = 0°$, ARI gain k = -0.152.

Part (a): Roll response with ARI active.

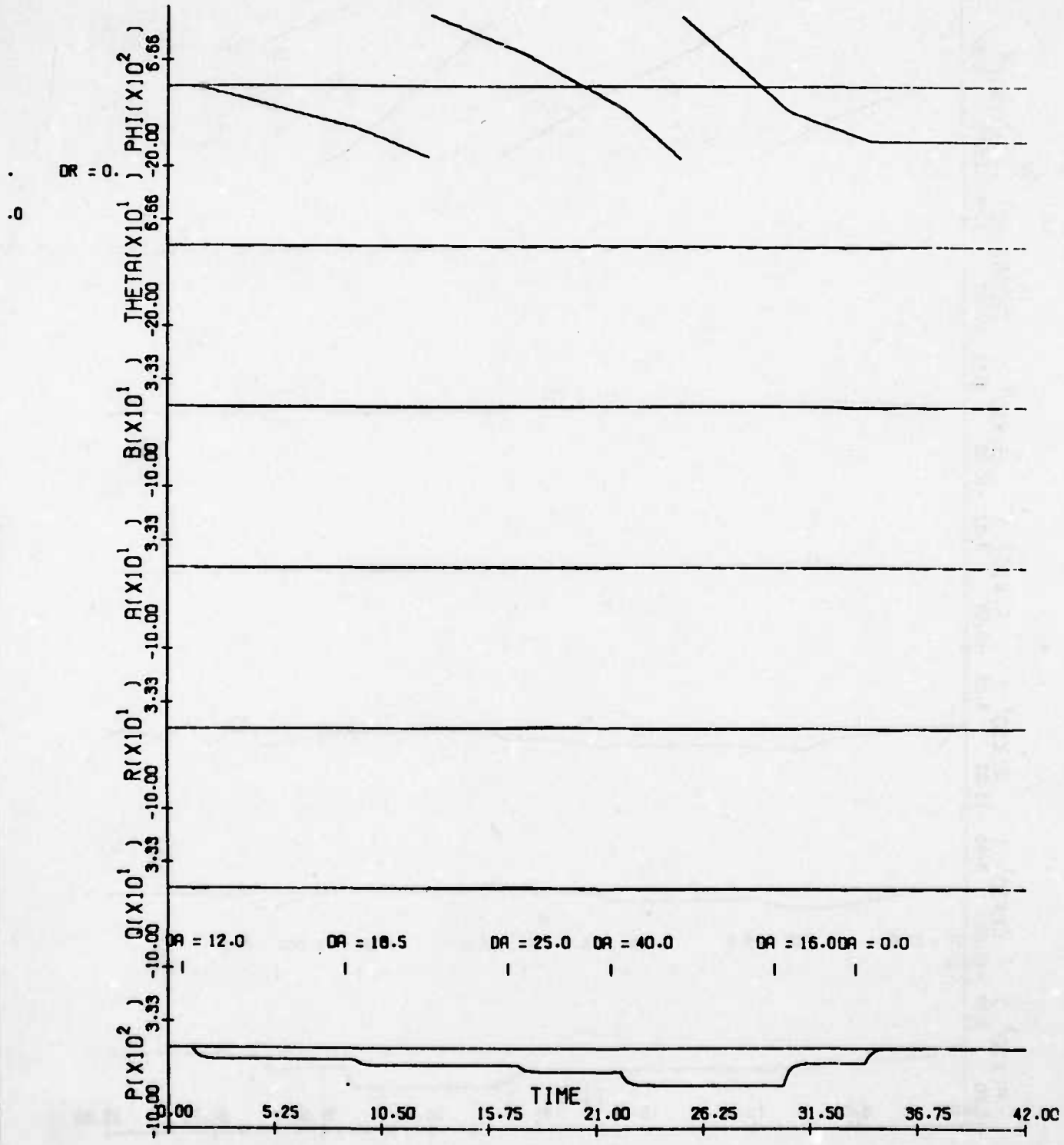

Fig. 3.96b: Effect of small positive root at $\delta a = 18.5°$.

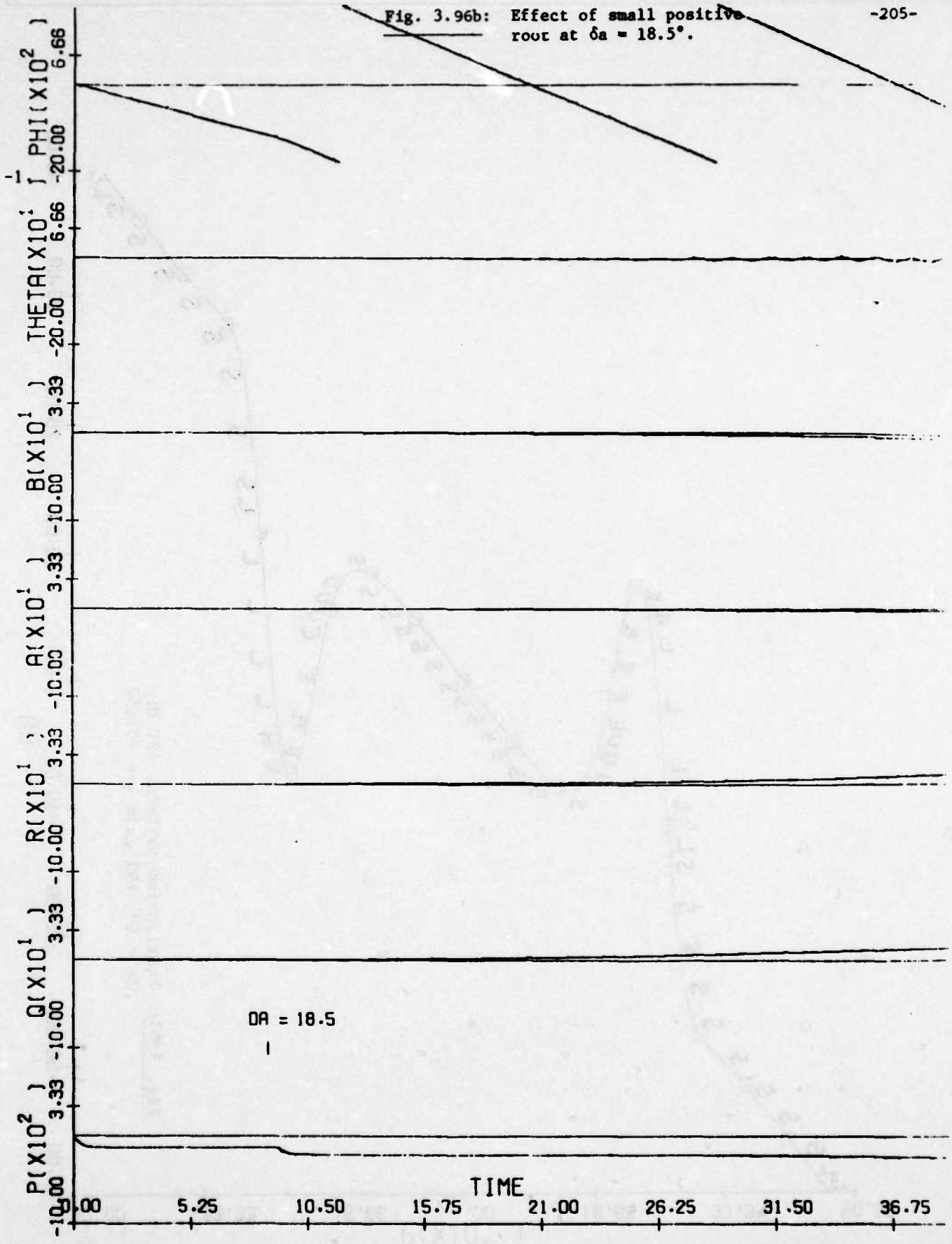

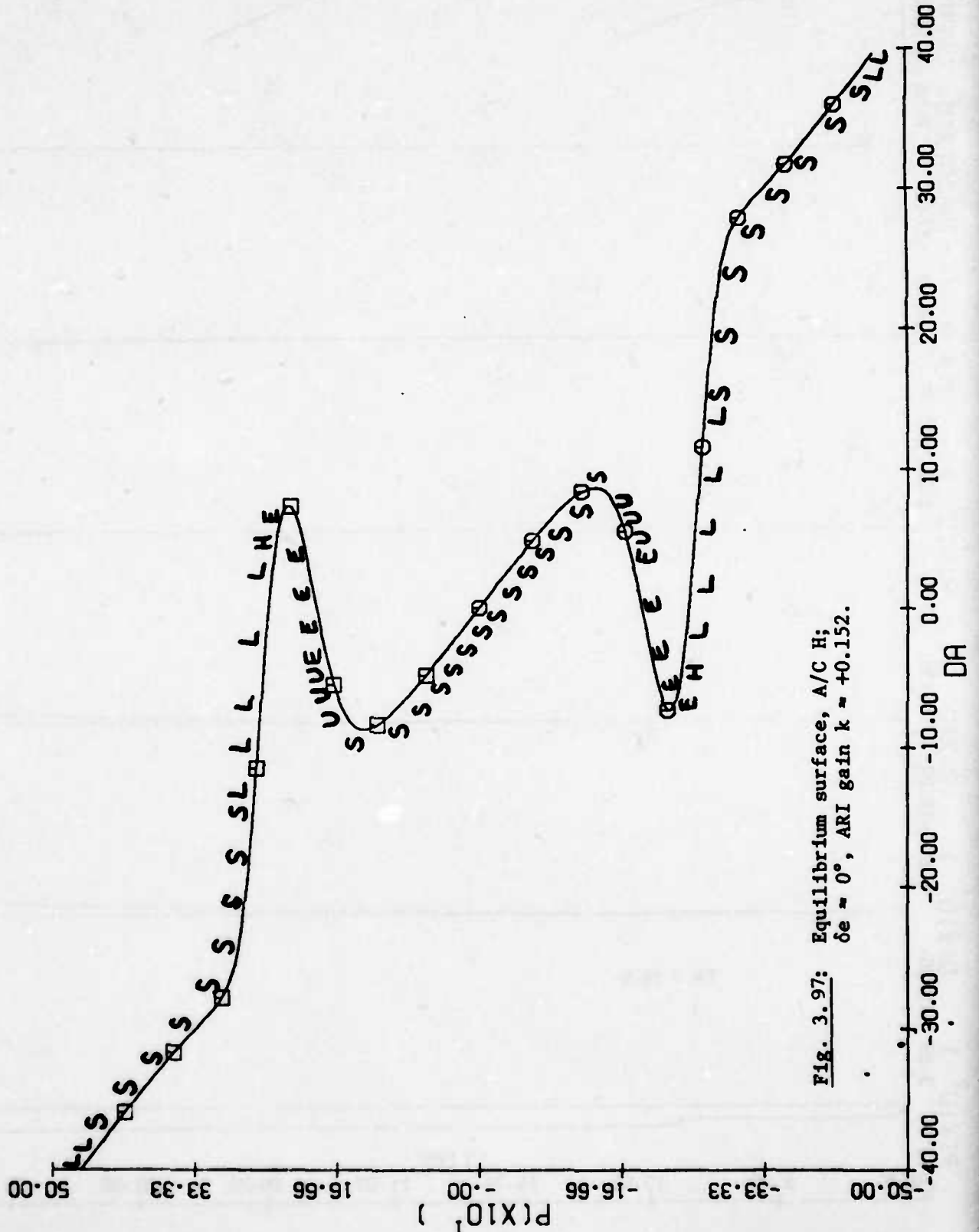

Fig. 3.97: Equilibrium surface, A/C H;
$\delta e = 0°$, ARI gain $k = +0.152$.

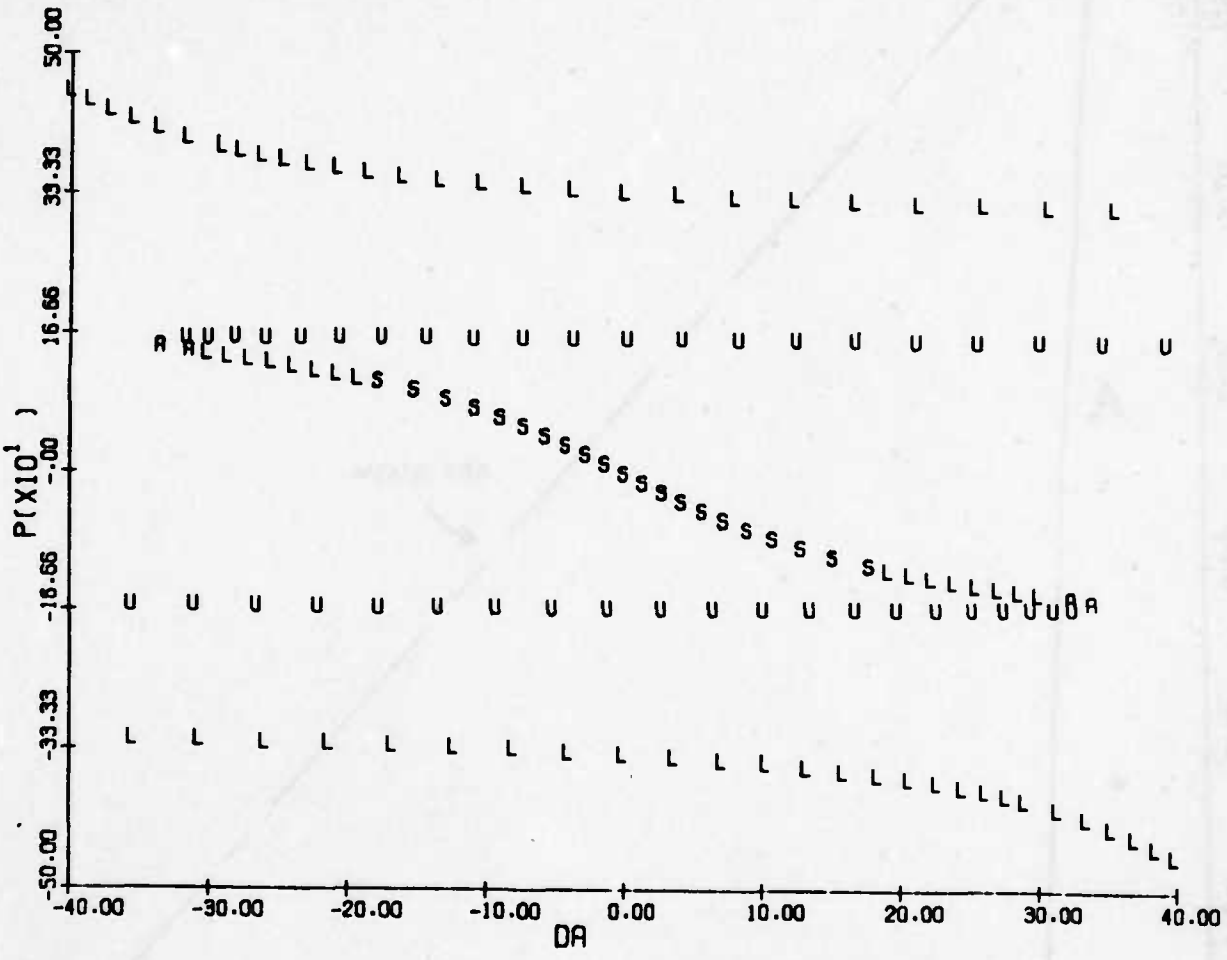

Fig. 3.98: Equilibrium surface, A/C H;
$\delta e = 5°$, ARI gain $k = -0.250$.

Fig. 3.99: Bifurcation locus in ($\delta a, \delta r$) plane (units, deg.). A/C H; $\delta e = 5°$. Only the major branches are shown.

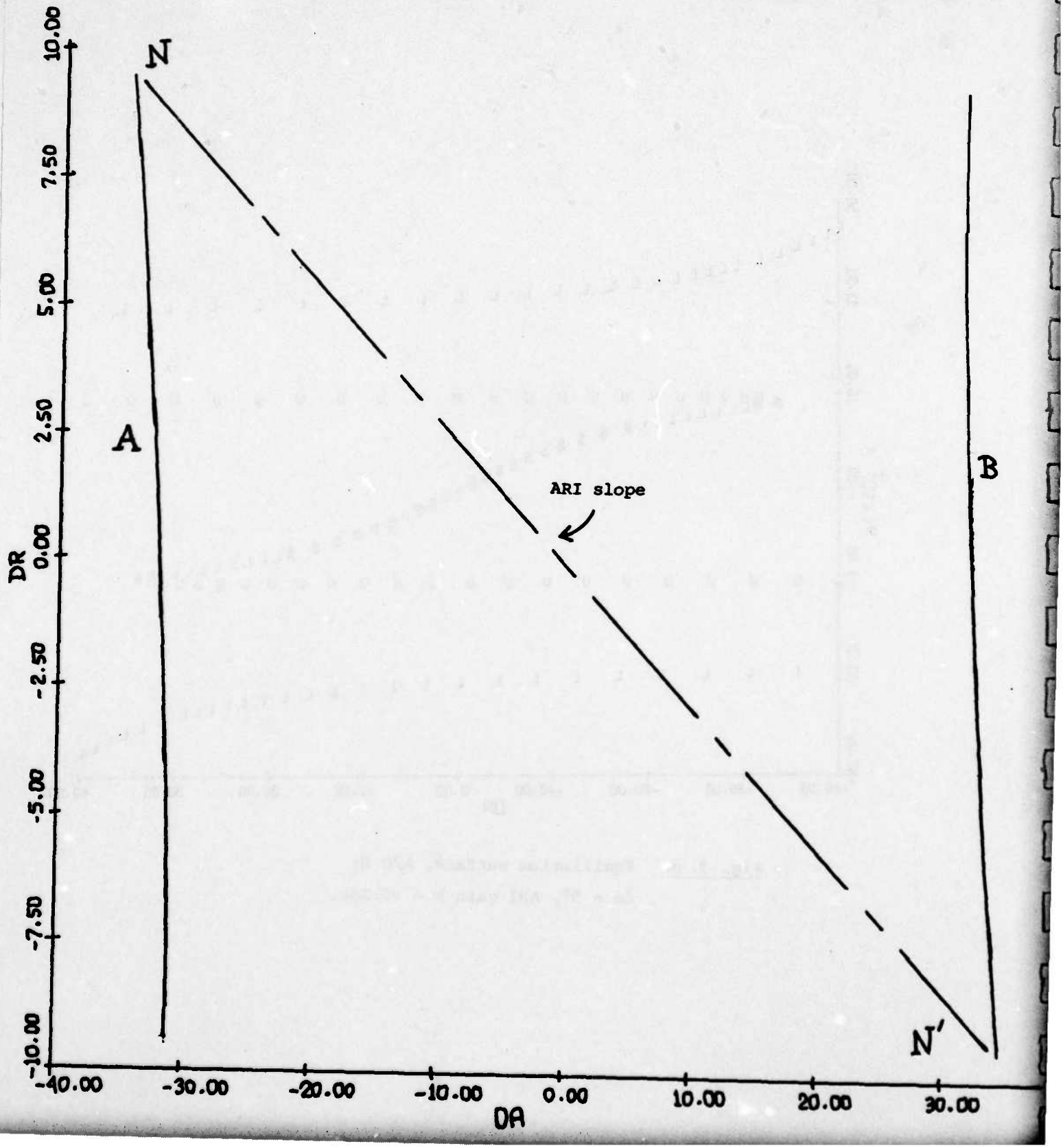

Fig. 3.100a: Time history, A/C H;
$\delta e = 5°$.

Part (a): ARI gain k = -0.250.

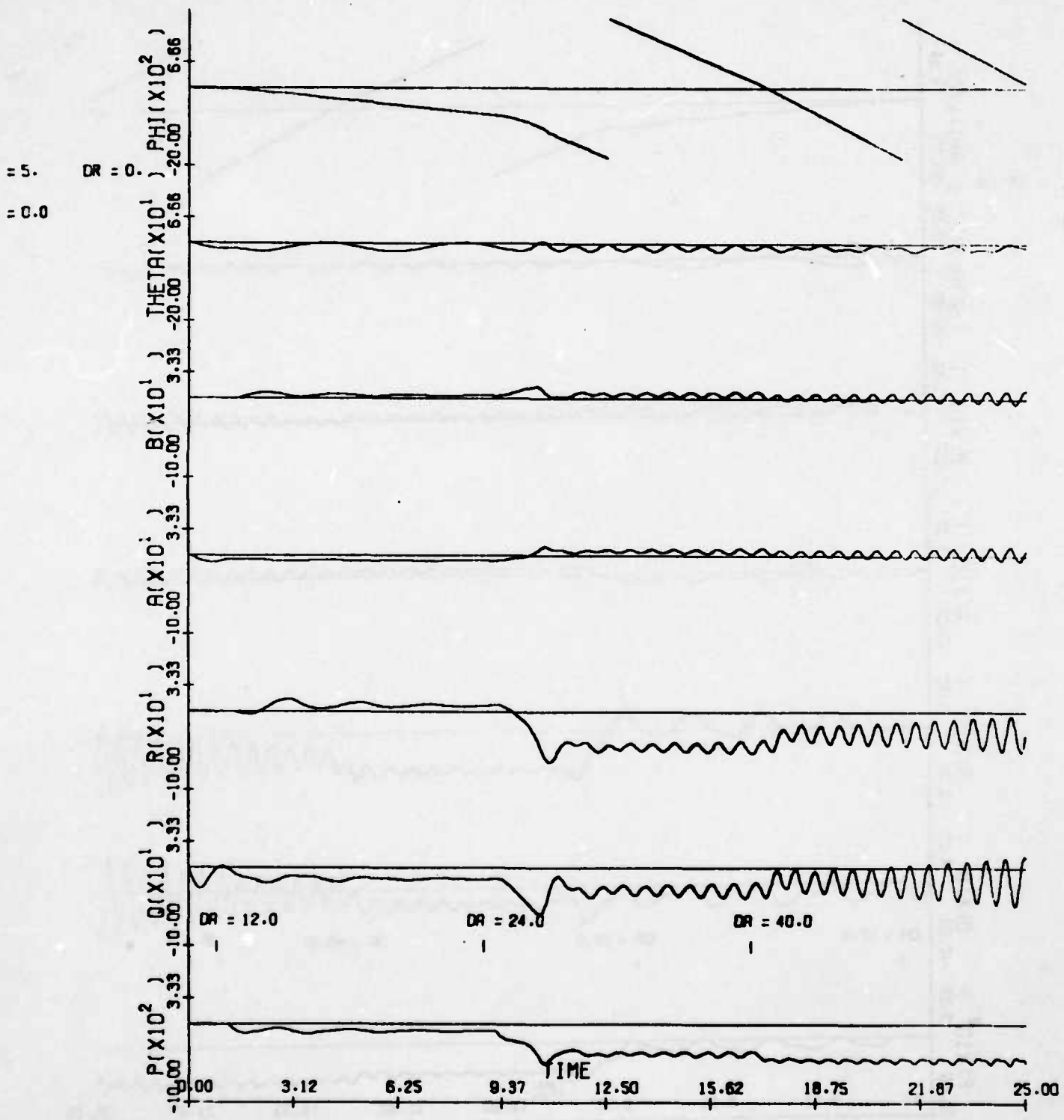

Fig. 3.100b:

Part (b): No ARI, $\delta r = 0°$.

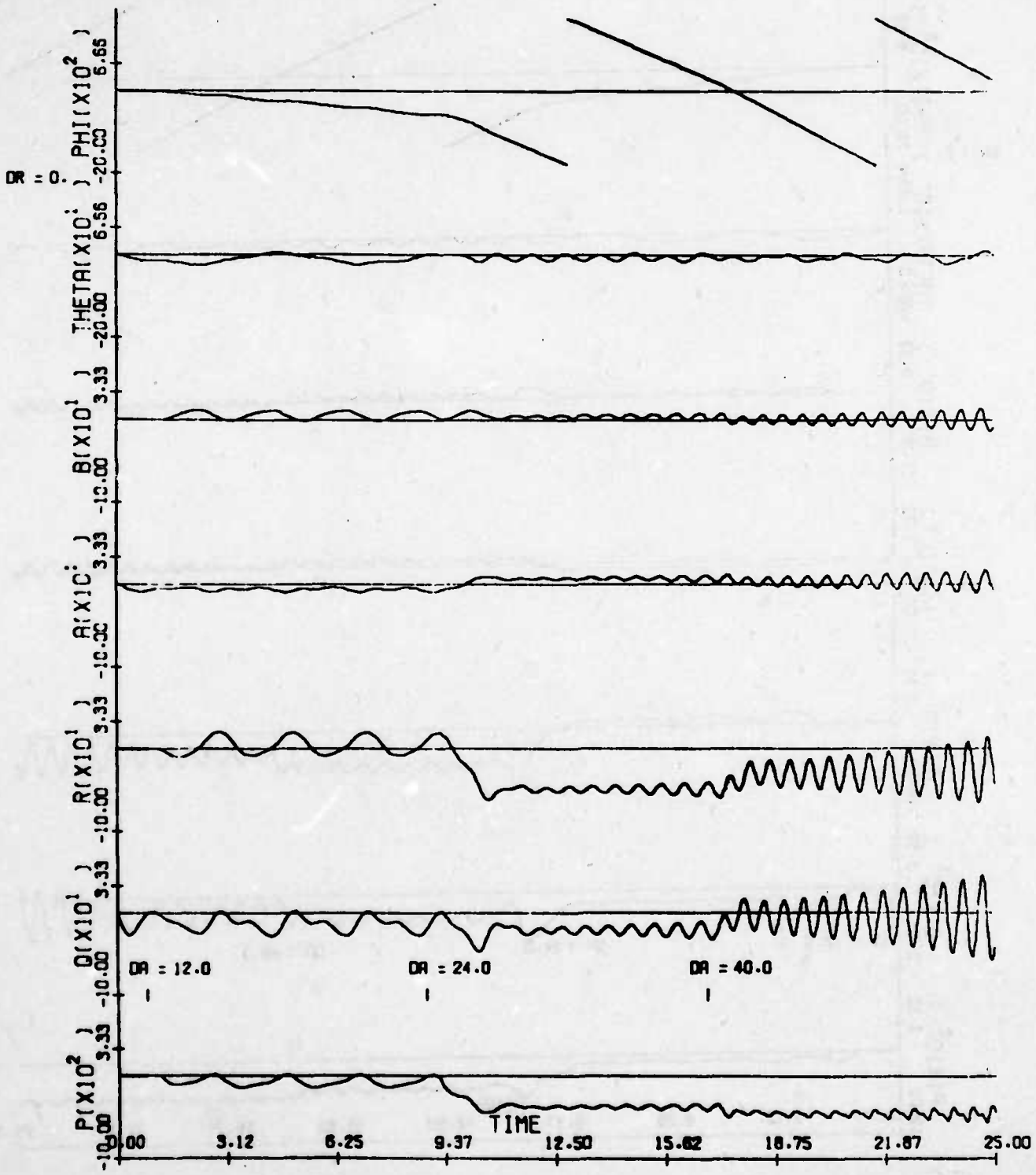

Fig. 3.101: Equilibrium surface, A/C H;
$\delta e = -5°$; ARI gain k = 0.118.

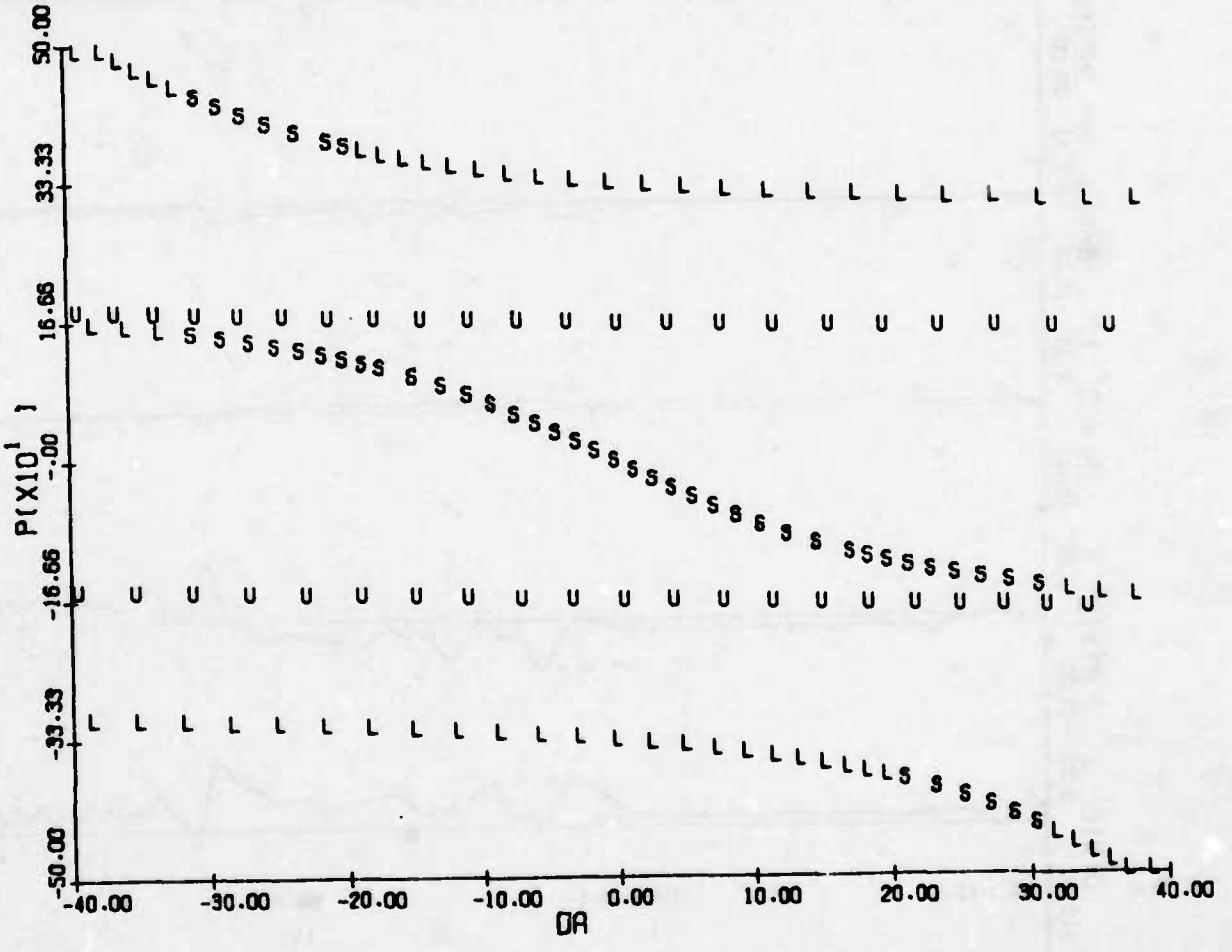

Fig. 3.102a: Time history, A/C H.

Part (a): ARI gain k = 0.118.

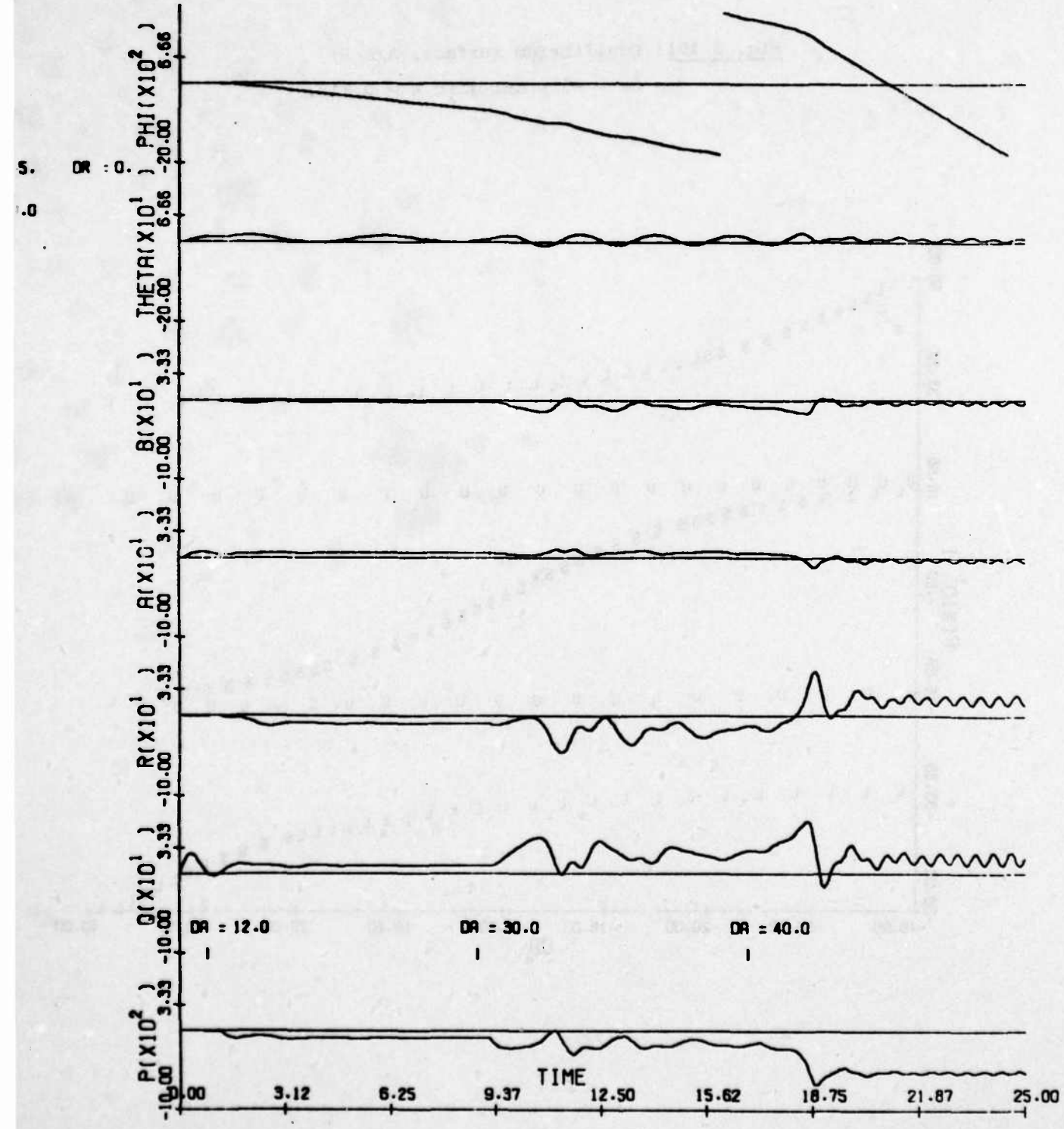

Fig. 3.102b: Time history, A/C H;

Part (b): ARI gain K = 0.118; transient response at $\delta a = 30°$.

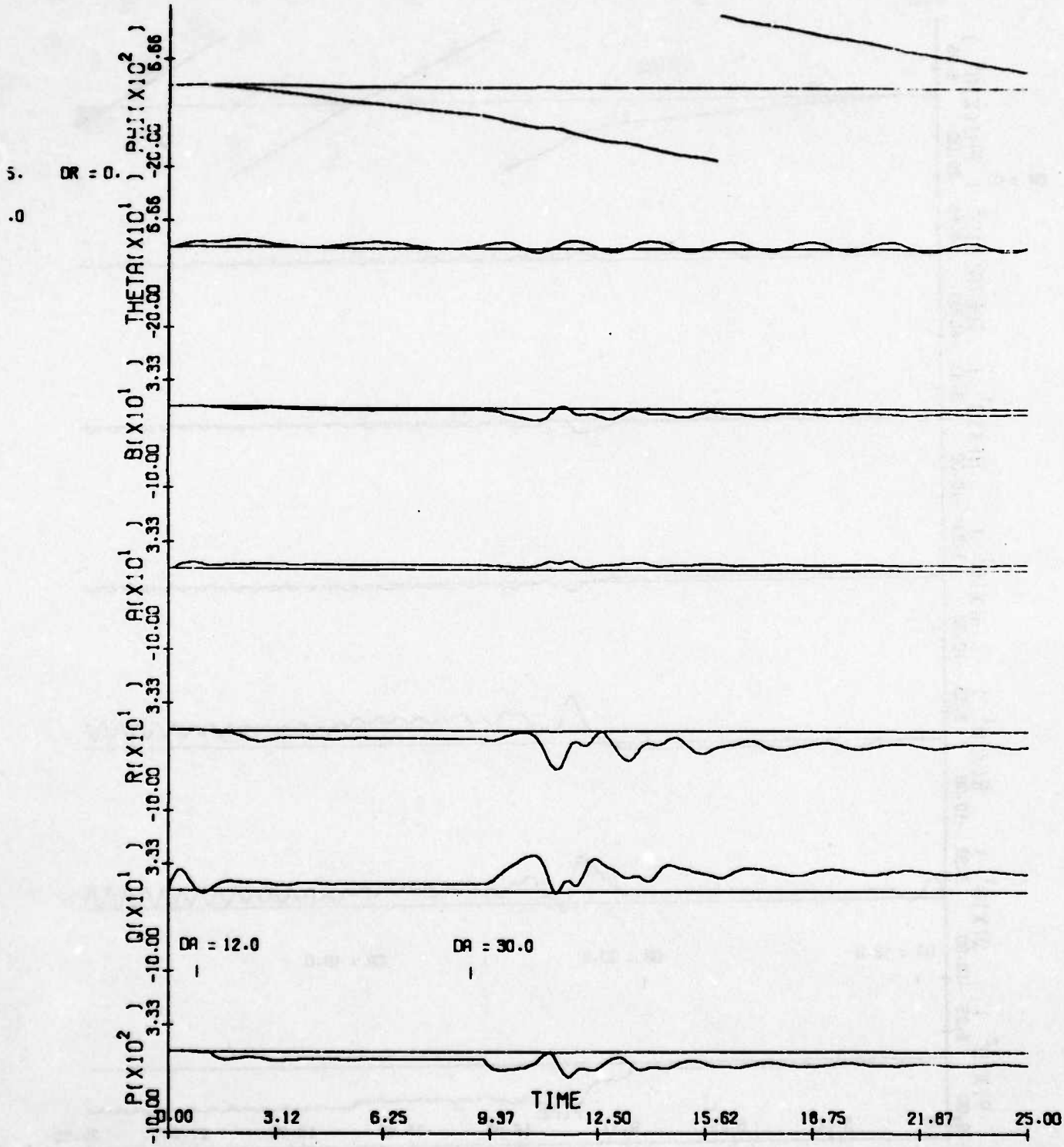

Fig. 3.102c: Time history, A/C H.
Part (c): No ARI, $\delta r = 0°$.

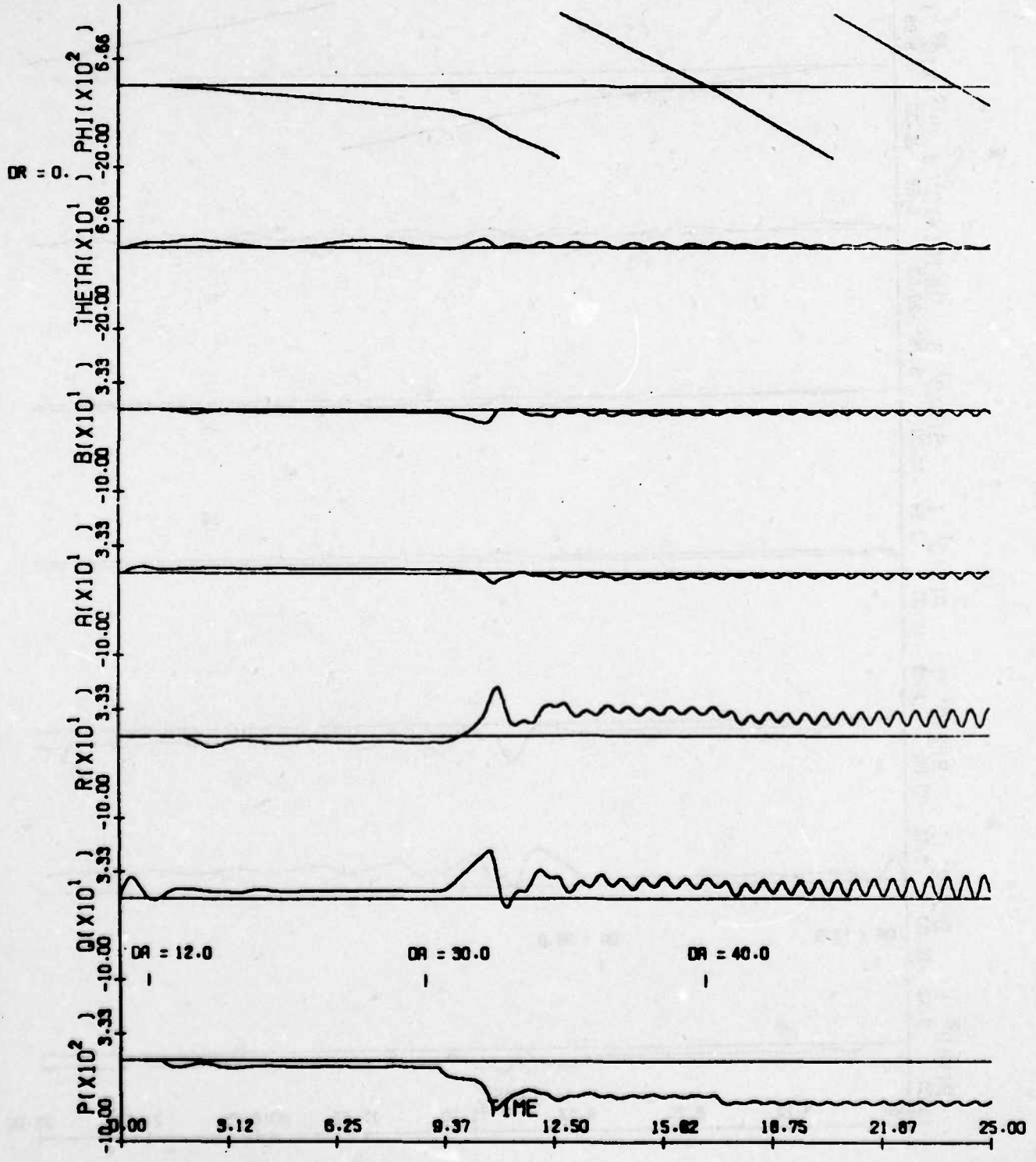

IV. Conclusions and Recommendations for Further Research

(4.1) Conclusions

Based on the analysis of nonlinear models for aircraft A, B and H, we can conclude that

(i) A large number of unstable, jump and limit cycle phenomena occurring at high angles-of-attack, can be analyzed in a unified fashion by using BACTM (Bifurcation Analysis and Catastrophe Theory Methodology).

(ii) BACTM provides a global representation of the equilibrium and bifurcation surfaces for nonlinear dynamic systems. The qualitative dynamics of the system for different initial conditions, controls and system parameters can be obtained easily from the equilibrium and bifurcation surfaces. In particular, the control and parameter values for which jumps and limit cycles appear as well as domains of attraction are obtained directly from the equilibrium and bifurcation surfaces. BACTM also provides insights into the control and identification problems for nonlinear dynamic systems.

(iii) Five degree-of-freedom nonlinear aircraft models in terms of roll rate p, yaw rate r, pitch rate q, angle-of-attack α and sidelip angle β with three control surface deflections $(\delta a, \delta e, \delta r)$, when analyzed using BACTM, reveal the presence of a large number of limit cycle and jump phenomena which encompass

roll coupling, directional divergence, wing rock, buffeting and other phenomena known to occur at high angles-of-attack.

(iv) For aircraft A and B represented using linear aerodynamics effects only, the five degree-of-freedom model can be reduced to a scalar fifth order polynomial model which is diffeomorphic to a "Butterfly" catastrophe. The stability and control properties of this model reveal two sets of jumps, hysteresis effects and autorotation for high values of elevator deflection. An analytical criterion is developed to predict the critical elevator deflection or angle-of-attack for autorotation. The effect of feedback control on bifurcation behavior is studied and it is shown that a control law which keeps the eigenvalues of the linearized system in the left half plane leads to bifurcation-free behavior. The results predicted by BACTM are in close agreement with the results obtained by numerical integration of the equations of motion, including the effects of gravity. Physical explanations are given for the bifurcations and jumps and it is shown that changes in yaw rate are an indicator of an incimpient jump condition.

(v) The five degree-of-freedom model for aircraft H involving several nonlinear aerodynamic effects exhibits Hopf Bifurcations to limit cycles. Several families of limit cycles are shown to exist and depending on the initial state and the control settings, the system trajectories converge either to one of the stable limit cycles or to a stable equilibrium point. The limit cycles themselves increase and decrease in magnitude and may correspond to phenomena such as wing rock, pre-stall buffeting and divergent oscillations towards spin conditions. A physical explanation in

terms of the exchange of kinetic and potential energies is developed for jump and limit cycle behavior. The extreme sensitivity observed at high angles-of-attack to minor design changes is also easily demonstrated in terms of the bifurcation and equilibrium surfaces.

(vi) Results on Aileron-Rudder Interconnect: In Sec. 3.7, the use of BACTM to synthesize a command augmentation system which schedules the rudder as a linear function of the aileron, the gain being a nonlinear function of elevon, has been demonstrated. The values of the ARI (aileron-rudder-interconnect) gains were derived directly from the plots of the bifurcation surfaces. These gains were seen to be nonlinear functions of angle-of-attack, when computed under the criterion of maximizing the range of aileron values which avoid jump or limit cycle behavior. Time history comparisons show significant improvement in dynamic response and performance using the BACTM ARI gain, as opposed to nulling the rudder. The results indicate that scheduling rudder as a general nonlinear function of both aileron and elevon would enhance globally the aircraft performance at high angles-of-attack.

(4.2) Recommendations for Future Research

The next step in the application of BACTM to high angle-of-attack phenomena is to use six degree-of-freedom equations and study spin entry, prevention and recovery.

The aircraft departure into spin followed by aircraft loss in several cases is a very serious problem. The methodology developed

under the current project provides a suitable tool for a complete analysis of this phenomenon. Certain dynamical jump behavior for aircraft B and H has already been observed which has similarities to departure into spin. An exact verification of this fact would require solving the spin equations of motion and relating the two sets of equilibirium points. A first step would be to use the spin equations used by previous investigators [1,2] and solve them for equilibrium surfaces and bifurcations using BACTM. By considering the most general set of equations, it would be possible to obtain spinning as well as nonspinning equilibrium states, including others that may not have been identified before. This will lead to a study of the post-stall departure phnomenon and entry into spin. Since the equilibrium and bifurcation surfaces will be obtained for different control values, techniques for spin prevention and recovery would be investigated easily. It would also be possible to explore the use of feedback laws, stability augmentation techniques and different aircraft configurations on the bifurcation surfaces. Notice that the characterization of bifurcation surfaces would make the concepts of incipient spin, stability margins, etc. much more exact compared to current heuristic methods for defining these variables.

Another direction for future research would be to consider applications of BACTM to other dynamic vehicles such as ships, submarines and missiles. Similar types of jumps and instabilities are known to occur in these vehicles. The use of BACTM for nonlinear control design, model structure determination and experimental design also needs further investigation.

References for Chapter I

[1] Phillips, William H., "Effect of Steady Rolling on Longitudinal and Directional Stability", TN 1627, 1948, NACA.

[2] Pinsker, W.J.G., "Aileron Control of Small Aspect Ratio Aircraft, in Particular, Delta Aircraft", Aeronautical Research Council, Reports and Memoranda 3188, 1953.

[3] Rhoads, D.W., and Schuler, J.M., "A Theoretical and Experimental Study of Airplane Dynamics in Large-Disturbance Maneuvers", Journal of Astronautical Sciences, Vol. XXIV, N. 7, July, 1957.

[4] Welch, J.D. and Wilson, R.E., "Cross Coupling Dynamics and the Problem of Automatic Control in Rapid Rolls", J. of Aeronautical Sciences, Oct. 1957.

[5] Abzug, M.J., "Effects of Centrain Steady Motions on Small Disturbance Airplane Dynamics", J. of the Aero. Sc., Vol. 21, No. 11, Nov. 1954, pp. 749-762.

[6] Moore, F.L., Anglin, E.L., Adams, M.S, Deal, P.O. and Person, L.J. Jr., "Utilization of a Fixed-Base Simulator to Study the Stall and Spin Characteristics of Fighter Airplanes", NASA TN D-6117, Washington, March 1971.

[7] Eney, J. A., and Chambers, J.R., "Piloted Simulation of Spin", ASD Stall/Post-Stall/Spin Symp., WPAFB, Dec. 1971.

[8] Adams, William M., Jr., "Analytic Prediction of Airpla-e Equilibrium Spin Characteristics", TN D-6926, 1972, NASA.

[9] Rutan, E.L., McElroy, C.E. and Gentry, J.R., "Stall/Near Stall Investigation of the F-4E Aircraft", Technical Report No. 70-20, Air Force Flight Test Center, Edward, California, August 1970.

[10] Stengel, R.F., Taylor, J.H., Broussard, J.R., and Berry, P.W., "High Angle-of-Attack Stability and Control", Report ONR-CR215-237-1, Office of Naval Research, April, 1976.

[11] Hall, W.E., Gupta, N.K., and Tyler, J.S., Jr., "Model Structure Determination and Parameter Identification for Nonlinear Aerodynamic Flight Regimes" in Methods for Aircraft State and Parameter Identification, AGARD-CP-172, Nov. 1974.

[12] Mehra, R.K. and Blum, E.H., "On the Dynamics of the Ignition of Paper and Catastrophe Theory", 1976 Joint Automatic Control Conference, Purdue Univ., Lafayette, Ind., June 1976.

[13] Blum, E.H., and Mehra, R.K., "Chemical Kinetics and Catastrophe Theory", IIASA RR-75-41, International Institute for Applied Systems Analysis, Laxenburg, Austria, Nov. 1975.

[14] Takens, F., (a) "Introduction to Global Analysis", and (b) "Notes on Force Oscillations" in Communications 2 and 3, Math. Inst. Rijksuniversiteit, Utrecht.

[15] Thom, R., "Structural Stability and Morphogenesis", Addison Wesley, Reading, Mass., 1974.

[16] Schy, A.A. and Hannah, M.E., "Prediction of Jump Phenomena in Roll-coupled Manuevers of Airplanes", AIAA Third Atmospheric Flight Mechanics Conference, Arlington, TEXAS, June, 1976.

References for Chapter II

[1] Thom, R., Structural Stability and Morphogenesis, Addison Wesley, Reading, Mass., 1974.

[2] Zeeman, E.C., "Differential Equations for the Heartbeat and Nerve Impulse", Towards a Theoretical Biology, Edinburg Univ. Press, 1972.

[3] Zeeman, E.C., "Levels of Structure in Catastrophe Theory", Invited Address, International Congress of Mathematicians, Vancouver, 1974.

[4] Zeeman, E.C., "Catastrophe Theory", Scientific American, April, 1976.

[5] Marsden, J.E., McCracken, M., The Hopf Bifurcation and Its Applications, Springer Verlag, New York, 1976.

[6] Antman, P., Keller, J., Bifurcation Theory and Nonlinear Eigenvalue Problems, Benjamin, 1969.

[7] Arnold, V.I., "Lectures on Bifurcations in Versal Families", Russian Maths. Surveys, 27, 1972.

[8] Poincare, H., "Les Methodes Novelles de la Mecanique Celeste", Vol. I., Paris, 1892.

[9] Andronov, A.A., Witt, A., "Sur la Theorie Mathematiques des Auto-oscillations", C.R. Acad. Sci., Paris, 190, 1930.

[10] Andronov, A.A., Pontryagin, "Coarse Systems", Dokl. Akad. Nak USSR, 14, 1937.

[11] Whitney, H., "On Singularities of Mappings of Euclidean Spaces, I: Mappings of the Plane into Plane", Ann. of Math. (2) 62, 1955.

[12] Thom, R., Levine, H., "Singularities of Differentiable Mappings", Bonn. Math. Schr. 6, Bonn, 1959.

[13] Arno'ld, V.I., "Singularities of Smooth Mappings", Uspekihi Mat. Nauk 23:1, 1968; Russian Math. Surveys 23:1, 1968.

[14] Mather, J.N., "Stability of C^{∞}-Mappings, III: Finitely Determined Map-germs", Inst. Hautes Etudes, Sci. Publ. Math., No. 35, 1968.

[15] Pliss, V.A., "A Reduction Principle in the Theory of Stability of Motion", Isv. Akad. Nauk., USSR. Ser. Mat. 28, 1964.

[16] Hopf, E., "Abzweigug einer Periodschen Losung eines Differential-systems", Akad. Wiss. Leipzig, 94, 1942.

[17] Palais, R.S., "Natural Operations on Differential Forms", Trans. Amer. Math. Soc., Vol. 92, July, 1959.

[18] Kelly, A., "The Stable, Centre-Stable, Centre, Centre-Unstable, Unstable Manifolds", J. Diff. Eqns. 3, 1967.

[19] Kopell, N., "Bifurcations and Trajectories Joining Critical Points", Advances in Maths., 19, 1976.

[20] Shoshitaishvili, A.N., "On the Bifurcation of Topological Type of a Vector Field Near a Singular Point", Funktsional. Anal. i Prilzhen, 6:2, 1972.

[21] Woodstock, A.E.R., Poston, T., A Geometrical Study of the Elementary Catastrophes, Springer Verlag Lecture Notes in Mathematics, 373, 1974.

[22] Amson, J.C., "Catastrophe Theory: A Contribution to the Study of Urban Systems?", Environment and Planning B, Vol. 2, 1975.

[23] Mehra, R.K. and Lainiotis, D.G., Ed., System Identification, Advances and Case Studies, Academic Press, 1976.

[24] Sussmann, H.J., and Zahler, R.S., "Catastrophe Theory as Applied to the Social and Biological Sciences: A Critique", Feb. 1977, to appear in Synthese.

[25] Zhabotinskii, A.M., Zaikin, A.N., "Auto-wave Processes in a Distributed Chemical System, J. Theor. Biol. 40, 1973, 45.

[26] Scarf, H., "The Approximation of Fixed Points of a Continuous Mapping", Siam. J. of Appl. Math. 15: 1328-43, 1967.

[27] Fox, J., Ed., Proceedings of the Symposium on Nonlinear Circuit Analysis, Polytechnic Institute of Brooklyn, New York, 1953.

[28] Minorsky, N., Nonlinear Oscillations, Van Nostrand, Princeton, 1962 (Reprinted, R.E. Krieger, Huntington, New York, 1974).

[29] Thompson, J.M.T. and Hunt, G.W., A General Theory of Elastic Stability, John Wiley & Sons, New York, 1973.

[30] A Uppal, Ray, W.H. and Poore, A.B., "The Classification of the Dynamic Behavior of Continuous Stirred Tank Reactor - - Influence of Reactor Residence Time", Chem. Eng. Soc., 1976.

[31] Takens, F., "Unfolding of Certain Singularities of Vector Fields: Generalized Hopf Bifurcations", J. Diff. Eq. 14, 476-493, 1973.

[32] Lasalle, J and Lefchetz, S., Stability by Liapunov's Direct Method, Academic Press, New York, 1961.

[33] Takahashi, Y., Rabins, M.J. and Auslander, D.M., Control and Dynamic Systems, Addison-Wesley Publishing Co., Reading, Mass., 1970.

[34] Gelb, A. and Van der Velde, W.E., Multiple-Input Describing Functions and Nonlinear System Design, McGraw-Hill, New York, 1968.

[35] Gantmacher, F.R., The Theory of Matrices, Vol. I, Chelsea Publishing Co., New York, N.Y., 1959.

References for Chapter III

[1] Rhoads, D.W., , and Schuler, J.M., "A Theoretical and Experimental Study of Airplane Dynamics in Large-Distrubance Maneuvers", Journal of Astronautical Sciences, Vol. XXIV, No. 7, July, 1957.

[2] Hacker, T. and Oprisiu, C., "A Discussion of the Roll Coupling Problem", Progress in Aerospace Sciences, Vol. 15, Pergamon Press, Oxford, 1974.

[3] Haddad, Emile, K., "Study of Stability of Large Maneuvers of Airplances:, CR-2447, 1974, NASA.

[4] Phillips, William H., "Effect of Steady Rolling on Longitudinal and Directional Stability", TN 1627, 1948, NACA.

[5] Etkin, Bernard, Dynamics of Atmospheric Flight, John Wiley and Sons, New York, 1972.

[6] Adams, William M., Jr., "Analytic Prediction of Airplane Equilibrium Spin Characteristics", TN D-6926, 1972, NASA.

[7] Young, J.W., "Optimal and Suboptimal Control Techniques for Aircraft Spin Recovery", TN D-7714, October, 1974, NASA.

[8] Gertler, M. and Hagen, G.R., "Standard Equations of Motion for Submarine Simulation", DTNSRDC Report 2510, June, 1967.

[9] Schy, A.A. and Hannah, M.E., "Prediction of Jump Phenomena in Roll-coupled Maneuvers of Airplanes", AIAA Third Atmospheric Flight Mechanics Conference, Arlington, Texas, June 1976.

[10] Rutan, E.L., McElroy, C.E. and Gentry, J.R., "Stall/Near Stall Investigation of the F-4E Aircraft", Technical Report No. 70-20, Air Force Flight Test Center, Edward, California, August 1970.

[11] Gilbert, W.P, et al., "Simulation Study of the Effectiveness of an Automatic Control System Designed to Improve the High Angle-of-Attack Characteristics of a Fighter Airplane", NASA TN D-8176, 1976.

[12] Ruelle, D. and Takens, F, "On the Nature of Turbulence", Comm. Math. Phy. 20, 1971.

[13] Pinsker, W.J.G., "Aileron Control of Small Aspect Ratio Aircraft, in Particular, Delta Aircraft", Aeronautical Research Council Reports and Memoranda 3188, 1953.

[14] Thom, R., "Structural Stability and Morphogenesis", Addison Wesley, Reading, Mass. 1974.

[15] Stengel, R.F., Taylor, J.H., Broussard, J.R., and Berry, P.W., "High Angle-of-Attack Stability and Control", Report ONR-CR215-237-1, Office of Naval Research, April, 1976.

References for Chapter IV

[1] Adams, William M., Jr., "Analytic Prediction of Airplane Equilibirum Spin Characteristics", TN D-6926, 1972, NASA.

[2] Young, J.W., "Optimal and Suboptimal Control Techniques for Aircraft Spin Recovery", TN D-7714, October, 1974, NASA.

APPENDIX A: MAIN THEOREMS OF BACTM

A.1 Center Manifold Theorem or Reduction Theorem, [18,19,20,24]:*

Suppose that a set of n Ordinary Differential Equations can be written as:

$$\dot{u} = Au + f_A(u,v,w) \qquad (A.1)$$
$$\dot{v} = Bv + f_B(u,v,w)$$
$$\dot{w} = Cw + f_C(u,v,w)$$

where A,B,C are square matrices of orders j,k,ℓ respectively ($j + k + \ell = n$) whose eigenvalues have their real parts <0, $= 0$, >0 resp. The nonlinear functions f_A, f_B, f_C are C^r differentiable ($r \geq 2$) and vanish along with their derivatives, at $(u,v,w) = 0$. Then there is a c^{r-1} submanifold $\tilde{M}$, of dimension k, which passes through $(u,v,w) = 0$, is tangent there to $u = 0$, $w = 0$, and which is invariant under the above equations (i.e., is composed of solution curves of those equations).

Proposition [20]: Suppose there is a curve $(u(\mu), v(\mu), w(\mu))$ depending on a parameter or control vector μ such that $(u(0), v(0), w(0)) = 0$ and for each $\mu \in R^m$, $[u(\mu), v(\mu), w(\mu)]$ is a fixed point for Eq. (A.1). Then for all sufficiently small μ, $[u(\mu), v(\mu), w(\mu)]$ lies in any center manifold $\tilde{M}$.

A.2 Main Theorem of Elementary Castrophe Theory [1,2,3]:

Let $x \in R^n$ and $c \in R^m$. Then $f(x,c) = 0$ is an m dimensional manifold M in R^{n+m}. Define the projection map $X: M \to C$ where C is the space of control variables.

---

* Reference numbers same as for Chapter II

Let F denote the space of c^∞ -functions on R^{m+n} with the Whitney c^∞-topology.

Theorem: If $m \leq 5$, there is an open dense set $F_0 \subset F$ which is the set of generic functions. If ϕ is generic, then

1) The manifold M_ϕ is an m-manifold;

2) Any singularity of the projection map X_ϕ is equivalent to one of a finite number of types called elementary catastrophes;

3) X_ϕ is stable under small perturbations of ϕ. The number of elementary catastrophes depends only upon m, the dimension of control space, as follows:

m	1	2	3	4	5	6
Elementary Catastrophes	1	2	5	7	11	∞

Here equivalence implies: two maps $X_\phi : M_\phi \to C_\phi$ and $X_g : M_g \to C_g$ are equivalent if there exist diffeomorphisms h and k such that the following diagram is commutative.

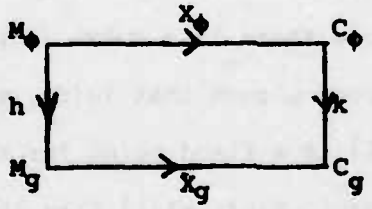

If X_ϕ and X_g have singularities at $x_\phi \in M_\phi$ and $x_g \in M_g$, respectively, then the singularities are equivalent if the above definition holds locally with $hx_\phi = x_g$. Stable means that X_ϕ is equivalent to X_g for all g in a neighborhood of ϕ in F.

A.3 The Hopf Theorem in R^2: [5]

The following theorem is essentially due to Andronov (1930) and Hopf (1942) and was suggested in the work of Poincare (1892). For detailed discussion see Ref. [5].

Theorem: Let X_μ be a C^k ($k\geq 4$) vector field on R^2 such that $X_\mu(0) = 0$ for all μ and $X = (X_\mu, 0)$ is also C^k. Let dX_μ $(0,0)$ denoting the linear part of X_μ have two distinct, complex conjugate eigenvalues $\lambda(\mu)$ and $\overline{\lambda(\mu)}$ such that for $\mu>0$, Re $\lambda(\mu)>0$. Also let $\left.\frac{d(\mathrm{Re}\lambda(\mu))}{d\mu}\right|_{\mu=0} > 0$

Then:

(a) There is a C^{k-2} function $\mu:(-\varepsilon,\varepsilon)\to R$ such that $(x_1,0,\mu(x_1))$ is on a closed orbit of period $\approx 2\pi/|\lambda(0)|$ and radius growing like $\sqrt{\mu}$ of X for $x_1\neq 0$ and such that $\mu(0)=0$.

(b) There is a neighborhood U of $(0,0,0)$ in R^3 such that any closed orbit in U is one of those above. Furthermore, if 0 is a "vague attractor" for X_0, then

(c) $\mu(x_1)>0$ for all $x_1\neq 0$ and the orbits are attracting.

The Hopf Theorem in R^n

Theorem: Let X_μ be a C^{k+1}, $k\geq 4$, vector field on R^n, with all the assumptions of the above Theorem holding except that we assume that the rest of the spectrum is distinct from the two assumed simple eigenvalues $\lambda(\mu), \overline{\lambda(\mu)}$. Then conclusion (a) is true. Conclusion (b) is true if the rest of the spectrum remains in the left half plane as μ crosses zero. Conclusion (c) is true if, relative to $\lambda(\mu), \overline{\lambda(\mu)}$, 0 is a "vague attractor" and if when coordinates are

chosen so that:

$$dx_0(0) = \begin{bmatrix} 0 & |\lambda(0)| & d_3x^1(0) \\ -|\lambda(0)| & 0 & d_3x^2(0) \\ 0 & 0 & d_3x^3(0) \end{bmatrix}, \quad \lambda(0) \notin \sigma(d_3x^3(0))$$

[i.e. $\lambda(0)$ does not belong to the spectrum of $d_3x^3(0)$].

A.4 Global Implicit Function Theorems [26,27]:

The following are extensions of Palais Theorem [17]:

Theorem 1: Let f be a continuously differentiable mapping of $E^m \times E^n$ into E^m. There then exists a unique continuously differentiable mapping g of $E^m \times E^n$ into E^m with the property that $g(y,u)=x$ for all $x,y \in E^n$ satisfying $f(x,u)=y$, provided that i) $\det[\partial f/\partial x]=0$ at each point in $E^m \times E^n$, and ii) for each $u \in E^n$, $||f(x,u)|| \to \infty$ as $||x|| \to \infty$.

Theorem 2: Let f be a continuously differentiable mapping of E^n into E^n. For $k=1, \ldots, n$, let J_k denote the matrix consisting of the elements in the first k rows and first k columns of the Jacobian matrix. Suppose there exist a positive constant ε such that

$$||\det J_1|| \geq \varepsilon, \left|\frac{\det J_2}{\det J_1}\right| \geq \varepsilon, \ldots, \left|\frac{\det J_n}{\det J_{n-1}}\right| \geq \varepsilon,$$

for all $x \in E^n$. Then there exist a unique solution of $x \in E^n$ for each $y \in E^n$.

Appendix B

Derivations of Equilibrium Equations and Analytic Stability Criterion for Autorotation

In this appendix, further details of the derivations of the equilibrium equations in terms of the roll rate and the critical elevator angle for autorotation are given (cf. Chapter III).

B.1 Derivation of Equlibrium Equation in Terms of Roll Rate, p.

Starting with the five equations of motion (gravity ignored): (α denotes deviation from trim).

$$\dot{\beta} = y_\beta \beta + p(\sin\alpha_o + \alpha) - r\cos\alpha_o + y_{\delta a}\delta a + y_{\delta r}\delta r =$$

$$f_\beta(\beta,\alpha,p,r,\delta a,\delta r) \tag{B.1}$$

$$\dot{\alpha} = q - p\beta + z_\alpha \alpha + z_{\delta e}\delta e = f_\alpha(\beta,\alpha,p,q,\delta e) \tag{B.2}$$

$$\dot{q} = \bar{m}_\alpha \alpha + m_q q + i_2 pr + m_{\delta e}\delta e - m_\alpha p\beta =$$

$$f_q(\beta,\alpha,p,q,r,\delta e) \tag{B.3}$$

$$\dot{r} = n_\beta \beta + n_{\alpha\delta a}\alpha\delta a + n_r r + n_p p + n_{p\alpha} p\alpha - i_3 pq$$

$$+ n_{\delta a}\delta a + n_{\delta r}\delta r = f_r(\beta,\alpha,p,q,r,\delta a,\delta r) \tag{B.4}$$

$$\dot{p} = \ell_\beta \beta + \ell_{\alpha\delta a}\alpha\delta a + \ell_q q + \ell_r r + \ell_p p + \ell_{\beta\alpha}\beta\alpha + \ell_{r\alpha} r\alpha$$

$$-i_1 qr + \ell_{\delta a}\delta a + \ell_{\delta r}\delta r = f_p(\beta,\alpha,p,q,r,\delta a,\delta r) \tag{B.5}$$

Setting all time derivatives to zero (i.e., f_β, f_α, f_q, f_r, $f_p = 0$), five equations in five unknowns are obtained. Equation B.2, correspondingly

is then solved for q:

$$q = p\beta - z_\alpha \alpha - z_{\delta e}\delta e = f(\beta,\alpha,p,\delta e) \qquad (B.6)$$

Substituting into the remaining four equations gives

$$0 = f_\beta(\beta,\alpha,p,r,\delta a,\delta e,\delta r) \quad \text{(from B.1)} \qquad (B.7)$$

$$0 = f_q(\beta,\alpha,p,r,\delta a,\delta e,\delta r) \quad \text{(from B.3)} \qquad (B.8)$$

$$0 = f_r(\beta,\alpha,p,p^2,r,\delta a,\delta e,\delta r) \quad \text{(from B.4)} \qquad (B.9)$$

$$0 = f_p(\beta,\alpha,p,r,\delta a,\delta e,\delta r) \quad \text{(from B.5)} \qquad (B.10)$$

B.7 is then solved for r and substituted into the others, leaving:

$$0 = f_q(\beta,\alpha,p,p^2,\delta a,\delta e,\delta r) \quad \text{(from B.3)} \qquad (B.11)$$

$$0 = f_r(\beta,\alpha,p,p^2,\delta a,\delta e,\delta r) \quad \text{(from B.4)} \qquad (B.12)$$

$$0 = f_p(\beta,\beta^2,\alpha,\alpha^2,p,p^2,\delta a,\delta e,\delta r) \quad \text{(from B.5)} \qquad (B.13)$$

Next, B.11 is solved for β and substituted into B.12 and B.13.

$$0 = f_r(\alpha,p,p^2,p^3,p^{-1},\delta a,\delta e,\delta r) \quad \text{(from B.4)} \qquad (B.14)$$

$$0 = f_q(\alpha,\alpha^2,p,p^2,p^3,p^{-1},\delta a,\delta e,\delta r) \quad \text{(from B.5)} \qquad (B.15)$$

Finally, B.14 is solved for α:

$$\alpha = \frac{f_{r1}(p,p^2,p^3,p^{-1},\delta a,\delta e,\delta r)}{f_{r2}(p,p^3,p^{-1},\delta a,\delta e,\delta r)} \tag{B.16}$$

This is substituted into B.15, leaving:

$$0 = f_p(p,p^2,p^3 \ldots p^{11},p^{-1},\delta a,\delta e,\delta r) \tag{B.17}$$

or

$$0 = f_p(p,p^2 \ldots p^{12},\delta a,\delta e,\delta r) \tag{B.18}$$

Equation B.18 is a quartic in δa [cf. Eq. (B.3)]. It simplifies to a cubic if $-i_1 qr$ term is negelected in Eq. (B.5) and to a quadratic if $n_{\alpha\delta a}$ is set to zero in Eq. (B.4). Finally, if all the nonlinear dynamic terms and $-i_1 qr$ are neglected, a fifth order polynomial in p is obtained (cf. Aircraft B, section 3.6.1).

B.2 Analytic Stability Criterion for Autorotation.

In this section, we derive an analytic expression for critical δe at which the equilibrium point ($\bar{p} = 0$, $\bar{r} = 0$, $\bar{\beta} = 0$, $\delta a = 0$, $\delta r = 0$) becomes unstable in the sense that a real eigenvalue crosses the origin from the left half plane. First, the equilibrium equations corresponding to $\dot{q} = 0$ and $\dot{\alpha} = 0$ [Eqs. (B.2) and (B.3)] are solved for $\bar{d}$ and $\bar{q}$ in terms of δe.

$$\bar{\alpha} = \frac{\bar{m}_q z_{\delta e} - m_{\delta e}}{\bar{m}_\alpha - \bar{m}_q z_\alpha} \delta e = K_\alpha \delta e \tag{B.19}$$

$$\bar{q} = \frac{z_\alpha \bar{m}_{\delta e} - z_{\delta e} \bar{m}_\alpha}{\bar{m}_\alpha - \bar{m}_q z_\alpha} \delta e = K_q \delta e \tag{B.20}$$

We now linearize the equations of motion (B.1-B.5) around ($p = r = \beta = 0$, $\bar{\alpha}$, $\bar{q}$) and set the determinant of the jacobian to zero. This leads to the following equation for critical δe (neglecting $-i_1 qr$):

$$a\delta e^2 + b\delta e + c = 0 \tag{B.21}$$

where

$$a = K_q K_\alpha (K_{\beta q} \ell_{\beta\alpha} + K_{rq} \ell_{r\alpha}) + K_\alpha^2 (K_{\beta\alpha} \ell_{\beta\alpha} + K_{r\alpha} \ell_{r\alpha}) \tag{B.22}$$

$$b = K_q (K_{\beta q} \ell_\beta + K_{rq} \ell_r) + K_\alpha (K_{\beta\alpha} \ell_\beta + K_{r\alpha} \ell_r + K_\beta \ell_{\beta\alpha} + K_r \ell_{r\alpha}) \tag{B.23}$$

$$c = K_\beta \ell_\beta + K_r \ell_r + \ell_p \tag{B.24}$$

and

$$K_{\beta q} = \frac{i_3}{n_\beta + n_r y_\beta}$$

$$K_{\beta\alpha} = -\frac{n_{p\alpha} + n_r}{n_\beta + n_r y_\beta}$$

$$K_\beta = \frac{-n_p}{n_\beta + n_r y_\beta}$$

$$K_{rq} = y_\beta K_{\beta q}$$

$$K_{r\alpha} = \frac{n_\beta - n_{p\alpha}}{n_\beta + n_r y_\beta}$$

$$K_r = y_\beta K_\beta$$

For the aircraft B model, Eq. (B.21) simplifies further since a = 0. Thus the critical elevator angle, $\delta_e^* = -\frac{c}{b} = 9.3$ deg. See Fig. 3.13. For aircraft H, two flight conditions from Rhoades and Schuler [1, Chapter III] were examined and for both these conditions, Eq. (B.21) was found to have imaginary roots. Thus, aircraft H model indicates that autorotation is not possible for $\delta a = \delta r = 0$. See Fig. 3.48 for confirmation of this observation.

The above analytical results are confirmed by the numerical simulation results given in section 3.6 of this report.

Appendix C

Nomenclature for Chapter 3

The orientation of the aircraft body axes [(x_b,y_b, z_b) in Fig. 3.1] with respect to inertial space, or earth-fixed axes, is defined by the following Euler angles, in sequence from reference to body axes: ψ(yaw), θ(pitch) and ϕ(roll). The orientation of wind axes (X_w,Y_w,Z_w), stability axes (X_s,Y_s,Z_s), and body axes and the conventions for linear velocities (u,v,w), angular velocities (p,q,r), forces (X,Y,Z), moments (L,M,N), and control surface deflections (δa,δe,δr) are all shown in Fig.3.1. The symbols and definitions used in this report are in as much agreement with convention as clarity allows. The body axes are oriented so as to align with the stability axes for straight and level flight in the reference flight condition.

ψ, θ, ϕ	orientation (Euler) angles of reference to body axes.
θ_o	reference value of θ
β	angle of sideslip
α	angle-of-attack
α_o	reference value of α
δa	aileron command deflection
δe	elevator command deflection
δr	rudder command deflection
u,v,w	body axis components of linear velocity
p,q,r	body axis components of angular velocity
$\vec{\omega}$	vector of angular velocity components, (p,q,r)
X,Y,Z	body axis components of force
L,M,N	body axis components of moment

m	mass (context distinguishes this from pitching moment per I_y,m).
t	time
I_x, I_y, I_z	moments of inertia
I	matrix (or tensor) of moments of inertia
$i_1 = (I_z - I_y)/I_x$	Non-dimensional Inertia Coefficients
$i_2 = (I_z - I_x)/I_y$	
$i_3 = (I_y - I_x)/I_z$	
E	vehicle kinetic energy
V	total aircraft velocity = $(u^2 + v^2 + w^2)^{\frac{1}{2}}$
$\bar{c}$	wing mean aerodynamic chord
b	wing span
S	lifting surface area
g	acceleration of gravity (=9.8, metric, 32.2, Eng.)
ρ	air density
$\bar{q}$	dynamic pressure, $\frac{1}{2}\rho V^2$; equilibrium pitch rate (distinguished by context from dynamic pressure)
ℓ	rolling moment per I_x
m	pitching moment per I_y
n	yawing moment per I_z
y	side force (over aircraft mass and speed)
z	aerodynamic force along Z_B axis (over mass and speed)

$C_y = Y/(\bar{q}S)$

$C_\ell, C_m, C_n = L/(\bar{q}Sb),\ M/(\bar{q}S\bar{c}),\ N/(\bar{q}Sb)$

Superscripts

$\bar{}$ equilibrium, or steady state, value

$\cdot$ time derivative in inertial, or earth-fixed, coordinates

0 reference value

Subscripts

$\alpha,\beta,\dot{\alpha},p,q,r,\ \delta a,\delta e,\delta r$ denote partial derivatives with respect to the relevant quantity (viz, C_y, C_ℓ, C_m, C_n for aircraft A and B; and y,z,ℓ,m,n for aircraft H). Thus, for example,

$$\ell_{\alpha\delta a} = \frac{\partial^2 \ell}{\partial\alpha\,\partial(\delta a)}$$

and

$$C_{\ell_\beta} = \frac{\partial C_\ell}{\partial\beta}$$

Special Definitions

$$\bar{m}_\alpha = m_\alpha + m_{\dot{\alpha}} z_\alpha$$

$$\bar{m}_q = m_q + m_{\dot{\alpha}}$$

Office of Naval Research
800 N. Quincy Street
Arlington, VA 22217
- Code 211 (CDR P. R. Hite) 4
- Code 102IP 6
- Code 455 (Mr. G. S. Malecki) 1

Office of Naval Research Branch Office
495 Summer Street
Boston, Mass 02210 1

Commander Defense Contract
Administrative Services-Boston
666 Summer Street
Boston, Mass 02210 1

U.S. Naval Research Laboratory
Washington, D. C.
- Code 2627 6

Defense Documentation Center
Bldg 5, Cameron Station
Alexandria, VA 22314 12

NASA Headquarters
Washington, D. C. 20546
- Code RE (Dr. P. Kurzhals) 1
- Code RO (Mr. K. Hodge) 1
- Code RT (Mr. R. Winblade) 1

NASA Langley Research Center
Hampton, VA 23665
- M/S 152 (Mr. W. H. Phillips) 1
- M/S 152A (Mr. J. R. Elliott) 1
- M/S 355 (Mr. J. R. Chambers) 1
- M/S 473 (Dr. T. M. Walsh) 1
- M/S 478 (Mr. A. A. Schy) 1
- M/S 494 (Dr. J. Creedon) 1

NASA Ames Research Center
Moffett Field, CA 94035
- M/S 200-3 (Mr. L. Roberts) 1
- M/S 210-9 (Mr. B. Y. Creer) 1
- M/S 211-2 (Dr. J. A. Franklin) 1
- M/S 227-5 (Mr. F. Stienly) 1

NASA Dryden Research Center
P.O. Box 273
Edwards, CA 93523
- Code R (Dr. H. Rediess) 1
- Code VDC (Mr. D. Deets) 1
- Code R (Dr. K. Iliff) 1

NASA Johnson Space Center
Houston, TX 77058
- Code EJ (Dr. K. J. Cox) 1
- Code EX (Mr. B. Redd) 1
- Code CA (Mr. W. North) 1

Naval Air Systems Command
Washington, D.C. 20361
- Air 03P34 (Mr. T. Momiyama) 1
- Air 320D (Mr. R. F. Siewert) 1
- Air 5102B (CDR W. Davis) 1
- Air 53011 (Mr. R. C. A'Harrah) 1
- Air 530111 (Mr. J. T. Lawrence) 1

Naval Air Development Center
Warminster, PA 18974
- Code 3015 (Mr. A. Piranian) 1
- Code 3015 (Mr. C. Mazza) 1
- Code 3042 (Mr. C. Abrams) 1
- Code 4023 (Dr. L. Hitchcock) 1

U.S. Naval Postgraduate School
Monterey, CA 93940
- Dept of Aeronautics (Dr. L. Schmidt) 1
- Ops Research (Dr. G. Poock) 1
- Library 1

Naval Air Test Center
NAS Patuxent River, MD 20670
- TPS (Mr. R. Bowes) 1
- SA43 (Mr. S. L. Porter) 1
- SA50G (Mr. J. Dunn) 1
- SA51 (Mr. W. M. Branch) 1

Pacific Missile Test Center
Point Mugu, CA 93042
- Code 1226 (LCDR W. Moroney) 1

Naval Material Command
Washington, D. C. 20362
- NMAT 0331 (Mr. H. G. Moore) 1

Naval Coastal Systems Laboratory
Panama City, FL 32401
- Code 794 (Dr. D. Humphreys) 1

Air Force Office of Scientific Research
Bolling AFB
Washington, D. C. 20332
Attn: Capt. C. Nefzger 1

Air Force Flight Dynamics Laboratory
Wright Patterson AFB, OH 45433
- Code FGC (Mr. E. H. Flinn) 1
- Code FGC (Mr. G. K. Heilman) 1
- Code FGL (Mr. P. Blatt) 1
- Code FGT (Mr. M. Ostgaard) 1
- Code FGD (Mr. R. O. Anderson) 1
- Code FGB (Mr. R. Swortzel) 1

Air Force Flight Test Center
Edwards, CA 93523
- Code DOY (Mr. C. L. Nagy) 1
- Code DOEEP (Mr. K. Martin) 1
- Code DOEEP (Mr. D. Wilson) 1

Massachusetts Institute of Technology
Cambridge, MASS 02139
- Attn: Prof. W. E. Vander Velde 1
- Prof. M. Athans 1
- Prof. T. B. Sheridan 1

University of Illinois
Savoy, Ill. 61874
- Attn: Dr. S. N. Roscoe 1

Grumman Aerosapce Company
Advanced Systems Plant 5
Bethpage, NY 11714
- Attn: Mr. J. Chen 1

Princeton University
Princeton, N.J. 08540
- Attn: Mr. D. Ellis 1
- Prof. D. Graham 1
- Prof. R. Stengel 1

System Technology Inc.
13766 S. Hawthorne Blvd
Hawthorne, CA 90250
- Attn: Mr. D. E. Johnston 1

Boeing Commercial Airplane Co.
Flight Control Technology
P.O. Box 3707
Seattle, WA 98124
- Attn: Mr. H.A. Shomber 1

Systems Control Inc.
1801 Page Mill Rd
Palo Alto, CA 94304
- Attn: Dr. E. Hall 1

Scientific Systems Inc.
1640 Massachusetts Avenue
Cambridge, MA 02138
- Attn: Dr. Raman Mehra 1

Federal Aviation Administration
Washington, D. C. 20591
- Code AEM20 (Mr. H. Verstynen) 1

David Taylor Naval Ship Research and Development Center
Bethesda, MD 20084
- Dr. Alan Powell, Tech. Dir. 1
- Code 1660 (Mr. L. Troubaugh) 1

Robert T.N. Chen
Mail Stop 211-2
Ames Research Center
Moffett Field, CA. 94035 1

Daniel R. Cichy
Rockwell International
Columbus Aircraft Division B6
4300 E 5th Ave.
Columbus, Ohio 43028 1

Kenneth K. Cobb
A.F. Armament Lab.
DLDL
Eglin AFB, Fla. 32542

N. Gregory
DRDS
British Defense Staff
3100 Massachusetts Ave., N.W.
Washington, D.C. 20001 1

John Hodgkinson
McDonnell Aircraft
P.O. Box 516
St. Louis, MO. 63106 1

David G. Hull,
Aerospace Engineering
University of Texas
Austin, Texas 78712 1

C.R. James, Jr. (unit 2-53300)
Vought Corporation
Box 5907
Dallas, Tx. 75222 1

Peter S. Maybeck
AFIT/ENG
Wright-Patterson AFB, Ohio 45433 1

Dean Mook
ESM Dept.
VPISU
Blacksburg, VA. 24061 1

B.L. Nagabhushan
Dept. 456G
Goodyear Aerospace Corp.
1210 Massillon Road
Akron, Ohio 44315 1

Ram Ramachandran
Dynamics Research Corp.
Wilmington, MA. 01887 1

Robert F. Ringland
Systems Technology, Inc.
13766 So. Hawthorne Blvd.
Hawthorne, CA. 90250 1

Jason L. Speyer
Aerospace Engineering
University of Texas
Austin, Texas 78712 1

H.L. Stalford
60 Concord St.
Dynamics Research Corp.
Wilmington, Mass. 01887 1

Darryl J. Trulin
General Dynamics/Pomona Div.
P.O. Box 2507
Pomona, CA. 91711 1

Dr. V. Klein
NASA Langley Research Center
Hampton, VA 23665 1

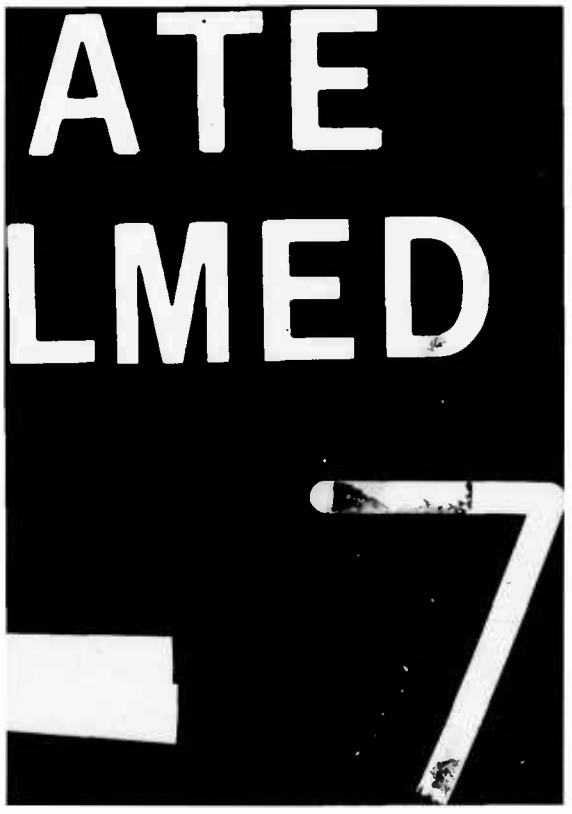
ATE
LMED
7